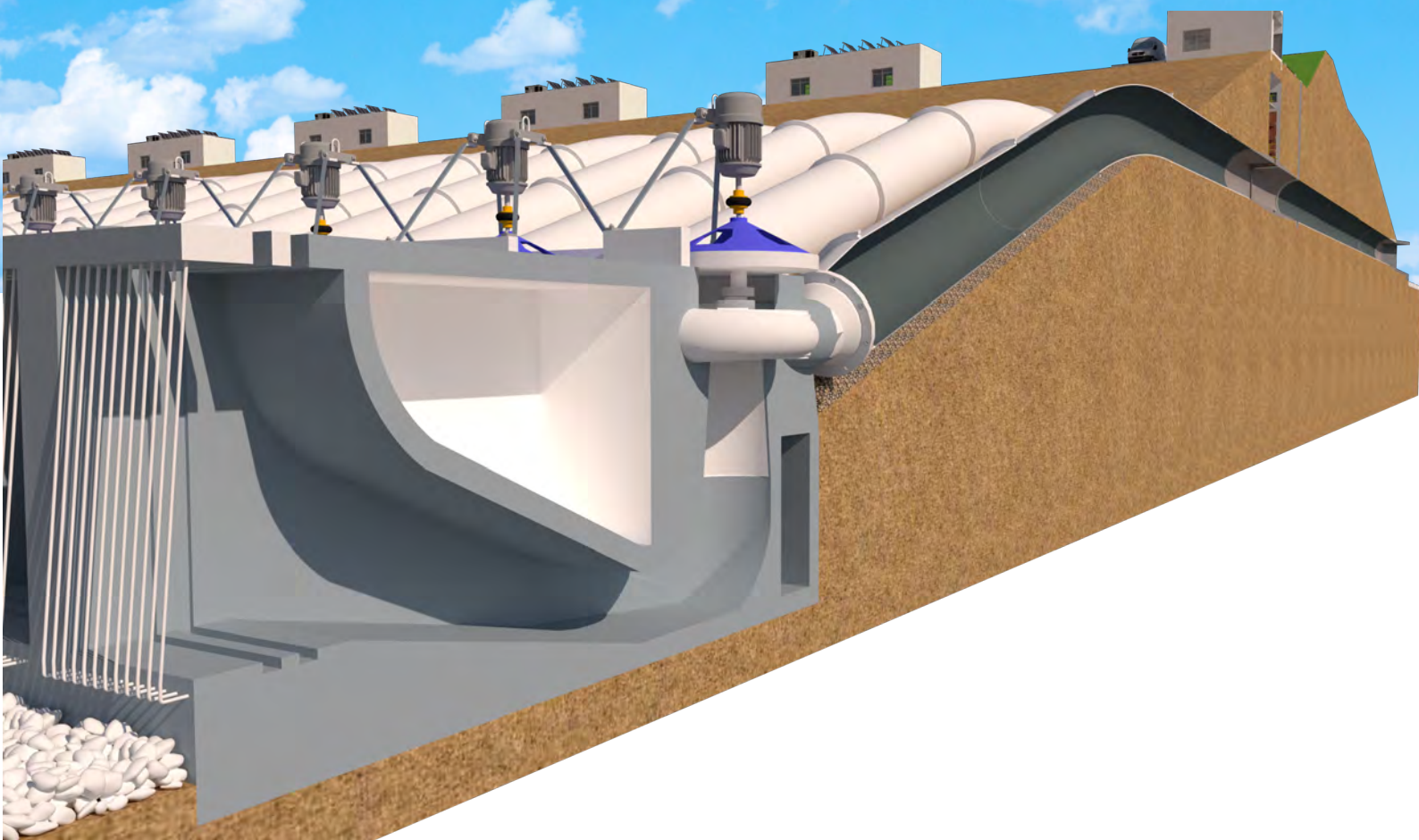


Delta21: Improved Design of the Pump-turbine Station

Loïc Jacquemin



MSc. Thesis Report

Delta21: Improved Design of the Pump-Turbine Station

by

L.J.E. Jacquemin

Student number: 4357426

Thesis committee: Dr. ir. J.D. Bricker, TU Delft, Chairman
Dr. ing. M.Z. Voorendt, TU Delft, Supervisor
Dr. ir. A. Jarquin Laguna, TU Delft, Supervisor
ing. G.E. van Beveren, Royal HaskoningDHV



Preface

The finalization of this report marks the end of my studies as a civil engineer.

My deepest thanks to the committee members who guided me very diligently along the way. All four of you; Mark, Antonio, Jeremy, and Guus, I would like to thank you for the time and effort you put into helping me complete a successful thesis project.

Thanks to all the Royal HaskoningDHV colleagues who provided their (virtual) support and expertise.

I also want to thank Huub and Leen for providing me with such an interesting topic and helping me find a company to pursue my thesis project at in the midst of a pandemic. Let us hope one day the realisation of the Delta21 concept will be a fact.

My final thanks go to my parents who showed me the world and made this all possible, to Linda for your unwavering support, and to all the friends along the way with whom I have shared unforgettable moments.

*L.J.E. Jacquemin
Rotterdam, August 2021*

Abstract

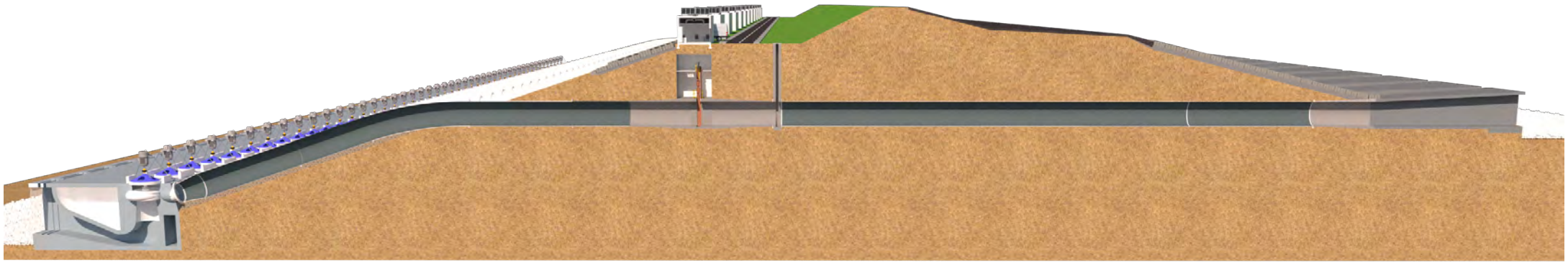
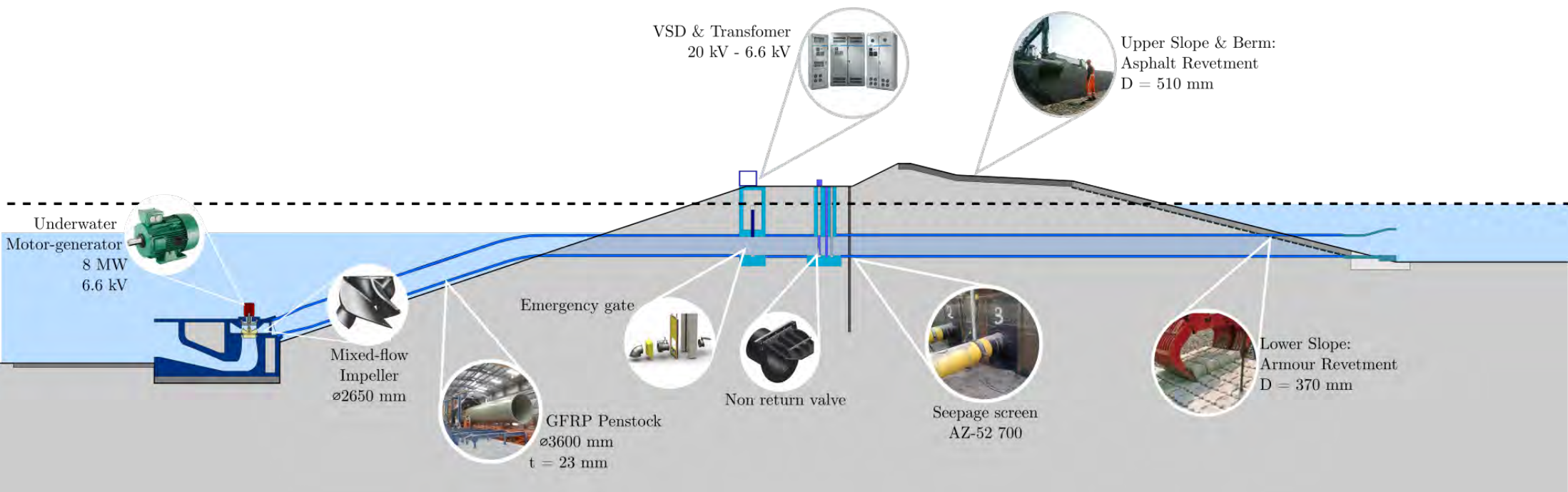
A changing climate means that the combination of storm surge and river flood waves is becoming increasingly likely. The turbine-pumping station of the Delta21 concept, is designed just for that. The energy storage lake and the pumps capable of up to 10,000 m³/s mean that even the highest river discharges can be sluiced to the North Sea in the event of closure of the storm surge barrier. When the pumps are not being operated to combat flood waves, the pump-turbines can be used for the purpose of storage of intermittent renewable energies.

The required capacity of the pumping station means that the total width of the structure is in the order of kilometers. Past studies into the conceptual design have shown that if the pumping station and flood barrier are integral then this results in a massive structure. Ansorena-Ruiz (2020) showed that such a massive structure performs very poorly in a life cycle analysis. For this reason, the goal of the thesis research is to develop an improved design for the turbine-pumping station in which the structure can be separated into two parts resulting in a less monolithic form.

The design is separated into two main parts: the hydraulic design and the structural design. The hydraulic design ensures that the turbine-pumping station can operate at the required functionality. A pump characteristic as well as a turbine characteristic was received from equipment manufacturer Pentair and was adjusted to the requirements of the Delta21 turbine-pumping station. A simulation showed that the total efficiency of the turbine-pumping system is around 67%. Using time-series of storm surges and predicted flood waves with various return periods, a simulation was also done of the response of the energy storage lake and pumping station. It showed that for flood waves of very low annual exceedance probability the required capacity of the turbine-pumping station should be larger than 10,000 m³/s, but however the storage function of the energy storage lake does contribute to the sluicing of the superfluous discharge. Various alternatives for the hydraulic design were conceived, and it was concluded that the draft tube shape of the intake is the optimal solution.

For the structural design the elements of the turbine-pumping installation were integrated into a sea dike. The dike acts as a flood defense, keeping the North Sea out of the energy storage lake, while the elements of the pumping station ensure control of the water level inside the lake. This separation of functions allows for a less imposing structure to be achieved, without compromising on the performance.

In this study, sea level rise and energy transition go hand in hand. On the one hand, pumping technology is used to protect delta areas from flooding, while on the other hand the technology of hydro-pumped storage is used to increase the productivity of renewable energies to offset further climate change. On top of this, the grid-balancing capabilities of the system make it financially attractive for potential investors. Hydro-pumped storage is already an upcoming technology in mountainous areas, but its potential in deltas and coastal regions is even bigger.



Contents

Preface	ii
Abstract	iii
Part 1: Introduction	1
1 Motivation, Relevancy, & Problem Statement	2
1.1 Motivation & Relevancy	2
1.2 Description of the Delta21 Concept	4
1.3 Operating Modes of the Energy Storage Lake	7
1.4 Findings of Past Designs of the Pump-turbine Station	8
2 Objective, Methodology, & Outline	9
2.1 Objective	9
2.2 Scope	9
2.3 Methodology	10
2.4 Report Outline	11
3 Basis of Design	13
3.1 Hydraulic Requirements	13
3.2 Structural Requirements	14
3.3 Starting Points	14
3.4 Boundary Conditions	15
Part 2: Hydraulic Design	22
4 Development of the Basic Design Concept for the Pump-turbine Station	23
4.1 Flood Defense System	23
4.2 Level Schematic and Preliminary Design	25
4.3 Selection of the Pump-turbine	27
4.4 System and Pump Characteristics	29

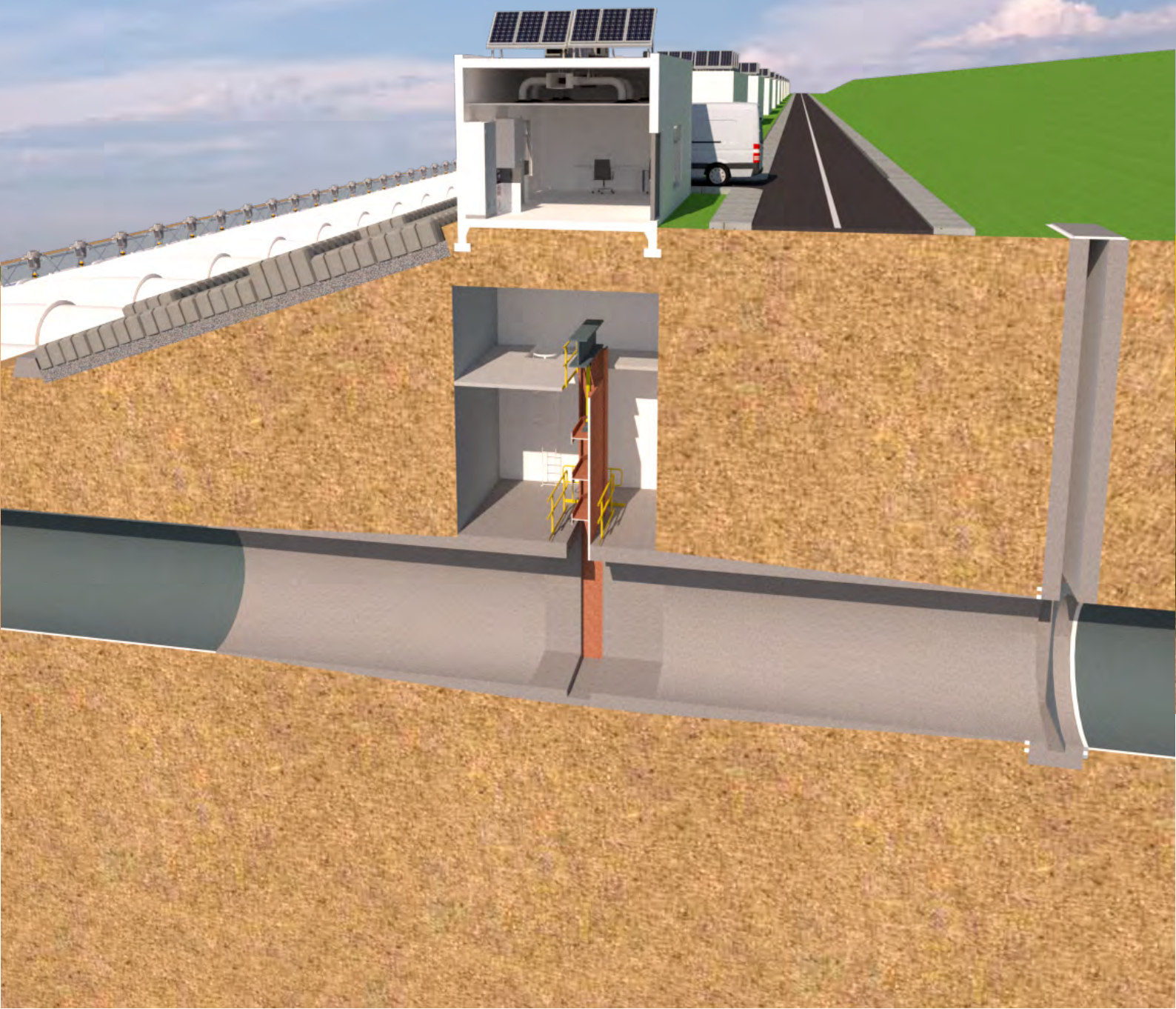
4.5	Turbine Characteristics	31
4.6	Hydraulic Sizing	32
4.7	Physical Sizing	34
4.8	Overview Schematic	35
4.9	System Efficiencies.	35
4.10	Analysis of Cavitation	36
4.11	Connection of the Pump-Turbines to Grid Power	36
4.12	Cooling of the Motor, Variable Speed Drives, and Transformers.	37
4.13	Standard Equipment	38
4.14	Operating Philosophy	39
4.15	Discussion of the Unstable Region for the Pump	47
4.16	Maintenance and Accessibility.	48
4.17	Selection of Materials in the Turbine-Pumping Installation	50
5	Variations on the Basic Design Concept	52
5.1	Analysing the Effect of an Increase in the Depth of the Pump-house	52
5.2	Analysing the Effects of a Change in Impeller Diameter	56
5.3	Analysing the Use of a Draft Tube Instead of Suction Box	58
6	Evaluation & Presentation of the Hydraulic Design	64
6.1	Introduction to the Evaluation of the Hydraulic Design	64
6.2	Concept Generation	64
6.3	Multi-criteria Analysis.	65
6.4	Cost Analysis	67
6.5	Evaluation & Selection	71
6.6	Presentation of the Preferred Hydraulic Design.	72
Part 3:	Structural Design	74
7	Constructability	75
7.1	Applied Construction Methods.	75
7.2	Construction Sequence	76

8 Stability	80
8.1 Stability of the Sea Dike	80
8.2 Piping Checks	85
8.3 Bed Protection Design and Stability	86
8.4 Stability of the Cofferdam	89
8.5 Stability of the Pumphouse.	91
8.6 Settlements	93
9 Strength	95
9.1 Structural Verification of the Cofferdam	95
9.2 Structural Verification of the Penstock.	101
Part 4: Conclusion	104
10 Presentation of the Final Design	105
11 Conclusions and Recommendations	109
11.1 Conclusions.	109
11.2 Recommendations	110
	112
References	113
Appendices	116
A Level Schematic	117
B System Characteristic Calculations	119
C Pump Characteristic	121
D System & Pump Characteristics	123
E System & Turbine Characteristics	125
F Flow Velocities Pump	127
G Flow Velocities Turbine	129
H Overview Schematic	131

I	NPSH Calculations	133
J	NPSH Head Losses	135
K	Single-line Diagram	137
L	System Efficiencies	139
M	Water Cooling Principle	141
N	NPSH Calculations: 180 rpm	143
O	System and Pump Curve: 180 rpm	145
P	NPSH Calculations: 190 rpm	147
Q	System and Pump Curve: 190 rpm	149
R	Cost Calculations	151
S	Level Schematic Selected Hydraulic Design	153
T	Construction Sequence: Construction Pit Method	155
U	Construction Sequence: Cofferdam Method	158
V	Construction Sequence: Caisson Method	164
W	Cone Penetration Test	167
X	Loads Acting on the Cofferdam	169
	X.1 Hydrostatic Pressure	169
	X.2 Wave Pressure	170
	X.3 Soil Pressures	170
Y	Loads Acting on the Pumphouse	171
	Y.1 Scenario's	171
	Y.2 Self-Weight	172
	Y.3 Center of Gravity	173
	Y.4 Buoyant Forces	174
	Y.5 Soil Pressures	174

Z	Loads Acting on the Penstock	175
Z.1	Scenario's and Load Combinations	175
Z.2	Loads	175
	Equivalent Beam Calculations	178
	Forces, Moments, and Displacements During Cofferdam Staging	180

Part 1: Introduction



1

Motivation, Relevancy, & Problem Statement

1.1. Motivation & Relevancy

1.1.1. The Climate and Energy Transition

Year by year, the effect that climate change is having on the Netherlands, as well as the rest of the world, is becoming clearer. Weather events are becoming more extreme, and the sea levels are expected to rise at an exponential rate, prompting the government to take action. On the one hand, the sourcing of renewable energy is a way to restrict emissions from fossil fuels and therefore limit further sea level rise. On the other hand, action is being taken by preparing for the worst and designing and strengthening the flood barriers to cope with this increased sea level. The concept of the Delta21 turbine-pumping station is a design which augments flood protection, while augmenting the efficiency of renewable energy, as well as preserving natural values.

1.1.2. Energy Transition

The European Union (EU) aims to be climate neutral - meaning zero emissions - by 2050. The result of this long-term strategy is a so-called 'energy transition' taking place in the Netherlands and other EU states. For European countries located on the coast of the North Sea offshore wind energy is proving to be a viable solution. A higher yield and lack of suitable areas onshore have pushed energy suppliers to source their energy from wind farms on the shallow shelf of the North Sea. Figure 1.1 shows the trend of offshore wind energy installations, which has been accelerating this past decade and is likely to continue doing so.

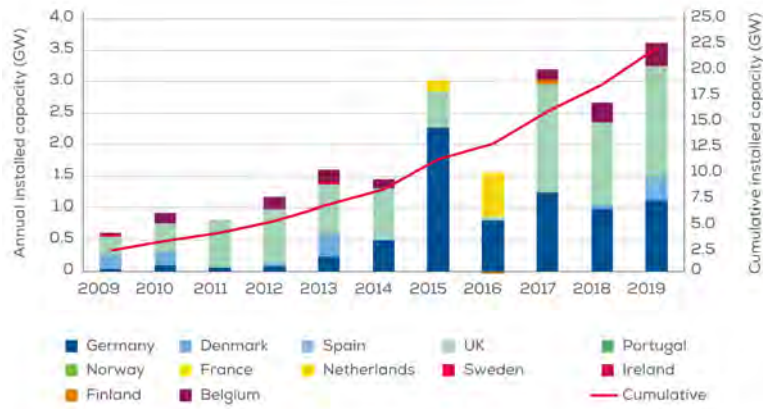


Figure 1.1: Installed Offshore Wind Capacity in Europe (WindEurope, 2020)

A major drawback of offshore wind energy is its intermittency, meaning power is only supplied when the wind is blowing. The fact that there is no large scale storage for wind-generated electricity means that the full potential of renewable energy is not yet unlocked. Pumped hydro storage is a potential solution for this, and it does so by storing energy in the form of hydraulic head. The principle works by pumping water (storage) when there is a surplus of generated wind or photovoltaic power, and if there is a shortage the water stored will be released through the turbines and will generate energy. As depicted in Figure 1.2, pumped hydro-storage is the optimal method for storing electricity and augmenting grid stability because it combines high efficiency with large capacities (Lechner, 2018).

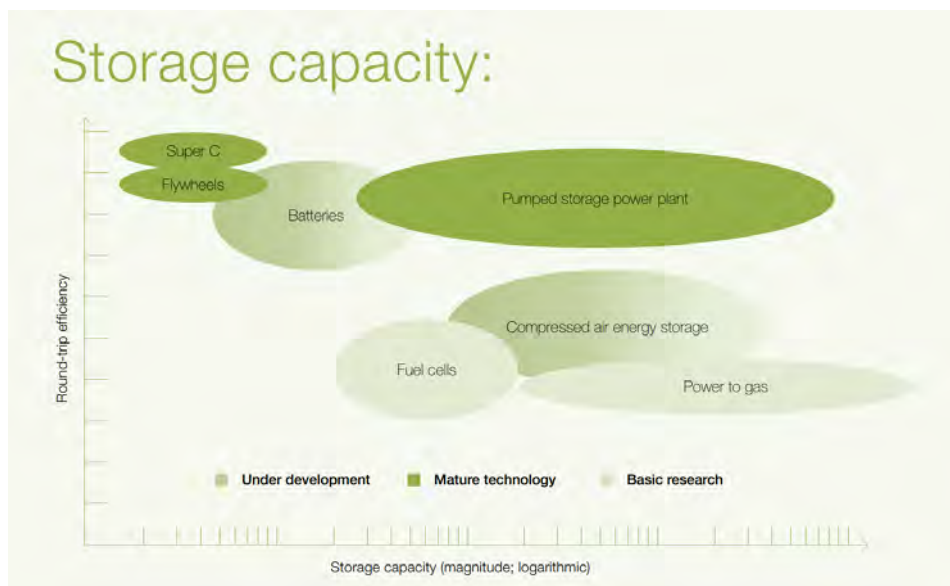


Figure 1.2: Comparison of electricity storage technologies (Lechner, 2018)

1.1.3. The Threat of Sea Level Rise

Not only is water from the sea threatening the coastal defences of the Netherlands, but climate change is also predicted to increase discharges from the rivers flowing through the Netherlands. Future flooding events in the Rhine river with discharges of up to 18,000 m³/s are considered 'plausible' (Hegnauer, Kwadijk, & Klijn, 2015). An example of the urgency of this two-sided problem is Project Afsluitdijk. The project, which was started in 2018 and predicted to end in 2022, includes a total reinforcement of the current dam. Rijkswaterstaat (2020) states the reasons for the necessary maintenance being sea

level rise, increased predicted discharges, and also includes plans for a pumping station with increased capacity to flush the IJsselmeer.

1.1.4. Delta21 as a Potential Solution

The Delta21 concept is an integrated solution for the future of the Haringvliet estuary, and appeals to 3 themes: Flood Protection, Energy, & Nature (Lavooij & Berke, 2019). The 'initiators', Huub Lavooij and Leen Berke, have been working on developing this concept for several years now with the help of students from Delft and Wageningen, as well as the collaboration of a range of companies, research centers, and government institutions. The full functioning of the Delta21 concept is elaborated in Section 1.2.

Part of the Delta21 concept is the construction of an Energy Storage Lake. The Energy Storage Lake, in combination with the pump-turbine station, will provide a means to pump superfluous discharge from the Haringvliet estuary which will improve the flood safety of the upstream reach of the Maas river. This will also mean that the river dikes will endure less harsh conditions and will save costs on dike maintenance and reparation works. Furthermore, the Energy Storage Lake and the pump-turbine station will function as a low-head pumped hydro-storage system. This will allow for a more efficient use of renewable energy, and will ultimately help achieve the goal of the EU to be carbon neutral in 2050.

1.1.5. Relevancy

Aside from its potential contribution to the Delta21 project, the development of a low-head pump-turbine station is also relevant in the bigger picture. Typically, pumped hydro storage uses reservoirs at altitude for water storage, and the increased head requires less discharge to generate the same amount of power. This requires a unique combination of topographical conditions, something which is not to the Netherlands. If low-head high-flow pumped storage is shown to be feasible, many countries who previously did not have access to large-scale grid energy storage could turn to this as a solution.

In addition to this, the use of the pumping station to empty the discharge of the Haringvliet is also an interesting feature. Cities around the world are facing issues with water management due to the rise in sea level. A good example of this is Jakarta, a city which is subsiding due to groundwater extraction and is flooding at increasingly frequent rates due to the rise in sea level (Lin & Hidayat, 2018). The pumping station, which is capable of handling discharges up to 10,000 m³/s, could prove to be a potential solution in many different possible cases such as the example named.

1.2. Description of the Delta21 Concept

If the concept of the Delta21 project is executed, it will form part of the Delta Works. It will be located at the mouth of the Haringvliet estuary, but its influence will also extend upstream into the Maas river and the cities and towns on its banks. Figure 1.3 shows the location of the proposed concept as well as its main parts.

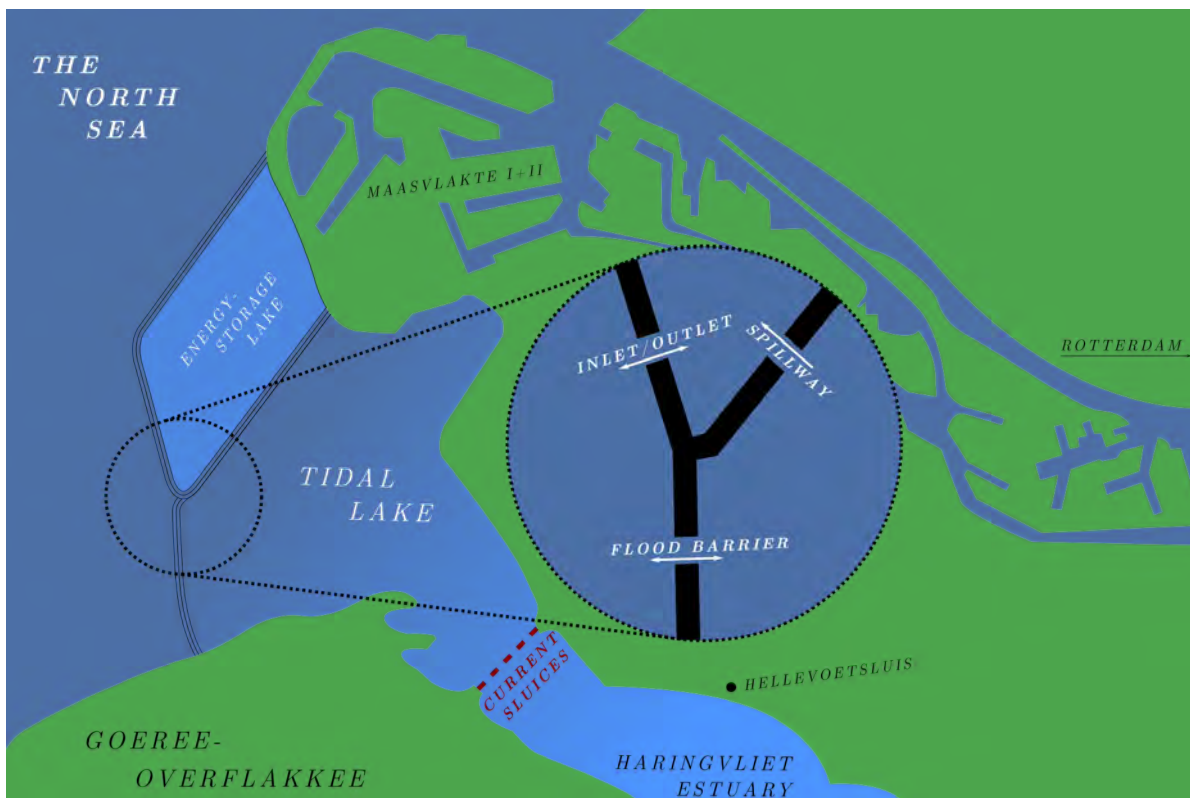


Figure 1.3: Diagram of Delta 21 Location and Elements

1.2.1. Current Situation

Built in 1970, the *Haringvlietdam* is a storm surge barrier on the mouth of the Haringvliet estuary which consists of a dam in combination with several gates and a navigation lock. The movable gates serve the purpose of closing off the estuary during high-water events, but also being able to discharge the flow from the Maas and Rhine rivers. The structure resulted in a separation between the saltwater environment on the North Sea side and the freshwater inland side. This basically removed the estuarine ecosystem which existed previously and was very detrimental to the biodiversity in the region (Hop, 2011).

In 2018 the government and other stakeholders decided to operate the Haringvliet sluices on the basis of a *kierbesluit*, meaning the gates would be partly open during flood to allow for saltwater intrusion. The goal of this was to allow for migration of fish and other species to restore the estuarine nature, while ensuring the freshwater intake points would not be impacted (Borm, 2018).

1.2.2. Proposed Changes

The proposed plan is to remove the current flood barrier (the *Haringvlietdam*) and to replace it with a series of dunes, a new flood barrier, and a pump-turbine station. The area now available around the vacated area will comprise the future Tidal Lake (*Getijmeer*).

The new flood barrier will be built at the North Sea side of the Tidal Lake, and it will remain open as long as it is not needed to ensure salt water intrusion and fish migration into the Haringvliet. If the closure of this barrier coincides with a high discharge of the Meuse or Rhine rivers, then water can still be pumped out. This is where the Energy-Storage Lake (*Valmeer*) comes into play. High water in the Tidal Lake will flow over into the Energy-Storage Lake via a spillway, whereafter it will be pumped into the North Sea via the pumping structure to ensure a safe upstream water level. The three main

elements (flood barrier, pumping station, and the spillway) are shown in Figure 1.3.

The use of the pumping station to remove superfluous discharge is only expected to occur once every 10 years. When this is not the case, the pump-turbines and the Energy Storage Lake can be used for pumped hydro-storage. Not only will this help with storage of renewable energy, but it will also make the Delta21 a financially attractive solution. By storing cheap energy during off-peak hours in the form of pumped storage and turbinning during peak hours when prices are higher, energy can be sold to the grid for a profit. Ultimately, this will make the Delta21 project interesting for investors (Lavooij & Berke, 2019).

1.2.3. System Diagram

The Delta21 concept and its systems are shown in Figure 1.4. The system which will be researched as part of this thesis project is the pump-turbine station. The subsystems and elements of the other systems of Delta21 are not included in the diagram.

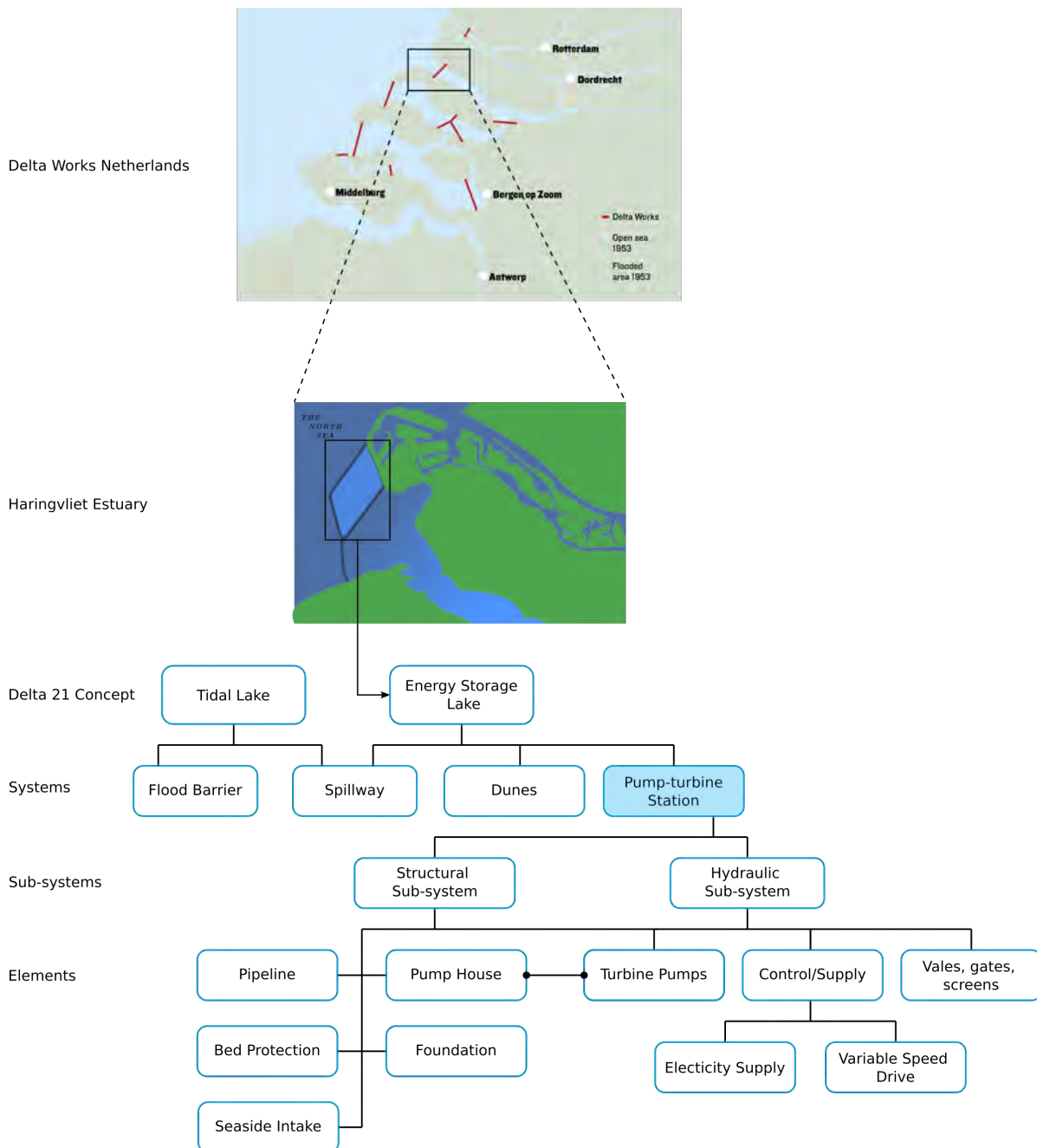


Figure 1.4: Delta 21 System Diagram

1.3. Operating Modes of the Energy Storage Lake

There are two main operating modes for the Energy Storage Lake. These operating modes will govern the function of the turbine-pumping station.

The critical operating mode of the pump-turbine station is to empty the river discharge of the Haringvliet if the storm surge barrier is close (which indicates high water in the North Sea). This is called the critical operation mode because it relates to flood protection, and it is governing for the design of the pump-turbine station. The closure of the flood barrier on the edge of the tidal lake will mean the river discharge is not flowing into the North Sea, meaning that the spillway needs to be adjusted so that excess discharge from the Maas river can flow into the energy storage lake and then be pumped out.

The large capacity of the energy storage lake means there is a buffer for the pumping. Nevertheless, the pumps should be designed for the maximal possible discharge of $10,000 \text{ m}^3/\text{s}$. This is a conservative estimate made by the initiators of Delta21, and is based on the maximal predicted discharge in the Rhine river which could go up to between $17,000$ and $18,000 \text{ m}^3/\text{s}$ (Hegnauer et al., 2015).

The second operation mode is the use of the Energy Storage Lake for the purpose of pumped hydro-storage. This can be split up into two sub-modes, one for pumping (storage of energy) and one for turbining (generating energy). The two sub-modes serve to balance out the intermittency of the offshore generated energy with the demand of the power grid. The storage will occur when there is a surplus of power being produced, while the turbining will take place when there is a shortage of renewable electricity being delivered. The Energy Storage Lake will be operating in this second mode for the majority of the time. Not only is this important for financial and sustainability reasons, but it is also important to keep the pump-turbines operational for maintenance and durability purposes. If the pumps were only used once every 10 years in the event of high water, they would not be as reliable and the chance of failure during operation would be much higher.

1.4. Findings of Past Designs of the Pump-turbine Station

Thus far two design studies have been done on the topic of the Energy Storage Lake. Both studies were preliminary designs for the pump-turbine station, and included a selection from a range of variants. It is also important to note that both designs were carried out for a location of the pumping station on the northern side of the Energy Storage Lake, where the water depth is deepest. Paasman (2020) used caissons as the base of their structural design, and the result was a mainly concrete section of 40 m height and 50 m wide, which can be seen in Figure 1.5. On the other hand, Ansorena-Ruiz (2020) focused more on hydraulic aspects such as piping and bed protection and also included a life-cycle analysis. Neither design focused on the selection of the pump/turbines and their hydraulic design.

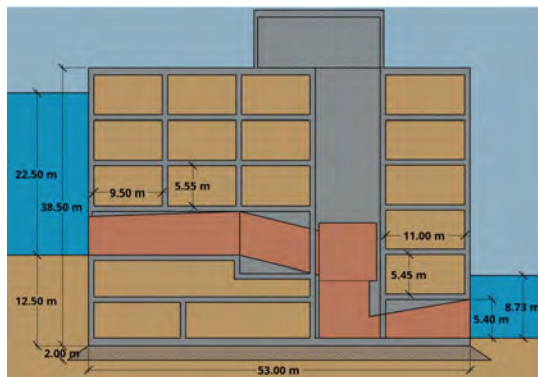


Figure 1.5: (Paasman, 2020)

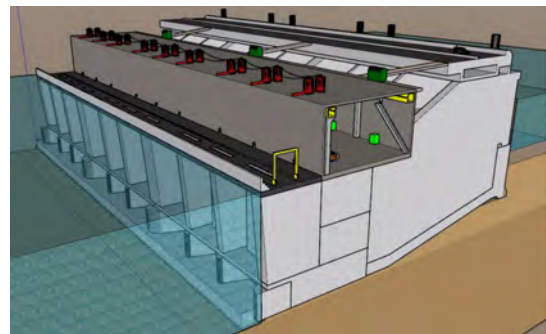


Figure 1.6: (Ansorena-Ruiz, 2020)

Both designs use the combined functions of a sea barrier as well as pump/turbine house for the superstructure. Combined with the large depth of the North Sea at this location, this resulted in designs for two very monolithic structures. As stated by Ansorena-Ruiz (2020), the large amount of concrete volume results in poor performance for the life-cycle analysis costs, something which could be optimized by using a smart construction.

The monolithic design is also favorable for in-situ construction due to the footprint being smaller. However, if the prefabrication of modular elements is possible, as well as the installation of these, then it could be interesting to see how this would positively affect a structure which is built up of different parts.

Objective, Methodology, & Outline

2.1. Objective

The objective of the thesis project is to create an improved design for the pump-turbine station of the Delta21 concept. This will include the hydraulic design of the turbine pumps as well as the structural design. The aim of the 'improved' design is to incorporate ideas, which reflect the shortcomings of past designs (Section 1.4). To this end, the initiators of the Delta21 concept can compare the designs to determine which type is more feasible.

The objective of the design is to provide a conceptual plan for a pump-turbine station that can store renewable energy at a large scale and high efficiency, is the most cost-efficient structure which is feasible from a constructive standpoint, and that ensures flood protection for the Dutch Delta.

2.2. Scope

The sub-systems and elements of the pumping station system shown in Figure 1.4 form the scope of this design. The items which are considered part of the scope of the design study are listed in Section 2.3. It is more suitable to explain what items will not be dealt with to define the scope.

The design study will not analyse the function of other parts of the Delta21 concept. The other parts of the Delta21 are still under development, meaning assumptions will need to be made as to their impact on the design of the pump-turbine station. Also, close contact with the initiators should be kept to determine the workings of the other systems in the Delta21 concept.

The choice of the location will not form part of the design considerations. This has already been prescribed by the client (initiators of Delta21). The location of the pump-turbine station will be kept at the south-western edge, as shown in Figure 1.3.

For the verification of the concepts, more precisely the structural checks, the loading due to earthquakes (or other seismic effects) will not be considered. Also, general dynamic loading will not be included in the structural calculations. The aim is to apply a pump-turbine that can be or is currently being made by pump manufacturers, such as Fairbanks-Nijhuis or Bosman. In the case that this is not possible, the specifications of the necessary pump-turbine should be determined. This includes the pump-curves and the necessary motor. Close contact will be kept with the pump-manufacturers to determine whether the required pump-turbine is achievable with the current technology at hand.

2.3. Methodology

2.3.1. General Approach

The general approach used in the design of the pump-turbine station will be based on a form of systems engineering, applied in civil engineering (Molenaar & Voorendt, 2019). This approach splits up the system into sub-systems and elements (as shown in Figure 1.4) and then defines the interaction between the sub-systems as well as their requirements. Once the basis of design is made, concepts are generated and verified. Finally, the verified concepts are evaluated and a selection is made. Based on the depth of the verification in the previous step, the selected alternative can be verified even further.

2.3.2. Applied Approach

The approach used that is more specific to this project will be the fact that the design process will be separated in two loops. First the hydraulic design is made. In this context, hydraulic refers to the design and functioning of the pump-turbine system. The second stage in the design is the structural part. The hydraulic design will serve as input for the structural design, and together these will form the integrated solution for the pump-turbine station of the Delta21 concept.

2.3.3. Hydraulic Design

At the start of the hydraulic design, all of the data which has an influence on the hydraulic functioning and requirements (pumping and turbinning) will be gathered, as well as the general boundary conditions (water safety, ecology, lifetime, etc.). This information will form the basis of the design. The starting points (or design assumptions) will be governed by the functioning of the pumps/turbines, something which is already partially covered in Section 1.3.

After the boundary conditions and the functioning of the pumps/turbines have been set, the next step is the creation of the level schematics. The level schematics shows all the water levels which the pump-turbine station is expected to experience. In essence, this schematic gives the boundaries of the system, and will thus govern its operational modes. In Appendix E a preliminary level schematic can be found.

Once the boundaries of the system have been established, the calculations can begin. A choice will need to be made for the turbine pump, and this will give both a pump curve and a turbine curve for the respective functions. The curves will form the basis for the calculations, and in the end the work area of the pump/turbine will be determined. Velocities and head losses will also be determined in this step.

Using norms and guidelines the sizing of the pump can be derived. In the end this will determine the lateral spacing of the pumps which will be crucial for the overall structure dimensions. After the hydraulic sizing is determined, the physical (final) sizing is established when the final details are added. This can be including the return valves, shutoff valves, access hatches, connections, and other necessary features.

The final result of the hydraulic design will yield the power and efficiency of the turbine pumps. This will allow for the verification of the operation modes.

2.3.4. Structural Design

As with the hydraulic design, the structural design will start with the gathering of boundary conditions, starting-points, functional/operational aspects, requirements, as well as the input of the hydraulic design. This first phase will form the basis of design.

Based on this first stage, various concepts can be developed on a sub-system level. Analyses and

calculations will be carried out, and the concepts will narrow down to a more detailed level, as shown in Figure 2.1.

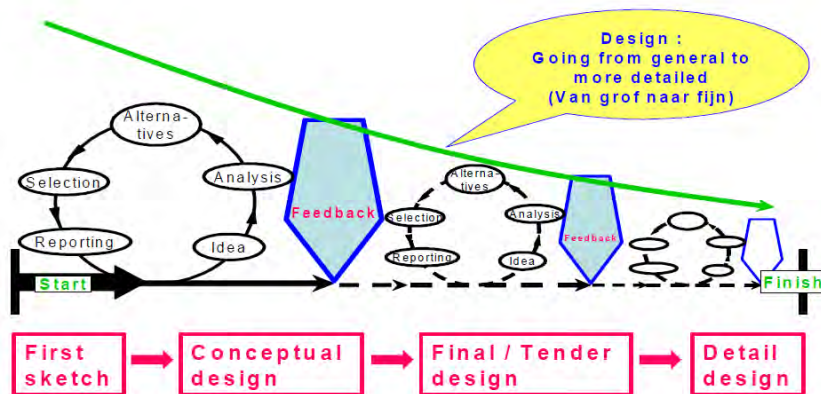


Figure 2.1: Cyclic Approach (Molenaar & Voorendt, 2019)

Structural calculations will be carried out as part of the verification of the concepts. In this step the strength and stability of the system as a whole, as well as its parts must be verified. Structural verification will include stability controls (rotational and translational), strength of structural elements, soil bearing capacity, piping and uplift checks, and bed protection. Also, special attention should be paid to constructability of the concepts. Not many structures of similar functions and sizes have been built, so determining feasible methods for construction will be an important part of the verification.

Once the concepts have been verified, they will be measured against one another using a multi-criteria analysis. Various criteria relating to the stakeholder wishes will be collected and given a weight, then the alternatives will be scored and a decision can be made on the selected alternative.

Final checks are then made on the selected variants, and additional verification steps can be taken.

2.4. Report Outline

The final report will be divided into four parts: the introduction, the hydraulic design, the structural design, and the conclusion and recommendations.

The introduction (Part I) will cover the motivation, relevancy, problem statement, objective, scope, methodology, and a reading guide. As well as this, the introduction will include a basis of design for both the hydraulic and structural design. In this chapter the boundary conditions, (functional) requirements, and starting points will be stated.

The next chapter will include the pump-turbine choice and the relevant calculations, including the pump and turbine curves, which will show the velocities and work area of the pump-turbine. These will then formulate the sizing of each pump-turbine unit. A chapter will also include the . The final chapter of this part will compile the relevant information which will form the hydraulic design input for the structural part.

The structural design (Part III) has three parts to it: constructability, stability, and strength. The constructability shows the construction methods that can be used to execute the turbine-pumping station, as well as three different sequences to accomplish it. One of these methods is chosen. The stability presents different stability issues during and after construction and works them out. For the final part, the strength of various elements throughout the construction phase and after execution is checked.

The final part (Part IV) will include a presentation of the final design, as well as a conclusions on the design and recommendations for any further research/design steps.

Basis of Design

3.1. Hydraulic Requirements

3.1.1. Functional Requirements

- H-FR1: The aim of the pump-turbine station is to control the water level inside the Energy Storage Lake (ESL)
- H-FR2: During high-water events, the pump-turbine station needs to be able to pump water out of the ESL at a rate of 10,000 m³/s (scenario 1)
- H-FR3: During normal operation, when there is a surplus of energy coming from renewable sources (offshore), the pump-turbine station will pump water out of the ESL until a minimum depth of N.A.P. – 22.5 meters in order to store energy. (scenario 2.1)
- H-FR4: During normal operation, when there is a shortage of renewable energy to the grid, the pump-turbine station will let water flow through the turbine into the ESL in order to generate power, until a maximal depth of NAP – 5 meters. (scenario 2.2)

3.1.2. Delta21 Requirements

- H-DR1: **Nature:** The pump-turbine station will be constructed and operated in a manner which preserves ecological values and enhances the local fauna and flora.
- H-DR2: **Flood Protection:** The design of the pump-turbine station will be such to augment the flood protection of the upstream reach of the Haringvliet estuary and its surroundings.
- H-DR3: **Energy:** The operation of the pump-turbine station will ensure an efficient usage of renewable energy in order to enhance grid stability. The round-trip efficiency should be maximized.

3.1.3. Operational and Maintenance Requirements

- H-OR1: In order to provide maintenance, inspection, and repairs, all parts of the pump-turbine station must be accessible in a safe manner
- H-OR2: To facilitate requirement H-OR1, the entire length of the pump-turbine station must be accessible for (heavy) traffic.
- H-OR3: Systems should be in place to ensure debris and other objects do not interfere with the system
- H-OR4: The power supplied to and generated by the pump-turbine station must be safely and securely connected to the grid.

3.1.4. Lifetime Requirements

The technical and economic lifetime of the hydraulic elements are collected in table 3.1.

	Economic Lifetime	Technical Lifetime
Mechanical	25 years	50 years
Electrical	15 years	20 years
Automation	10 years	10 years

Table 3.1: Hydraulic Lifetime

3.2. Structural Requirements

3.2.1. Functional Requirements

- S-FR1: The structure should facilitate the hydraulic functioning of the pump-turbine station.
- S-FR2: The structure should protect the pump-turbine station from environmental factors.
- S-FR3: The structure should be able to resist a storm with a yearly exceedance probability of 10^{-4} .
- S-FR4: The structure's technical lifetime should be 100 years, and should thus be designed with a corresponding predicted sea-level rise.

3.2.2. Aspect Requirements

- S-AR1: The structure should integrate well with its surroundings.
- S-AR2: Construction of the structure should have minimal impact on the environment and aim to minimize carbon emissions.
- S-AR3: The structure should be constructable, stable, and strong.

It should be noted that in the Netherlands, flood defense systems are no longer designed according to exceedance probabilities. By law, a calculation of the failure probability of the structure must be carried out.

3.3. Starting Points

3.3.1. Location & Layout

For the hydraulic design, the layout of the energy storage lake is of interest as it governs the total amount of space available for the pump-turbine station. Especially the available width is of interest.

Figure 3.1 shows the layout of the energy storage lake, based on the latest update (Lavooij & Berke, 2019). The location of the pump-turbine station is a starting point for the design, and will be on the southern-most edge of the energy storage lake. According to the diagram, an area 3 to 4 kilometers wide will be available for the construction of the pump-turbine station.

The total area of the basin will be approximately 20 km^2 , this is represented by the boxes of 1 km^2 shown in Figure 3.1.



Figure 3.1: Spatial Design of the Energy Storage Lake and Approximate Location of the Pump-turbine Station

3.3.2. Water Levels: Energy Storage Lake

The water levels inside the energy storage lake are governed by the operation of the pump-turbines and are therefore a design choice. The minimal water level inside the energy storage lake is NAP - 22.5 m, which is limited by the potential bursting of the bottom of the lake if dug out further (Lavooij & Berke, 2019). The maximal water level inside the energy storage lake is NAP - 5 m, due to the minimal head required for the turbine operation (Lavooij & Berke, 2019).

It is noteworthy that a change of water level inside the energy storage lake due to environmental factors such as precipitation or wind set-up is neglected.

3.4. Boundary Conditions

3.4.1. Water Levels: North Sea

The water levels in the North Sea adjacent to the pump stations have been collected in table 3.3. Sea level rise for the structural lifetime of the pump-turbine station (100 years) is included in the extreme high water level. The extreme-high water level is found in Hydra-NL with an exceedance probability of 1:10,000 years, which corresponds to the failure of the dike itself described in Chapter 3.2.

The maximal water levels on the North Sea at the Haringvliet as a result of storm surge for various return periods, based on the Hydra-NL model are given in Table 3.2.

Return Period [years]	Maximal Water Level [m + NAP]
10	3.227
30	3.521
100	3.854
300	4.169
1000	4.526
3000	4.868
10000	5.257
30000	5.627
100000	6.042

Table 3.2: Maximal Water Levels as a Result of Storm Surge for Various Return Periods

Using the software Waterstandverloop the maximal water level as given in Table 3.2 can be transformed into a time series as is shown for the case of a return period of 10000 years in Figure 3.2.

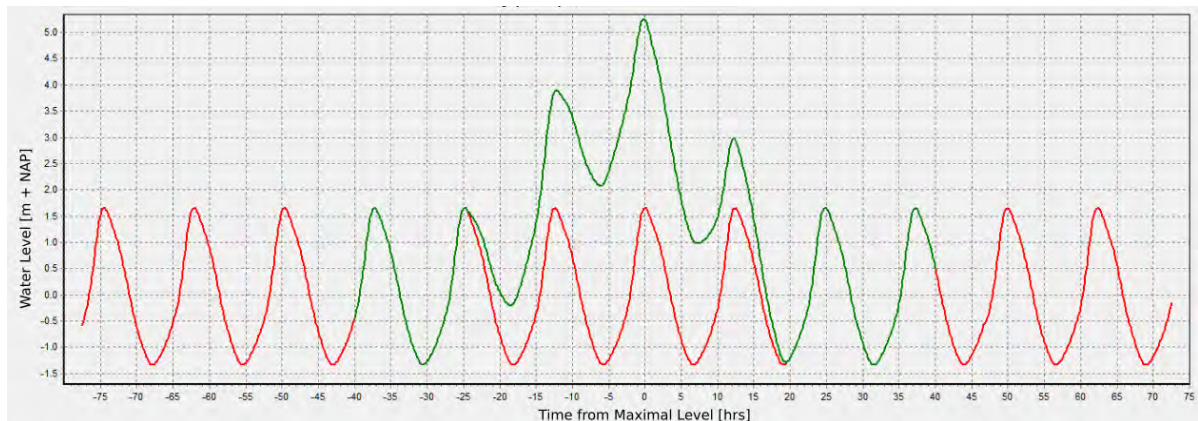


Figure 3.2: Storm Surge Time Series for Return Period of 10000 years (HydraNL [Computer Software], 2017)

The additional sea level rise of 0,65 m is the median value for the projected sea-level rise until 2100 of various studies according to the RCP4.5 pathway (medium), retrieved from Oppenheimer et al. (2019).

For the tidal range, the mean high-water (MHW) and mean low-water (MLW) of the Haringvliet outer delta (Haringvliet Tidal Station 10, location shown in Figure 3.3) have been taken, retrieved from Colina-Alonso (2018).

	Level [m ± NAP]
Extreme	+5.65
High-tide	+1.22
Average	+0.19
Low-tide	-0.85

Table 3.3: Water levels in the North Sea

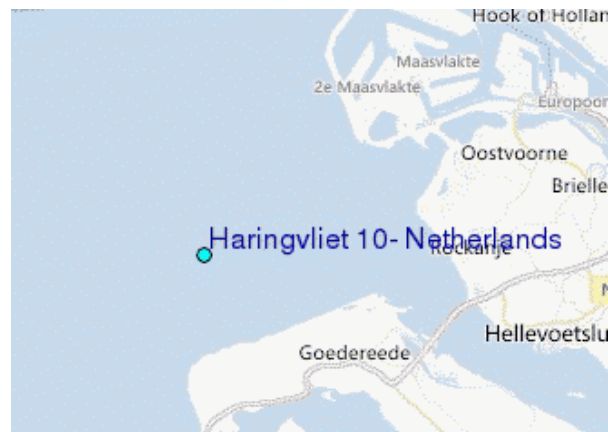


Figure 3.3: Location of the tidal station (HydraNL [Computer Software], 2017)

3.4.2. Waves

The oscillatory water levels such as waves are neglected for the hydraulic design.

For the structural design the waves are of interest in order to determine the structural integrity. As well as the maximal water levels in case of a storm surge, the Hydra-NL software provides the significant wave height with various return periods, as shown in Table 3.4.

Return Period [years]	Significant Wave Height (H_{m0}) [m]
10	2.349
30	2.556
100	2.784
300	2.992
1000	3.223
3000	3.437
10000	3.674
30000	3.896
100000	4.144

Table 3.4: Significant Wave Heights for Various Return Periods at the Haringvliet

As can be seen from Table 3.5 the generation of the waves with the highest exceedance probability comes from those with a wind with a bearing between 300 and 360.

Wind Heading [deg]	Contribution to Exceedance Probability [%]
30.0	0.0
60.0	0.0
90.0	0.0
120.0	0.0
150.0	0.0
180.0	0.0
210.0	0.0
240.0	0.0
270.0	2.3
300.0	36.6
330.0	58.6
360.0	2.6
Sum [%]	100

Table 3.5: Contribution of Wind Directions to the Maximal Wave Height

Figure 3.4 shows how the fetch distances for headings between 330 and 360 degrees are much larger (in excess of 1000 km). The fetch distances for waves coming from the west (headings between 270 and 300) are approximately 200 km.

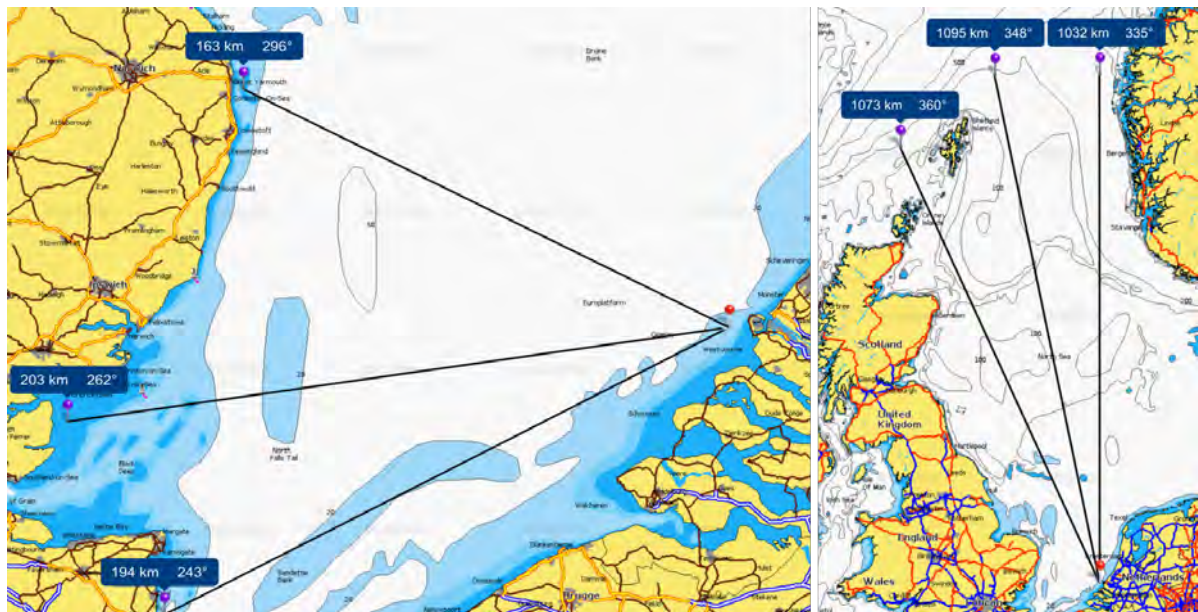


Figure 3.4: Long vs. Short Fetch Headings

Bretschneider (1965) gives a relationship of the wave height (H) and the period (T) as a function of wind speed (U), water depth (D) and fetch distance (F), the formulas of which are given in Equations 3.1 and 3.2.

$$\frac{gH}{U^2} = 0.283 \tanh \left\{ 0.530 \left[\frac{gD}{U^2} \right]^{0.75} \right\} \tanh \left\{ \frac{0.0125 \left[\frac{gF}{U^2} \right]^{0.42}}{\tanh \left\{ 0.530 \left[\frac{gD}{U^2} \right]^{0.75} \right\}} \right\} \quad (3.1)$$

$$\frac{gT}{U} = 7.540 \tanh \left\{ 0.833 \left[\frac{gD}{U^2} \right]^{0.375} \right\} \tanh \left\{ \frac{0.0770 \left[\frac{gF}{U^2} \right]^{0.25}}{\tanh \left\{ 0.833 \left[\frac{gD}{U^2} \right]^{0.375} \right\}} \right\} \quad (3.2)$$

The sheltered location of the Delta21 pump-turbine station means that the significant wave heights measured at the Haringvliet and given in Table 3.4 cannot reach the turbine-pumping station. Rather, the waves striking the turbine-pumping station will be of a reduced fetch distance than those from the north. By applying the Bretschneider equations the reduced wave heights are given in Table 3.6, as well as the significant wave period. The depth for both the predicted and the reduced fetch wave equations is kept at 30 meters.

Return Period [years]	Predicted H_{m0} (Hydra) [m]	Reduced H_{m0} [m]	Significant Period (T_s) [sec]
100	2.78	2.08	5.56
1000	3.22	2.43	6.01
10000	3.67	2.82	6.49
100000	4.14	3.23	6.95

Table 3.6: Significant Wave Heights and Periods Based on Reduced Fetch

For wave generation inside the energy storage lake the Bretschneider equations, Equations 3.1 and 3.2, can be used as well. The maximal fetch distance of 5000 meters is used, and a wind speed equal to 35.7 m/s which is found to correspond to a exceedance probability of 1/10000 years at this location. The wave conditions depend on the level of the energy storage lake and are collected in Table 3.7.

Water Level [m \pm NAP]	Depth [m]	Sig. Wave Height [m]	Significant Wave Period [sec]
-5	22.5	2.02	4.90
-13.25	14.25	1.92	4.79
-22.5	5	1.44	4.37

Table 3.7: Wave Conditions Inside the Energy Storage Lake

3.4.3. Geotechnical Boundary Conditions

A nearby cone penetration test (number S36H00033) can give insight into the soil characteristics at the site of the turbine-pumping station. The location of the test in relation to the predicted layout of the energy storage lake is given in Figure 3.5.



Figure 3.5: Location of the CPT Test

The full result of the cone penetration test can be found in Appendix W. At two locations in the soil column a combination of low resistance and a high friction ratio show evidence of clay layers. These layers are from NAP - 20.5 m to NAP - 23.5 m and a thin layer from NAP - 27.25 m to NAP - 27.75 m. The rest of the soil column has the characteristic of sand, with a friction ratio that is largely less than 1.0 %. The sand above the first clay layer has a lower resistance than that of the deeper sand, suggesting that the deeper sand is of the coarser variant.

The model based on the cone penetration test and the corresponding soil properties that are used for the design of the pump-turbine station are found in Figure 3.6 and Table 3.8, respectively. The soil properties are adapted from NEN-EN 1997-1 (2019).

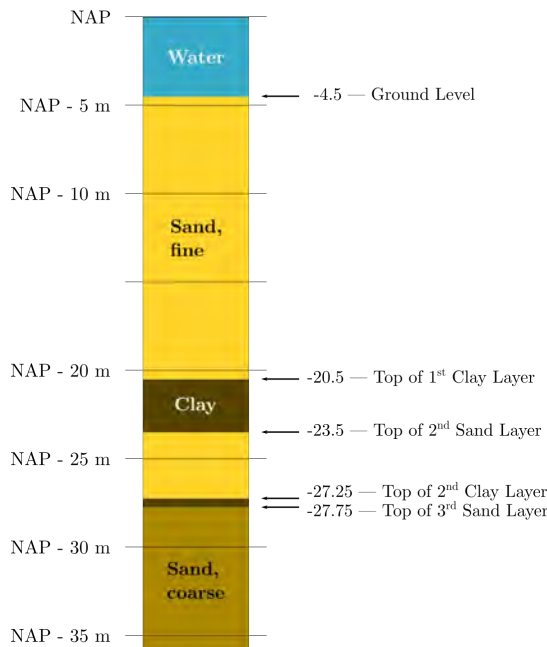


Figure 3.6: Model for the Soil Profile

	Symbol	Clay	Sand, dense	Sand, loose
Volumetric Weight [kN/m^3]	γ	17	19	17
Saturated Weight [kN/m^3]	γ_s	17	20	18
Friction Angle [$^\circ$]	ϕ	17.5	35	30
Cohesive Strength [kPa]	c'	5	-	-
Active Soil Coeff. [-]	K_a	0.54	0.27	0.33
Neutral Soil Coeff. [-]	K_0	0.3	0.57	0.5
Passive Soil Coeff. [-]	K_p	1.86	3.69	3

Table 3.8: Soil Properties

A sieve analysis of the sand nearby to the construction location of the turbine-pumping station is also included and can be found in Figure 3.7.

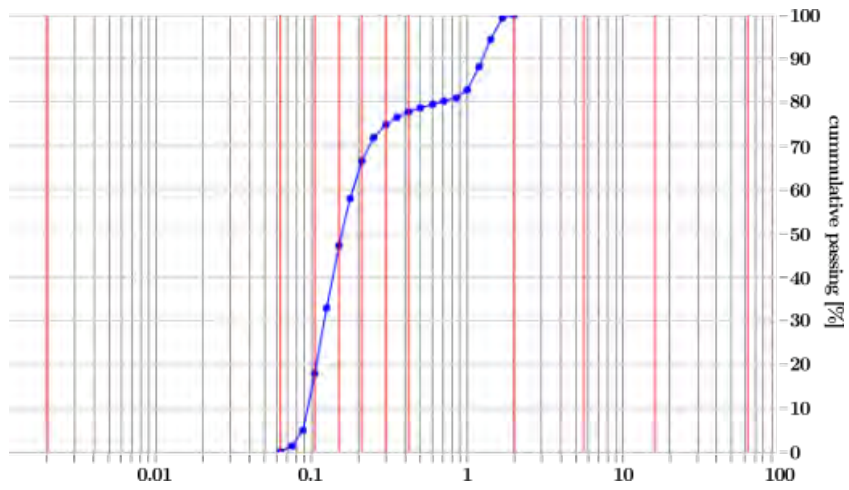
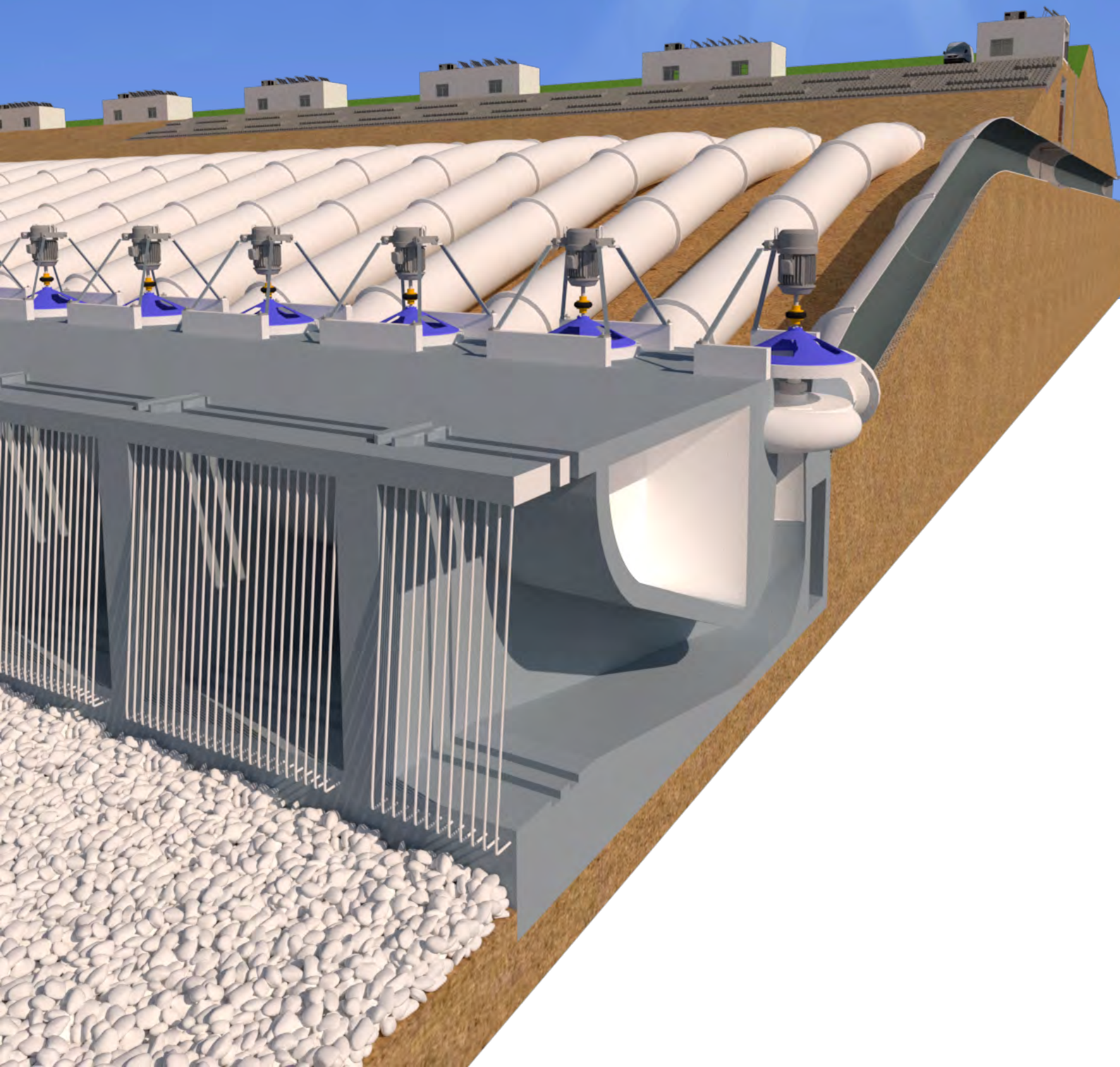


Figure 3.7: Sand Gradation

Part 2: Hydraulic Design



Development of the Basic Design Concept for the Pump-turbine Station

In this chapter, a basic design concept will be created in accordance to the basis of design for the hydraulic design. This basic design concept is a conceptual design in which certain design choice are made, and the design is verified accordingly. The design choices will be substantiated, and in Chapter 8 the effect of the variation of these choices will be analysed and discussed.

4.1. Flood Defense System

Upon construction, the Delta21 project will connect to the primary flood defense along the Maasvlakte 2 and the coast of Goeree Overflakkee. As shown by in Figure 4.1, the arrangement of the Delta21 elements can be such that either the spillway serves as a primary flood defense (Figure 4.1 Right) or the turbine-pumping station is the primary flood defense (Figure 4.1 Left).



Figure 4.1: Connection of the Delta21 Elements to the Current Primary Flood Defense System (Red Line)

Since the northern part of the Maasvlakte is not a primary flood defense, the more economical and technically feasible approach would be to have the spillway section of the energy storage lake function as a primary flood defense.

Whether or not the turbine-pumping station serves as a primary flood defense system, it will always

serve as an indirect primary flood defense system. This is because when there is a storm surge and flood wave simultaneously, the turbine-pumping station will have the function of supporting the river dikes, by ensuring the water levels upstream remain at an acceptable level by ensuring discharge can properly be sluiced.

The fault tree for flooding due to a combination of storm surge and flood wave is given in Figure 4.2. If the turbine-pumping station is a primary flood defense then the fault tree from storm surge is shown in Figure 4.3. If the turbine-pumping station is a primary flood defense then the fault tree from a combination of storm surge and flood wave is still the same as if it is not a primary flood defense (Figure 4.2).

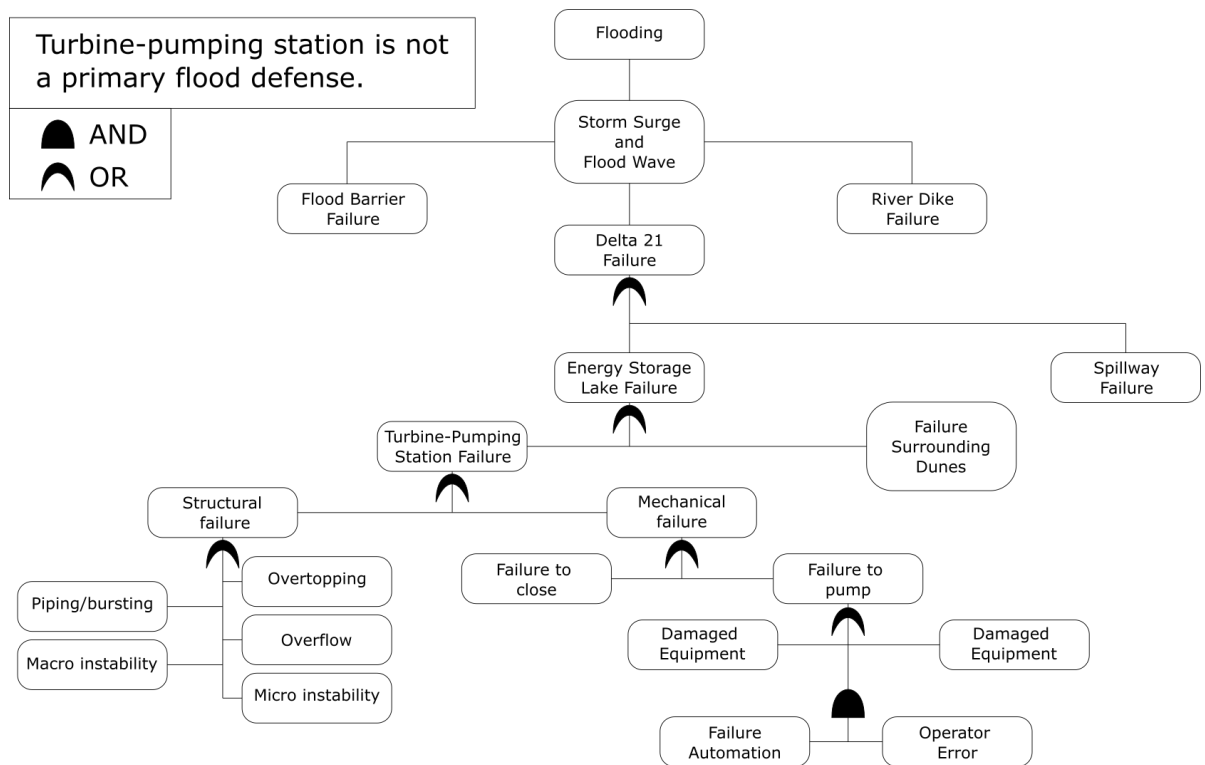


Figure 4.2: Fault Tree During a Combination of Storm Surge and River Flood Wave

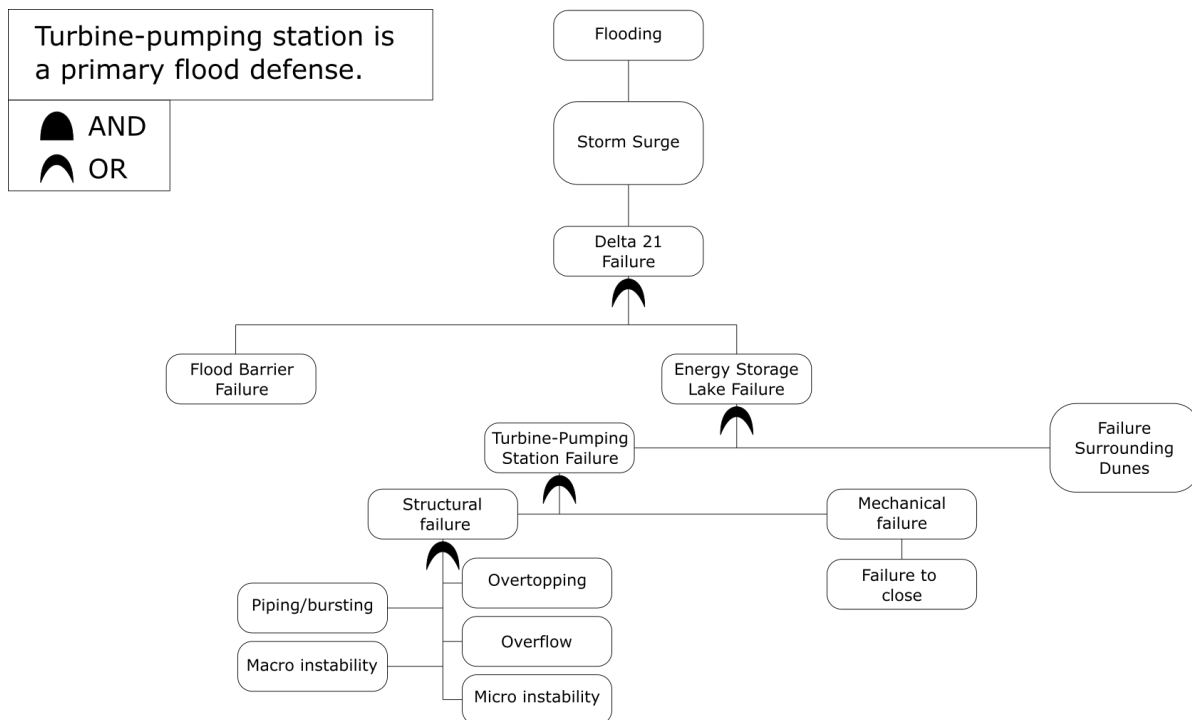


Figure 4.3: Fault Tree for Primary Flood Defense During Storm Surge

4.2. Level Schematic and Preliminary Design

A pumping (and turbine) installation typically consists of an inlet, the pump-turbine itself, a penstock, and an outlet. As well as these features, the necessary standard equipment such as non-return valves, stop logs, and trash racks also form the basis of the installation.

The design of the pumping installation is governed primarily by the water levels on either side, as well as the flow velocities. This is called the hydraulic sizing. Next, the design is adapted to be able to fit the required standard equipment, the result of this is the physical sizing. The physical sizing will be verified on the basis of the requirements such as safety, accessibility and maintenance.

Finally, the design must be fit into a structure which fulfills the civil requirements, in this report this final design step is discussed in part 3.

The selected pump will be of the concrete-volute type. In the Netherlands, these are the most widely used types of pumps for drainage and flood control. A combination of the medium head and flow-rate requirements mean that this type of pump is ideal, combined with the fact that the integration into the structure is practical and reliable means that the concrete volute pump (CVP) is the optimal choice for the basic design concept for the Delta21 turbine-pumping station (Joshi & Kulkarni, 2004). Furthermore, the geometry of the suction box is such that the construction depth required is much smaller than for other types of pumps, more information on the suction box is included in Section 4.6 (Joshi & Kulkarni, 2004). Figure 4.4 shows the casting of the concrete volute in situ at the Bergsche Maas pumping station. It is also possible to prefabricate the entire casing of the concrete volute pump.



Figure 4.4: Preparation of the Casing for a CVP (Van Der Ven, 2020)

The level schematic, displayed in Figure 4.5, as well as in higher quality in Appendix A, is a side view of the entire pumping station in which the water levels (set in Section 3.3.2 and 3.4.1) are displayed on either side. The level schematic also serves the purpose of a preliminary design for the structural part of the pump. This is something that needs to be chosen at this point because the system characteristics (Section 4.4) are dependent on the overall sizing and dimensions of the pump-turbine station. During part 3 when the structural design of the pump-turbine station is adapted, then this will impact the system characteristic, so this will need to be recalculated, although a large change is not expected.

The levels in the energy storage are categorized maximal, mean, and minimal. On the sea-side the levels are . The chosen levels are collected in Table 4.1

Water Level Lake	Water Level North Sea	Static Head Difference [m + NAP]	Color
Minimal	Mean	22.80	Orange
Mean	Mean	14.30	Purple
Maximal	Maximal	10.20	Green
Maximal	Mean	5.80	Blue
Maximal	Low	3.93	Red

Table 4.1: Levels

The level with the color code green and the static head of NAP + 10.20 m is relevant as it shows the minimal static head that can occur for the operation of the pumps for flood protection. During this scenario, it is expected that the water level in the north sea will be at its maximal level. The lowest head will thus be expected to return the highest possible discharge, and since the maximal discharge in this scenario (10,000 m³/s) is governing for the pumps, this level is also governing.

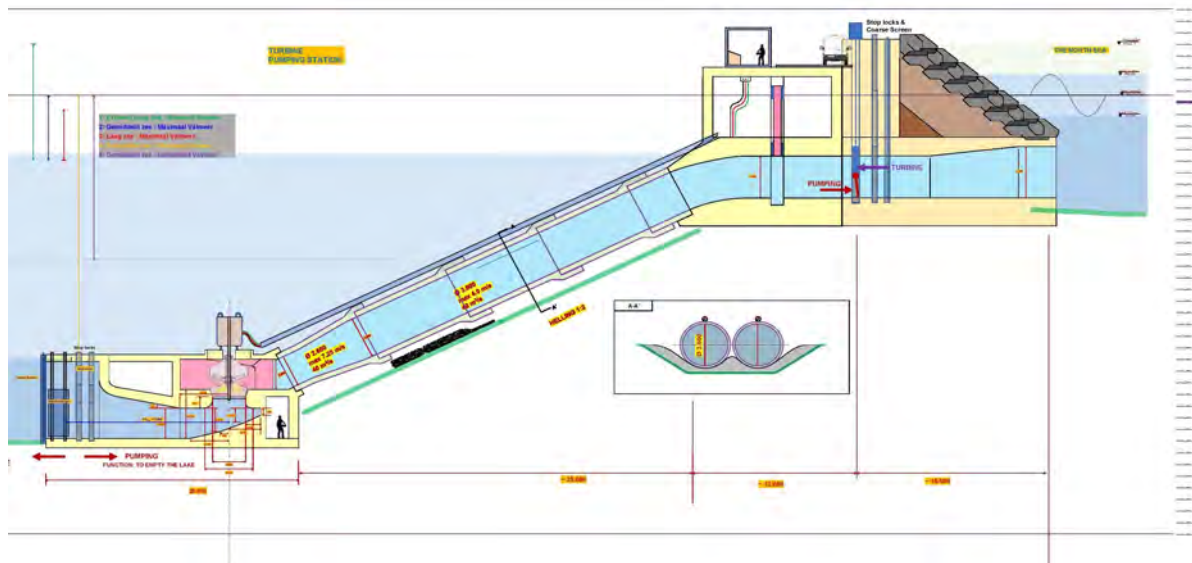


Figure 4.5: Level Schematic

4.3. Selection of the Pump-turbine

Depending on the required operation and the hydraulic boundary conditions a centrifugal pump can be chosen to have axial flow or radial flow. The type of flow is dependent on the shape of its blades (or runners) as shown in Figure 4.6 and 4.7 for axial and radial flow, respectively.

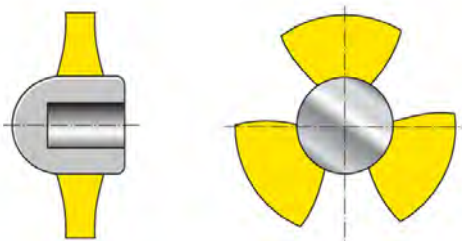


Figure 4.6: Axial-flow Impeller (Klein, Schanzlin Becker Aktiengesellschaft, n.d.)

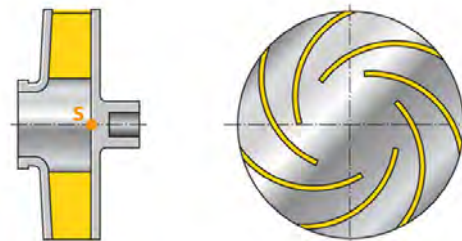


Figure 4.7: Radial-Flow Impeller (Klein, Schanzlin Becker Aktiengesellschaft, n.d.)

Radial flow impeller have lower specific speeds ($n_s = 16-80$) and this means they are more suitable for high-head applications, while sacrificing the flow rate. On the other hand, axial flow impellers have high specific speeds ($n_s = 160 - 400$), meaning they are suited to high flow rates but at lower heads (Klein, Schanzlin Becker Aktiengesellschaft, n.d.).

Combining these two concepts is the mixed-flow impeller, the shape of the blades is shown in Figure 4.8. Operating at specific speeds from 80 to 160, the mixed-flow impeller has the advantage of combining both high flow rates and hydraulic head, doing so at a high efficiency (up to 85%). Furthermore, when the mixed-flow impeller is run in reverse it can function as a Francis turbine, meaning the mixed-flow centrifugal pump is ideal to be used as a Pump-as-Turbine (Agarwal, 2012). For this reason, the type of pump used for the Delta21 turbine-pumping station is a mixed-flow centrifugal pump in a concrete volute.

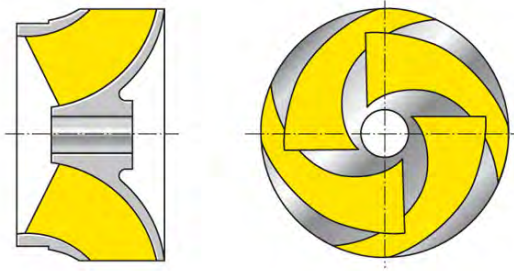


Figure 4.8: Mixed-Flow Impeller (Klein, Schanzlin Becker Aktiengesellschaft, n.d.)

Each pump has a pump curve, also defined as a pump characteristic, which defines the rated head as a function of the flow rate. The pump curve also shows the hydraulic efficiency of the pump at various flow rates. The pump characteristic, delivered by the manufacturer Pentair is for a specific speed of 108. The specific speed is selected based on the suction specific speed (usually constant around 3.5) and the available NPSH (typically 6 meters at the design head). This combination of suction specific speed and available NPSH delivers the smallest and cheapest pump. If a lower specific speed is taken, then the pump becomes larger and more expensive, and although the efficiency becomes higher, this difference is marginal (Arnold & Nijhuis, 2004).

The pump characteristic delivered by Pentair is shown in Figure 4.9 as well as Appendix C.

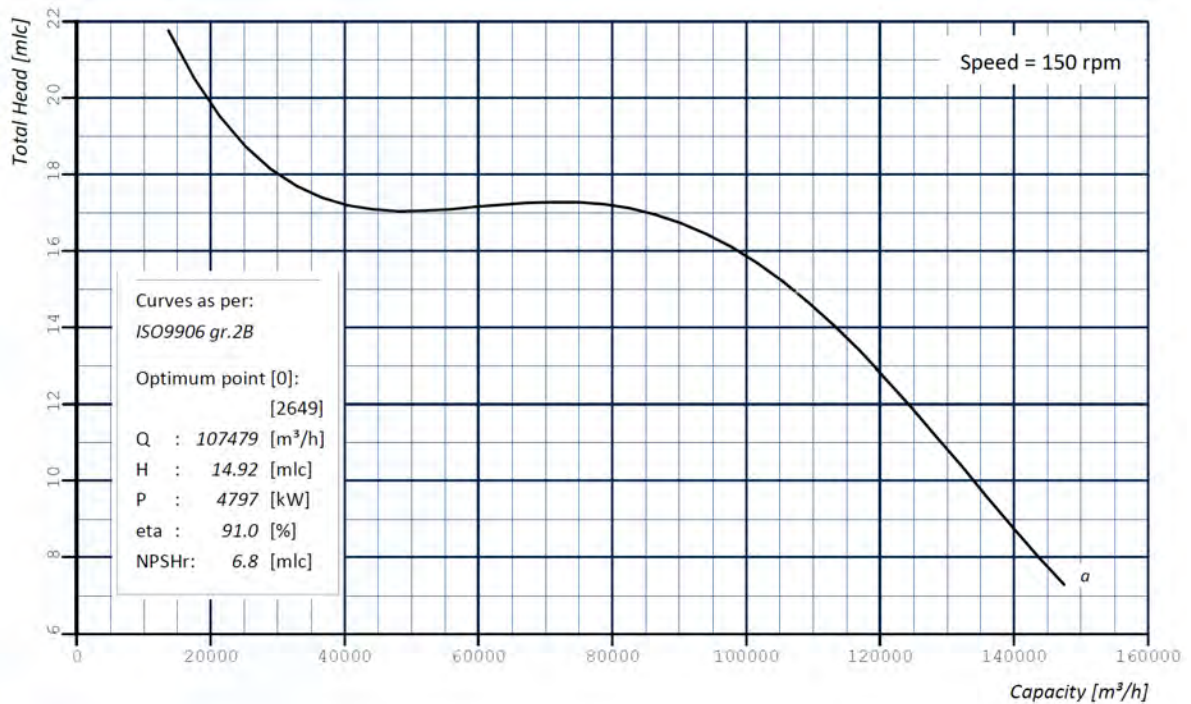


Figure 4.9: Pump Characteristic as Delivered by the Manufacturer

4.4. System and Pump Characteristics

Using the conceptual design of the pump installation, the entire distance from the inlet to the outlet constitutes the system characteristic. The system has a head loss along its length, and this dynamic head loss increases with the discharge. The dynamic head losses include inlet and outlet losses, friction losses, losses in the turning, and losses from the equipment such as non-return valves, pumps and trash racks. The calculations can be found in Appendix B.

The system characteristic is plotted for each difference in water level (h) shown in the level schematic (Figure 4.5 & Appendix A) as a function of the discharge (Q). The result is the lines which correspond in color to those depicted in the level schematic.

The pump curve as shown in the Selection of the Pump, Section 4.3 is for the rated speed of 150 rpm. For the purposes of the Delta21 turbine-pumping installation, the required discharge and the maximal pumping head is larger, so the speed of the blades has been increased to 175 rpm. When scaling back the speed of the motor (ω), and thus the impeller blades, the relationship between the flow rate at the new speed (Q_{i+1}) and the original speed (Q_i) is given in Equation 4.1

$$Q_{i+1} = \frac{\omega_{i+1}}{\omega_i} \cdot Q_i \quad (4.1)$$

For the relation in delivery head at the lower speed (Q_{i+1}) the proportion is different as the squared value of the rotational speed is used, as shown in Equation 4.2

$$h_{i+1} = \frac{\omega_{i+1}^2}{\omega_i^2} \cdot h_i \quad (4.2)$$

The pump and system characteristics with the working points for pump operation is shown in Figure 4.10 as well as in Appendix D.

The top-most curve is the pump operating at 100% of its adjusted rated speed, while the curves underneath show its operation at a reduced speed. The corresponding speeds of these so-called isolines are given in the top right legend of the diagram.

The reduction of the speed of the impeller is done so that the pumps can be operated at a same head but increased efficiency. The maximal efficiency of the uppermost region of the pump curves (light blue) is from 190 to 163 rpm, while the region of the lower rated speed (dark blue) is operated from 140 rpm to 113 rpm. Each of these regions has the same maximal efficiency, but at a different discharge rate. During the actual operation, the speed of the pump will be adjusted gradually in between these ranges, instead of at these specific values.

The intersection of the system characteristics and the pump curve shows the point at which the pumping station will be operating, this is called the working point. From this, the various flow rates can be determined, and have also been labeled on the diagram. When the energy storage lake is full and the North Sea is at an average depth (indicated by point 5), the pump is operating at its maximal discharge of 40 m³/s. This flow rate can be slightly increased at low-tide, however this situation is not expected to occur frequently so it can be neglected.

The lower two graphs show the shaft power required as well as the efficiency of the pump. The shaft power is defined as the hydraulic power divided by the efficiency at this point. The hydraulic power is simply related to the head [H] and discharge [Q] as given in Equation 4.3:

$$P_{hydr} = Q \cdot H \cdot \rho \cdot g \quad (4.3)$$

The hydraulic efficiency only looks at the losses relating to the amount of water that the pumps can handle at a specific head. During the actual operation there will be other losses included, which will

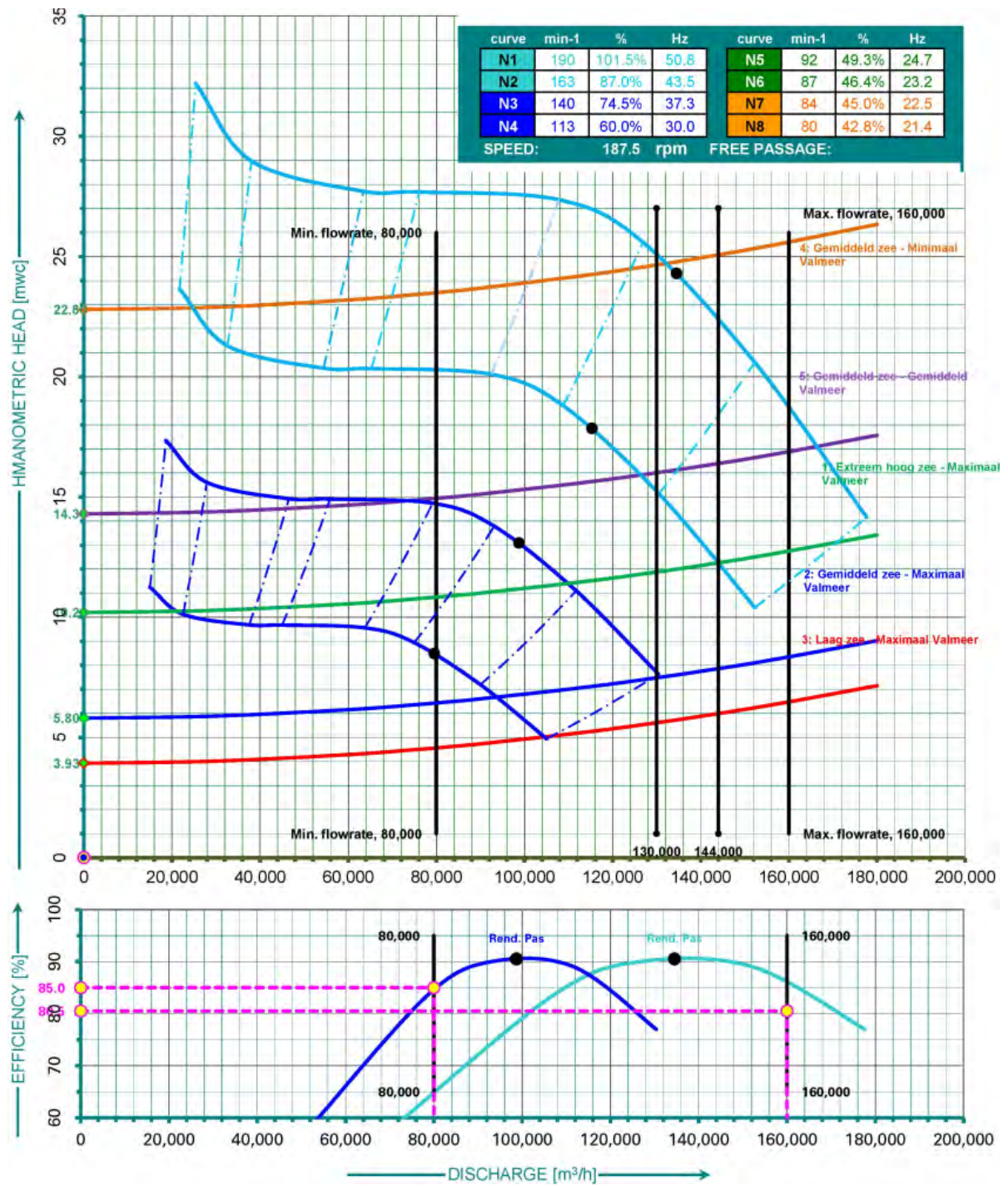


Figure 4.10: System and Pump Characteristics

further increase the power needed to pump the water out at each point. These losses include elements such as the motors, variable speed drives and transformers and will be further handled in Section 4.9.

4.5. Turbine Characteristics

For the basic design concept, the turbine is designed by means of a 'pump-as-turbine'. This means that the performance of the turbine is determined as if the geometry of the pump stays exactly the same but the flow of water is reversed. CFD modelling can be applied to this system and the flow analysed to determine the characteristic of the pump-as-turbine.

Typically steps can be taken to optimise the pump and achieve a higher hydraulic efficiency for its operation as a turbine when the flow is reversed. These steps can include a modification to the casing or to the impeller, such as a change in the angle of the impeller blades. However, the benefits of using a PaT is in its simplicity and the reduction in costs. The turbine curve delivered by the pump-turbine manufacturer Pentair can be found in Figure 4.11.

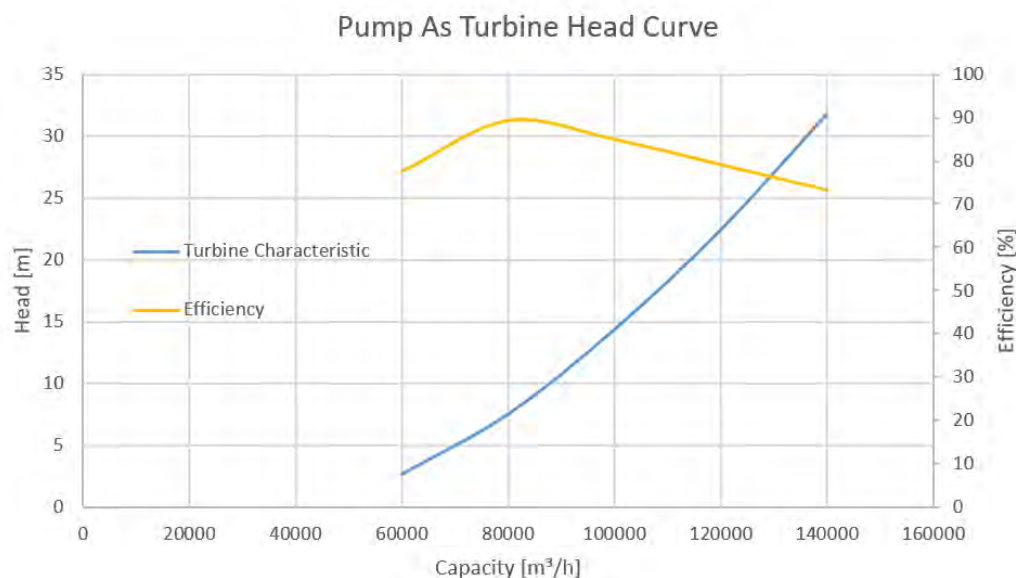


Figure 4.11: Turbine Flow rate-Head Curve

The system and turbine characteristics can be found in Figure 4.12 as well as in Appendix E. The system characteristics are largely the same as with the system and pump characteristics, however the shape of the system characteristic is of a negative parabola in the case of turbine operation. This is because the head losses incurred decrease the head available for energy generation. The geometry of the system is identical whether the flow is in pumping mode or turbine mode, meaning that the magnitude of the system curve is similar in both cases. However, the dynamic head loss is slightly increased in the case of the turbines, which due to the shape of the suction box which is optimized for pumping applications and therefore the head loss over this part of the system is larger for turbine applications. Another difference in the system and turbine characteristics is that the calculation of the hydraulic efficiency reduces the amount of power generated instead of adding to the power, which is the case in the pumping mode.

As can be seen from Figure 4.12, the speed of the impeller varies between 96 rpm at high heads to 47 rpm at lower heads. Also, the maximal flow rate varies from 115,000 m³/h (32 m³/s) to 56,000 m³/h (15.6 m³/s).

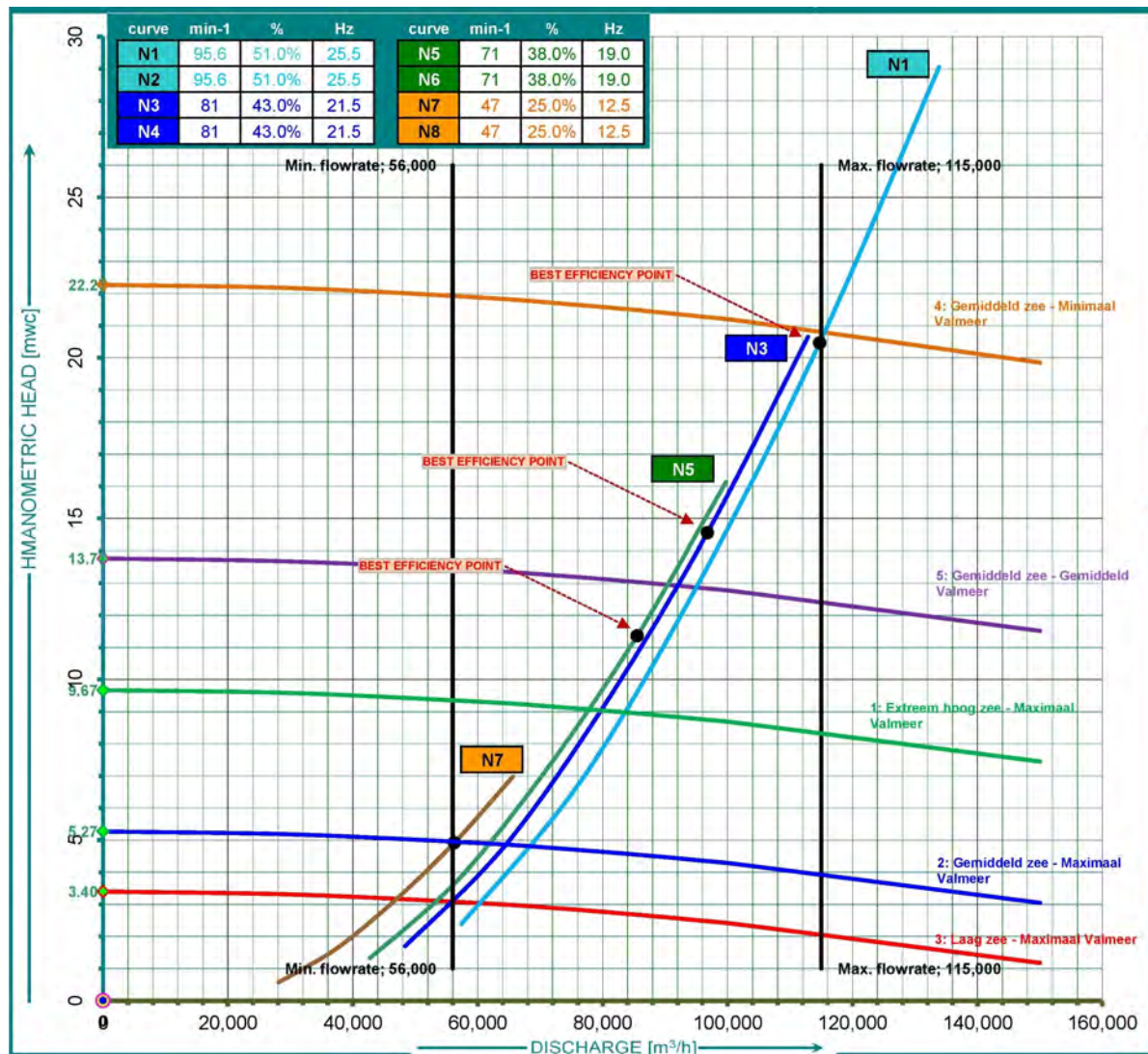


Figure 4.12: System and Turbine Characteristic

Comparing the operation of the turbine to that of the pump is difficult. It is not possible to compare the two characteristics based on flow rate or rotational speed, rather the available head and the power generated need to be analysed. In Figure 4.12 at the maximal head (orange line), the rotational speed of the turbines is much lower than that of the pump, however much more power is being generated due to the higher flow rate. However, as the lake is slowly filled and the head decreased, the flow rate and the rotational speed both decrease and the power generated does so too.

The motor and variable speed drive play a large role in the operation of the turbine. By decreasing the frequency and thus essentially braking the motor, the variable speed drive can regulate the flow into energy storage lake and keep the turbine as close as possible to its highest efficiency point at all times.

4.6. Hydraulic Sizing

The hydraulic sizing looks at the flow velocities through the pumping/turbine installation. The geometry of the conduit of the installation is finely tuned in accordance to the requirements for fish-friendliness and the dynamic head. As stated in Requirement H-DR1, the pumping-turbine installation must protect

the ecological values. Part of this is to either prevent the fish from entering the installation, or if entry is not prevented, to reduce the mortality rate for fish that enter the installation to an acceptable level. If fish entry is to be prevented, then the maximal flow velocities at the fish screens as a result of pumping or turbine operation must not pass a threshold level, thus enabling fish to swim away from the screens (van Berkel et al., 2018). For the geometry of the conduits in relation to the pump operation, it follows that a higher velocity will generate a higher dynamic head loss. Put simply, the head loss related to the increased velocity will create a steeper system characteristic, as shown in Appendix D. The steepness of the system characteristic determines the operation point of the pump, meaning that for the same level, the pump will operate at a lower discharge. Because of the inverse relation between the velocity and the area (and thus the diameter) for a constant discharge, decreasing the size of the conduit will generate a higher velocity and more head losses due to friction. In Figure 4.13 the effect is shown of a decrease in 1 meter of the penstock.

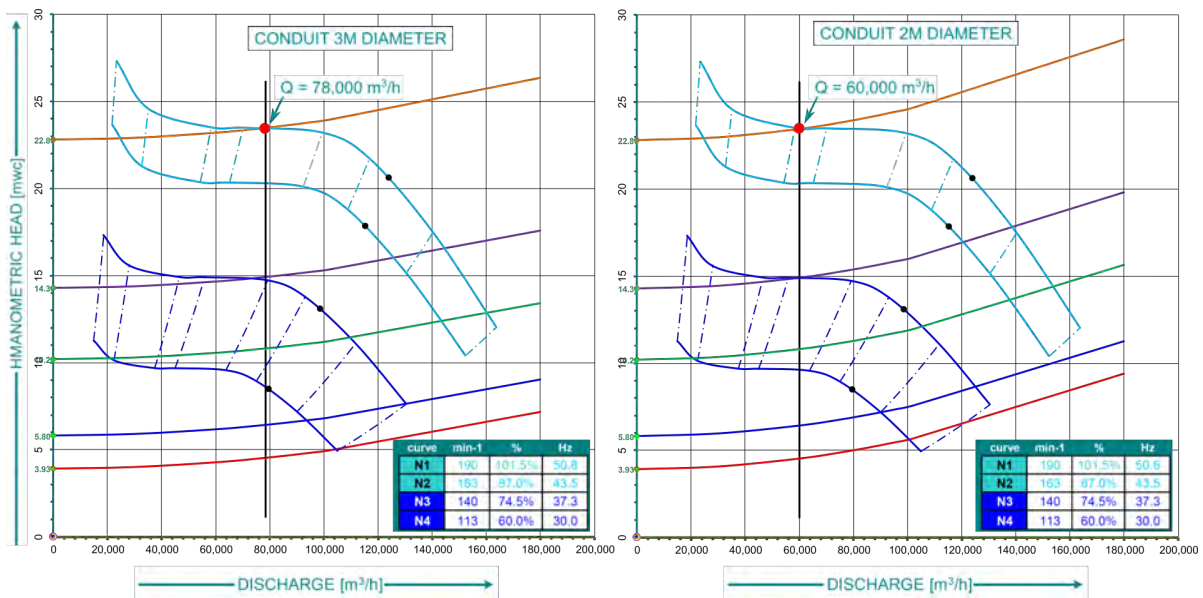


Figure 4.13: Effect of Conduit Geometry on System Characteristics

Although the difference 1 meter diameter in the penstock appears subtle, this results in a decrease of the flow rate of nearly 20,000 m³/h (5.5 m³/s) for the working point with the highest head (orange line). In this case, the choice to enlarge the diameter (left side of Figure 4.13) means that the pump is prevented from operating in the instable region of 40,000 to 60,000 m³/h.

For the flow velocities concerning the eco-friendliness requirement (H-DR1) the assumption is made that there are fish-screens present. This means that the velocity inside the system is not limited by the eco-friendliness requirements, however the flow velocities at the intake must be restricted to a value where the fish can still swim away.

4.6.1. Flow Velocities: Pumping Mode

For the pumping mode the flow velocities are presented in Table 4.2 as well as more schematically in Appendix F. Although it is uncertain whether there are fish present in the energy storage lake, for ecological safety it is assumed that fish and other marine life are present in the lake. Therefore inflow needs to be restricted to 1 m/s during the operation of the pumps to avoid sucking in fish against the fish screens. As can be seen in Appendix F the intake velocities are well below that point.

Level Lake [m + NAP]	-22	-13	-13.5	-5
Level Sea [m + NAP]	0	5	0	0
Velocity Lake Inlet [m/s]	0.38	0.61	0.33	0.24
Velocity Inside Pumphouse [m/s]	0.45	0.74	0.82	0.91
Velocity Volute [m/s]	4.28	6.96	7.71	8.56
Velocity Inside Conduit [m/s]	2.18	3.55	3.93	4.36
Velocity Before Outlet Sea [m/s]	1.71	2.79	3.09	3.43
Velocity Outlet Sea [m/s]	0.97	1.58	1.75	1.94

Table 4.2: Flow Velocities through the Installation - Pumping

4.6.2. Flow Velocities: Turbine Mode

For the turbine operation the flow velocities are presented in Table 4.3 as well as more schematically in Appendix G. In this case the critical velocities are at the sea-side inlet, as the flow should be restricted to not suck fish from the sea into the fish screens. If the flow velocity stays low then it gives the fish the possibility to swim away. In order to achieve this the dimensions of the outlet at the sea-side have been increased to 6.6 meters wide and 5.4 meters high. The restriction in the height increase is that the inlet height should not come above the minimal water level to prevent the intrusion of air. The restriction in width is the total width of the pump house, so that the entire structure does not become unnecessarily wide. Also the slope of the widening should be restricted to 1:7 to restrict any additional head losses. Furthermore, the operation of the turbine should be such that the flow rate of the pump is maximum 35 m³/s. The restricted flow rate and the enlarged dimension ensures a flow velocity of 1 m/s at the inlet of the turbine which passes the ecological requirements.

Level Lake [m + NAP]	-22	-13	-13.5	-5
Level Sea [m + NAP]	0	5	0	0
Velocity Lake Inlet [m/s]	0.54	0.21	0.18	0.08
Velocity Inside Pumphouse [m/s]	0.65	0.55	0.45	0.32
Velocity Volute [m/s]	6.16	5.14	4.28	3.00
Velocity Inside Conduit [m/s]	3.14	2.62	2.18	1.53
Velocity Before Outlet Sea [m/s]	2.46	2.06	1.71	1.20
Velocity Outlet Sea [m/s]	1.40	1.17	0.97	0.44

Table 4.3: Flow Velocities through the Installation - Turbine Operation

4.7. Physical Sizing

The sizing of the suction box is determined by the norm as shown in Figure 4.14. The size of the suction box in all cases is directly proportional to the impeller diameter (D). This norm has been developed by manufacturers and is based on computer simulations and empirical research on physical models. The result is a maximal efficiency for CVP's and minimal creation of vortices.

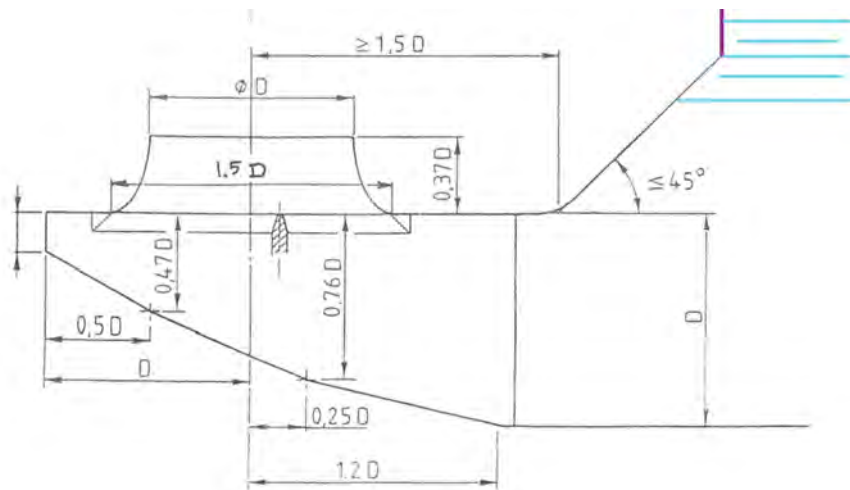


Figure 4.14: Suction Box Sizing

The impeller diameter has been specified by the manufacturer and can be found in Appendix C to be 2649mm. The result of the sizing is found in the level schematic (Appendix A).

Other than the suction box the physical sizing determines the general arrangement of the elements to incorporate all the necessary equipment, such as penstocks, stop-logs, fish screens, etc. For the penstock, an initial inner slope of the energy storage lake has been assumed to be 1:2. Although in reality this may be longer, the impact that a change in length of the penstock will have on the system characteristic will be negligible, so long as it is in the same order.

4.8. Overview Schematic

The overview schematic (Appendix H) shows the bird-eye view of the pump-turbine installations. With a maximal flowrate of 44.4 m³/s, a total number of 226 turbines will be required to achieve the maximal pumping discharge of 10,000 m³/s. With the total amount of pump-turbines required as well as the sizing of each unit, the total width of the structure can be derived. Walls of 600 mm thick at either side are added to the total width of each unit as an estimate of the eventual added spacing between the pump-houses. As per the guidelines for the suction box design, the intake width is 2.8 times the impeller diameter. This means the total width (w_t) of the turbine-pumping station is given in Equation 4.4.

$$w_t = N_{pt} \cdot (2.8 \cdot D_{imp} + 1.2) + 1.2 \quad (4.4)$$

The total amount of pump-turbines is indicated by N_{pt} while the impeller diameter is D_{imp} .

The overview schematic also shows the general infrastructure required for a good operation of the turbine-pumping station, mainly the access road connecting the electrical installations, which are grouped per 4 pumps.

4.9. System Efficiencies

Each working point, as discussed in Section 4.4, has a corresponding shaft power and operating efficiency. The efficiencies presented in the system and pump characteristics (Appendix D) are only for the hydraulic performance of the pump, so the hydraulic power required to operate at this working point. In addition to the hydraulic losses associated with the pump, there are losses related to the motor,

variable speed drive, transformers and the cables. Typically, the higher the power of the motor, the less the losses will be. However, the losses in the electrical components are typically quite small, in the order of 2 to 5%.

The overall efficiencies of the system are given in Appendix L. For the determination of the efficiencies, the performance of the pumping station Bergsche Maas have been used as samples values because the motors are of a similar voltage and power. The working points in the calculation for the system efficiencies can be found in the pump and system characteristic (Appendix D), with each point's corresponding efficiency. For the working points operating close to the maximal power, the efficiency of the motor was chosen as $\eta_{\text{motor}} = 95\%$. For the working points at lesser power (between 1 and 5 MW), this was chosen at 92%.

4.10. Analysis of Cavitation

An important step in the verification of the design is making sure that cavitation does not occur. The occurrence of cavitation can severely damage the pump, but it can be prevented by making sure the available net positive suction head ($NPSH_a$) is always larger than the net positive suction head required ($NPSH_r$). The required net positive suction head is a property which is dependent on the pump design, and is usually provided by the manufacturer of the pump along with the pump characteristics. The required NSPH for the basic design concept can be found plotted in the pump characteristic in Appendix C. On the other hand, the available net positive suction head is a property of the system and the vapour pressure of the fluid being transported.

Based on the geometry of the system as well as the material properties (the roughness taken in this case as $k = 0.2\text{mm}$) the head losses in the conduit are determined. These losses are dependent on the amount of flow. As well as this the losses related to the shapes of the system (inlet, outlet, bends) are added, but are not dependent on the flow. Combined, these two losses give the total head loss, and the calculations can be found in Appendix J. The total head losses as a function of the amount of discharge passing through the pumps is used as input for the available net positive suction head.

The head described previously which is dependent on the flow is also called the dynamic head (H_{dyn}). Next to this, the static head (H_{stat}) is simply the difference in the height between the impeller blade center-line and the water level inside the lake. This can be negative if the pump is situated above the water line, which could be the case when the water level inside the lake is at its minimal point (NAP - 22.5 m). The positive head and the atmospheric pressure are added up. From this the dynamic losses in the pipe are subtracted, as well as the vapour pressure of the liquid. The remainder is given as the available net positive suction head. The values and graph can be found in Appendix I. In the graph a dashed line is visible at 1 meter under the calculated available net positive suction head level. This line serves as a safety factor. As can be see from the graph in Appendix I, the safety level of 1 meter intersects with the required net positive suction head level at a flowrate of $160,000\text{ m}^3/\text{h}$, so this is the limit for the maximum flowrate of the pump for this type of system.

4.11. Connection of the Pump-Turbines to Grid Power

4.11.1. Components of the Electrotechnical Installation

The most vital element of the electrotechnical installation is the motor. The motor will be directly attached to the shaft of the impeller, and although the impeller blade will be placed in the volute, the motor will be placed outside the pump house meaning it will be underwater most of the time. This will make accessibility to the motor easier since underwater pressurized chambers will not be required. More information about the maintenance can be found in Subsection 4.16.2. The underwater placement also means that the cooling of the motor can be done by the water it is placed in, removing the need for a complicated underwater air-cooling solution. More information on the cooling of the motor can be found in Section 4.12. The motor is 6,6 kV. This amount of voltage corresponds to the high power

requirements, and also allows for the variable speed drive and the transformer to be placed further away, on dry land.

Another vital element in the connection of the motor to the grid power is the variable speed drive. The variable speed drive adjusts the power supply to the motor and hence controls the frequency of the motor. The control of the frequency allows the motor to adjust its speed, which is critical in its flexibility, allowing the turbine-pumping station to control the flow rate precisely among the 250 pumps. The variable speed drive is also a critical element in the system in the operation of the turbines. The frequency control allows the torque in the motor to increase during flow to restrict the rate of flow. This is critical as it means no extra equipment is needed in the turbine operation to restrict the flow of water.

The last important link to the grid is the transformers. There are 3 separate voltages for the entire pumping station. The highest voltage is that of the grid, and is usually 120 kV. Then, along the entire turbine-pumping the various electrical installations are connected by 20 kV power. This allows for the large distances to be bridged with minimal loss. Finally from the electrical installation to the motor the voltage is 6,6 kV, which matches the voltage of the pump. Between each

4.11.2. Single-line Diagram

The single-line diagram shows how the components of the electrotechnical installation are connected to one another and to the grid.

4.11.3. Layout of the Electric Installations

The transformers and variable frequency drives are quite large and have a required space around them needed to extract parts if required. The variable frequency drives are largest and are 2.5 meters deep and 8 meters wide. The transformers only require 1 meter by 1 meter. Since the 4 pump-turbines are grouped together to one electric installations, 4 groups of variable speed drives and transformers will mean the total area required for each group of electrical installations is 18x10 meters.

4.12. Cooling of the Motor, Variable Speed Drives, and Transformers

In each turbine-pumping installation the motor, variable speed drive (VSD) and transformer will produce heat, which will need to be removed in one way or another to ensure proper operation of the entire unit. The motor, VSD, and transformer each have their inefficiency, meaning that this proportion of the power is converted into heat.

On a smaller scale, pumps and frequency inverters are typically air-cooled. The increased scale and the unique style of proposed Delta21 turbine-pumping station, however, means that an innovative measure needs to be found in order to tackle the cooling problem. For this, a reference case is used in the shape of the Intake Pumping Station Bergsche Maas (*Innamepompstation Bersche Mass*). This pumping station, commissioned by Evides, is designed by Royal HaskoningDHV and has recently started its operations in the area of the Biesbosch in order to pump water into a nearby freshwater reservoir. The 3 mixed-flow pumps at the pumping station are powered by a high-voltage asynchronous motor with a rated power of 1100 kW. The unique feature of this pumping station is that the motors and the variable speed drives are cooled using water flowing in front of the pumps.

Due to the fact that the motors of the Delta21 turbine-pumping station are underwater for a large part of the operation, the water flowing around the pumps can be used to directly cool the motors. However, as can be seen from the level schematic (Appendix A), the motor is no longer underwater when the level inside the lake is close to its minimum level. The solution for this problem is to place a heat exchanger in front of the pump house and to use this flowing water to cool not only the motor,

but also the frequency inverter and transformer located at the sea-side inlet. Auxiliary pumps will be required to provide cooled water to the elements, and the heat exchanger will need to be at an ample distance from the pump house not to interfere with the flow in front of the turbine-pump. The principle of how the heat exchanger provides cool water for the motor and transformers/variable speed drive is shown in Appendix M.

The heat exchanger element can also be provided with UV-C light as a protection from environmental factors such as fouling or other growth. An example of such a cooler can be found in Figure 4.15. If required, the heat exchanger can also be removed with the same principles described in Section 4.16.

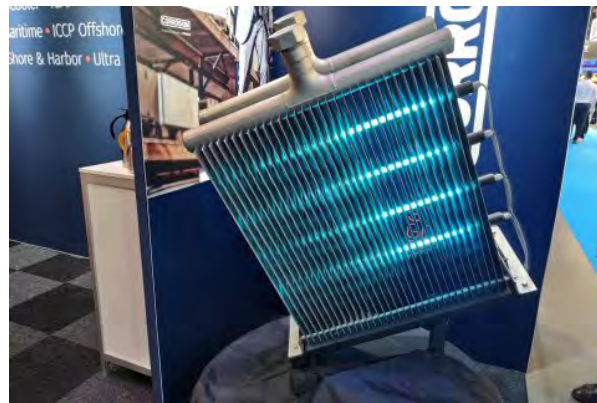


Figure 4.15: UV-C Light Cooler Box (Buitendijk, 2019)

4.13. Standard Equipment

Apart from the pump-turbines and the electrical equipment used to operate them, there is also a range of other equipment required to allow for successful operation of the pump-turbine station. The level of detail can go very far in describing all of the equipment, until the coffee maker in the electrical installation chamber, however this section will restrict itself to the more significant and basic items.

The first piece of equipment mentioned is the non-return valve. This valve, depicted in the level schematic as a flap-type element, is used to make sure that when the pumps are not in used, the water does not flow back into the energy storage lake due to gravity. Typically, non-return valves consist of valves which can only open one way, and are automatically opened when the flow in the direction of pumping is active, and automatically close for flow in the opposite direction. This means that during pumping operations or when there is no flow, the non-return valves do not require any mechanical operation. Finally a valve that bypasses the non-return valves should be included. The non-return valves are used for pumping mode, but when switching to turbine operation the water should be allowed to flow back into the energy storage lake.

On either side of the pumping installation there should be two separate means to stop the flow. At the lake-side of the installation this is done with a pair of stop logs. Stop logs are typically installed inside a groove in the structure, lined with rubber or similar materials to create a watertight seal. The stop logs are installed manually as they are only required during maintenance, inspection, or repair to provide accessibility. An example of such a stop log is given in Figure 4.16.

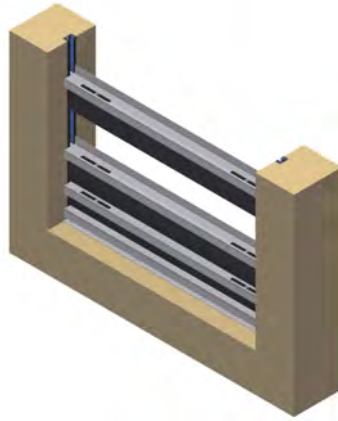


Figure 4.16: Stop Logs (KWT Waterbeheersing, 2018)

At the sea-side of the installation, only one stop log is required as an emergency gate is also presented. This gate is integrated into the structure and is operated hydraulically when the energy storage lake is not in use, but also for maintenance, inspection, or repair.

4.14. Operating Philosophy

4.14.1. Operating Philosophy for Flood Protection

When the pumping station is used for flood protection, this means that the flood barrier connecting the tidal lake to the North Sea is shut, and discharge from the Haringvliet estuary cannot flush naturally into the sea. In this case, the spillway connecting the tidal lake to the energy storage lake will open, and the river discharge will flow into the energy storage lake and will then be pumped out into the North Sea.

Following from Requirement H-FR2 in Section 3.1, the maximal discharge that will need to be pumped out in this situation is 10,000 m³/s. The reasoning behind this quantity is that in the next 100 years (the structural lifetime of the pumping station) the peak river discharge from a flood wave flowing through the Haringvliet will be 20,000 m³/s. Since the energy storage lake has a capacity of 430 million m³, the pumps will only need to be able to pump out half of this peak discharge, while the storage capacity of the energy storage lake can handle the rest. Knowing this, there are two different approaches that can be taken for which the pumps can be operated in case of the scenario relating to flood protection is occurring.

The first approach is preemptively emptying the energy storage lake in anticipation of the flood wave. This approach is based on the assumption that the flood wave and its size can be predicted and modelled correctly. With the current state of monitoring technology and the fact that it takes several days for a flood wave to pass through to the Haringvliet from the upper reaches of the Rhine and Maas, this assumption is seen as quite reasonable. Emptying the energy storage lake before the arrival of the flood wave will allow the storage capacity to remain maximal. The disadvantage of this tactic is however that the head difference of the water inside the storage lake compared to that at the North Sea will be very large. This large head difference will mean that the pumps will operate at a lower flow rate, even when the speed is at 100%. Another disadvantage of this approach is that the preemptive emptying of the storage lake will cost electricity which cannot be stored. In summary, this approach to the use of the pumping station for flood protection should be reserved for when the size of the flood wave is considerable, and all available storage and pumping capacity is required, regardless of the electricity costs.

The other approach to pumping the superfluous discharge from the Haringvliet that is flowing into

the energy storage lake via the spillway is without any interference beforehand, or even by filling the energy storage lake preemptively. This ensures that the pumping head remains small(er) and this thus means the flowrate of the pumps is at its maximal level. As calculated in Section 4.8, a total of 250 pumps pumping at 40 m³/s will achieve the total of 10,000 m³/s which is the requirement for the pumping station. However, this maximal flowrate only occurs at the lowest head difference, when the energy storage lake is full. This means that there is no storage capacity beyond this. Therefore, this strategy for the operating philosophy can only be used in a scenario where the peak discharge of the flood wave is no higher than 10,000 m³/s.

Both approaches can be fine tuned in accordance to the expected peak discharge of the incoming wave. For each flood wave, an optimization can be made for the operating philosophy of the pump. The predictable nature of a flood wave and the capacity to monitor it can allow for a pumping solution that is as efficient as possible. By regulating the speed of the pumps and thus the flow of the pumping station, the pumps can be kept at their peak operating efficiency, while safely dealing with the flood wave.

It should also be known that in general, keeping a pump as close as possible to its best efficiency point is good practice, as this will prolong its lifetime. As well as saving costs on energy, it will help potential costly repairs in the future which are more likely if the pump is operated outside of its designated area. Furthermore, the entire pumping station consists of 250 pumps. This means if it is desirable to pump at a very low discharge, it is better to operate half the pumps at their best efficiency point than to switch on all the pumps at a sub-optimal working point. This combined with the fact that the pumps are all of variable speed means the pumping station is very flexible in its operation.

4.14.2. Operating Philosophy for Energy Storage

When the pumping installation is not in use for flood protection, the pumps are put to use for the storage of renewable energy coming from (offshore) wind and solar farms when this is surplus to grid requirements, while the turbines are used for the generation of electricity when there is a shortage of renewable energy. The use of the pumps for flood protection will happen less than once a year on average, therefore the use of the turbine-pumping station for pumped-storage hydroelectricity is considered its daily use.

The operation of the pumps and turbines for pumped-storage is governed on the one hand by the demand of the grid, and on the other hand of the availability of renewable energy. As can be seen from Figure 4.17, the variations in demand of grid power follow a strong pattern, with the demand during weekends (shaded dark green) being less than week days.

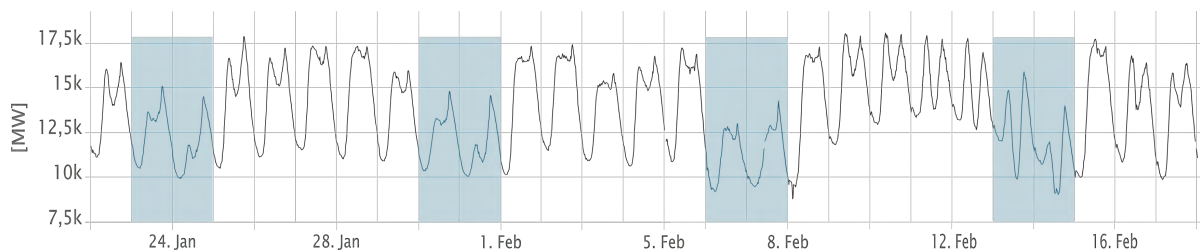


Figure 4.17: Daily Demand From the Grid. Data retrieved from <https://www.tennet.eu/nl/elektriciteitsmarkt/data-dashboard/productie/>

On the other hand, Figures 4.18a and 4.18b show the unpredictability of wind energy, and while solar power is more predictable in its nature, it is still dependent on the weather, as can be seen in the large differences in energy produced on days with different weather.

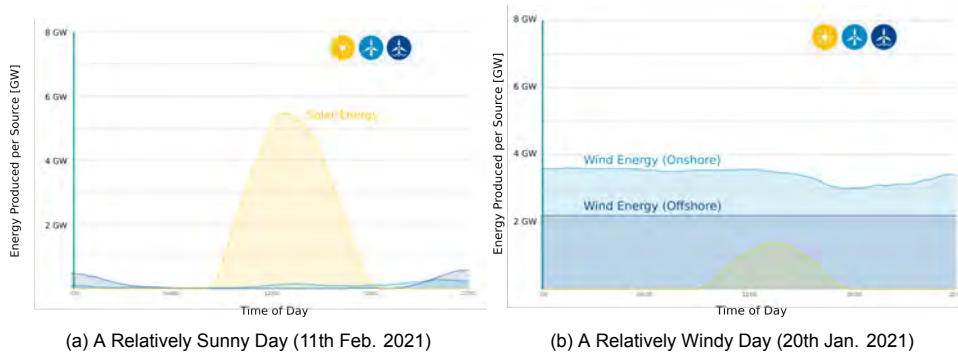


Figure 4.18: Influence of Weather on Renewable Energy Sources. Sourced from <https://energieopwek.nl/>

In accordance with the requirement H-DR3, the goal of the turbine-pumping station is to deal with electricity in a sustainable manner, and to maximize the amount of renewable energy that is stored. For the operation of the pumps and turbines in the energy storage mode this means that the pumps and turbines should be kept as close as possible to their best efficiency point. The speed of the pumps and turbines can be adjusted so that the flow rate is regulated while maintaining the optimal hydraulic efficiency. However, the periods during which there is a surplus of renewable energy are restricted, meaning that the goal is to pump as much of the lake empty to store. Again, this is a case optimizing the operation of the pumps and turbines to maximize the storage and production of renewable energy in the time frame where there is a demand or supply for it.

4.14.3. Simulation of Emptying and Filling the Energy Storage Lake

The working point of a pump depends on the available static head and the speed at which the pump is being operated. Using the small basin approximation and a numerical procedure a simulation can be carried out which shows the operation of a pump based on certain initial conditions and the pump and system characteristics. The small basin approximation states that the area of a body of water is constant with the depth and therefore the volume balance for this body of water can be written as shown in Equation 4.5 (Battjes & Labeur, 2017).

$$Q_{in} - Q_{out} = A_b \frac{dh}{dt} \quad (4.5)$$

The area of the basin in this case is A_b , while $\frac{dh}{dt}$ represents the change in level inside the energy storage lake over time.

Since the working point is dependent on the static head available, but the water levels in the lake change according to the working point, a numerical method is needed as a solution. For the simulation of the emptying and filling of the energy storage lake the Euler forward method is used. The Euler forward method approximates a function as shown in Equation 4.6 (Atkinson, 1989).

$$y_{n+1} = y_n + \Delta t \cdot f(y_n, t_n) \quad (4.6)$$

In case the emptying of the lake by means of the pump only ($Q_{in} = 0$), this means the simulation will combine Equations 4.5 and 4.6 the static head and the level in the energy storage lake (which are interdependent) can be written as follows.

$$h_{n+1} = h_n + \Delta t f(h_n, t_n) \quad (4.7)$$

$$f(h_n, t_n) = \frac{dh}{dt} = -\frac{Q_{out}(h_{s,n})}{A_b} \quad (4.8)$$

In Equation 4.7 the term h refers to the level inside the energy storage lake, while the term h_s refers to the static head, so the difference in the levels inside the energy storage lake and on the North Sea. As stated previously, the pump flow rate is a function of this static head, therefore the flow rate is given as $Q_{out}(h_{s,n})$. The step size for this numeric method is 1 minute, so $\Delta t = 60\text{sec.}$

The working point is found by solving the equations for the system characteristic and the pump characteristic at its given speed. An example of such is seen in Figure 4.19.

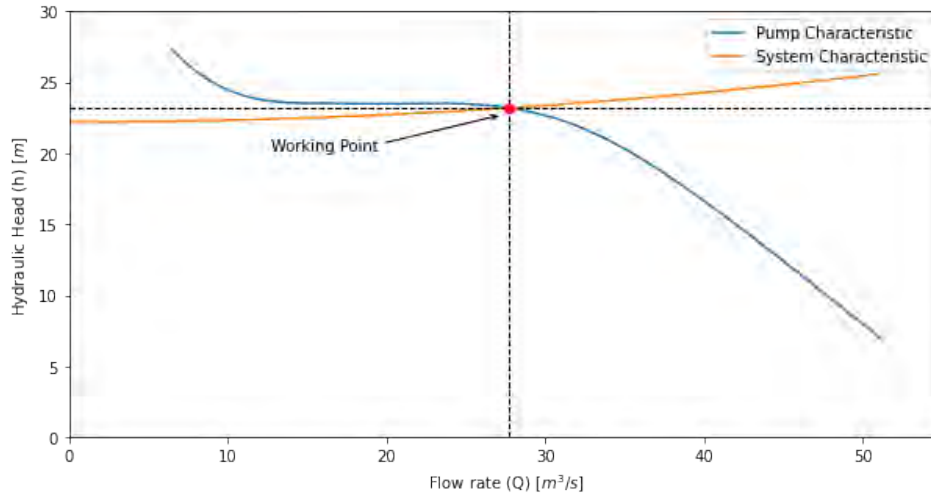


Figure 4.19: Working Point at 100% Rated Speed

The first simulation done is to simply empty the lake from the lowest ($h_{ESL} = NAP - 22\text{m}$) to the maximal ($h_{ESL} = NAP - 5\text{m}$) level at a constant maximal rated speed of the motor (175 rpm). The level on the North Sea is assumed to be constant for this simulation so the static head at the start (the initial condition) is 22 meters. The result of such a simulation is shown in Figure 4.20.

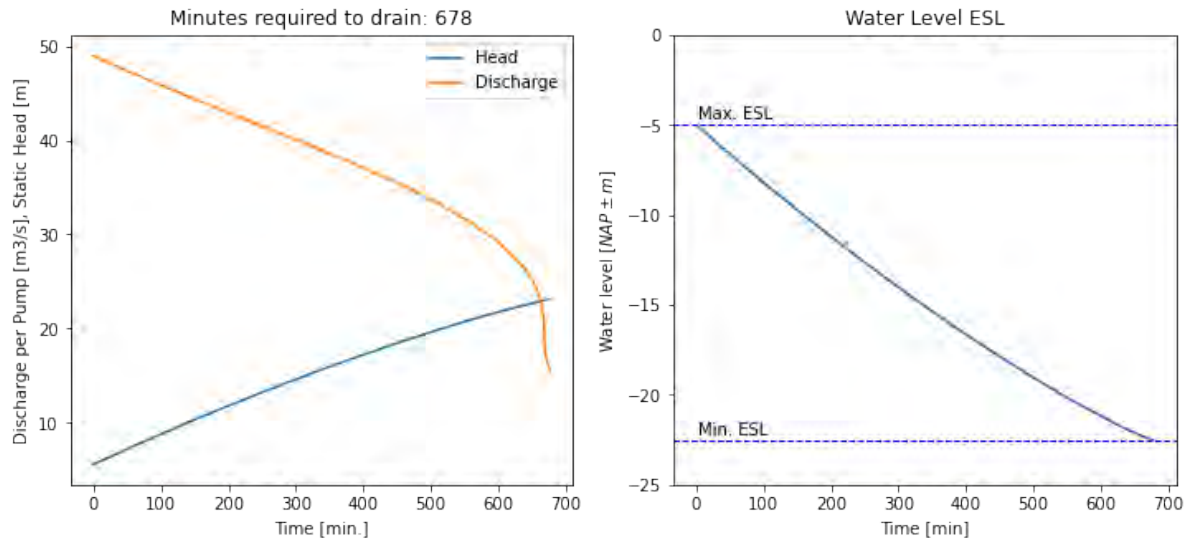


Figure 4.20: Simulation of Emptying Energy Storage Lake

By adding the efficiencies from the pump curve, the power consumption for emptying the lake can be determined. This is done in a piece-wise manner, and as can be seen from Figure 4.21, the pump is really inefficient at lower hydraulic heads due to the fact that the speed is still at 100%. This shows

the need to manage the motor speed during operation of the pumps.

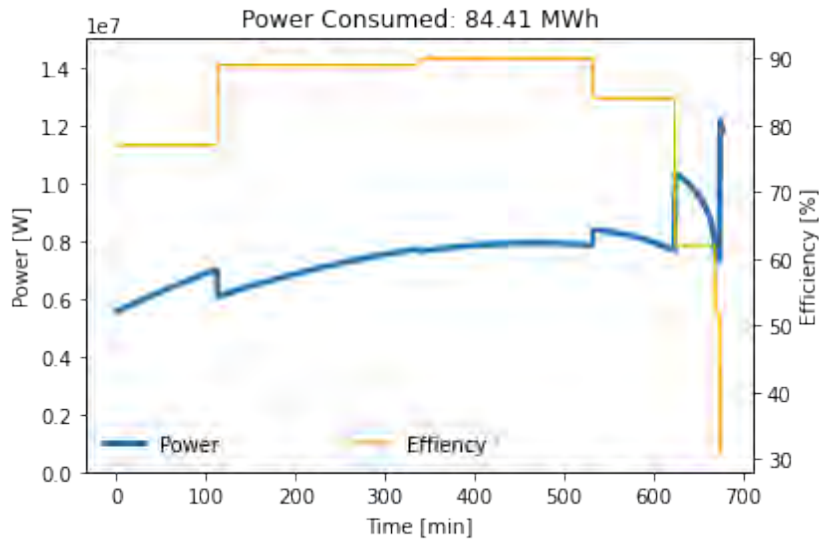


Figure 4.21: Power Consumption of the Pump to Empty the Lake

Using the same technique as with pumping, a simulation can be made of the lake being filled with the turbine operation. The only difference now is the sign of the flow rate into the energy storage lake (Q_{in}) is changed, as well as the system characteristic which is inverted. Since the operation of the turbine is sensitive to the rotational speed of the motor, the adjusting of the motor speed is included in the simulation, keeping the speed so that the working point is always near to the maximal efficiency point. This is done step-wise and is dependent on the static head available as shown in Table 4.4 and Figure 4.22.

Static Head Max. [m]	Static Head Min. [m]	Rotational Speed [rpm]
22.27	18.02	92
18.02	13.77	71
13.77	9.52	61
9.52	5.27	56

Table 4.4: Turbine Motor Speed Based on Static Head

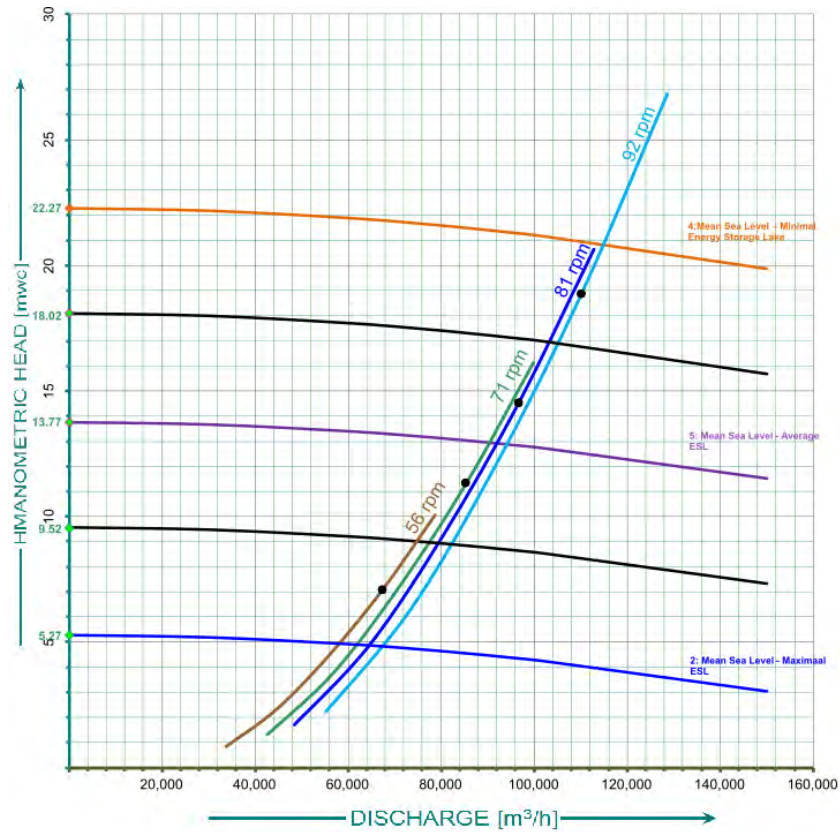


Figure 4.22: Turbine Characteristics Based on Static Head and Rotational Speed from Table 4.4

4.14.4. Simulation of a Flood Wave

The peak discharge of $20,000 \text{ m}^3/\text{s}$ used as a requirement for the energy storage lake and the pump installation to remove superfluous discharge from the Haringvliet is a very conservative value. However, the GRADE Report for the Rhine and Meuse basins does indeed calculate a peak discharge of $19,480 \text{ m}^3/\text{s}$ for a return period of 10,000 years at Lobith (without upstream flooding) as well as a peak discharge of $4,400 \text{ m}^3/\text{s}$ at Borgharen for the same return period (Hegnauer, Beersma, van den Boogaard, Buishand, & Passchier, 2014). The locations of Lobith and Borgharen refer to the location where the Rhine and Meuse river enter the Netherlands, respectively.

Using the pump operation simulation described in Subsection 4.14.3 as well as the inclusion of the discharge from the flood wave, the response of the energy storage lake can be modelled. In addition to the numerical solution to the operation of the pumps, the volume coming into the energy storage lake per unit time is taken. The Q_{out} term in Equation 4.5 is now equal to the integral of the flood wave along the same time step (Δt) as in Equation 4.6. A diagram of this model can be found in Figure 4.23.

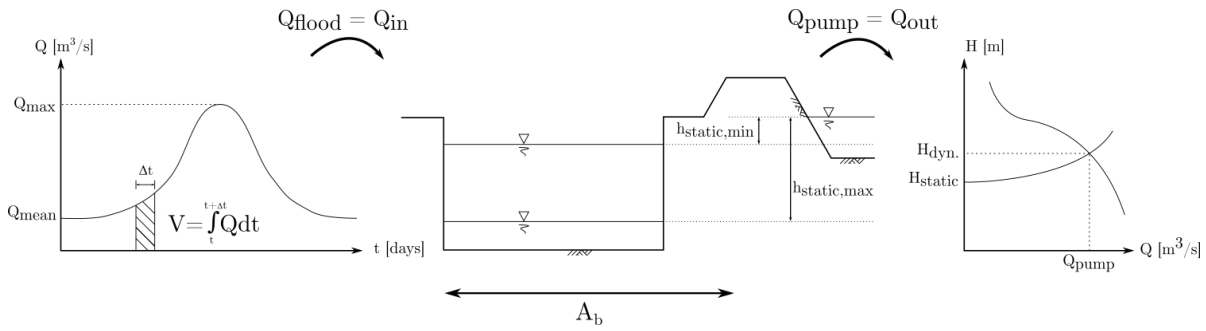


Figure 4.23: Model Used to Simulate the Operation of the Pumps During a Floodwave

Return Period [years]	Borgharen [m^3/s]	Lobith [m^3/s]	Q_{total} [m^3/s]	Q_{max} [m^3/s]	Q_{mean} [m^3/s]
5	1970	7970	9940	7455	2485
10	2300	9130	11430	8572.5	2857.5
50	2970	11710	14680	11010	3670
100	3220	12580	15800	11850	3950
250	3520	13390	16910	12682.5	4227.5
500	3700	13890	17590	13192.5	4397.5
1250	3910	14350	18260	13695	4565
4000	4180	14940	19120	14340	4780
10000	4400	15400	19800	14850	4950
100000	4930	16560	21490	16117.5	5372.5

Table 4.5: Peak Flood Wave Discharges for Various Return Periods (Hegnauer et al., 2014)

Figure 4.24 shows the response of the energy storage lake and the pumps for the whole duration of a flood wave, which is 20 days. From this it can be concluded that the for such a large discharge during such a long time the storage function of the energy storage lake is negligible. Furthermore, it can be concluded that the flow rate of the pumps is very much dependent on the static head, as can be seen from the fluctuation of the flow rate with the tidal signal.

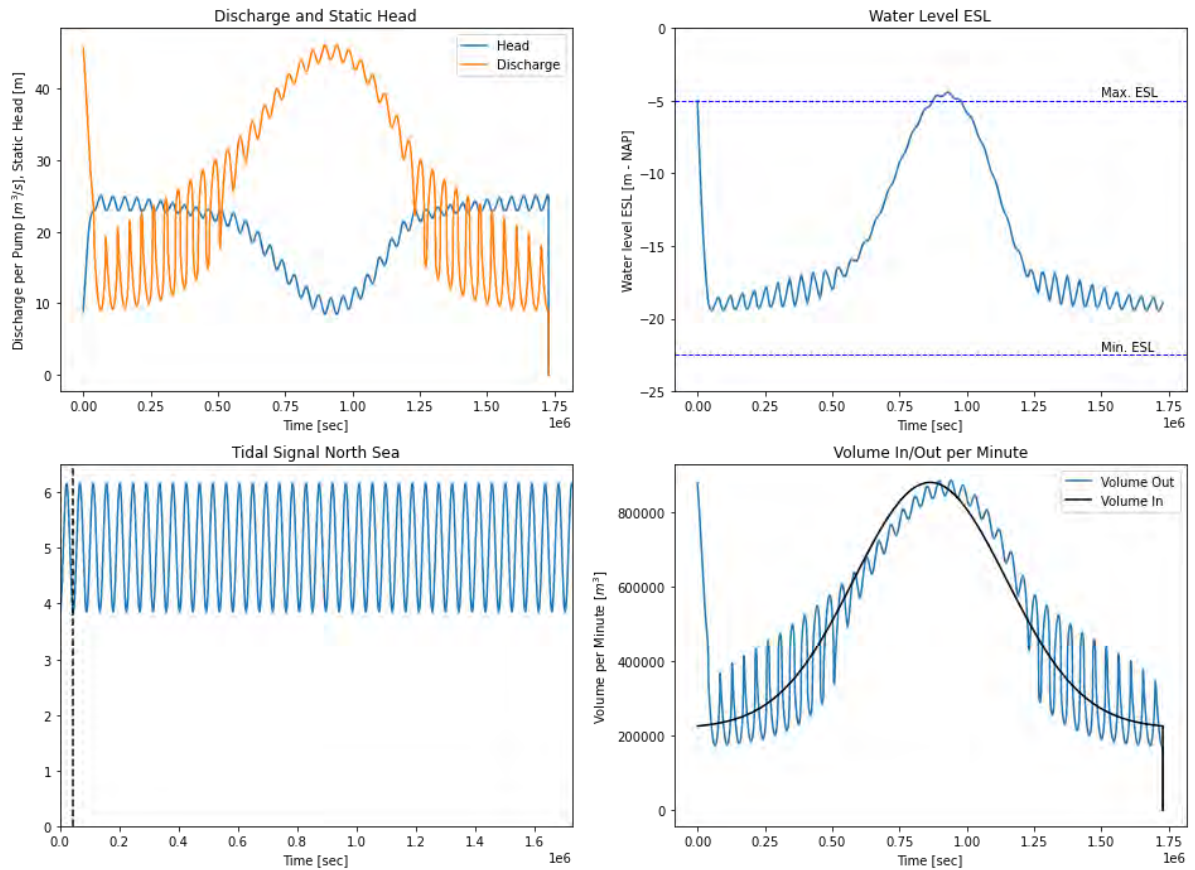


Figure 4.24: Simulation of the Energy Storage Lake Response to a Floodwave (20 days)

4.14.5. Simulation of a Flood Wave During Storm Surge

A more realistic situation for simulating the operation of the energy storage lake is where a storm surge on the North Sea coincides with the arrival of a flood wave. The storm surge will require a closure of the barrier which will then mean the superfluous discharge from the flood wave needs to be discharged via the spillway energy storage lake. Furthermore, instead of taking the full discharge of the Borgharen and Lobith discharges, 70% will be taken, as referenced by (Rijkswaterstaat, n.d.). Figure 4.25 shows the worst case of such an event, where the peak discharge of the flood wave coincides with the highest water level of the storm surge. The vertical dashed black lines represent the effective duration of the storm surge and show when the barriers will open and close, meaning the time for which the energy storage lake is receiving the flood wave discharge through the spillway.

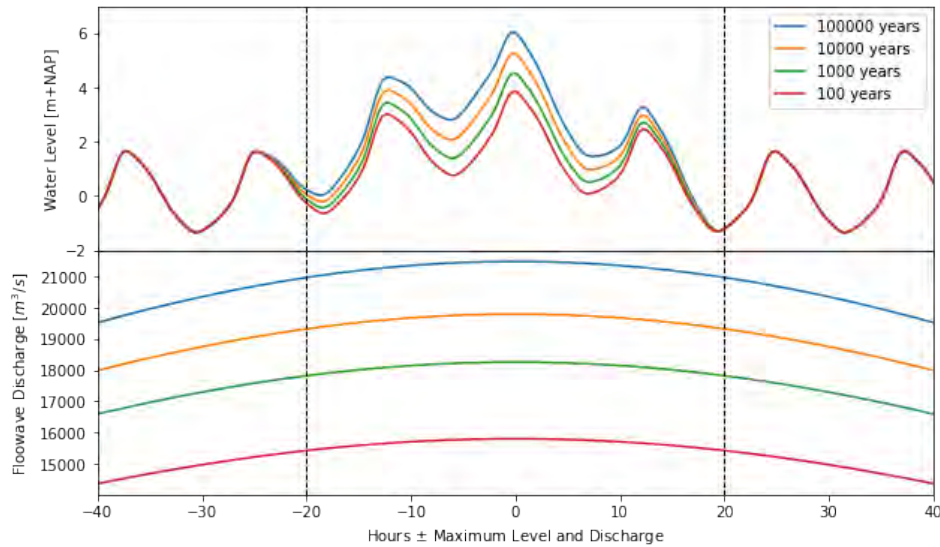


Figure 4.25: Water Levels During Storm Surge and Flood Wave Discharges for Various Return Periods

The maximal values of the storm surge sea levels are determined using the applications Hydra-NL and Waterstandverloop. The flood wave peak discharges are taken from Table 4.5 but now only 70% of the peak and mean values.

4.15. Discussion of the Unstable Region for the Pump

From the pump characteristic shown in Figure 4.26 it can be seen that the pump has a region which is unstable. As shown by the red lines, within these discharges the same delivery head corresponds to two separate discharges. This means that if the pump operates at this delivery head, the discharge can suddenly fluctuate, which can potentially be damaging to the pump.

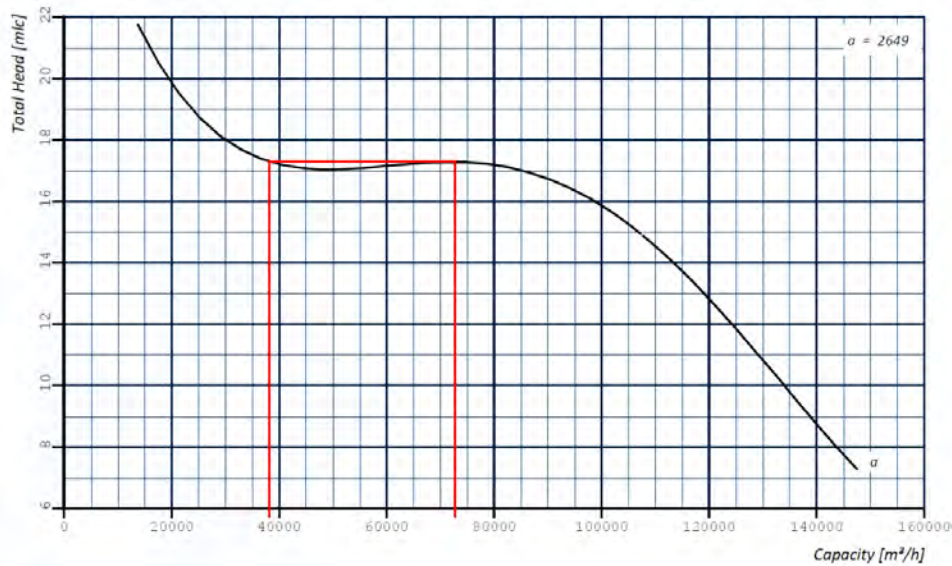


Figure 4.26: Unstable Region Indicated on the Pump Characteristic

One solution for this issue is to operate the pump outside of the unstable region. By avoiding the

range for which the pump characteristic is unstable, any damage to the system can be avoided. The stable region in which the pump can be operated is shown in Figure 4.27.

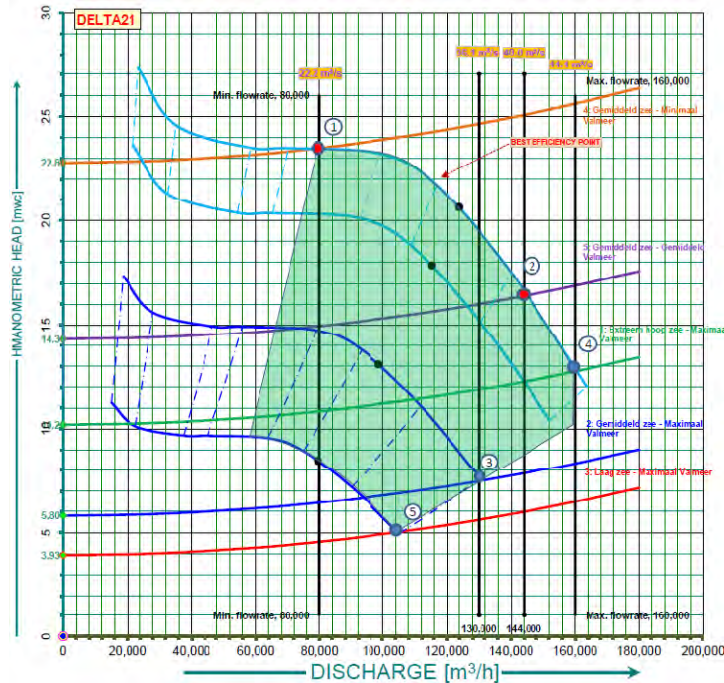


Figure 4.27: Stable Region

Apart from avoiding the unstable region while operating the pump, the penstock and impeller blade should also be able to absorb the impact generated by a sudden change in discharge, for example water hammer, which could cause an excess pressure in the pipe. The maximal change in discharge that can suddenly occur for the unstable region increases with an increase in the rotational speed of the impeller. At the maximal speed of 180 rpm, the maximal change in flow rate which could occur is from 88,000 m³/h to 44,000 m³/h, equal to 12 m³/s. The effects of waterhammer on the penstock are further discussed in Section 9.2 and Appendix Z.

4.16. Maintenance and Accessibility

4.16.1. Halting Flow Through the Installation

For the majority of the maintenance procedures access will be required inside the conduits. In order to do this in a safe fashion the flow through the turbine-pumping installation must be stopped, and an auxiliary pump can be used to further drain the installation. For safety, there must be two barriers present at each inlet and outlet. The level schematic (Appendix A) shows the inclusion of two stop logs at the energy storage lake-side of the installation, and one stop lock at the North Sea-side as well as the emergency gate. The stop logs at the sea-side can be installed and removed using a mobile crane. At the lake-side the installation of stop logs can be done by placement using a crane positioned on a vessel, such as described in Subsection 4.16.2.

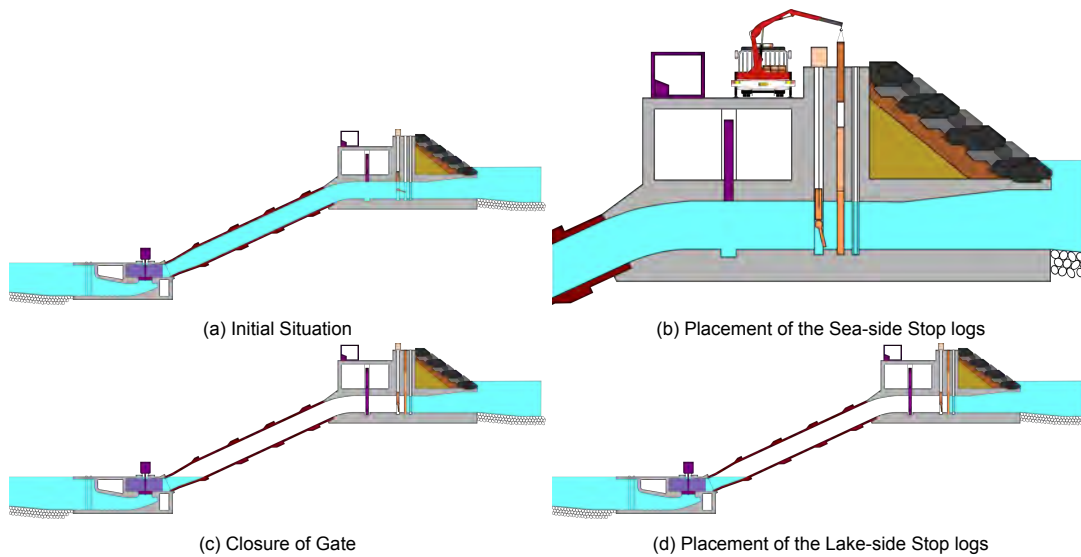


Figure 4.28: Halting Flow in the Pump-turbine Installation

4.16.2. Removal of the Motors, Blades

The most critical maintenance is the removal of the motor and the blades. This could be for inspection, repair or replacement. This will be done using a vessel with a crane, as shown in Figures 4.29a, 4.29b, and 4.29c. The first step is to lower the water level and to halt the flow in the necessary turbine-pumping installations, as described in Subsection 4.16.1. The assumption here is that even if there are damaged pumps which will need replacement or repair, the total amount of pumps is such that the water level can still be lowered to the required level. The next step, before attaching the motor and blades to the crane is to disconnect the motor from the cables, and break the watertight seal between the impeller and the volute. After this, the crane of the maintenance boat can be attached to the motor, and the entire motor-impeller system can be removed from the pump-house.

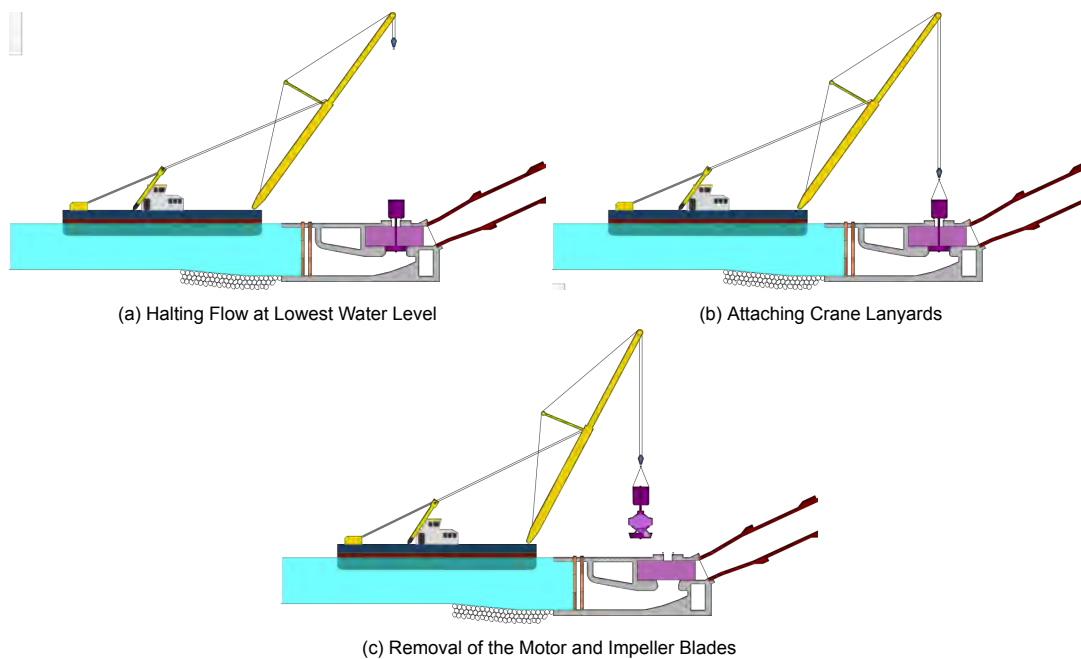


Figure 4.29: Maintenance of Motor and Blades

As discussed at the start of Chapter 4, the benefits of a concrete volute pump are in the ease of installation and maintenance. As can be seen in a real-life example in Figure 4.30, the motor and impeller element is designed to be hoisted into the concrete installation with ease.



Figure 4.30: Hoisting of a CVP Impeller Blade and Bearing (Van Der Ven, 2020)

The next question is determining what to do with the motor and blade assembly once they have been removed from the pump house and are being transported. In order to transport the necessary items from the pump house to dry land, the water level needs to be restored to the maximal level of the energy storage lake. During operation of the energy storage lake for the storage and generation of renewable energy - which is expected to be more or less daily - the water level will vary between the maximal and minimal level various times per day. This means that for maintenance when elements need to be removed from the pump house, no special measures need to be taken that interfere with the operation of the energy storage lake. This only means that the turbine-pumping station will be operating at a slightly reduced capacity, but in this case the large amount of pumps is an advantage when it comes to maintenance or repair procedures.

When the energy storage lake is at its minimal level and the maintenance vessel has removed the required parts, the vessel needs to wait for the water to flow back into the energy storage lake and then transport the parts to the shore. At this point, it is also recommended to remove the lake-side stop logs from the pump house otherwise these will be exposed to very high water pressure when the lake is filled back up.

4.17. Selection of Materials in the Turbine-Pumping Installation

4.17.1. Penstock

Ductile iron pipelines are most common in hydropower applications. These type of pipelines can take up large stresses and deformations, and are also available at larger diameters ($D_N > 2000mm$). The application of ductile iron or even steel as penstock material is the poor corrosive resistance of ferrous metals. For this reason, using steel or ductile iron would require a coating on both the inside and outside

of the penstock. Furthermore, the coating would require thorough maintenance and inspection which would drastically increase the lifetime costs, and may make it interesting to invest in a more suitable material.

The world's first example of a seawater pumped storage station was the Okinawa Yanbaru experiment. This high-head seawater storage system used fibre-reinforced polymers (FRP) for the penstock and tailrace, the main reason for this the high resistance of FRP to corrosion (Pandey, Srivastav, Kulmi, & Prasad, 2016). Furthermore, the frictional properties of FRP are comparable to steel, resulting in low frictional head losses. FRP is also lighter than steel, which would facilitate the installation of the sections during construction (Katsaprakakis, Christakis, Stefanakis, Spanos, & Stefanakis, 2013). The disadvantage of FRP is the lower pressures that can be handled compared to steel of similar sizes.

Rajendran, Arkadu, Dinakaran, Ganapathy, and Murthy (2018) studied the application of FRP pipelines in coastal waters and gave a typical cross section of the pipeline for such a system, the buildup of the layers can be seen in Figure 4.31.

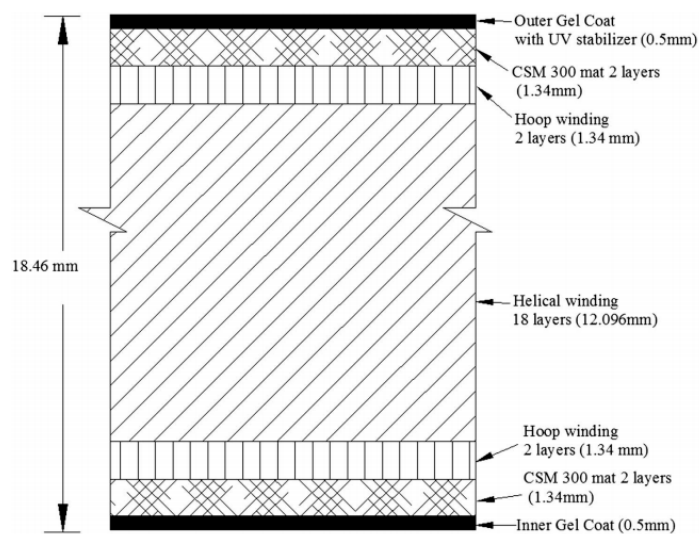


Figure 4.31: Contribution of Winding Layers to FRP Pipe Thickness (Rajendran et al., 2018)

4.17.2. Impeller

Also of importance is the selection of the material of the impeller. Typically in freshwater/brackish pumping applications the material chosen for impellers is an aluminium-bronze alloy. As stated by Gouriou, Robin, and Wintzer (2018), aluminium-alloys have good corrosion resistance, while also maintaining good biofouling properties compared to steel alloys. However, one weakness is the fact that this alloy should be properly heat treated to develop these properties. If there are any manufacturing discrepancies, the impeller blade will quickly be rendered unusable.

An alternative to aluminium-bronze is stainless steel, used frequently in wastewater applications due to the material's corrosive resistance. Stainless steel impeller blades were also used in the Okinawa experiment, and a cathodic protection was applied to further increase the resistance to corrosion Fujihara, Imano, and Oshima (1998). Finally, chrome white iron is another alternative. Chrome white iron is applied mainly in dredging pumps. However, these impeller blades are used for transporting material and designed to avoid abrasion, therefore their application for pumping water would be slightly overdesigned.

Variations on the Basic Design Concept

In Chapter 4 a conceptual design of the turbine-pumping station was made. Several design decisions were made and the reason for the choice was explained. In this chapter, several parameters will be varied. The impact of the varied parameter will be estimated and any other impacts discussed.

5.1. Analysing the Effect of an Increase in the Depth of the Pump-house

As discussed in Section 4.4, the maximal flow rate that the pump can be operated at ($160,000 \text{ m}^3/\text{h}$) is restricted by the cavitation requirements. Section 4.10 describes that the available net positive suction head must always be 1 meter higher than the required net positive suction head. The available net positive suction head is dependent on the available head and this can be increased by decreasing the level of the impeller relative to the water level in the energy storage lake, as shown in Figure 5.1.

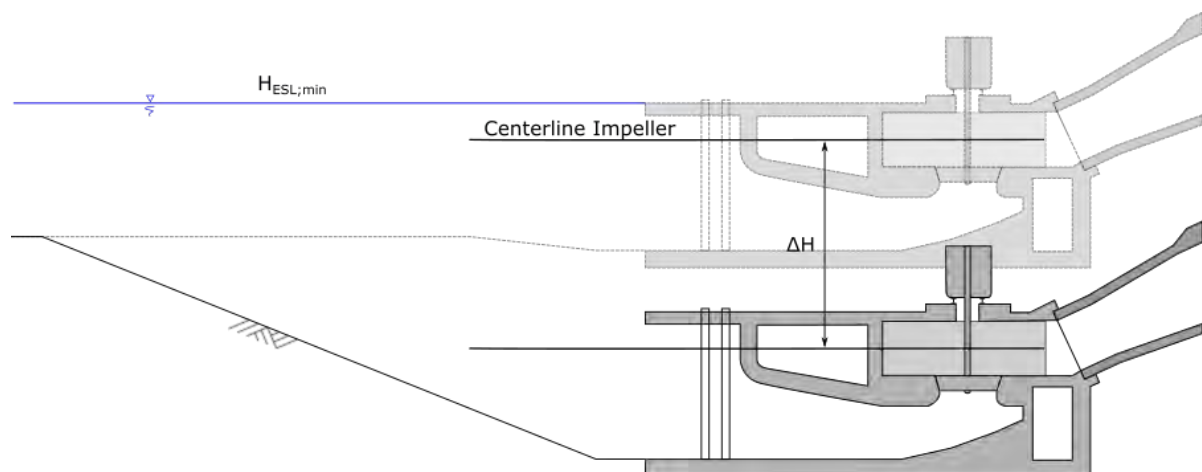


Figure 5.1: Deepening of the Impeller Centerline

Increasing the depth of the pump-house, while maintaining the same minimal water level inside the energy storage lake will allow the pressure head in front of the pump to increase, allowing as well for an increase in the speed of the motor and thus a higher flow rate. The higher flow rate will mean that less pumps are required, decreasing the total width and the material costs. However, the excavation will need to be deeper, which adds to the costs.

5.1.1. Effects of Increased Impeller Speed - 180 rpm

An increase of the speed of the impeller will mean the required net positive suction head is also larger, so an increase of the available net positive suction head is necessary to avoid cavitation. As discussed previously, the increase of the depth of the impeller (as well as the whole pump house) is a straightforward way to increase the available net positive suction head, due to the increase of the static head in front of the pump.

The net positive suction head calculations for 180rpm (Appendix N) show that the impeller will need to be lowered to NAP - 25 m to provide the available net positive suction head with an additional meter of safety margin. This is an increase in depth of 4 meter for the structure as compared to the basic design concept. This increased speed, however, will allow the flow rate to be increased to 46.1 m³/s as can also be seen in Appendix (x). For a flow rate of 46.1 m³/s the total required pumps will be 217 to reach the required 10,000 m³/s. Since the impeller diameter remains the same size, the total width of the turbine-pumping station will be 1867.4 meters in this case, based on the resultant intake width per pump house as discussed in Section 4.8.

5.1.2. Effects of Increased Impeller Speed - 190 rpm

In order to further increase the impeller speed, the depth of the impeller needs to be lowered even more. At an impeller centerline at NAP - 30 meters, the impeller speed can be increased to 190 rpm, which is shown in Appendix P. As can be seen in Appendix Q, the speed of 190 rpm will allow the pump to reach a flow rate of 50 m³/s. The required decrease in depth for this is NAP - 30 m, meaning that the total decrease in depth in comparison to the basic design concept is 9 meters. The increased flow rate will mean only 200 pumps are required for the flood protection requirement, and thus the total width of the turbine-pumping station is reduced to 1721.2 meters.

Speeding up the motor to 190 rpm will mean the peak power of the motor is approximately 10 MW. This is a significant shaft power and will require extra attention to detail to be installed underwater.

5.1.3. Drawbacks of an Increased Impeller Speed

In both cases with a higher impeller speed than the basic design concept the flow rate of the pump is increased quite drastically, but the efficiency of the system suffers as a result. This is even more so the case for the 190 rpm version, and in the system and pump characteristic (Appendix (x)) can be seen that the shift of the pump curves means that the pump is operating mostly in the range of 70 to 80% efficiency. The motor speed can be reduced to increase the efficiency at the same delivery head, but this defeats the purpose of achieving a higher flow rate by increasing the motor speed.

Compared to the basic design concept the total width of the structure is decreased by 238.8 meters and 430 meters for the 180 rpm and 190 rpm versions, respectively. However, the excavation will need to be deeper, and on top of this, the slope leading to the pump house also needs to be at a shallow angle (approximately 1:7) meaning that a significant volume of sand needs to be removed on top of what is originally required for the energy storage lake. If the inner slope of the energy storage lake is also maintained at the same slope as in the basic design concept (1:2) this will mean that the increased depth also means more sand needs to be removed at this side of the pump house. Figure 5.2 gives a schematic reproduction of the additional excavation area required for the two proposed changes to the impeller depth.

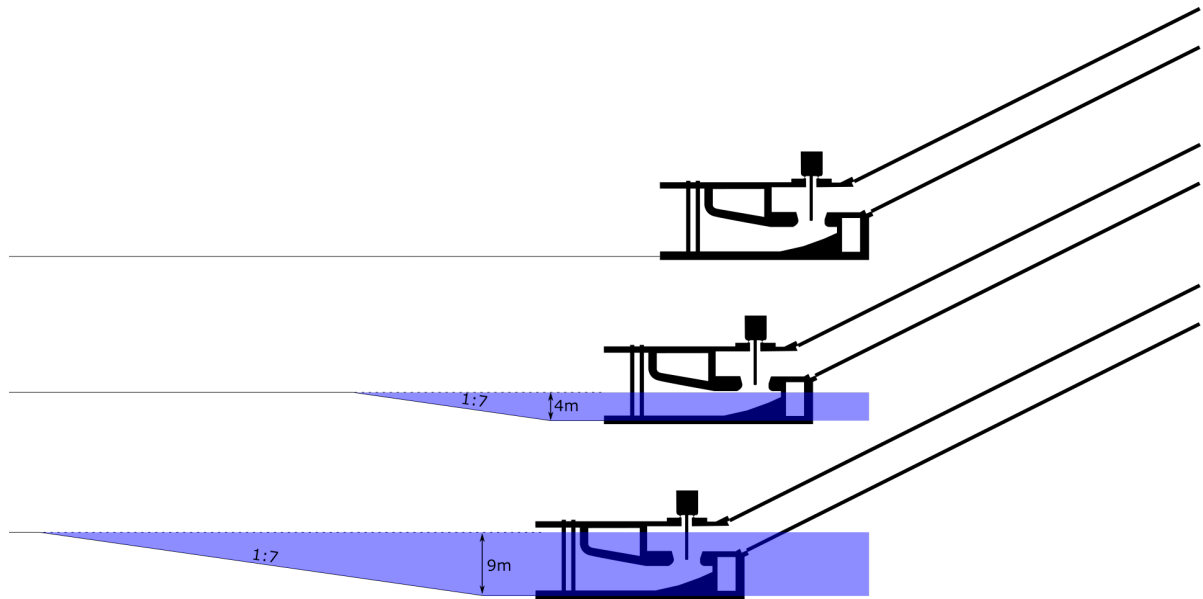


Figure 5.2: Blue Shaded Region Showing the Increased Excavation Volume Required

Using this cross section multiplied by the new width, the total extra excavation volume as well as the increased penstock distance is given in Table 5.1.

Rated Speed [min^{-1}]	Additional Excavation Volume [m^3]	Additional Penstock Length [m]
180	433,237	8.9
190	1,324,450	20.1

Table 5.1: Additional Excavation and Penstock Distance Per Variant

As well as the need to excavate extra material, attention is required to the potential bursting of the bottom due to if the difference of water levels inside and outside the energy storage lake becomes too large during installation. It has been calculated that the maximal depth of the bottom of the energy storage lake is NAP - 27 m to ensure the bottom does not burst open. However due to the increased excavation depth, measures need to be taken to ensure that this does not compromise the stability of the bed of the energy storage lake. During the lifetime of the structure this should not be an issue because the weight of the pump house applies enough surcharge to the soil to compensate for the upward water pressure. However, before installation of the pump houses the water level inside the energy storage lake must be kept above a certain limit. This also means the energy storage lake cannot be emptied before placement of the pump-house, so in-situ construction techniques must be ruled out for these variations.

Finally, the issue of maintenance needs to be addressed for the new variants where the pump house is moved further down. The minimal water level inside the energy storage lake stays the same, but the pump house is deepened. This means that the connection of the motor to the crane for removal of the impeller blades needs to be done underwater. This will extend the duration of maintenance and increase the costs.

5.1.4. Conclusion on the Effects of Increasing Depth and Rotational Speed and Cost Analysis

Table 5.2 shows the results of increasing the depth of the excavation compared to the basic design concept (175 rpm).

Rated Speed [min^{-1}]	Centerline Depth [m - NAP]	Amount of Pumps Required	Total Structure Width [m]
175	21	226	1949.3
180	25	217	1867.4
190	30	200	1721.2

Table 5.2: Results of Various Rated Speeds at Various Depths

In the case of a motor speed of 180 rpm, the reduction in the number of pumps required from 250 to 217 is quite drastic.

Above 180 rpm, the required additional excavation volume and the extra penstock length is quite significant. Although the increase of flow rate is only 11% for the 190 rpm version compared to 180 rpm, the extra excavation necessary is threefold, and a larger motor of 10MW will require extra technical attention to develop for an underwater CVP. In conclusion, it is possible to increase the rotational speed of the pump in order to achieve a flow rate of $50 \text{ m}^3/\text{s}$, but this will likely need special equipment to achieve this.

By analysing the costs related to the extra excavations and the costs saved by decreasing the amount of units, this can help determine whether or not the excavation to increase the net positive suction head is worthwhile.

For the excavation costs, only the extra operational costs related to the dredging will be taken into account. The dredging volume for the entire energy storage lake is approximated at 240 million m^3 , therefore the capital costs will have been made already, and the extra time taken to dredge deeper to accommodate a deeper pump house will be represented in extra operational costs.

For a project of considerable size like Delta21, larger dredgers such as trailing suction hopper dredgers or cutter suction dredgers will most likely be used. The material dredged will most likely be transported to another part of the site to be used for the dunes surrounding the energy storage lake, so the suction dredger used will be discharging with a floating pipeline. The weekly costs of a dredging ship are dependent on its size and power, and according to Bray (2009) this can range from €300,000 for a 1750 kW cutter suction dredger to €930,000 for a dredger with 7600 kW of cutting power. These prices are for 2009 and earlier, so accounting for inflation the equivalents today would be €350,000 and €1,007,000, respectively.

Predicting the duration needed to dredge out the extra necessary material is a difficult task due to the fact that the production of a cutter suction dredger or trailing suction dredger is dependent on so many factors. According to Vlasblom (2005) several factors determining the production rate for a cutter suction dredger are the depth, material type, the pump capacity, pipeline diameter, cutting power, spud arrangement, and the spillage. Furthermore, the weekly dredging production is also dependent on the hours and days worked. Based on the critical velocity and a concentration of $C_{vd} = 30\%$, Vlasblom (2005) made a relation between the diameter of the suction pipe and the production, which can be found in Figure 5.3.

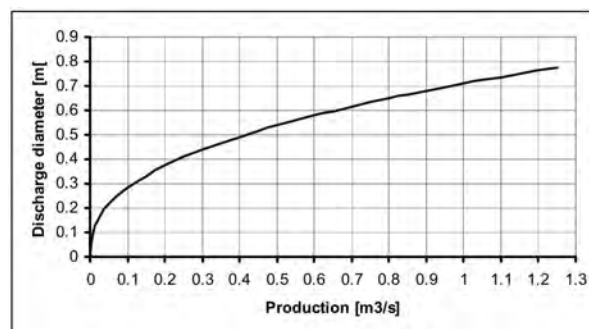


Figure 5.3: Dredging Production based on Pipeline Diameter (Vlasblom, 2005)

Helios is a cutter suction dredger owned by marine contractor Boskalis and has a cutting power of up to 7000 kW and can work at 35 meters depth (Boskalis, 2017). The diameter of the pipeline on the ship is 1000 mm, so according to Figure 5.3 the production on this ship would be 0.7 m³/s. Vlasblom (2005) also explains that more material is produced in the middle of a cut, so when taking the production by the hour, this is 20-30% less than the production by second. All-in-all, accounting for the movement of the ship and a working week of 168 hours (continuous operation) at 75% efficiency, the weekly production is estimated at 254016 m³/week. 1.7 weeks extra would be required for the excavation until 25 meters, while 5.2 weeks would be needed to excavate until 30 meters.

Using the price data from Bray (2009) for a large ship such as the Helios, the extra costs for the 25 meter-deep variant would total at €1.71 million, while for the 30 meter-deep variant this would be coming in at a price of €5.25 million. The weekly production estimates and the price data returns a price of 3.96 €/m³. This estimation can be compared to the price calculated by de Vilder (2017) who estimated it at 3.4 €/m³ for only the operational costs in a similar project but using the grab dredging technique.

5.2. Analysing the Effects of a Change in Impeller Diameter

The so-called affinity laws state how a change in pump rotational speed (Ω) and impeller diameter (D) affect the flow rate (Q) and hydraulic head (H). In Formulas 5.1 and 5.2 the subscript 0 represent the original pump characteristic, speed, and size, while the subscript 1 denotes the adjusted pump variables (Arnold & Nijhuis, 2004).

$$\frac{Q_1}{Q_0} = \frac{\Omega_1}{\Omega_0} \cdot \frac{D_1^3}{D_0^3} \quad (5.1)$$

$$\frac{H_1}{H_0} = \frac{\Omega_1^2}{\Omega_0^2} \cdot \frac{D_1^2}{D_0^2} \quad (5.2)$$

The effect of a change in the pump characteristics can be visualized in Figure 5.4. The parameters of the adjusted pump characteristics (blue) can be seen at the top left and top right of each subfigure.

By adapting the diameter as well as the rotational speed, the pump characteristic can be modified. However, a change in the diameter of the impeller does impact several other things such as the system characteristics and the geometry of the suction box including the total width required per pump. This section will take a look at several options of adjusting the diameter and rotational speed in order to optimize the performance of the pump for the Delta21 turbine-pumping station.

According to Grundfos (2004), a reduction of the impeller diameter which reduces the flow by 20%, will deliver a 33% decrease in the power consumption, as shown in Figure 5.5.

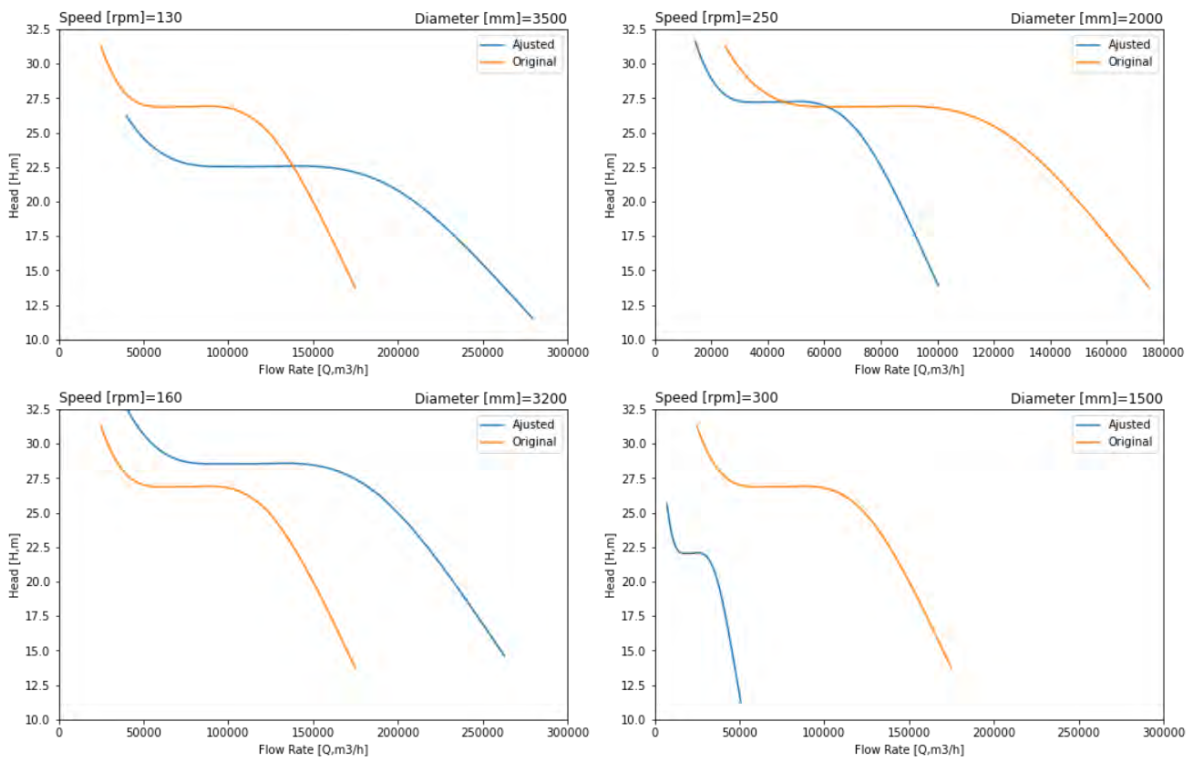


Figure 5.4: Example of the Impact of a Change in Diameter on the Pump Curve

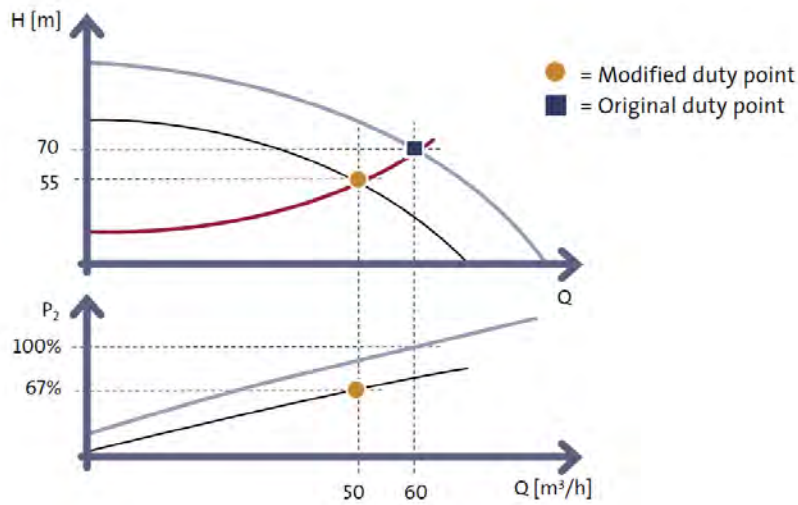


Figure 5.5: Result of a Change in Impeller Diameter (Grundfos, 2004)

In order to determine the effect of the change in diameter impeller, several steps are required and are listed as follows:

1. Generate a pump characteristic based on the original impeller diameter and the affinity laws (Equations 5.1 and 5.2)
2. Insert the new pump characteristic into the system and pump characteristics graph
3. Modify the system characteristics based on the newly chosen impeller diameter. The system characteristics are adjusted such that the flow velocities for pump operation are identical to those

from the basic design concept

4. Apply the new geometries into the system characteristics and adjust the working points of the pump. Since the flow rate and the geometry of the system are interdependent, steps 3 and 4 may need to be iterated.
5. Verify whether the available net positive suction head is adequate based on the steps described in Section 4.10.
6. Based on the maximal flow rate in the flood protection mode (working point #4), determine the number of pumps required to achieve a flow rate of 10,000 m³/s.
7. Calculate the intake width of the suction box as described in Section 4.7. Based on this width the total width of the turbine-pumping station can be determined.

For this analysis, two diameters larger and two diameters smaller than the basic design concept were taken. For the larger diameters the rotational speed of the motor was not changed from the basic design concept (175 rpm). The smaller diameters required an increased rotational speed otherwise the results from these pump characteristics would not be feasible as the required head would not be achieved. For the impeller diameter of 2400 mm, the speed was increased to 206 rpm, whereas for the 2200 mm impeller the required speed was 225 rpm.

Impeller Diameter [mm]	Q_{max} [m ³ /s]	Number of Pumps Required [-]	Total Width [m]	Peak Power [kW]
2200	34.4	291	2142.96	6500
2400	40.3	249	1973.29	7800
2650	44.4	226	1949.32	7800
2800	52.8	190	1714.04	10400
3000	65.2	154	1473.69	14600

Table 5.3: Results of a Change in Impeller Diameter

The result of the analysis of the impeller diameter shows that the decreased intake width due to the smaller impeller diameter does not compensate the lack of flow rate achieved in order to reduce the total width of the structure. The case of the diameter of 2400 mm is an anomaly however, the increase in rotational speed means that a higher discharge can be achieved while the intake width remains relatively small.

For the larger diameters, the results are quite promising, with the total width of the turbine-pumping station well under 2 kilometers. The power required (10-15 MW) to handle these heads and flow rates are quite unrealistic at this stage, taking into account that up to 10% extra power will be required when counting the losses from the electric installations, VSDs, and slip.

Other conclusions are that the change in the system characteristic from a variation of the geometry are quite minuscule and do not impact the working points. This is likely because the system characteristics are relatively flat to begin with.

5.3. Analysing the Use of a Draft Tube Instead of Suction Box

5.3.1. Comparing the Geometry of a Draft Tube vs. Suction Box

In the basic design concept, the lake side pump house has been designed including a so-called suction box. As explained in Section 4.7, the goal of the suction box is to minimize the losses associated with the intake, while optimizing the use of space. The reason for the inclusion of a suction box in the basic design concept is that for mixed-flow pumps this is the most efficient geometry, especially in combination with a concrete volute. The combination of the precast concrete volute and the specialized shape of the intake for the pump means that for pumping operations this suction box is the ideal solution.

On the other hand, for turbine operation, the flow of water is reversed and this means that this suction box shape is not so optimal. Typically turbines use what's called a draft tube. The draft tube is fitted at the end of the impeller for a vertical (Kaplan or Francis) turbine and redirects the flow. The goal of this gradual redirection of flow is in order to preserve the kinetic energy in the flow and convert it to useful potential energy (Soni, Roghelia, Desai, & Chauhan, 2010). The recovery of this static head allows for a more efficient turbine operation, therefore increasing the energy generated by the turbine.

Gubin (1970) collected data from a large range of Soviet and foreign hydro-electric stations. The dimensions of the draft tubes were recorded and a study was done to optimize these. In Figure 5.6 a comparison is made between the draft tube for a turbine and that of a suction box as well as the difference in height. The dimensions used for the draft tube are those recommended for use with mixed-flow turbines of medium and high specific speeds (Gubin, 1970). The geometry for higher specific speeds is different to that of lower specific speeds as the higher specific speeds require more kinetic energy to be recovered.

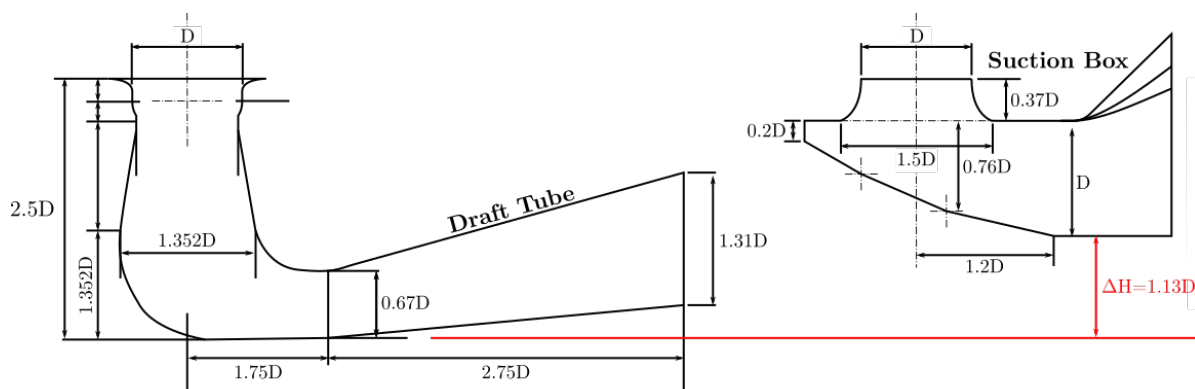


Figure 5.6: Comparison of Draft Tube and Suction Box Geometry

As can be deduced from Figure 5.6 a draft tube requires a greater construction depth equal to 1.13 times the impeller diameter when compared to a suction box and the bottom of the impeller is used as a common datum. For an impeller of 2.65 meters as used in the basic design concept, the extra required excavation depth for the suction box would be 3 meters.

The differences in total structure width are not taken into account for this analysis. The recommended width for a suction box is $2.8D$ while for a draft tube this is $2.74D$. These differences are negligible and are not looked at further. In terms of the length of the structure for the draft tube or suction box no comparison is made either. In the case of the Delta21 turbine-pumping station the length of the pump house required due to the equipment (such as the cooling box which needs to be at a distance of $5D$ from the impeller) is larger than the length suggested by the recommended dimensions. Thus the length required for the equipment is governing and no comparison for this dimension will be made between the suction box and draft tube.

5.3.2. Comparing the Performance of a Draft Tube vs. Suction Box

Due to its shape which is optimized for redirecting flow in both directions, the draft tube is equally capable as the suction box to provide an optimal solution for intake in the case of pumping. Therefore, when comparing the performance of each variant, only the turbine operation will be taken into account. It is assumed that the impact on hydraulic efficiency associated with pumping is equal in both cases.

Without a full computational fluid dynamics (CFD) or other numeric analysis, it is difficult to determine the exact differences in performance associated with a draft tube versus a suction box. However, a crude analysis can be done to give an idea of how the draft tube can improve the energy-generating capabilities of a pump-turbine, compared to a suction box. In order to compare the hydraulic efficiency

of both variants of outlet geometry, it is assumed that in the case of the draft tube the flow is redirected through to the exit without any losses. In the design including the suction box, it is assumed that there is a full loss of kinetic energy at the exit of the impeller blade. By comparing these two results, an idea can be had about the impact hydraulic efficiency in terms of the ability to generate energy.

When discussing kinetic energy in flow, this is best represented by Bernoulli's equation. Equation 5.3 shows the same three terms on either side. The first term, is the potential energy and is simply dependent on the vertical position. The second term, which is dependent on the flow velocity (v), shows the kinetic energy, while the pressure energy is the last term. The difference between the two levels of energy is the energy loss (H_{loss}), which is simply given in meters.

$$z_0 + \frac{v_0^2}{2g} + \frac{p_0}{\rho g} = z_1 + \frac{v_1^2}{2g} + \frac{p_1}{\rho g} + \Delta H_{loss} \quad (5.3)$$

For the design including the draft tube, the loss of the kinetic energy will be taken at the exit of the draft tube, after the flow has been redirected and the tube is widened. In the design with the suction box, the loss of kinetic energy will be taken at the exit of the impeller blade. Both cases will also include friction losses over the entire length of the system. The friction losses are determined by Equation 5.4.

$$\begin{aligned} \Delta H_{loss} &= L \frac{\lambda}{D_h} \frac{v^2}{2g} & (5.4) \\ D_h &= 4R_h \\ \lambda &= \frac{8g}{C^2} \\ C &= 18 \log \frac{12R_h}{k} \end{aligned}$$

In Equation 5.4 R_h is the hydraulic radius, k is the roughness taken as 1 mm, and L is the total length over which the friction loss is calculated. If a constant circular diameter ($\emptyset 3.6m$) is taken and the total length is approximated at 60 meters, the friction losses in the system are equal to $0.000216Q^2$.

The energy losses of both systems are equal to the kinetic energy at the respective outlet points. For the suction box this is at the impeller blade, as shown in Equation 5.5 and 5.6.

$$\Delta H_{loss} = \frac{v^2}{2g} = \frac{Q^2}{2A^2g} \quad (5.5)$$

$$A = 0.25\pi D^2 \quad (5.6)$$

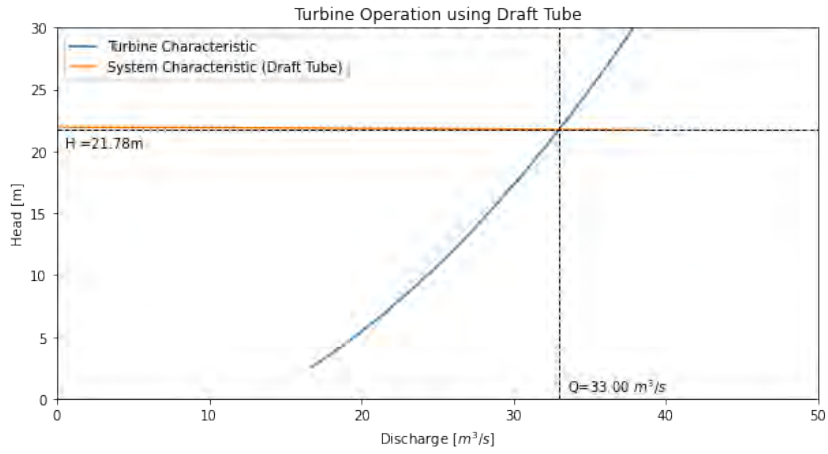
As mentioned in Subsection 5.3.1, the width and height for the exit of the draft tube are equal to $1.31D$ and $2.47D$, respectively. Therefore, the head loss at the outlet for the draft tube design is given in Equation 5.7 and 5.8.

$$\Delta H_{loss} = \frac{v^2}{2g} = \frac{Q^2}{2A^2g} \quad (5.7)$$

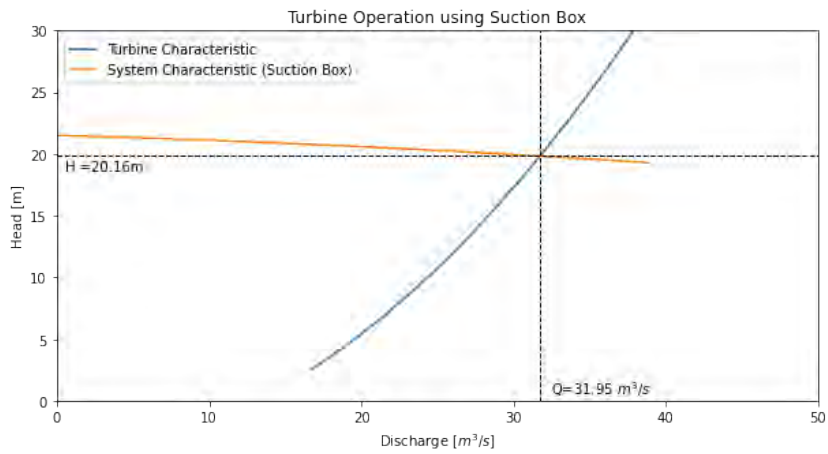
$$A = 1.31D \times 2.74D = 3.56D^2 \quad (5.8)$$

For a diameter of 2.65 meters as used in the basic design concept, the head losses at the exit of the draft tube are in the order of 10^{-5} so these are neglected. As explained in Section 4.4, the system curve represents the head losses in the system. Figures 5.7a and 5.7b show the effect of the system curve on the operation of the turbines for a system fitted with a draft tube and a suction box, respectively.

The available static head in both cases is 22 meters, however the 'useful' resulting head is lower in the case of the suction box, also resulting in a lower flow rate.



(a) Working Point for a Draft Tube at $H_{static} = 22m$



(b) Working Point for a Suction Box at $H_{static} = 22m$

Figure 5.7: Visualization of the Performance Differences Between Draft Tubes and Suction Boxes

Putting both these system curves in the simulation for filling the lake (described in Subsection 4.14.3), the result is shown in Table 5.4 as well as in Figure 5.8.

	Duration to Fill Lake [min]	Total Energy Generated per Pump [MWh]
Draft Tube	1040	54.38
Suction Box	1075	50.63

Table 5.4: Results of the Simulation for Turbine Operation

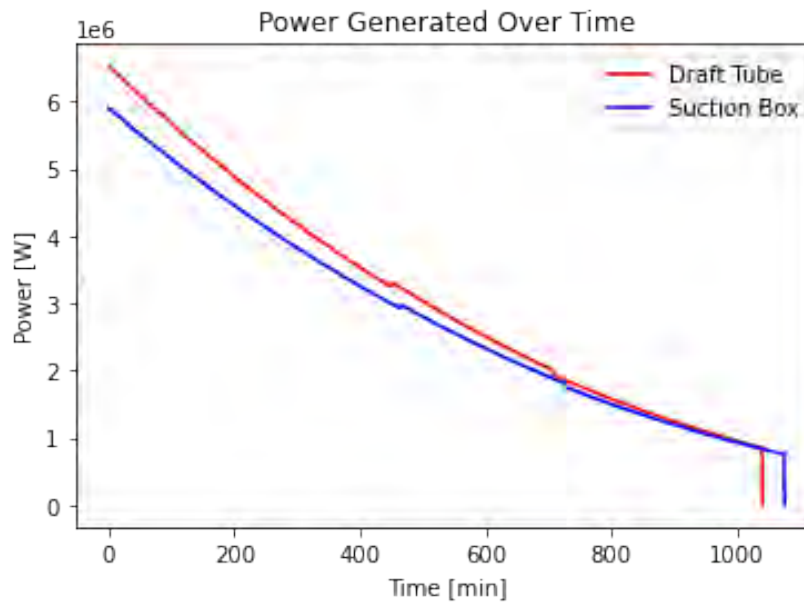


Figure 5.8: Power Generated Over Time

Not only does the draft tube allow for 3.75 MWh more energy generated during a filling cycle of the lake, but the increased speed in which the lake can be filled means the energy storage lake can cycle between generating and storing energy at a faster rate.

5.3.3. Analysing the Costs and Benefits of a Draft Tube vs. Suction Box

In order to evaluate whether or not the draft tube is a worthwhile investment in the scope of the Delta21 turbine-pumping station, a closer look is taken at the investment costs relating to the required excavation and the extra revenue that can be generated as a result of more efficient hydraulics.

For the extra investment costs needed in order to construct the draft tube, only the costs related to the deeper excavation will be examined. Other incurred costs may include the slightly larger structure for the pump houses and the extra material required for this, but these fall outside the scope of this study. The excavation will need to be 3 meters deeper along the entire width of the structure. Using the dimensions from the basic design concept, meaning a width of 1950 meters and a length of 20 meters, the extra excavation required will be equal to 117,000 m³. To determine the cost of this the same approach will be used as in Subsection 5.1.4. The price of 3.96 €/m³ means the investment required to excavate 3 meters further to accommodate the draft tube will be €463,000.

In terms of determining the benefits of a draft tube, this will be calculated by taking the extra revenue coming from the energy generated. The price at which a supplier sells their electricity is quite variant, depending on the demand (time of day) and the source. Currently for the Delta21 energy storage lake, the price at which electricity is bought is estimated to be 0.01 €/kWh and the selling price at 0.05 €/kWh. In the case of the Basic Design Concept, 226 pumps will be operational. With a profit margin of 0.04 €/kWh and a total system efficiency of 65%, the revenue that is gained in filling the lake from NAP - 22 meters to NAP - 5 meters (one full cycle) is €22,330 more with a draft tube as compared to a suction box. If the fact that the draft tube decreases the time to fill the lake by 3.3% is taken into account, then this increased revenue is €23,080 per cycle. A full cycle takes approximately 30 hours, so it can safely be assumed that in accordance to grid demands, every 2 days a full cycle is completed.

If the draft tube increases the profitability of the energy storage lake by €23,000 every 2 days, then it can be assumed that within a month of full-time operation the costs for deeper excavation have been earned back. Furthermore, the benefits of the inclusion of a draft tube go further than the monetary

aspects. Benefits of a better hydraulic efficiency also mean that the mechanical and structural parts endure a longer lifetime, which returns in a lowering of the maintenance costs.

Evaluation & Presentation of the Hydraulic Design

6.1. Introduction to the Evaluation of the Hydraulic Design

So far in the hydraulic design of the Delta21 turbine-pumping station the basis of design has been drawn up, and on the basis of this a reference case has been made. In the Variation on the Basic Design Concept, Chapter 5, certain aspects of the design were discussed which would enable an optimization of the turbine-pumping station. In order to evaluate this analysis various concepts will be generated and then scored based on certain criteria in a multi-criteria analysis (MCA). The MCA will determine the value of each of the concepts, then a cost analysis will be done. Based on the value and the costs, a selection will be made for the best alternative.

6.2. Concept Generation

6.2.1. Parameters for Concept Generation

For each concept, there are 3 parameters that will be changed. The parameters that vary for each alternative are the impeller diameter, the impeller centerline, and whether the intake for the pump will be a suction box or a draft tube. Six concepts are generated and the chosen parameters for these are given in Table 6.1. Concept 1 is the reference case.

	Impeller Diameter (D_{imp}) [mm]	Impeller centerline [meters below NAP]	Intake Design
Concept 1	2650	21	Suction Box
Concept 2	2400	25	Draft Tube
Concept 3	2650	21	Draft Tube
Concept 4	2800	25	Suction Box
Concept 5	2650	30	Suction Box
Concept 6	2650	25	Draft Tube

Table 6.1: Parameters for the Concept Generation

With the amount of pumps required known the total width of the structure can be determined. Since the intake width is dependent on the impeller diameter, the diameter as well as the number of pumps required will return the total width of the structure. The procedure for doing this is found in the Overview Schematic of the reference case, in Section 4.8.

Based on depth of the impeller centerline the maximal rotational speed of the turbine is determined, as per the cavitation verification. These follow from the increasing of the excavation depth, in Section 5.1. The maximal rotational speed, as well as the impeller diameter, will determine the maximal flow

rate (Q_{max}) which can be achieved for each concept.

6.2.2. Characteristics of the Concepts

The selection of the parameters for each concept will determine the characteristics for the design of the turbine-pumping station in each concept. The characteristics will enable the scoring for each criterion to be carried out, as well as giving an indication for the cost analysis.

First, the physical properties of each concept is presented in Table 6.2. This includes the number of pumps required in order to satisfy the flood protection requirement H-DR2. Previously, the flood protection requirement was determined by making the flow-rate equal to 10,000 m³/s, as listed in requirement H-FR2. However, for the verification of the flood protection requirement the number of pumps required will be tested by simulating a storm surge with return period of 1 in 10000 years in combination with a flood wave with a return period of 1 in 1000 years. The amount of pumps required to withstand these two events occurring simultaneously will be used to determine the design of the turbine-pumping station. By withstand, it is understood that the water level in the energy storage lake does not pass above the maximal level (NAP - 5 meters) for the duration of the storm surge. The amount of pumps required and the impeller diameter determine the total width of the structure, which is another physical property. Also, based on the impeller centerline and the draft tube requirements the bottom of the structure can be calculated.

	Pumps Required [-]	Total Width of Structure [m]	Bottom of Structure [m below NAP]
Concept 1	258	2225	30.0
Concept 2	333	2638	36.7
Concept 3	258	2225	33.0
Concept 4	227	2053	34.0
Concept 5	226	1949	39.0
Concept 6	247	2130	37.0

Table 6.2: Physical Characteristics of the Concepts

As well as the physical characteristics of the concepts, the technical characteristics are determined from the simulations. The maximal discharge and pumping power for each concept is given, as well as the power consumed and the power generated by filling the lake. These are collected in Table 6.3.

	Max. Flow Rate [m ³ /s]	Max. Power [MW]	Power Consumed [MWh]	Power Generated [MWh]
Concept 1	44.4	8.39	18597	11467
Concept 2	46.1	7.80	28161	12376
Concept 3	44.4	8.39	18597	12316
Concept 4	46.1	11.36	18403	10981
Concept 5	50.0	10.15	19147	11467
Concept 6	44.4	9.13	18184	12316

Table 6.3: Technical Characteristics of the Concepts

6.3. Multi-criteria Analysis

6.3.1. Criteria for the Determining the Value

In order to determine the value of each concept, the concepts are scored based on several criteria. The first criterion is performance. The performance of each concept is determined by analysing the concepts on three sub-criteria: efficiency, speed, and power generated. The values for these three sub-criteria are taken from running a simulation for emptying the energy storage lake (pumping) and filling the energy storage lake (turbine operation). In terms of efficiency, the ratio is taken between the energy generated from filling the lake to the energy that is consumed while pumping the lake. It is noteworthy

that this is not the peak efficiency of the system, nor the round-trip efficiency. The efficiency value is merely a result of the 2 simulations and indicates the proportion of energy conserved in a full cycle of pumping and turbine operation. Next to efficiency, the speed of the system is determined by adding the time taken to empty the lake and the time to fill the lake. The speed shows the responsiveness of the system and although in real-life operation the lake may not be filled and emptied completely every time, the speed of the total cycle is important for energy storage and generation for augmenting grid stability. Finally, the third sub-criterion for performance is the total power generated by the turbines when filling the lake. This sub-criterion simply takes a look at the magnitude of power generated, regardless of the efficiency or cycle speed.

Constructability and maintenance is another criterium. Constructability takes into account the potential difficulties that may be encountered during the construction phase by some concepts compared to others. For this criterion concepts which require a greater depth during the construction are penalized due to the difficulties and extra construction steps that are required for these concepts. The maintainability is paired with the constructability criterion since the same is valid for maintenance. As described in the Maintenance part of the reference case, Section 4.16, concepts where the impeller centerline is located lower than NAP - 21 meters will required special attention during maintenance. The constructability criterion looks at the total depth required during construction, while the maintainability criterion looks at the depth of the impeller centerline to determine the score.

The eco-friendliness criterion looks mainly at fish survivability rates in the pump-turbine installation. Based on the maximal impeller speed and the flow velocity (dependent on the flow rate) a score is given for eco-friendliness. Higher impeller speeds and flow velocities decrease the fish survivability rate and therefore count for a lower score.

The final criterion is the sensitivity to failure. If one or more pumps breaks down or become damaged, then the energy storage lake must still be able to operate while maintenance is carried out. For this criterion, concepts with a larger number of pumps are considered favorable. The larger amount of pumps will mean that if one pump cannot operate, the total operation of the energy storage lake will be less impacted than if the amount of pumps is smaller to begin with.

6.3.2. Weighting of the Criteria

By far the most important criterion is the performance. Not only is the performance of the system critical in increasing sustainable energy on the grid by storing renewable energy, but the performance is also key to making the energy storage lake financially viable, and therefore making it attractive to investors. Taking this into account, the total weight of the performance criterion will be 0.6. This will be divided into efficiency (0.35), speed (0.15), and power generated (0.1).

The Maintainability & Constructability criterion is weighed at 0.25. The Delta21 project will be already be a technically difficult project to execute, therefore it is important to make sure that the constructability is kept to a maximum. Maintenance will also be an important part of the life cycle of the structure and its elements, therefore it is also important to make sure that this can occur as smoothly as possible.

The weight of the eco-friendliness criterion is 0.1. There will be fish screens stopping marine life from entering the pumping installation in the first place, therefore making sure the fish mortality rates are decreased is more of a backup for if the fish screens fail.

Finally, the sensitivity to failure criterion has a weight of 0.05. The number of pumps for all concepts is between 226 and 333. This number is large enough so that for all the concepts even if 5-10 pumps fail at once (which is highly unlikely) then the percentage decrease in performance is still relatively negligible. It is therefore only a minor benefit to have more pumps.

6.3.3. Scoring of the Concepts for the Multi-criteria Analysis

Scoring of the concepts is done by determining the relative merit, meaning the concepts are ranked in such a way that the best concept(s) for each criterion gets the highest value score (6) and the concept(s) performing the worst for each criterion receives the lowest score (1). The results of the multi-criteria analysis are given in Table 6.4

	Value
Concept 1	4.650
Concept 2	2.550
Concept 3	4.775
Concept 4	3.425
Concept 5	2.200
Concept 6	4.525

Table 6.4: Results of the Multi-criteria Analysis

By comparing the relative merit of each concept to their prices, the best concept can be chosen.

6.4. Cost Analysis

6.4.1. Breakdown of the Costs for the Pump-turbine Station

Much like the scope for the entire hydraulic and civil design of the Delta21 pumping-turbine station, the scope of the costs will only include those directly related to the pump-turbine station. The excavation of the entire energy storage lake as well as the forming of the dunes around it are not taken into account while determining the costs.

The full breakdown of the costs can be split into 3 main categories: mechanical, civil, and electro-technical. These categories are made up by various parts and are listed as follows.

- Mechanical
 - Pump-turbine, drive, and housing
 - Standard Equipment
- Civil
 - Powerhouse
 - ◊ Lake-side Powerhouse
 - ◊ Sea-side Powerhouse
 - ◊ Emergency Gate Housing
 - ◊ Electrical Component Housing
 - Penstock
 - Bed Protection
 - Ground Improvement
 - Dredging/Excavation
- Electrical

In Figure 6.1 a visualization can be found of the components which are included in the determination of the costs.

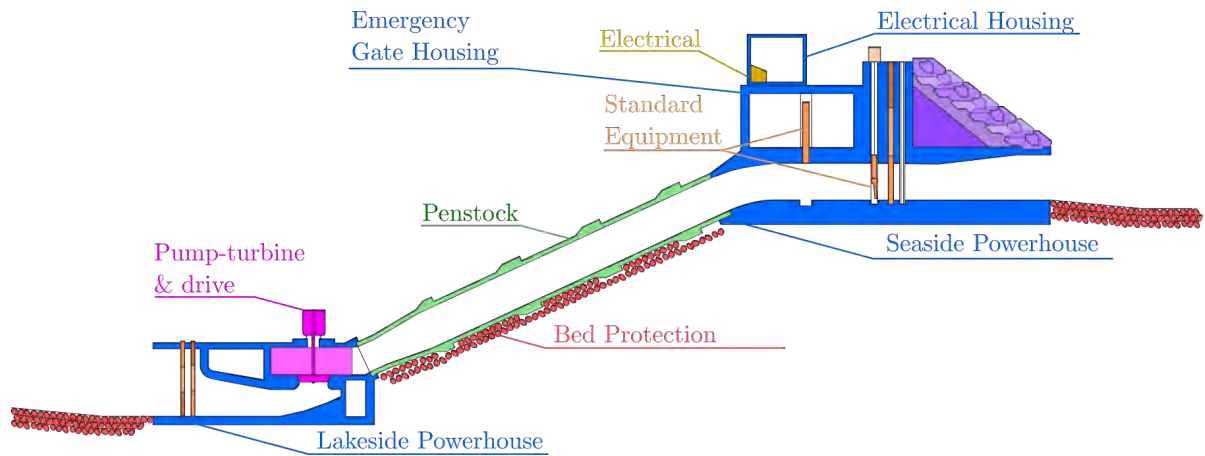


Figure 6.1: Components of the Pump-turbine Installation

6.4.2. Determining the Costs of the Pump-turbine Units

The largest share of the costs will be for the pump-turbine units. Various studies have attempted to determine the price of such a unit based on certain characteristics. Swane (2007) estimated the total price of the turbines (C_t) based on the rated hydraulic head (H_r) as well as the turbine impeller diameter (D_t) per turbine unit (N_t). The price in USD (\$) is given in Equation 6.1. Swane (2007) estimated this price for a tidal power plant in South Korea

$$C_t = 5,500,000 + 118,500 \cdot H_r^{0.18} \cdot N_t \cdot D_t^2 \quad (6.1)$$

Similarly, Vrijling, van Duivendijk, Jonkman, Gilles, and Mooyaart (2008) also determined the cost of a tidal power plant in the Western Scheldt estuary based on the power of the turbine (P_t) as well as the rated head (H_r), per unit (N_t). The estimated cost in EUR (€) is shown in Equation 6.2.

$$C_t = 10,646 \cdot N_t \cdot P_t^{0.7} \cdot H^{-0.26} \quad (6.2)$$

A more accurate description of the cost of a pump-turbine unit is from Pentair. Although the exact calculation method is confidential, the cost is dependent on the maximal power, the rated speed of the motor, and the impeller diameter. The cost is totally inclusive and includes the following:

- Impeller blade and casing
- Motor, gears, and drives
- Design, engineering, quality control
- Testing and installation

The costs of pump-turbine units as determined by Pentair, which will be used, are given in Table 6.5. As can be seen, the two other sources have a large variation ($\pm 25\%$), however the price given by Pentair is still within the range. Also, the price determined by Swane (2007) and Vrijling et al. (2008) do not vary much based on the parameters.

	Pentair	(Vrijling et al., 2008)	(Swane, 2007)
Concept 1	€4,393,192	€3,013,697	€5,467,216
Concept 2	€4,026,378	€2,863,733	€5,275,352
Concept 3	€4,393,192	€3,013,697	€5,467,216
Concept 4	€5,476,618	€3,725,899	€5,467,216
Concept 5	€4,962,376	€3,443,440	€5,591,452
Concept 6	€4,632,508	€3,197,392	€5,467,216

Table 6.5: Prices of Pump-turbine Units

Furthermore, since the Delta21 project will require many units, it is safe to assume a bulk discount on the units is possible. For 200 or more units the bulk discount is assumed to be 10%, while for 300 or more this is assumed to be 15%.

6.4.3. Determining the Costs of the Powerhouse

The 4 components that make up the powerhouse are all made from reinforced concrete. Although all made from the same material, different parts of each structure have different prices. This is because, for example, a floor requires much less formwork and framework than a wall or a column, thus decreasing the labor costs which are included in the price per cubic meter.

Based on estimations from past studies regarding hydropower constructions, a collection of the various prices per cubic meter of reinforced concrete is given in Table 6.6.

	(Paasman, 2020)	(Mooyaart, 2009)	(Swane, 2007)	(Vrijling et al., 2008)			
	Price [€/m ³]	Price [€/m ³]	Price [€/m ³]	Price [€/m ³]			
Roof	550	Wall	850	Reinforced concrete	477	Reinforced concrete	360
Wall	860	Floor	400				
Floor	275						
Column	1600						

Table 6.6: Unit Prices of Reinforced Concrete for Various Structural Elements

In order to be on the safe side, the maximal price for each part of the structure is used in determining the costs. The lakeside powerhouse is split up into walls, floor, roof, and the general price. The other components of the powerhouse structure are calculated using the unit price of reinforced concrete, irrespective of the structural element. Finally, the lakeside powerhouse, the seaside powerhouse, and the emergency gate housing, the calculated volume of Concept 4 has been multiplied by a factor 1.1 as a way of accounting the extra size of the structure due to the larger diameter. For Concept 2 the total volume is multiplied by 0.9 due to the smaller diameter (2400 mm) leading to a smaller structure.

Dimensions for the powerhouse components are taken from the level schematic, Section 4.2. The total costs of the powerhouse for each unit is found by multiplying the amount of units required by the cost per unit.

6.4.4. Determining the Costs of the Penstock

Glass fibre reinforced polymer (GFRP) is determined to be the most suitable material for the penstock due to its corrosion resistance properties, and it still maintains a high degree of strength relative to steel. van Stormbroek (2008) states that the price of GFRP is 4 €/kg. Taking inflation into account and a density of 1800 kg/m³, this is equal to 8406 €/kg in today's world.

Concepts where the impeller centerline is lower have a longer penstock length. This extra length is determined in the Analysis of Increased Depth, Section 5.1. Also, in accordance with the hydraulic

sizing verification steps, the diameter of the penstock along the majority of its length is approximated to be 1 meter larger than the impeller diameter. These two parameters determine the dimensions of the penstock per unit. Finally, the volume of the unit is multiplied by 1.2 in order to account for the overlap of the joints as well as for the possible increase in price due to special treatment applied to the pipes because of their installation in seawater.

6.4.5. Determining the Costs of Bed Protection and Ground Improvement

Bed protection will be required at either side of the turbine-pumping installation as well as under the penstock. Ground improvement will be required in order to provide a stable foundation for the lakeside and seaside powerhouses. Ground improvement will also be required in the cases where the impeller centerline is deeper than NAP - 21 meters, in order to provide stability to the downward sloping pump intake. In both cases, the width that the bed protection and ground improvement is required will be calculated over the total width of the structure.

The unit price for bed protection is 50 €/m³, referenced from Mooyaart (2009). In this study, it is also stated that a safe method for predicting the distance required for the bed protection is to set it equal to the length of the structure. Therefore, it is predicted the length of bed protection on both the seaside and lakeside of the structure is 20 meters, at a thickness of 1 meter. For the bed protection underneath the penstock less is required, so a thickness of 0.5 meter is assumed. Although not technically required, the width for the bed protection under the penstock is taken as the total width of the structure.

Mooyaart (2009) also states that the unit price of ground improvement for the foundation is 10 €/m³. However, due to the complicated, underwater nature of the installation, the unit price is assumed to be 50 €/m³. For all concepts the cost of ground improvement underneath the powerhouse is included. For the concepts where the impeller centerline is lower than 21 meters below NAP, the cost of ground improvements of the slope leading down towards the lakeside powerhouse is taken. The slope is assumed at 1:7, so the length over which it is required is approximately 7 times the depth to which the excavation is required. The ground improvement over the total width of the structure is once again used.

6.4.6. Determining the Costs of Electrical and Automation Installations

The costs of the electrical installations (including the electric installation housing) has been estimated by an electrical expert within Royal HaskoningDHV. For this reason, the costs are much higher than the civil costs even though they are less substantial. The electrical costs can be found summarized in Table 6.7, this instance is an example for Concept 1 with 258 pumps.

	Units	Unit Price		Total Cost
Transformer 120/11kv 250MW	10	€ 5,000,000.00		€ 50,000,000.00
Switchyard 120 kV	2	€ 15,000,000.00		€ 30,000,000.00
MS Switches incl. measuring points	258	€ 100,000.00		€ 25,800,000.00
VSD incl. transformer 8,5MW	258	€ 800,000.00		€ 206,400,000.00
110kV cables	2	€ 25,000,000.00		€ 50,000,000.00
11kV cables	4	€ 50,000,000.00		€ 200,000,000.00
Electrical Installation Housing	258	€ 150,000.00		€ 38,700,000.00
Automation Pumphouses	258	€ 100,000.00		€ 25,800,000.00
Automation General	2	€ 500,000.00		€ 1,000,000.00
				€ 627,700,000.00
Unforeseen			25%	€ 156,925,000.00
Totaal				€ 784,625,000.00

Table 6.7: Costs of the Electrical Installations

6.4.7. Presentation of the Total Costs per Concept

Based on the costs for various elements and the calculations which can be found in Appendix R, a breakdown of the total cost is given in Table 6.8. The civil costs have been multiplied by 1.2 in order to account for extra installation costs or further unforeseen costs.

	Civil (x1.2)	Mechanical	Electrical	Total
Concept 1	€ 274,520,872	€ 1,020,099,320	€ 784,625,000	€ 2,079,245,192
Concept 2	€ 332,607,491	€ 1,139,666,429	€ 892,437,500	€ 2,364,711,421
Concept 3	€ 275,154,147	€ 1,020,099,320	€ 784,625,000	€ 2,079,878,467
Concept 4	€ 273,490,415	€ 1,118,873,084	€ 740,062,500	€ 2,132,425,999
Concept 5	€ 259,724,008	€ 1,009,347,399	€ 738,625,000	€ 2,007,696,407
Concept 6	€ 272,880,148	€ 1,029,806,660	€ 768,812,500	€ 2,071,499,308

Table 6.8: Total Costs per Concept

6.5. Evaluation & Selection

As can be seen from the breakdown of the total costs in Table 6.8 the mechanical costs account for the vast majority of the total costs, from 77% to 81%. Also, the difference between the mechanical costs are quite low. Between the concept with the highest mechanical cost (Concept 2) and the one with the lowest cost (Concept 3) there is only a 10% difference. What this tells us is that the even though the concepts with high power and high flow rates require less units in total, the high costs of these units put together does make the concepts cheaper than the ones with more units but at lower costs per unit.

Seeing as the price of the mechanical elements (pump-turbine unit and motor) dominates the costs, it is interesting for the Delta21 concept to find a way to reduce this. Making the concepts with the larger pump-turbines and motors less expensive would allow for a reduction in the civil costs, and subsequently make the Delta21 an economically viable and attractive project.

In terms of the variability for civil costs, this is slightly larger than for the mechanical costs, with a difference of 22% between the most expensive civil concept (Concept 2) and the cheapest concept in terms of civil costs (Concept 5). As can be from Figure 6.2 there is a strong link between the width of the total structure and the civil costs.

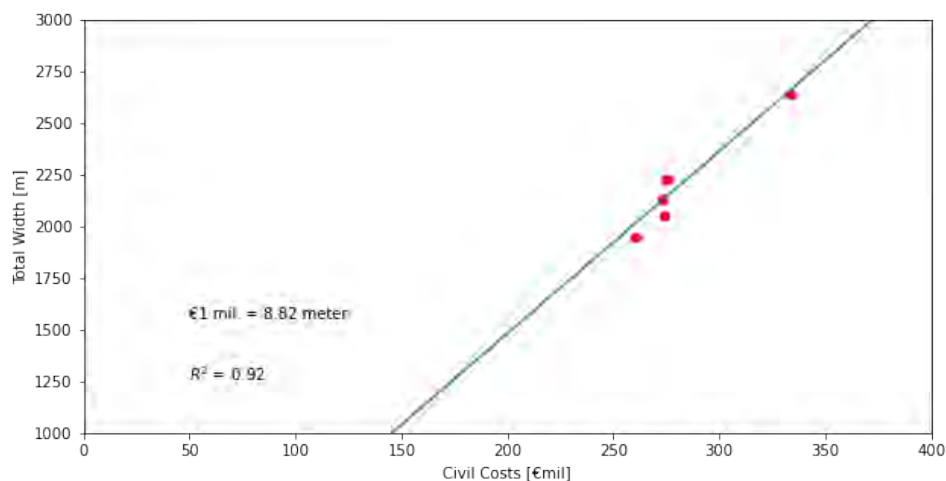


Figure 6.2: Costs per Width

However, the link between the construction depth and the costs of the civil works is not clear. As can be seen from Figure 6.3 there is no clear relation between the construction depth of each concept

and the costs of the civil works. This is possibly due to the very low costs of the dredging works which is maximally 0.5%, and even when the price of the dredging works is increased to 10 €/m³ this accounts for maximum 1.3% of the total costs. Another reason is the link between the depth of the construction and the lesser width required. However, the fact that the width is relevant to the total civil cost is not in line with the fact that for most civil projects the costs increase for greater construction depths as opposed to greater widths.

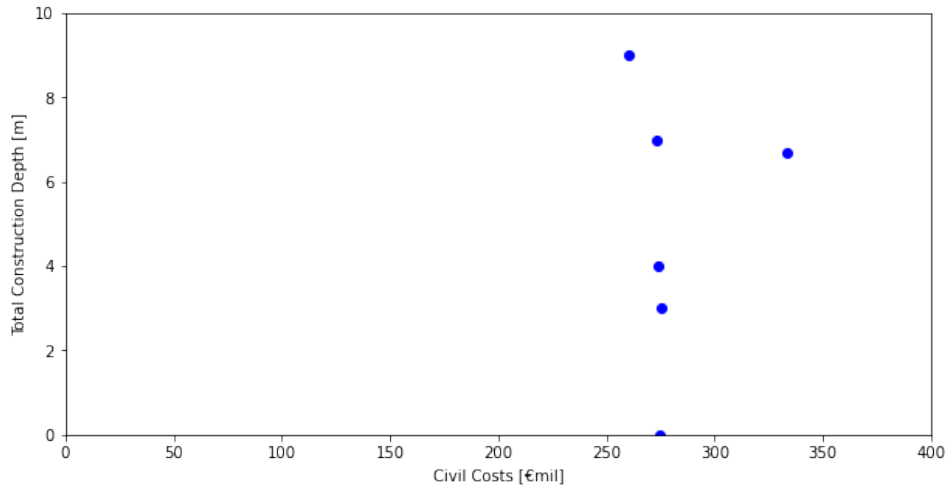


Figure 6.3: Costs per Depth

In order to make a selection, the value and costs of the concepts are compared with each other. This can be done by plotting the costs and value of each concept against one another. This is shown in Figure 6.4. From this figure it can be seen that Concept 3 marginally outperforms Concept 1 and Concept 6. Concept 5 offers a financially more attractive solution, however scores quite low. The relative price of Concept 2 is much too high to consider, while Concept 4 also performs poorly.

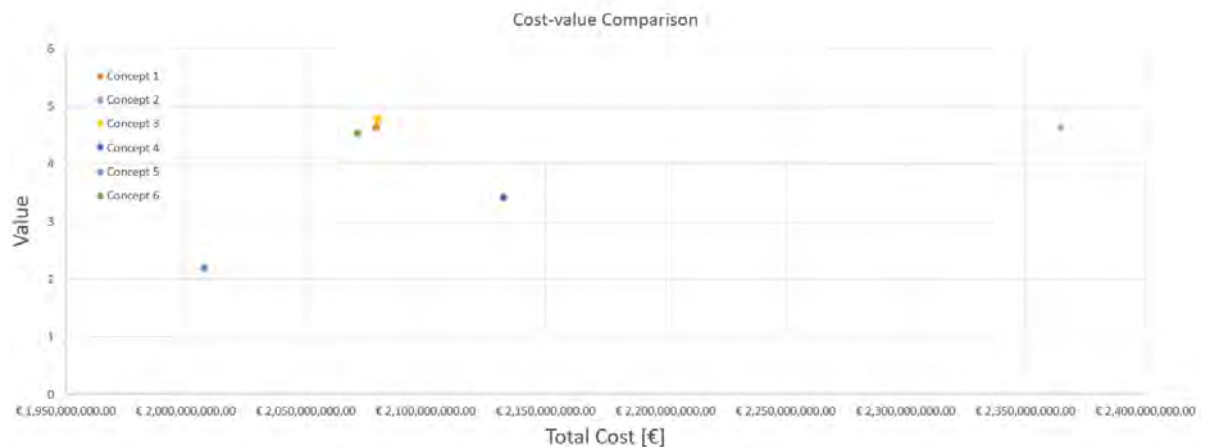


Figure 6.4: Cost-Value Analysis

6.6. Presentation of the Preferred Hydraulic Design

The chosen concept (Concept 3) is the same as the concept which was worked out in the Basic Design Concept, Chapter 4, except that instead of a suction-box design for the pump inlet, the lakeside powerhouse has the draft tube shape. Part of the level schematic for this adjusted design can be found in Figure 6.5. The full level schematic can be found in Appendix S

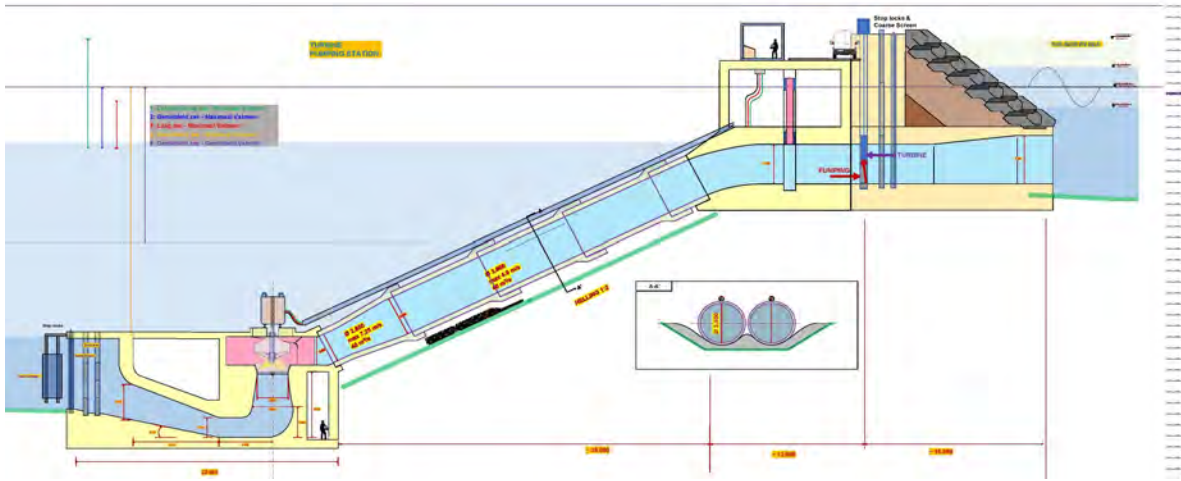
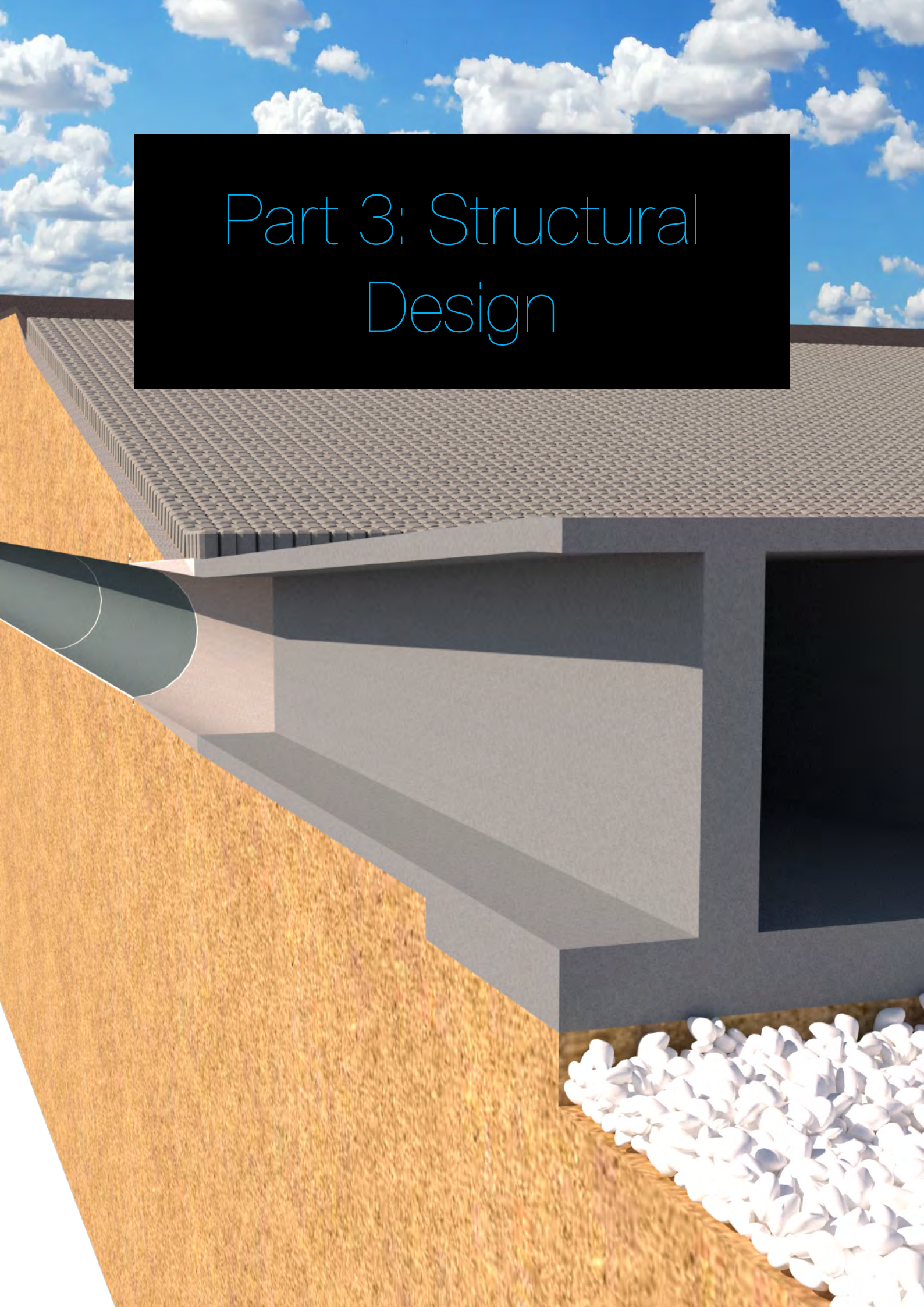


Figure 6.5: Level Schematic for the Chosen Hydraulic Design

Part 3: Structural Design



Constructability

7.1. Applied Construction Methods

In Appendices V, T, and U three different construction methods are presented for the execution of the turbine-pumping station. The difference in these methods is the selection of the temporary retaining structure. This section will discuss the advantages and disadvantages of each method, and in Section 7.2.2 the chosen construction method and sequence is presented. The construction method using caissons (Appendix V) and the method using a cofferdam (Appendix U) are a combination of prefab and in-situ methods, while the construction pit method (Appendix T) is completed entirely in-situ.

The caisson method (Appendix V) involves the use of caissons as temporary structures in order to create a building pit for the construction of the emergency gate housing, sea-side inlet, and electrical installations. Special attention should be paid to the connection between the sheet piles and the caissons in order to create a watertight connection. A seal can be applied to the underside of the caisson which forms a special connection to the top of the sheet piles, and monitoring equipment should also be used to check for potential leakage. The turbine-pumping station is built in segments, and caisson elements are reused for each segment. For this a trade-off needs to be made in the amount of caissons that are being reused and the speed of construction. Using less caissons will leave a smaller environmental footprint due to less concrete used, but will mean the duration of the construction will be prolonged. The main drawbacks of this method are the techniques required to ensure watertightness and the extra duration due to needing to transport the caissons and subsequently fill them with ballast, and then empty them and transport them again when the in-situ construction is finalized. The main advantages are that the construction of the lake-side pumphouse can be done simultaneously with the sea-side elements, cutting the duration of the project, as well as the fact that the space required is less than that of the construction pit.

The cofferdam method (Appendix U) is similar to the caisson method, except sheet piles are used for the entire depth of the construction pit. Due to the large depth to which they have to be installed the sheet piles are braced, which decreases the size of the building pit compared to the caisson method. However, if good execution of the sheet piles is ensured, then watertightness should not be an issue. If the strength/stiffness aspects are not fulfilled for sheet piles, they can be upgraded to combi-walls. The main advantage of this method is that sheet-piles are the cheapest option for temporary retaining structures as they can be reused. Also, this method is likely to be the fastest since the installation and removal of the sheet piles takes less time than the retaining measures of the other two methods. As with the caisson method, the prefabrication and installation of the lake-side pumphouse can be done during the cofferdam execution of the sea-side elements. The disadvantage of this method is that the space available inside the cofferdam is restricted based on the maximal length of the struts.

The construction pit (Appendix T) allows for a total construction of the turbine-pumping station in-situ. The embankments on either side of the pit can be made from local material, which is a large advantage. However, due to the large width and length of the turbine-pumping station, a very large construction pit will be made. This presents the main challenge, which is dewatering this large volume.

It estimated the total width of the construction pit will be 550 meters, and approximately 2 kilometers long. Aside from this, the construction pit method is a tried-and-tested method and was the chosen construction method for the Haringvlietdam, as can be seen in Figure 7.1.



Figure 7.1: Construction Pit for the Haringvlietdam (Slagboom, 1965)

7.2. Construction Sequence

7.2.1. Construction Sequence for the Energy Storage Lake

Although the energy storage lake as a whole does not form part of the scope of the structural design, a general description of the construction sequence for the energy storage lake itself is given.

Figure 7.2 shows the initial situation and red dashed line shows the area that is to be excavated to provide the main basin area for the energy storage lake.

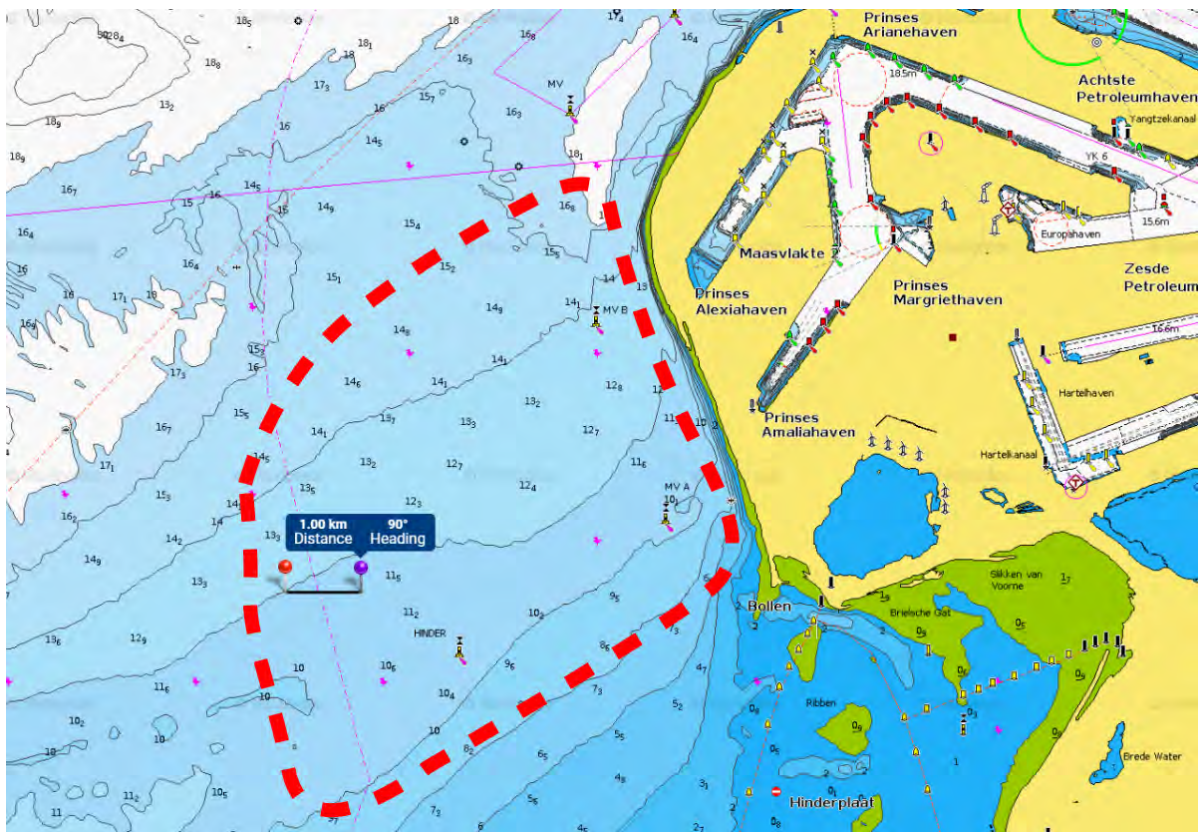


Figure 7.2: Initial Situation and To-be Excavated Area (Red Dashed Area)

The area of the basin, which is 20 km^2 , initially has a depth varying between 9 and 14 meters. If the average depth of 12.5 meters is taken, and the depth to which the energy storage lake is 27.5 meters, then the total volume of sand that will be excavated is approximately $3 \cdot 10^8 \text{ m}^3$.

The dunes which are going to form the outer banks of the energy storage lake have an average cross section of approximately 10500 m^2 , following from the size of the dune as given in Figure 7.3.

Considering the average sand needed per meter of dune section, the volume excavated is good for approximately 29 kilometers of dune. Since the area of the turbine-pumping station requires less material, as well as the eastern border which is located landwards, this is more than enough, and means no extra sand will be required for the construction of the energy storage lake.

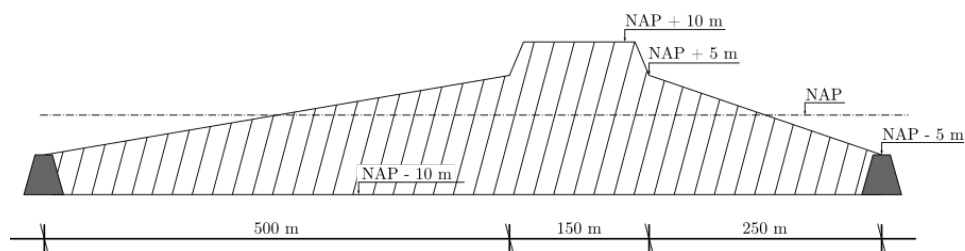


Figure 7.3: Average Cross Section of a Dune, Adapted from Lavooij and Berke (2019)

The first step of the construction of the energy storage lake, as shown in Figure 7.4, involves the creation of the dunes at the northern edge of the lake. The dredging of the approximately 8 kilometers of dunes will require 84 million m^3 of sand, so about a third of the excavated area of the energy storage lake. The placement of the dunes at the northern edge first will allow for sheltered conditions from

waves for the rest of the construction of the energy storage lake and the turbine-pumping station. The dunes at the northern edge will also allow for land access to the construction site of the turbine-pumping station.



Figure 7.4: Step 1: Establishment of the Northern Dune Front

After the reclamation of the dune area at the north, the work island as well as part of the southern edge can be constructed, as shown in Figure 7.5. During this step a road connection can be made for the work island as well as for the construction area of the turbine-pumping station.



Figure 7.5: Step 2: Construction of the Work Island and Infrastructure

The final dunes are placed at the south-western edge of the energy storage lake, as shown in Figure 7.6. As well as this, the bottom of the bed at the location of the turbine-pumping station is made level.



Figure 7.6: Step 3: Construction of the Southern Dunes Connecting the Spillway, Barrier and Pumping Station

After the last construction phase for the energy storage lake itself, the turbine-pumping station will be constructed, after which the spillway can be constructed. The construction of the pumping station first will mean that the energy storage lake is not closed off from the north sea yet. When the spillway is being constructed and the energy storage lake is closed off from the north sea, the turbines or pumps in the pumping station can be used to regulate the level of the energy storage lake and possibly compensate for the tidal current velocities during closure.

7.2.2. Construction Sequence for the Turbine-Pumping Station

The chosen construction method is the cofferdam method. The steps are presented in the following figures. A more detailed construction sequence can be found in Appendix U.



Figure 7.7: Installation of the Prefabricated Pumphouse

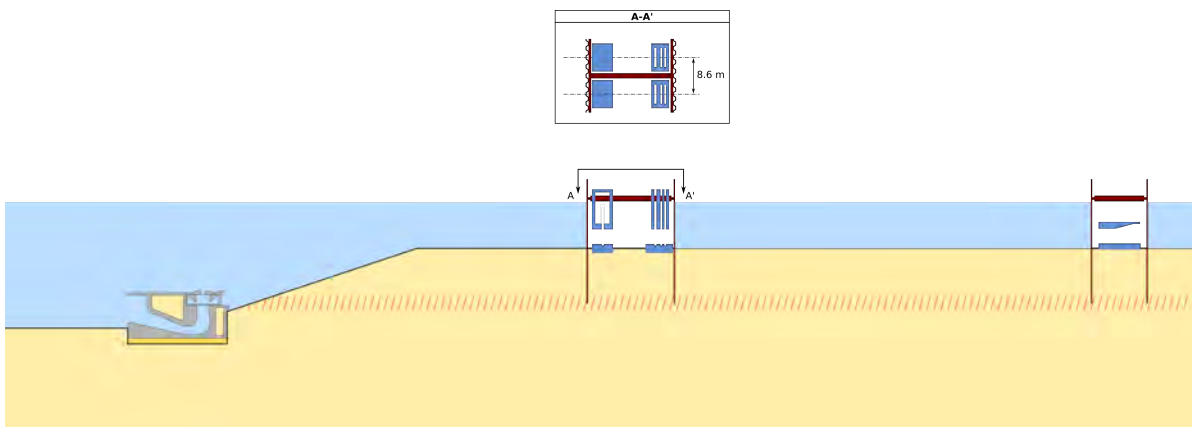


Figure 7.8: In-situ construction of the emergency gate housing and sea-side inlet inside cofferdams

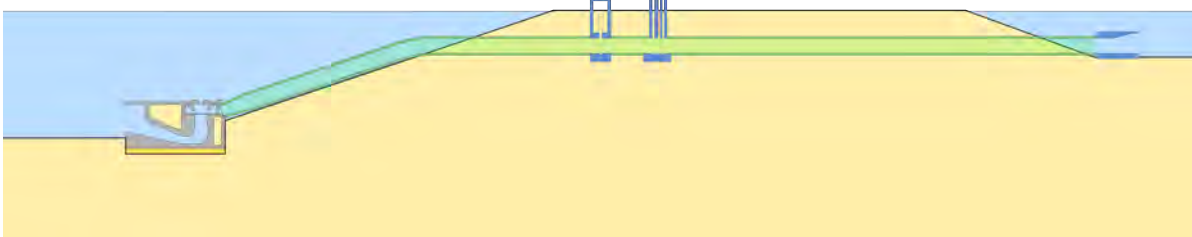


Figure 7.9: Removal of the cofferdams and backfilling of the dike core material

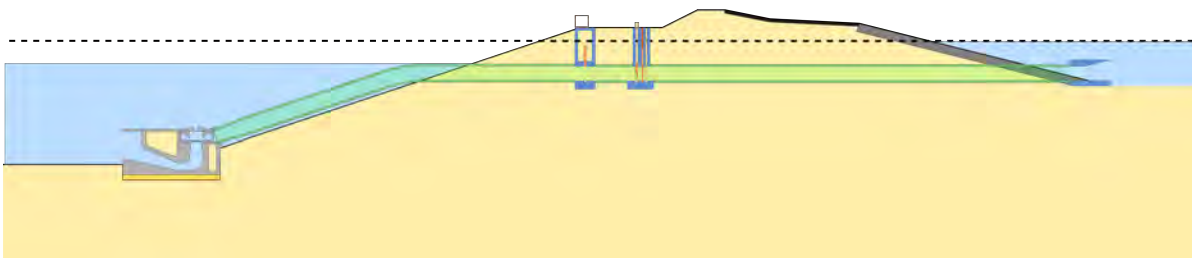


Figure 7.10: Construction of the dike revetment, finishing of the powerhouse, and installation of the standard equipment

8.1. Stability of the Sea Dike

8.1.1. Design of the Sea Dike

The body of the dike will incorporate the main elements of the turbine-pumping station and will function as the main barrier between the energy storage lake and the North Sea. The outer slope of the dike, facing the North Sea, will consist of two slopes separated by a berm. The outer slopes will be 1:4 while the berm is at a slope of 1:20. Following the outer slopes, there will be a narrow crest (2m) behind which there will be area for the emergency gate housing, electrical installations, and an access road. The inner slope leading to the energy storage lake will be sloped at 1:3. The integration of the elements of the turbine-pumping station into the sea dike is shown in Figure 8.1.

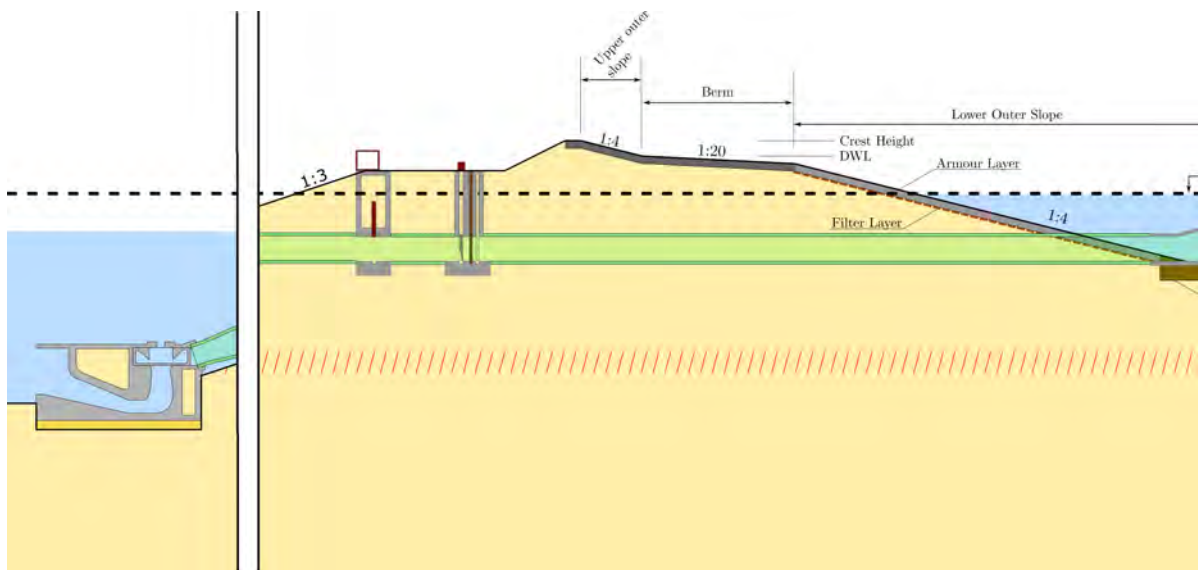


Figure 8.1: Visualization of the Integration of the Elements into Sea Dike

For the berm width, TAW - LZEM (1999) recommends a width of approximately $4 \cdot H_{m0}$, while EurOtop (2007) states that a berm loses its functions if it is wider than a quarter wavelength (L_0). Using the significant wave period determined in Subsection 3.4.2, the deep water wave length can be found using Equation 8.1 (Holthuisen, 2007).

$$L_0 = \frac{g \cdot T_s^2}{2\pi} = 65.76[m] \quad (8.1)$$

The chosen berm width is 12 meters, which is between the required widths suggested by EurOtop (2007) and TAW - LZeM (1999).

8.1.2. Determining the Crest Height

Apart from the design water level (DWL) for a given reference period, there are several surcharges in addition to this which determine the height of a dike or other hydraulic structure. According to TAW - WRWOD (2002) these are as follows:

- (a) Oscillations, storm surge, seiches
- (b) Predicted sea level rise during the lifetime of the structure
- (c) Wave overtopping
- (d) Settlements, compaction and/or ground subsidence

Figure 8.2 visualizes the required construction height for a dike.

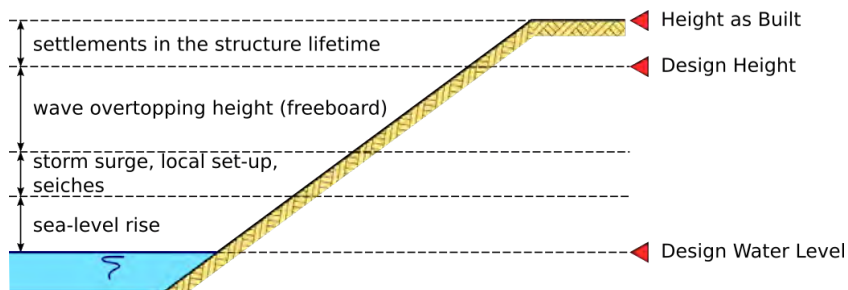


Figure 8.2: Calculation of Dike Height, Adapted from TAW - WRWOD (2002)

The water level of NAP + 5.26 m with an exceedance probability of 1:10,000 years which was determined in the Hydraulic Boundary Conditions, Section 3.4.1, already takes the surcharge (a) into account. Also discussed in 3.4.1 is the predicted sea level rise of 0.65 m in the lifetime of the structure. According to Schiereck (2005) the settlement for an embankment can be estimated at 0.5 meters, however, due to the limited presence of weak soil layers (clay), the settlement will be estimated at 0.3 meters.

Finally, in order to determine the crest height of the sea dike as built the wave overtopping height, or freeboard, needs to be calculated. The calculation of the freeboard takes into account the allowable overtopping discharge, which is usually measured in l/s/m or if divided by a factor 10^3 , $m^3/s/m$. The Overtopping Manual classifies the overtopping discharges as shown in Table 8.1 (EurOtop, 2007).

Overtopping Discharge	Result
$q < 0.1$ l/s per m:	Insignificant with respect to strength of crest and rear of structure.
$q = 1$ l/s per m:	On crest and inner slopes grass and/or clay may start to erode.
$q = 10$ l/s per m:	Significant overtopping for dikes and embankments. Some overtopping for rubble mound breakwaters.
$q = 100$ l/s per m:	Crest and inner slopes of dikes have to be protected by asphalt or concrete; for rubble mound breakwaters transmitted waves may be generated.

Table 8.1: Overtopping Discharge Classification as Shown in EurOtop (2007)

Due to the fact that the energy storage lake is located behind the dike and that overtopping will not directly have a negative impact on the surroundings, the allowable overtopping discharge of 10 l/s/m is

chosen. However, this does mean special attention to the overtopping discharges must be taken into account in the design of the inner slope.

For certain hydraulic conditions and dike geometry, the overtopping discharge (q) is dependent on the freeboard height (R_C) as shown in Equation 8.2 (EurOtop, 2007).

$$\frac{q}{\sqrt{g \cdot H_{m0}^3}} = \frac{0.067}{\sqrt{\tan \alpha}} \gamma_b \cdot \xi_{m-1,0} \cdot \exp\left(-4.75 \frac{R_C}{\xi_{m-1,0} \cdot H_{m0} \cdot \gamma_b \cdot \gamma_f \cdot \gamma_\beta \cdot \gamma_v}\right) \quad (8.2)$$

In Equation 8.2, the constants γ_b , γ_β , γ_f , γ_v are the influence factors for the berm, wave angle of attack, roughness, and for a vertical wall, respectively. The presence of a berm means the parameter γ_b is equal to 0.65. The rest of the influence factor parameters are equal to 1.

The breaker parameter ($\xi_{m-1,0}$) relates the wave steepness ($H_{m,0}/L_0$) to the slope steepness ($\tan \alpha$), in this case 1/4. From Subsection 3.4.2, the significant wave height and the period are 2.82 meters and 6.49 seconds. This returns a deep water wave length of $L_0 = 65.8$ meters, and therefore the breaker parameter is 1.2.

Filling in these variables for Equation 8.2, shows that a freeboard height of 2 meters allows a mean overtopping discharge of 13 l/s/m during governing wave conditions. This is determined to be acceptable. Furthermore, the settlement is estimated to be 0.3 meters, this is on the safe side for a structure built entirely on sand, but is verified in Section 8.6. Finally, the surcharge of sea level is 0.65 meters, this is established in the boundary conditions, in Section 3.4.1.

NAP + 5.26 m: Design water level (1/10000 years)
+ 0.65 m: Sea level rise
+ 0.30 m: Settlements
+ 2.00 m: Freeboard
NAP + 8.21 m: Crest Height as Built

8.1.3. Stability of the Armour Layer

The armour layer located on the lower slope will be subject to a large quantity of wave attacks, so first it should be determined what kind of wave is breaking on the slope. For the wave parameters discussed earlier, the breaker parameter (ξ) is around 1.2 indicating it is a plunging breaker.

Klein Breteler (1992) developed a numerical method for determining the thickness required (D) for an armour layer of placed blocks. The numerical method was simplified into an equation, for which the one for a plunging breaker type is given in Equation 8.4.

$$\Gamma \Delta D \cos \alpha = \left(\frac{\Lambda \sin \alpha}{0,34 \xi_0} \cdot \left\{ 1 - \exp\left(\frac{-0,061 \cdot \xi_0^2 \cdot H}{\Lambda \sin \alpha \cdot \sqrt{\tan \alpha}}\right) \right\} + \frac{\Delta \sin \alpha}{2} \right) \cdot \left(1 - \exp\left(\frac{-0,72 \cdot \xi_0 H}{\Lambda \sin \alpha \cdot \sqrt{\tan \alpha}}\right) \right) \quad (8.3)$$

$$\Gamma = \Gamma_1 + \Gamma_2 + \Gamma_3 \quad (8.4)$$

$$(8.5)$$

The parameter Γ is an influence parameter which combines the effects of friction, inertia, and in-flow. Using several diagrams it was taken at 1.425. The leakage length (Λ) was taken as 1.5 which corresponds to the value for blocks. Finally, the resulting required thickness was found to be 37 cm.

Using the graphic from Figure 8.3, also by Klein Breteler (1992), returns a slightly smaller thickness of 0.3 meters, with $a = 0.9$ and $\xi = 1.2$, the failure wave height ($\frac{H}{\Delta D}$) is 4.5.

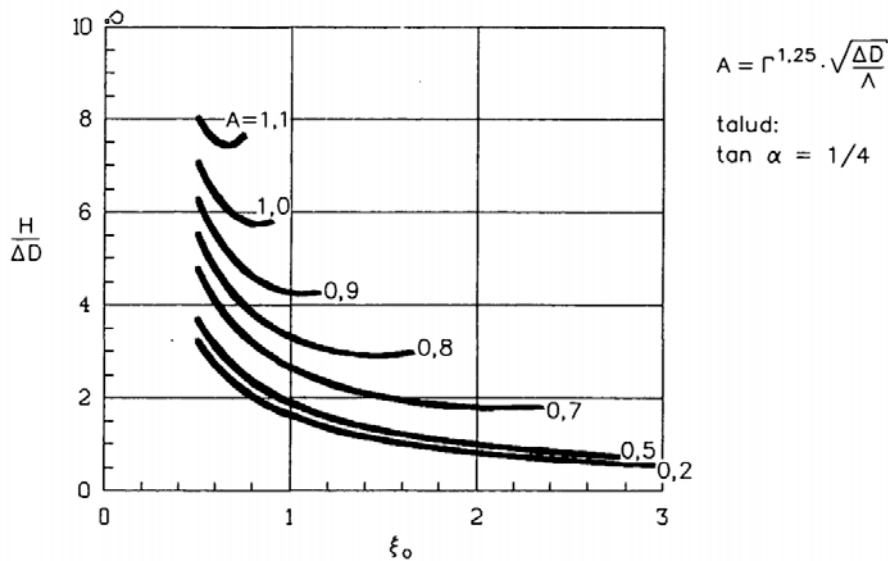


Figure 8.3: Wave Breaker Parameter vs. Failure Wave Height (Klein Breteler, 1992)

8.1.4. Stability of the Asphalt Revetment

Waves The primary check to determine whether the thickness of the asphalt layer (h) is suitable is for the wave impacts that can be expected during a storm. The stress (σ) in the asphalt due to wave impact can be determined by using a flexible beam model which was schematized by TAW (2002) and the formulas for which can be found in Equations 8.6 and 8.7.

$$\sigma = \frac{p_{\max}}{4\beta^2\beta z} [1 - e^{(-\beta z)}(\cos(\beta z) + \sin(\beta z))] \frac{6}{h^2} \quad (8.6)$$

$$\beta = \sqrt[4]{\frac{3c(1 - \nu^2)}{Sh^3}} \quad (8.7)$$

p_{\max} : maximal wave impact pressure [Pa]

z : width of the wave impact ($= \frac{H}{2}$)

c : Winkler bedding constant of sand = $100 \cdot 10^6$ [Pa/m]

S : asphalt E-Modulus = $10 \cdot 10^9$ [Pa]

ν : Poisson constant of asphalt = 0.33 [-]

Equation 8.6 requires an extensive computation due to the various wave impacts during a storm and the fatigue behaviour of asphalt that decreases the failure stress. Therefore the results of these equations for a storm of duration 10-20 hours is given by Figure 8.4. For asphalt on a sand layer with a significant wave height of 2.82 meters, the required thickness is approximately 0.15 meters.

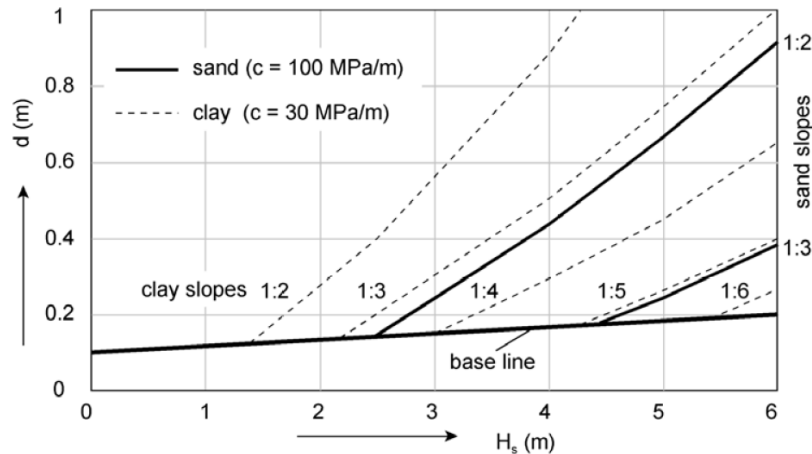


Figure 8.4: Required Asphalt Thickness Based on Significant Wave Height (Schiereck, 2005)

As can be seen in Figure 8.4, the required thickness for asphalt on shallow sand layers is quite low, even for large significant wave heights. This is due to the high stiffness of the sand layer.

Uplift & Shear Due to the fact that the asphalt is directly on a permeable layer, there is a chance that excess pore pressures cause uplift or shear. The uplift force (H) on an impervious layer is shown in Figure 8.5 and can be determined using Equation 8.8 (Schiereck, 2005).

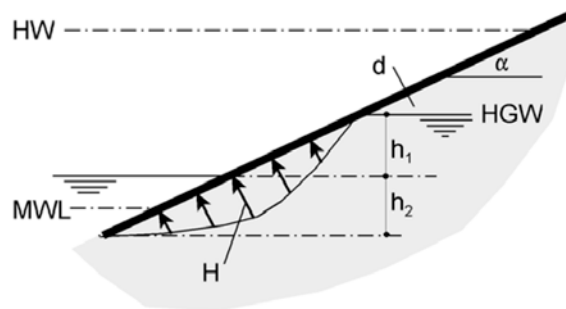


Figure 8.5: Uplift Force on an Asphalt Layer (Schiereck, 2005)

$$H = \frac{h_1}{\pi} \arccos \left[2 \left(\frac{h_1 + h \cos \alpha}{h_1 + h_2} \right)^{\frac{\pi}{\arctan(\cot \alpha) + \pi/2}} - 1 \right] \quad (8.8)$$

In these equations Δ represents the relative weight of asphalt concrete to water, so is equal to 1.4. The f in Equation 8.10 represents the friction coefficient between asphalt and sand, estimated at 0.5. For the shear check, Schiereck (2005) states that spring tide conditions are suitable to determine the required conditions. However, for uplift design conditions must be used, so in this case a storm surge of NAP + 5.56 m is taken.

For coastal areas, the high ground water level (HGW) can be approximated as $0.5(HW-MWL)$, where $HW-MWL$ is the difference between high water and average water level.

The checks for uplift and shear check the vertical and horizontal balance of the layer of asphalt perpendicular to the slope, respectively. The thickness required (h) due to uplift is given in Equation 8.9 and due to shear in Equation 8.10.

$$\frac{H}{\Delta h} = \cos \alpha \quad (8.9)$$

$$\frac{H}{\Delta h} = \frac{f \cos \alpha - \sin \alpha}{f} \quad (8.10)$$

For the uplift check an initial value of $h = 0.15$ m is taken. This returns an upward excess pressure (H) of 0.7, which then returns a required thickness $h = 0.67$. The calculation is repeated several times and the required thickness converges at 0.51 meters.

For spring tide conditions ($HW = NAP + 1.22$ m) the thickness 0.51 meters returns an excess pressure $H = 0.24$ m. After repetition of the calculation of Equation 8.8 and 8.10, the thickness required to resist shear during spring tide conditions is 0.32 meters.

The resistance of the asphalt layer to uplift is governing in the case of the Delta21 turbine-pumping station and the required thickness is 0.51 meters. The transition between the upper slope asphalt revetment and the lower slope block armour layer is shown in Figure 8.6. The bottom of the layer flares out in order to distribute the normal stresses in the layer as a result of the self-weight of the asphalt layer shearing off the slope. The filter layer underneath the armour block layer becomes encapsulated in the transition between the asphalt and block layers.

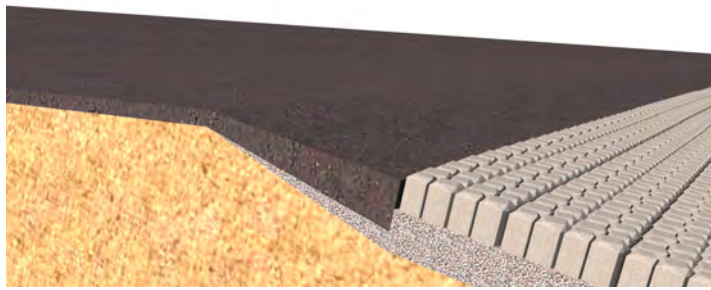


Figure 8.6: Transition Between the Asphalt and Block Layers

8.2. Piping Checks

Piping is a phenomenon which occurs when a difference in water level causes a flow of water through sediment (usually sand and more permeable soils), which causes the soil underneath the structure to erode. This erosion can cause the entire superstructure to become unstable, hence why it needs to be checked. The head difference on either side of the structure is the main propagator in erosion which is why it is determined first. The development of piping can take time, which is why in the case of piping underneath the turbine-pumping station a head difference (ΔH) of 22.5 meters is taken, neglecting the storm surge level which could increase the head difference but does not occur for longer than 48 hours.

Lane and Bligh each determined a formula to determine the seepage length, given in Equation 8.11 and 8.12, respectively.

$$L \geq \gamma \cdot C_L \cdot \Delta H, \text{ where: } L = \sum L_{\text{vert}} + \sum \frac{1}{3} L_{\text{hor}} \quad (8.11)$$

$$L \geq \gamma \cdot C_B \cdot \Delta H, \text{ where: } L = \sum L_{\text{vert}} + \sum L_{\text{hor}} \quad (8.12)$$

Neglecting the presence of the clay layer at NAP - 22 meters and the seepage screen, the governing (largest) seepage length is given by Bligh is 405 meters, and for Blane's method this is 168.75 meters. The horizontal seepage distance from the toe of the dike at the seaside is 125 meters, so according to Bligh 4 sheet piles (or other seepage screens) would be required to a depth of NAP - 45 meters

($\sum L_{\text{vert}} = 35$ m per screen), and according to Lane 3 seepage screens would be needed to extend down to NAP - 31 meters ($\sum L_{\text{vert}} = 21$ m per screen). These piping prevention measures are quite strenuous.

Fortunately, however, the CPT for the location nearby the turbine-pumping station indicates a clay layer 3 meters thick around 22 meters below NAP, and another thinner layer located below the bottom of the energy storage lake. Unfortunately, on the other hand, it can not be assumed that these indicated clay layers are present everywhere along the turbine-pumping station.

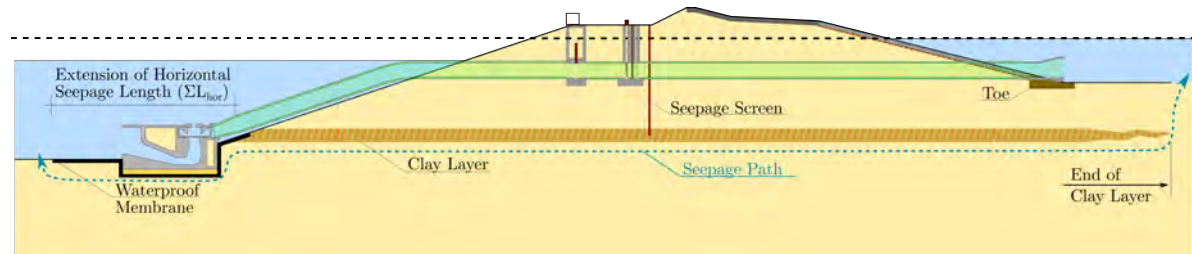


Figure 8.7: Extending the Horizontal Piping Distance by Means of a Waterproof Membrane

8.3. Bed Protection Design and Stability

8.3.1. Flow Velocities

Due to the fact that they are the main drivers of sediment transport, the flow velocities need to be determined in order to check the stability of the bed protection at the sea-side and lake-side of the structure. At the sea-side, the velocities are comprised of three components: the orbital motion as a result of wave action, the flow velocity as a result of the pump-turbine operation, and the velocity as a result of tidal currents. In the case of the sea-side bed protection the maximal flow velocity is either a combination of ebb currents and pumping operation, or flood currents and turbine operation.

IJntema (2021) studied the predicted impact of the construction of the Delta21 project on the tidal flow. Three models were used to predict the tidal flow velocities at varying locations. For the sea-side of the pumping station the average flow velocity of the three models was predicted to be 0.70 m/s for flood and 0.89 m/s for ebb.

The flow velocities are discussed in the Hydraulic Sizing, Section 4.6. The maximal flow velocity at the sea-side outlet during pumping is 1.94 m/s, while for turbine operation this is 1.40 m/s. Combining the effects of the tides and the operation of the pump-turbines, the maximal flow velocity to be expected at the sea-side outlet is 2.64 m/s.

The maximal orbital velocity at the bed (u_b) is added with the velocity of the currents in order to

At a depth of 10 meters, the waves are their transition between deep and shallow water, thus the wavelength must be calculated iteratively using Equation 8.13. With the wave parameters known, the orbital velocity can be determined, shown in Equation 8.14 (Schierneck, 2005).

$$L = \frac{gT^2}{2\pi} \tanh kh = 54.16 \text{ m} \quad (8.13)$$

$$u_b = \frac{\omega a}{\sinh(kh)} = 0.95 \text{ m/s, where: } k = \frac{2\pi}{L} \text{ and } \omega = \frac{2\pi}{T} \quad (8.14)$$

8.3.2. Bed Protection at the Sea-side Inlet

The Chezy coefficient (C in Equation 8.16), indicates the roughness. The formula for the Chezy coefficient is given in Equation 8.15, where the hydraulic radius has been simplified to the depth (since the width of the area is not stated). Accounting for irregularities in dumping the bed protection from barges, the value k_r is taken as $5d_{n50}$ (Schierreck, 2005).

$$C = 18 \log \left(\frac{12h}{k_r} \right) \quad (8.15)$$

The flow velocity and the sizing of the bed protection are interdependent, therefore they must be solved iteratively. Using Shields's formula for the threshold of motion, the median nominal diameter of the topmost layer of bed protection can be found. Schierreck (2005) states that a good value for the Shields criteria (ψ) is 0.03. Using Equation 8.16 the median nominal diameter can be found.

$$d_{n50} = \frac{\bar{u}_c^2}{\psi_c \Delta C^2}, \text{ where } \psi_c = 0.03, \Delta = \frac{\rho_s - \rho_w}{\rho_w} = 1.65, \bar{u}_c = 3.59 \text{ m/s} \quad (8.16)$$

Solving Equations 8.15 and 8.16 iteratively results in a bed protection with a median nominal diameter (d_{n50}) of 0.18 meters, which gives a Chezy value of $38.4 \sqrt{\text{m/s}}$. No safety factor is attached to this because the likelihood of the tidal currents, pumping currents, and the orbital velocity from the waves all creating a flow velocity in the same direction are quite small.

The resultant median nominal diameter corresponds to a quarry stone with gradation 5 - 40 kg, with nominal diameters of 0.17 - 0.21 meters (Laan, 1996). This class (LM_A 5-40) requires a minimum thickness of 255 mm, 1.5 times the d_{n50} . The sand upon which the bed protection is placed has a d_{85B} of 1 mm, following Worman's formula the filter layer above it should have a d_{15T} of 13.5 mm. Although a bit large, the coarse grading CP32/90 can be used as a filter layer, which would only require a bed protection consisting of two layers.

The sand which is located at the site of the turbine-pumping station has a median diameter of 0.15 mm, or 0.00015 m. Rearranging Equation 8.16, and setting the critical Shields parameter (ψ_c) equal to 0.05, the critical velocity (\bar{u}_c) for sediment transport can be found using Equation 8.17.

$$\bar{u}_c = C \cdot \sqrt{\Delta \cdot d_{n50} \cdot \psi_c} = 0.355 \text{ m/s} \quad (8.17)$$

The eventual scour hole that will form behind the sea-side bed protection can be estimated by assuming the velocity in the scour hole reaches a depth such that the velocity is equal to the critical velocity for sediment transport. To this end, the depth of the scour hole can be (conservatively) approximated. Using Equation 8.18 and Figure 8.8 as reference, the length required for the bed protection can be determined (Schierreck, 2005).

$$\frac{h_{se}}{h_0} = \frac{0.5\alpha\bar{u} - \bar{u}_c}{\bar{u}_c} \quad (8.18)$$

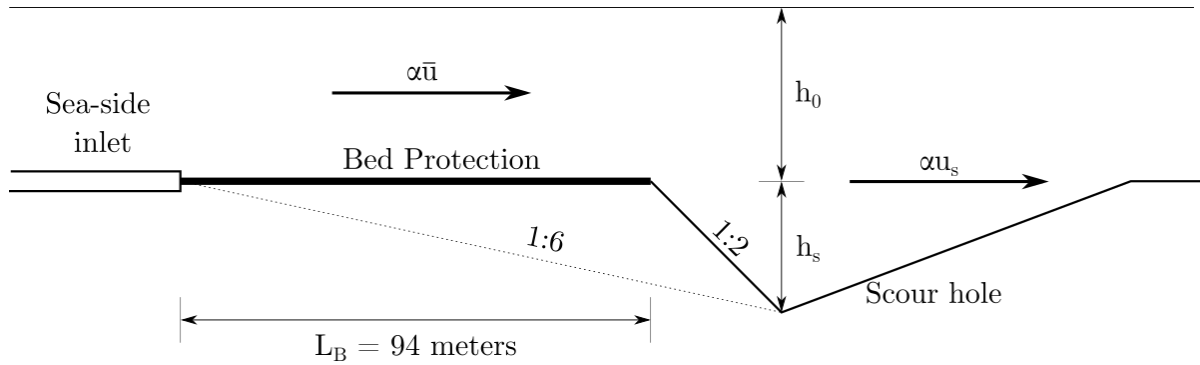


Figure 8.8: Scour Hole and Bed Protection Length, adapted from Schiereck (2005)

In Equation 8.18 the influence of the turbine pumping station has been left out, since it is at a suitable distance away from the scour hole. Also the value for α is 2.5. This results in a scour hole of 23.5 meters and thus a total distance of 94 meters for the bed protection.

8.3.3. Bed Protection at the Lake-side Inlet

For the design of the bed protection at the lake-side inlet the influence of the tides can be left out of the calculations. For the rest, the procedure to determine the size and distance of the bed protection is the same as in the sea-side design, Subsection 8.3.2.

Since the wave conditions and the pumping/turbine discharges vary for different levels inside the energy storage lake, the situation which results in the velocity needs to be determined. The maximal velocities for pumping and turbinning can be found in Appendix F and G, while the maximal orbital velocities from wave actions are found using Equation 8.14. The resulting velocities for different water levels inside the energy storage lake are compiled in Table 8.2

Level ESL [m \pm NAP]	Depth [m]	Pumping Flow Velocity [m/s]	Turbine Flow Velocity [m/s]	Orbital Bed Velocity [m/s]
-5	22.5	0.91	0.32	0.06
-13.25	14.25	0.82	0.42	0.20
-22.5	5	0.74	0.65	0.65

Table 8.2: Flow Velocities Inside the ESL for Different Water Levels

From Table 8.2 it can be found that the governing flow velocity is at the minimal depth of the storage lake, during turbinning operations. At this point the combined flow velocity is 1.39 m/s.

Once again iterating Equations 8.16 and 8.15, the value for d_{n50} is 0.01 m, and the Chezy coefficient (C) is $60.3 \sqrt{m}/s$. This median nominal diameter corresponds to a mine stone with gradation 0/70 mm (Laan, 1983).

The variability of the water level inside the energy storage lake makes it hard to determine a suitable length of the bed protection. However, it can be seen that at deeper water levels the actions of waves are negligible, and that the flow velocity from turbine or pump operation is reduced by the depth of the lake. Therefore, it is assumed the water level of NAP - 22.5 m (depth of 5 meters) is the critical level for scour development, and a bed protection length of $10 \cdot h_0 = 50$ m is selected.

8.4. Stability of the Cofferdam

8.4.1. Design of the Cofferdam Structure

The cofferdams in which the emergency gate housing and the sea-side inlet will be constructed are installed to a depth of NAP - 22 meters, in the middle of the first (thicker) clay layer. In that way they form a natural seal and water can be pumped out without having to install an underwater concrete floor for the entire length of the cofferdam.

For the retaining height of the temporary structures, significant wave height and storm surge water levels are taken into account. Since the structures are temporary and no danger is present to the general public the acceptable failure probability can be assumed much lower than that of the finished structure. Still, the safety of the workers should be considered, and an acceptable probability of 1 in 100 years is assumed. This leads to a maximal water level of NAP + 3.85 meters and a significant (reduced) wave height of 2.08 meter with a period of 5.56 seconds. The reduction of the wave height based on the geography of the construction site is elaborated in the Boundary Conditions, Subsection 3.4.2.

8.4.2. Bursting of the Bottom

During the step 2 (Figure 7.8) of the construction sequence, Subsection 7.2.2, a cofferdam is used as a temporary retaining structure. The cofferdam is pumped dry and part of the bottom is excavated. In this section, the stability of the bottom will be checked for heave of the clay layer at NAP . If the check returns negative, underwater concrete and/or tension piles will need to be installed to ensure the watertightness of the cofferdam.

Bursting of the bottom occurs when the water pressure under the clay layer is greater than the pressure of the clay layer itself and the layers on top of it. The governing situation, when the cofferdam is empty and the water level has been decreased to a level of NAP - 12 m (1 meter below the bottom of the construction pit), is shown in Figure 8.9.

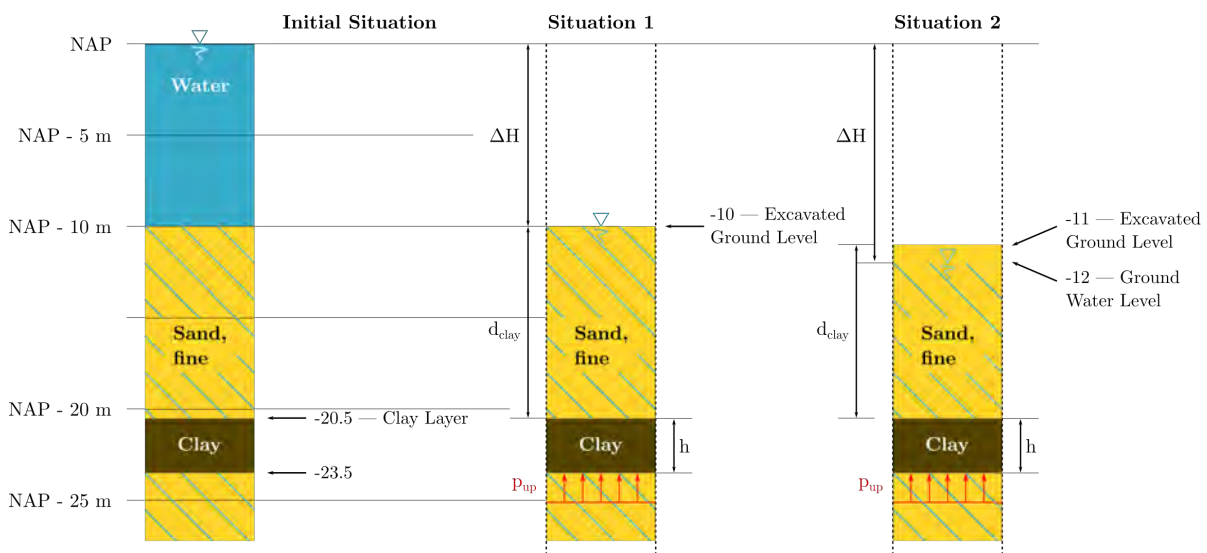


Figure 8.9: Bursting of the Bottom

The upward pressure beneath the clay layer is determined using Equation 8.19. The downward pressure in the case of the situation in Figure 8.9 is equal to that stated in Equation 8.20 (Korff, 2018).

$$p_{up} = \rho_w \cdot g \cdot \Delta H \tag{8.19}$$

$$p_{down} = (\rho_{clay} - \rho_w) \cdot h \cdot g + (\rho_{sand} - \rho_w) \cdot d_{clay} \cdot g \quad (8.20)$$

The results of dividing Equation 8.20 by 8.19 gives a factor of safety. For the scenario shown by Situation 1 in Figure 8.9 ($\Delta H = 10$ m, $d_{clay} = 10.5$ m), the factor of safety is 1.24. However, for Situation 2 ($\Delta H = 12$ m, $d_{clay} = 9.5$ m) the factor of safety is only 1.04. This is a very low factor of safety, so in order to improve the watertightness of the cofferdam measures should be taken such as elongating the walls to a deeper impermeable layer, grouting of the clay layer, or adding heavier layers at the surface of the cofferdam (Korff, 2018). Furthermore, the factor of safety can be increased by draining the groundwater in the excavation to a further level. The additional downward stress created by the dry soil compensates for the additional upward force of the water.

8.4.3. Embedded Depth of the Sheet Piles

The embedded depth of the piles with regards to the watertightness of the structure is to a depth of NAP - 22 m. In this section the method of equivalent beam developed by Blum will be used to determine whether the embedded depth is also suitable for the horizontal stability of the cofferdam structure. Blum proposes that the toe of the sheet pile is free and that the rotational stability of the bottom of the sheet pile is ensured by a substitute force. The calculated embedded depth is then increased with a factor α to ensure the toe does in fact remain in place (Voorendt & Molenaar, 2020). Blum's schematisation in the case of the cofferdam structure in question is shown in Figure 8.10.

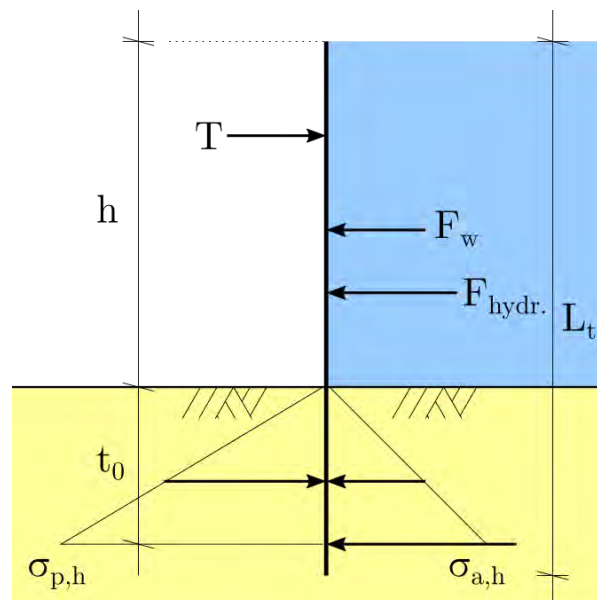


Figure 8.10: Blum Schematisation based on (Voorendt & Molenaar, 2020)

The loads acting on the sheet piles are presented in Appendix X. The equivalent beam method assumes that the sheet pile can be schematised by two simply supported beams. For the topmost beam the strut serves as a pivot, while the point of zero pressure serves as the other pivot. The moment is assumed to be zero at the strut and at the point of zero pressure, which allows the forces in the strut and the restoring force (R) to be determined. The second beam is from the point of contraflexure to the bottom of the beam. The moment is again assumed zero at the bottom of the second beam. The length of this beam required for a balance of moments returns the required embedded depth. Finally this depth is multiplied the factor α equal to 1.2 (United States Steel, 1984).

Based on the governing combination of loads shown in Appendix X, the calculations for the equivalent beam formulation show that the embedded depth required is 8.2 meters. The calculations can be found in Appendix . For the calculation a section with a moment of inertia of $I_y = 130140 \text{ cm}^4$ was

taken. This corresponds to a ArcelorMittal profile AZ-52 700.

8.5. Stability of the Pumphouse

8.5.1. Checking the Bearing Capacity

The pumphouse has a shallow foundation, meaning it is not built on foundation piles. In order to check whether the soil underneath can resist the weight of the structure, the bearing capacity must be determined. Since soil behaves unpredictably, the bearing capacity (p_R) must be one and a half as large as the maximal vertical load exerted by the pumphouse ($p_{max,Ed}$). This is written in a limit state in Equation 8.21.

$$p_R > 1.5 \cdot p_{max,Ed} \quad (8.21)$$

As derived in Appendix Y, the maximal self-weight of the structure amounts to 34,477 kN. Combined with a buoyant force of 11,702 kN, the maximal downward pressure exerted by the pumphouse is $p_{max,E} = 120$ kPa. The design value is taken by multiplying by 1.2, since this is a static load, resulting in $p_{max,Ed} = 144$ kPa. A quick rule of thumb tells us that this is within the limits for loose sand (<200 kPa), and well within the limits for medium and densely-packed sand (<400-600 kPa) (Voorendt & Molenaar, 2020).

The bearing capacity of the soil can be further analysed using the Brinch Hansen method. Brinch Hansen extended Prandtl's formula based on slip planes to find the bearing capacity by a strip foundation (p), which is given in Equation 8.22 (Verruijt, 2001).

$$p = i_c s_c c N_c + i_q s_q q N_q + i_\gamma s_\gamma \frac{1}{2} \gamma B N_\gamma \quad (8.22)$$

This equation takes into account the effects of inclination, shape, and the influence of the depth of the foundation in the form of a surcharge ($q = \gamma d$), where d indicates the depth of the foundation. It should also be noted that in Equation 8.22 the term for the gravitational weight of the soil (γ) should be taken as the effective volumetric weight ($\gamma_s - \gamma_w$) for saturated conditions.

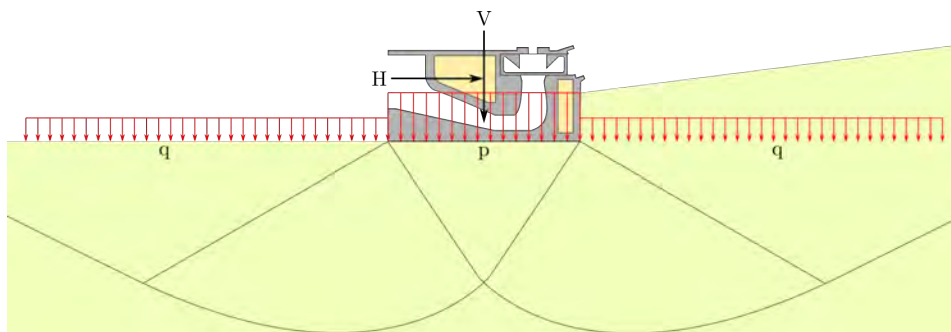


Figure 8.11: Brinch Hansen Method

From Verruijt (2001) it follows that:

$$N_q = 37.8 \quad (8.23)$$

$$N_\gamma = 53.4 \quad (8.24)$$

$$s_q = 1 + \frac{B}{L} \sin(\phi) = 1.12 \quad (8.25)$$

$$s_\gamma = 1 - 0.3 \frac{B}{L} = 0.21 \quad (8.26)$$

$$i_q = i_\gamma = 1 \quad (8.27)$$

Using these parameters and a surcharge of 3 meters of sand, the bearing capacity is p_R 4726 kPa, so more than strong enough not to require deep foundations. Due to the proximity of the center of mass to the middle of the bottom of the structure, the additional stresses on the soil due to moments were not taken into account.

8.5.2. Horizontal Stability

The shear capacity of the soil is determined using Coulomb's theory, given in Equation 8.28 (Verruijt, 2001).

$$\tau_f = c + \sigma' \tan \phi \quad (8.28)$$

The angle of friction (ϕ) between sand and concrete is in the range of 40-50% according to Voorendt and Molenaar (2020), while the cohesion (c) of sand can be neglected. The minimal effective stress underneath the pumphouse occurs during maintenance, when the pumphouse is empty and the buoyant forces are largest. The self weight minus the buoyancy is 15300 kN, and the water depth is 5 meters, resulting in an effective stress under the foundation of 30.9 kPa. This however, is still enough to resist the maximal shear force of 5.5 kPa.

8.5.3. Rotational Stability

The tensile capacity of sandy soil is negligible, therefore only the compressive forces of the ground are able to support the shallow foundation. The rule of thumb states that the working point of the sum of the horizontal and vertical forces should not act more than one sixth the width away from the middle of the bottom of the structure, as shown in Equation 8.29 Voorendt and Molenaar (2020).

$$e_R = \frac{\Sigma M}{\Sigma V} \leq \frac{1}{6} b \quad (8.29)$$

In this case, the acting load is the overturning moments, while the vertical loads and the extrusion of the working point from the center (e_R) provide the resistance. Again, a safety factor of 1.5 is taken, which results in the following limit state function, given in Equation 8.30.

$$\Sigma M_{Ed} < M_{Rd} = \frac{1}{9} \cdot b \cdot \Sigma V_{Rd} \quad (8.30)$$

The critical combination in this case is during maintenance, when the buoyancy is acting in the middle of the structure and the self weight is offset by 0.9 meters. The resultant moment is a result of static forces, so is multiplied by 1.2, resulting in $M_{Ed} = 33638$ kNm. The vertical forces are unfavorable for the stability, thus multiplied by 0.9, equaling $V_{Rd} = 13992$ kN

Filling in the limit state, the total resistance is $M_{Rd} = 34203$, while the acting moments are $M_{Ed} = 33638$ kNm, so this narrowly passes the verification, with a unit check of 0.98.

8.6. Settlements

Settlements on either side of the turbine-pumping stations should be checked, because uneven settlements can mean large stresses and strains occurring for the penstock. If the difference in settlements is too large then the penstock needs to be designed in order to take up the rotation and elongation due to differential settlements. Furthermore, if the settlement in the pumphouse is large then this will also affect the hydraulic operation, something which should also be taken into account.

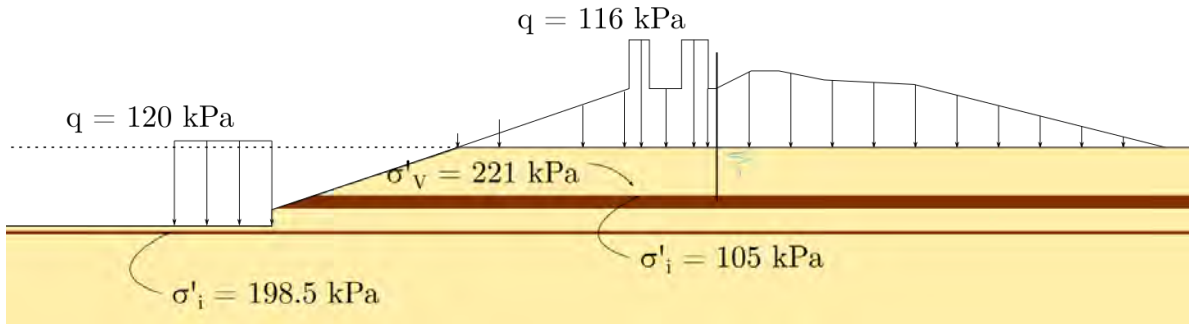


Figure 8.12: Loads Acting on the Original Soil Profile (Dotted Line)

Settlement is determined using the Koppejan method, which assumes a splitting of settlements into the primary and secondary (creep) components, which is essentially a combination of the formulas from Terzaghi and Buisman. The Koppejan settlement is given in Equation 8.31 (Verruijt, 2001).

$$\varepsilon = - \left[\frac{1}{C_p} + \frac{1}{C_s} \log \left(\frac{t}{t_0} \right) \right] \log \left(\frac{\sigma}{\sigma_1} \right) \quad (8.31)$$

The settlement checks at the seaside, underneath the sea dike, will be done for the clay layer located at NAP - 20.5 meters, and is 3 meters thick. The smaller clay layer situated deeper will be neglected. The initial vertical pressure on the layer is 10.5 meters of saturated sand, below water level, so equal to 105 kPa. After construction of the turbine-pumping station the emergency gate housing will provide the largest surcharge load. It is estimated the concrete volume is 75.84 m³ on a surface of 4 m², as well as the sand layer this results in a final effective stress of 221 kPa.

According to Arbib (2014), for a clay with saturated volumetric weight (γ_{clay}) 18 kN/m³, the consolidation parameters given in Equation 8.32 (primary consolidation) and Equation 8.33 (secondary consolidation) are valid.

$$\frac{1}{C_p} = 0.0388 \quad (8.32)$$

$$\frac{1}{C_s} = 0.0042 \quad (8.33)$$

Solving the Koppejan settlement problem gives $\varepsilon = 0.0593$. It is assumed the degree of consolidation (U) is equal to 1 (fully consolidated) and that the time period ($\frac{t}{t_0}$) is 10,000 days, which is enough to achieve equilibrium according to Voorendt and Molenaar (2020).

A shrinkage of 6% on a layer of 3 meters thick results in a settlement of 17.8 centimeters.

On the other hand, as can be seen from Figure 8.12, the effective stress above the lower clay layer at the pumphouse is smaller after installation of the pumphouse. This can result in relaxation (swell) of the soil layer. The swell for a layer of soil is given by Equation 8.34, where $\Delta\sigma$ represents the reduction in effective stress on the soil layer.

$$\varepsilon_{sw} = \frac{\Delta h_{\text{total}}}{h} = \frac{C_{sw}}{(1 + e_0)} \cdot \log\left(\frac{\sigma'_i + \Delta\sigma}{\sigma'_i}\right) \quad (8.34)$$

NEN-EN 1997-1 (2005) gives various values of the swell coefficient $\left(\frac{C_{sw}}{(1+e_0)}\right)$ for clay. These range from 0.0055 for very sandy clay to 0.1905 to weak clay, meaning a discrepancy of 30 times. For the location of the turbine pumping station it is assumed the clay is moderately sandy so a value of 0.0383 is taken. A decrease of the effective pressure by 78.1 kPa thus returns a swell in the clay layer of 3 mm. Even if assuming the weakest clay quality the swell is still less than 1 centimeter, so can be neglected.

9.1. Structural Verification of the Cofferdam

9.1.1. Strength and Stiffness of the Sheet Piles

The programme D-Sheet Piling is used in order to determine the load distribution and the internal stresses and displacements on the sheet piles. The initial design as discussed in the stability of the cofferdam, Section 8.4, included sheet piles with a profile AZ52 - 700 and one strut at NAP. However, it is quickly obvious that the single strut is not enough to withstand the governing load combination, shown in Figure 9.1. Normally, in a cofferdam, the underwater concrete floor serves as an extra strut layer but in this case it is not present.

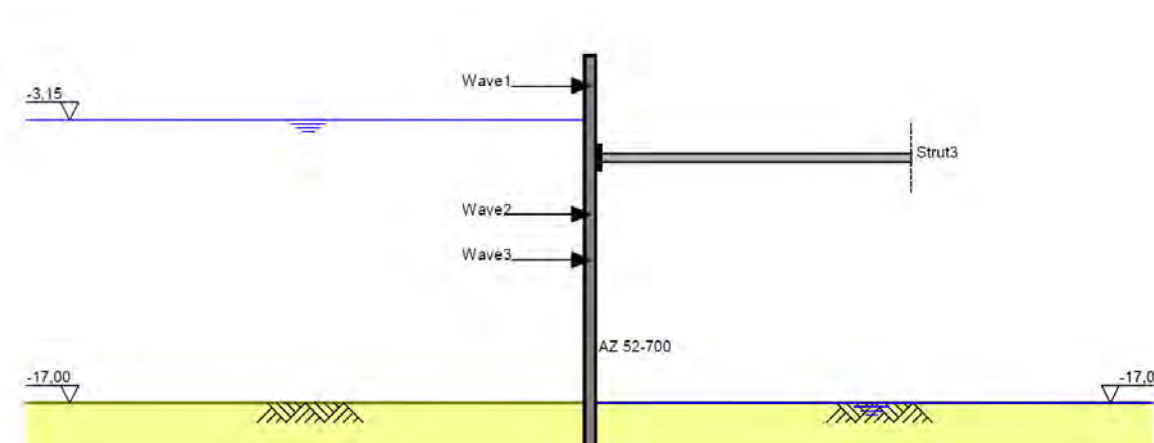


Figure 9.1: Load Combination for the Scenario with 1 Strut

The values for the wave forces are determined in Appendix X. The combined line loads from significant wave action sum up to 271.5 kN/m'. For this load combination, the variable loads (the waves) are multiplied by a factor of 1.3. The result of the governing load combination of waves and hydrostatic pressure would result in a failure of the cofferdam as shown in Figure 9.2, with displacements up to 0.8 meters and bending moments of 4500 kNm.

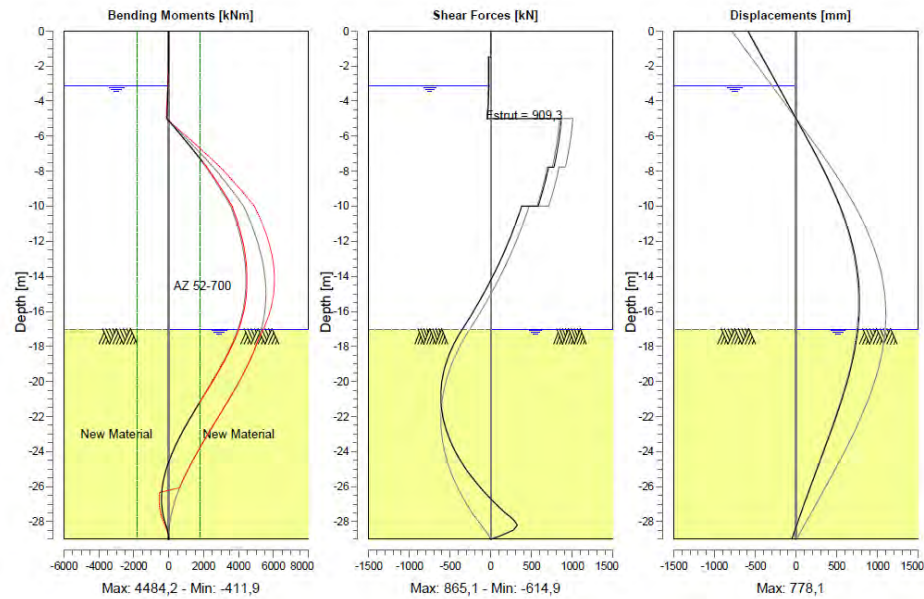


Figure 9.2: Displacements, Moments, and Shear Force for a Single Strut

Rather, three struts are needed in order to resist the combination of storm surge water levels and significant wave impacts. As can be seen in Figure 9.3, the struts are located at levels of NAP + 2 m, NAP - 3 m, and NAP - 8 m.

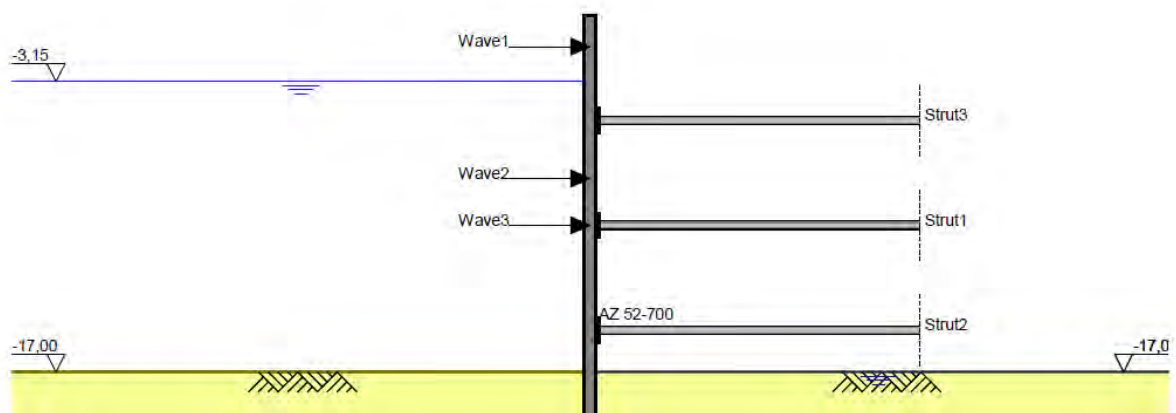


Figure 9.3: Governing Load Combination for Three Struts

The maximal moment in the sheet piles for the ULS load combination is 535.5 kNm, and the maximal displacement for the SLS is 10 mm. The full results of the stresses and displacements can be found in Appendix . The design section modulus (W_y) for the sheet pile profile is 5155 cm³ or 5.155 · 10⁶ mm³. This means the maximal stress occurring in the sheet pile is 100 MPa, well within the design yield stress of 355 MPa for steel class S355. For the SLS displacement, the maximal tolerable displacement is L/250. For the 29 meter long sheet pile, the maximal displacement (98 mm) falls just inside the tolerable displacement of 116 mm.

The various stages of installing the struts also needs to be verified. The stages are depicted in Figures .1 through .6. The results of the forces, moments, and displacements are found in Appendix .

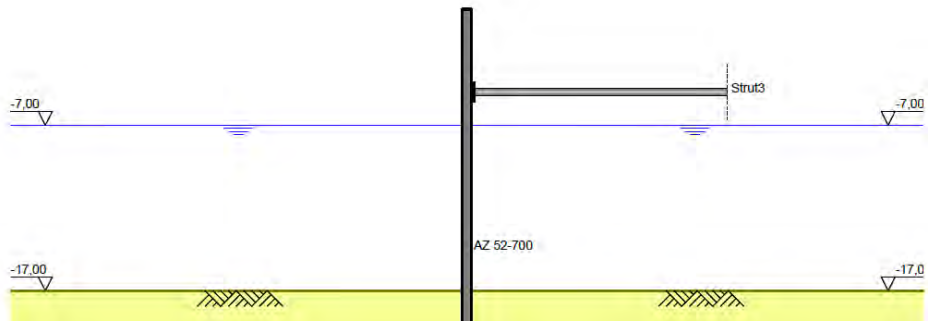


Figure 9.4: Stage 1

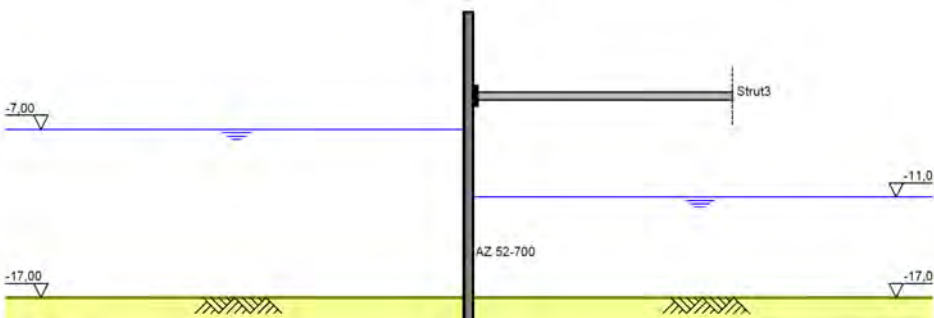


Figure 9.5: Stage 2

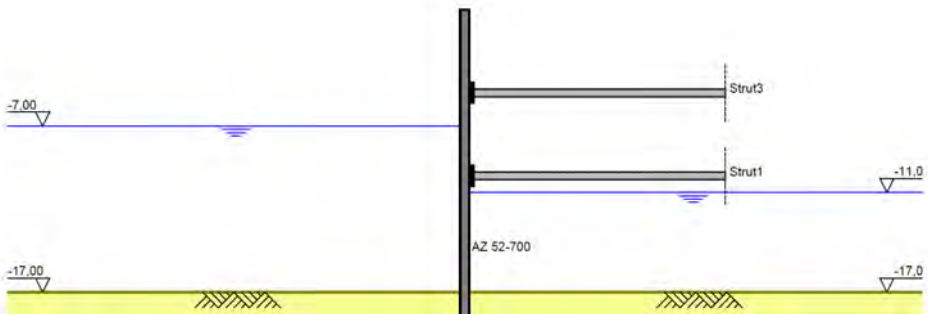


Figure 9.6: Stage 3

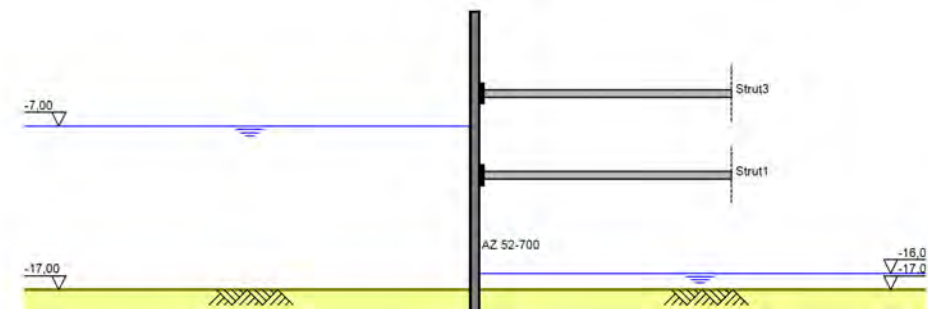


Figure 9.7: Stage 4

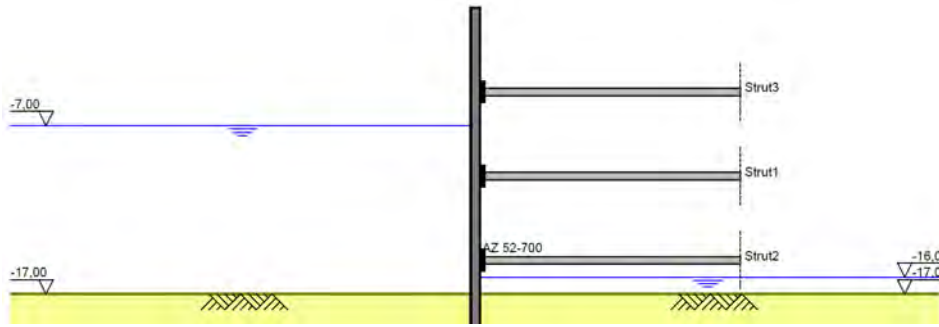


Figure 9.8: Stage 5

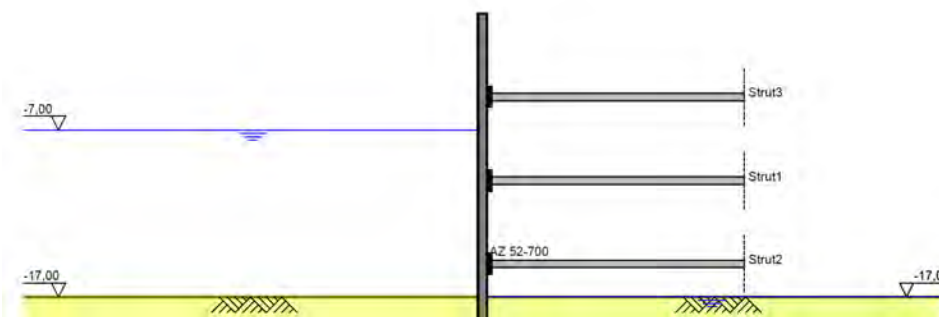


Figure 9.9: Stage 6

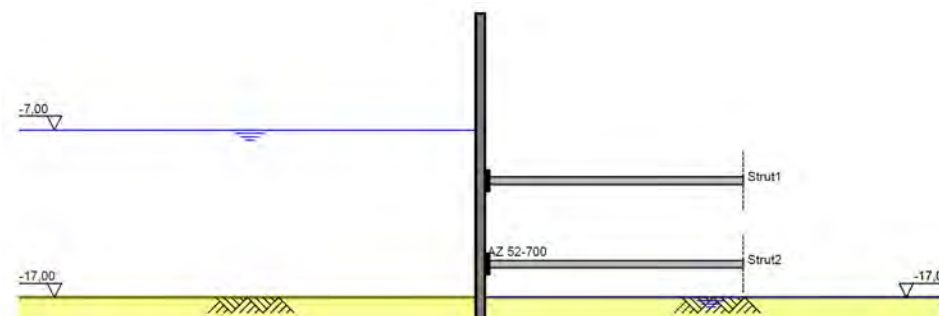


Figure 9.10: Stage 7

9.1.2. Verification of the Struts and Wales

The struts which support the cofferdam are attached to the sheet piles by means of a wale and a welded connecting plate. The arrangement is shown in Figure 9.11, and the spacing of the struts is at 8.6 meter intervals.

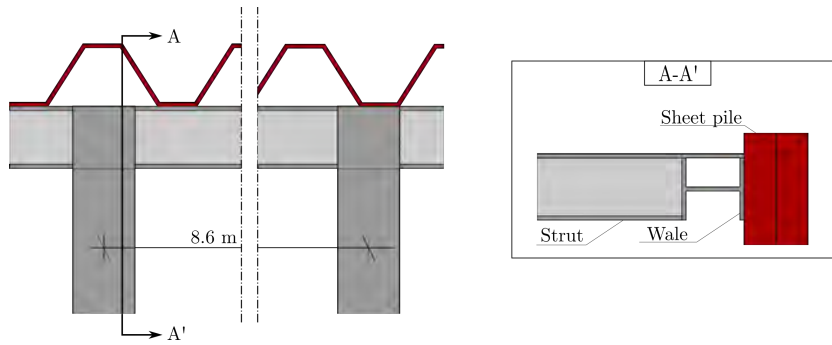


Figure 9.11: Top View of the Arrangement of the Struts and Wales

The maximal ULS load on the strut is on the upper struts and is equal to a normal force of 854.5 kN per meter width, or a distributed load of 854.5 kN/m acting on the wales. The welded plates form a rigid connection between the wales and the struts, hence the wales can be schematized as shown in Figure 9.12.

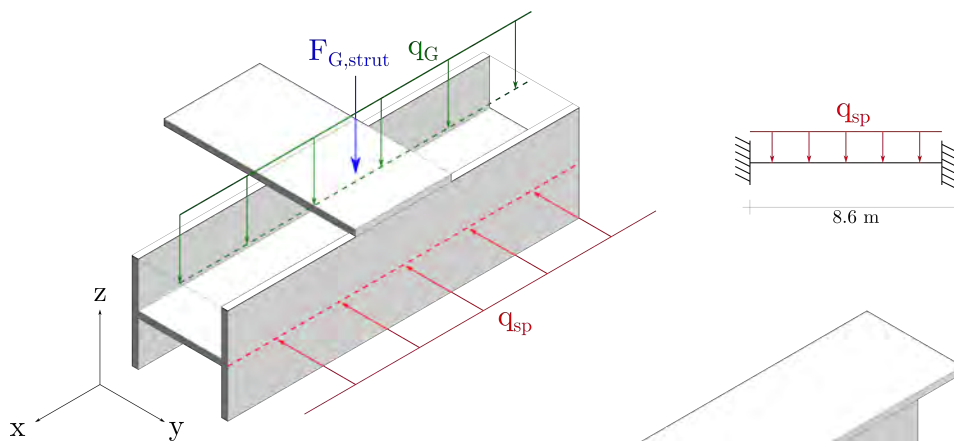


Figure 9.12: Schematization of the Wale Forces

The vertical loads of the self-weight of the wale and the weight of the strut will be neglected, as it is assumed they are transferred directly to the sheet pile. For a fixed-fixed beam, the maximal moment occurs at the supports and is equal to $\frac{1}{12} \cdot q \cdot l^2$, which returns $M_{Ed} = 5266.6 \text{ kNm}$. The required section modulus would be $1483 \cdot 10^3 \text{ mm}^3$. This corresponds to a profile HE 300 B for a steel quality S355.

The reaction force in the rigid support for the wale is 7345.7 kN, meaning this is the design normal force (N_{Ed}) for the struts. The struts will be checked for resistance to buckling and maximal yield stress. As of yet, the required width of the cofferdam is not yet determined. A wider cofferdam is optimal, with the extra space made available important for construction purposes.

Figure 9.13 shows the combination of the moment due to self-weight as well as the normal force. It is unlikely the wave impacts will be acting on both sides of the cofferdam simultaneously, so a reduced value of the normal force ($N_{E,red}$) is taken, equal to the strut force in normal conditions, 289 kN.

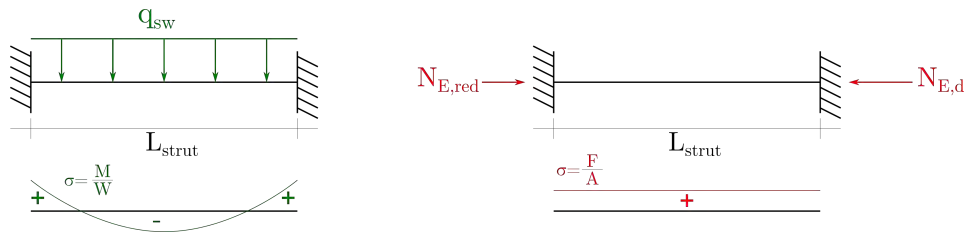


Figure 9.13: Schematization of the Strut Stresses

For a fixed-fixed beam the effective buckling length (l_{eff}) is half the total length. Using Euler's formula (Equation 9.1) the critical buckling force can be found.

$$F_{cr} = \frac{\pi^2 \cdot EI}{l_{eff}^2} \quad (9.1)$$

$$uc_{buc.} = \frac{F_{Ed}}{F_{cr}} \quad (9.2)$$

$$uc_{stress} = \frac{\frac{M_{Ed}}{W_y} + \frac{N_{Ed}}{A}}{\sigma_{Rd}} \quad (9.3)$$

The relationship between the length of the struts and the unity check for buckling (Equation 9.2) and the unity check for stress (Equation 9.3) can be found in the graphs in Figures 9.14 and 9.15, respectively.

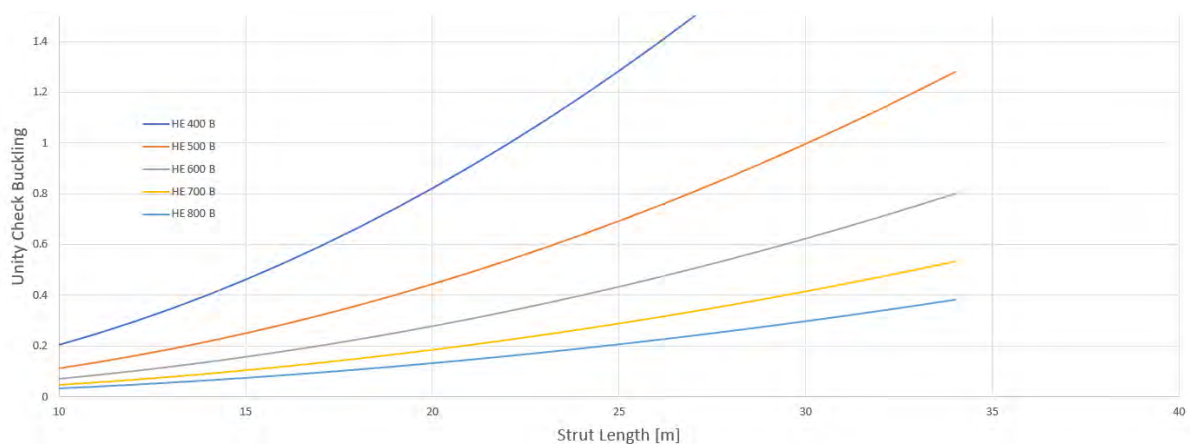


Figure 9.14: Unity Check for Buckling vs. Strut Length

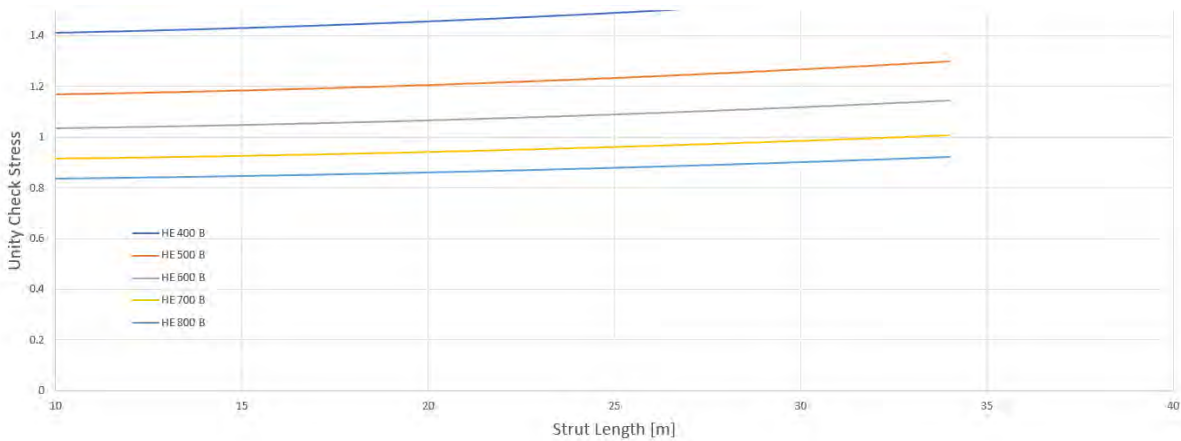


Figure 9.15: Unity Check for Stress vs. Strut Length

For the final design of the cofferdam, the strut with profile HEB 700B is selected. This profile is large enough to span 25 meters, allowing for room for the structure itself as well as extra room around for storage of materials or other purposes. The final design of the cofferdam is shown in Figure 9.16.

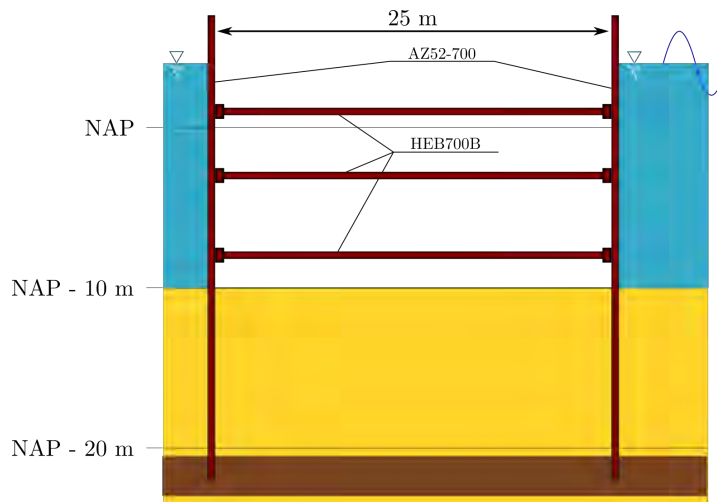


Figure 9.16: Final Design of the Cofferdam

9.2. Structural Verification of the Penstock

9.2.1. Stress

The penstock should be able to handle the pressure associated with hydrodynamic forces and soil loading. As explained in Appendix Z the combination of loads from the soil and from the hydraulics are mutually exclusive so they will be examined separately.

The mechanical properties of FRP are very variant, since FRP is an entire class of materials and can use many components, as well as a fact that a lot depends on the buildup of the material in question and the method of fabrication (how it is wrapped, how many layers, etc.). For the design of the penstock, the use of glass fibre reinforced polymer (GFRP) will be analysed as it is cheaper and more suitable to this use than its high-strength polymer friends such as aramid- and carbon-fibre reinforced polymers (Katsarakakis et al., 2013). Various literature has quoted the axial tensile strength of GFRP between 542 MPa ((Ju, Lee, & Park, 2017)) until 4580 MPa ((Gudonis et al., 2013)) for high strength classes. Also, the transverse strength of GFRP has also shown to be much lower than its axial tension. Important

however, is that a study by Gunoz, Kepir, and Kara (2020) showed the strength of GFRP pipelines (6 layered) to reduce after prolonged exposure to seawater, as shown in Figure 9.17.

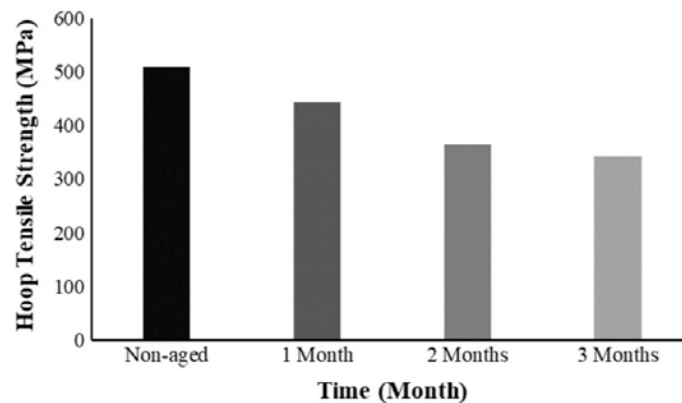


Figure 9.17: Tensile Strength of GFRP vs. Duration of Exposure to Saltwater

Gunoz et al. (2020) found that after 3 months of submergence in seawater the tensile strength of the GFRP pipe was reduced by an average of 33% to 342.2 MPa. The trend along the first 3 months showed a decrease in the rate of decay of strength, therefore a design yield strength for the GFRP penstock will be taken at 250 MPa.

For the pressure of the water hammer, the E-Modulus of the pipe is of importance. The E-Modulus of GFRP is lower than that of steel, at around 72.4 GPa Shakir Abbood, aldeen Odaa, Hasan, and Jasim (2021). Based on the equations in Appendix Z, a penstock thickness of 23 mm returns a water hammer over-pressure of 1.29 MPa, and at 41 mm this is 1.61 MPa. On top of this the hydrostatic pressure and the flow pressure add an additional 280 kPa of pressure.

For the hydraulic pressure inside a pipeline, Barlow's theorem gives a relation between the diameter (D) and thickness of the pipe (t), the design stress that can be handle (σ_h), and the acting pressure on the pipe (P), given in Equation 9.4, and depicted in Figure 9.18 (Amaya-Gomez, Sanchez-Silva, Bastidas-Arteagac, Schoefsc, & Munoz, 2018).

$$P = \frac{2\sigma_h t}{D} \quad (9.4)$$

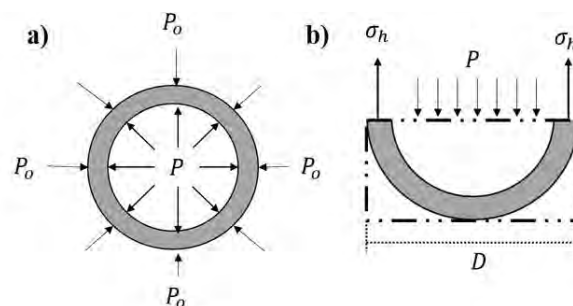


Figure 9.18: Barlow's Theorem Visualized (Amaya-Gomez et al., 2018)

The result for the hydraulic pressure shows that a thickness of 23 mm is required to achieve a factor of safety of 2.0 for Barlow's theorem of acceptable pressure in the pipe, while for a factor of safety of 3.0, 41 mm is required.

9.2.2. Strain

Due to the uneven settlements between the emergency gate housing and the pumphouse, as discussed in Section 8.6, the penstock may experience strains. According to Gunoz et al. (2020), the tolerable strain for GFRP before rupture is 1.5%. The maximal differential settlement of the penstock is expected to be 18 centimeters, between the pumphouse and the emergency gate housing. The total length of the penstock between the pumphouse and emergency gate housing is 80 meters, resulting in a strain of only 0.2%.

Part 4: Conclusion



10

Presentation of the Final Design

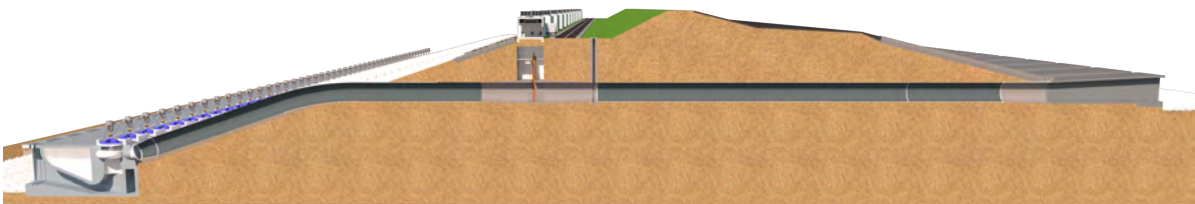


Figure 10.1: Cross-Section of the Turbine-Pumping Station

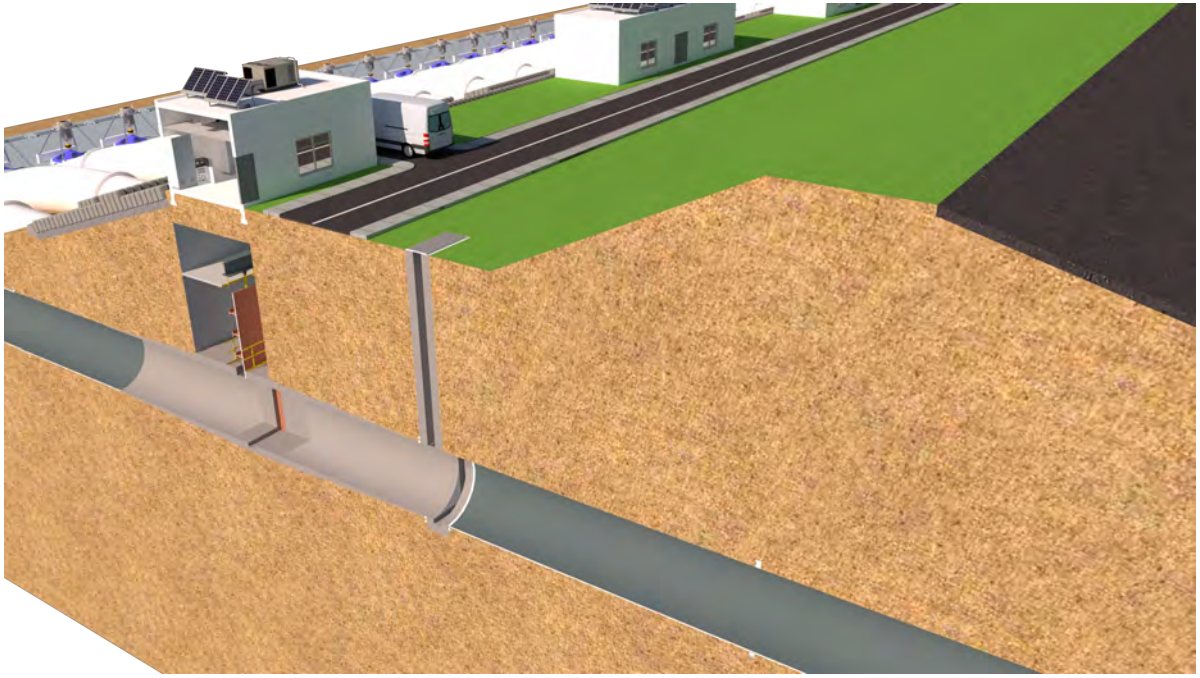


Figure 10.2: 3D Impression of the Top of the Sea Dike

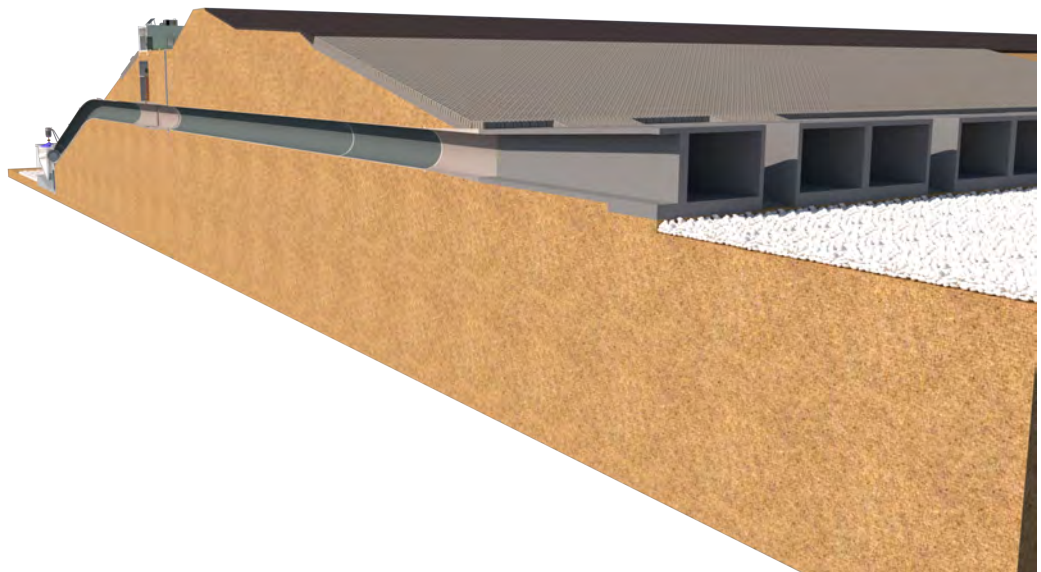


Figure 10.3: 3D Impression of the Sea-side Intake

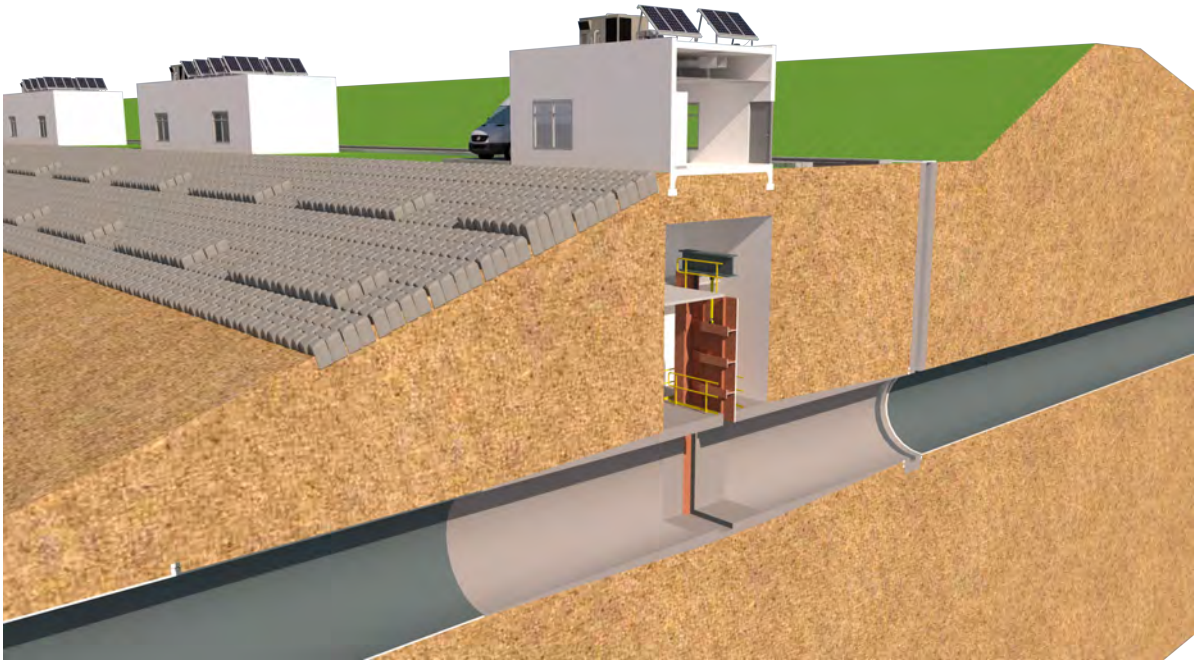


Figure 10.4: 3D Impression of the Emergency Gate Housing and Electrical Installations

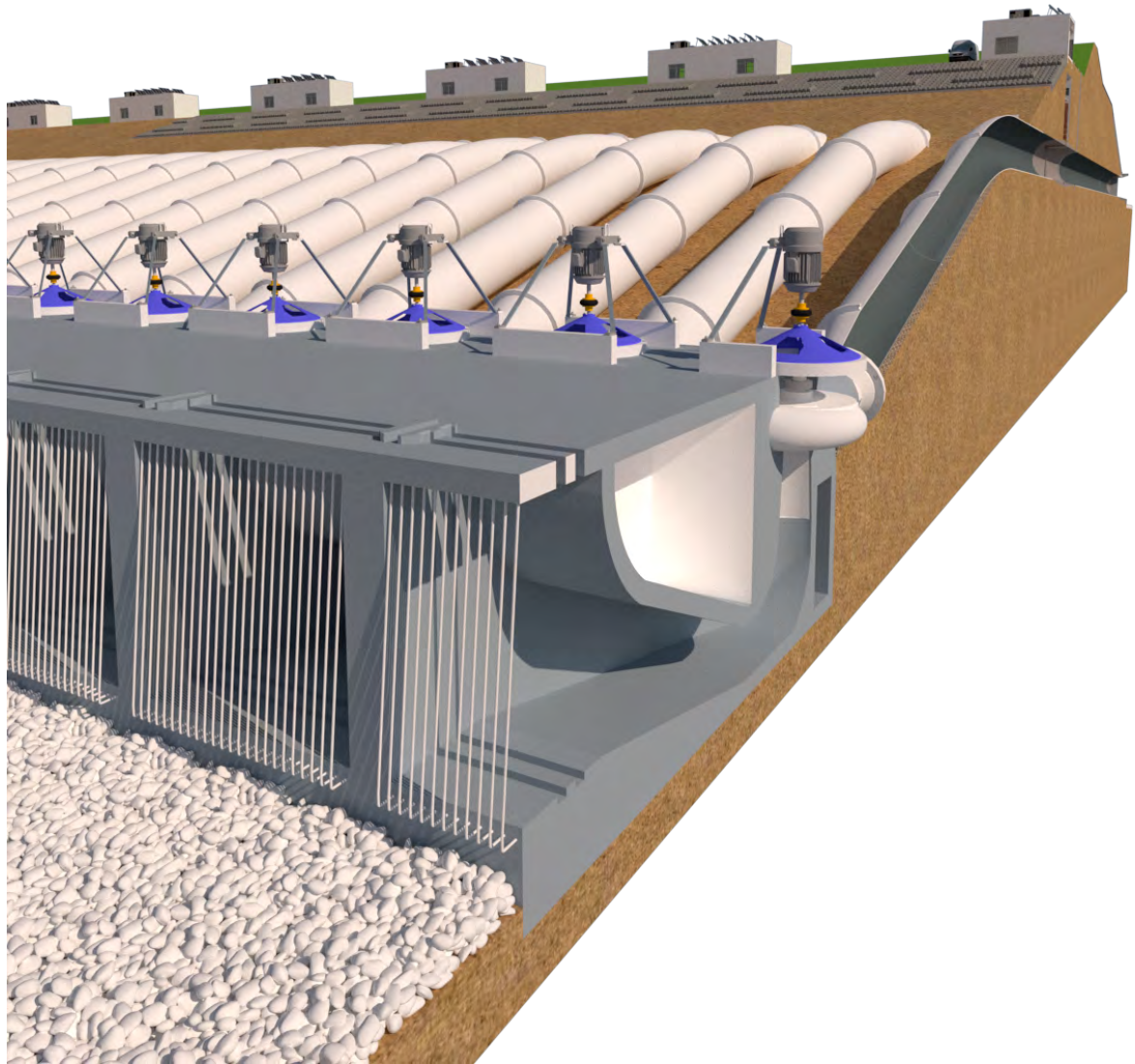
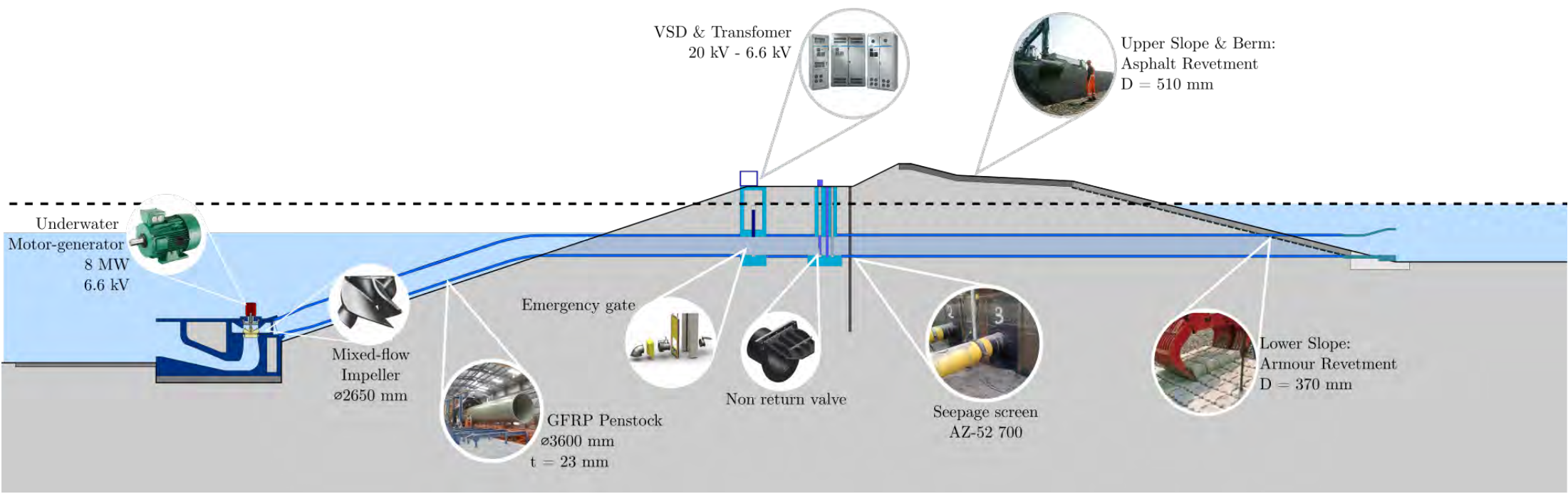


Figure 10.5: 3D Impression of the Pumphouse



Conclusions and Recommendations

11.1. Conclusions

In this report a conceptual design was made in order to demonstrate the feasibility of an alternative turbine-pumping station for the Delta21 project. This alternative design pays attention to splitting the structure into two main parts and integrating this into a dike. This way an imposing, monolithic structure is avoided, which would otherwise be needed in order to resist a head difference of 22.5 meters.

In the hydraulic design a concept was generated in which a pump characteristic is fitted to the needs of the energy storage lake of the Delta21 concept. The pump characteristic delivered by Pentair fit well with the system characteristic when the speed was increased to around 180 rpm. The fact that a manufacturer's pump curve fits the system shows the realization of the Delta21 project is realistic. It was found that the pump characteristic and the system characteristic resulted in a maximal discharge of 44.4 m³/s. It was found that this discharge was limited due to the cavitation requirements. To achieve a total discharge of 10,000 m³/s the entire turbine-pumping station would require 226 units, resulting in a total width of the structure equal to 1945 meters. A study showed that the total width of the structure could be further reduced by increasing the capacity of each unit and therefore decreasing the total amount of units required. For the capacity to be increased, the depth at which the pump-turbines are placed needed to be lower, requiring excavation lower than the bottom of the energy storage lake. Another study also demonstrated that the system's overall efficiency could be increased by changing the shape of the intake from a suction box to a draft tube. The draft tube requires a deeper structure than the suction box, but it was shown that the costs of lowering the installation depth of the turbines could quickly be earned back due to the increased efficiency allowing for a greater revenue from the sale of stored energy.

The evaluation of the hydraulic designed showed that although the pumps can be made larger and thus the structure is less wide with less units required, the high price of each units outweighed the costs saved by having a narrower excavation. However, this was mainly due to the fact that the civil costs were predicted at the lower end, with price estimates only marginally including the operational and man-hour costs. A strength of the design is that the installation is very modular, and can be optimized for various different cases. Since flood defenses in delta regions now also need to cope with the combination of flood waves and high water, pumps required to remove superfluous discharge can also be used as turbines for the storage of electricity. By operating the pump-turbines when they are not required for flood safety, a return on investment can be achieved by sale of the energy stored, as well as the fact that continuous operation of the pump-turbines will mean they are better prepared for flood events.

The simulations for flood safety indicated that for combined floodwaves from the Meuse and Rhine rivers required more than a maximum pumping capacity of 10,000 m³/s for large return periods. However, this model was quite improbable considering the fact that the river floodwaves are simultaneous and the combined discharges and storm surges result in a combined exceedance probability of 10⁻⁸.

The simulations of the energy storage capabilities showed that the total efficiency of a full cycle of pumping and turbine operation is around 66%, even when not operating at maximal efficiency. Although certain smaller inefficiencies such as variable speed drive losses and cable losses are not included, it goes to show that pumped hydro storage can indeed provide a large scale and high efficiency solution to grid balancing. However, for the Delta21 turbine-pumping station to serve as a grid-balancing element then special attention should be paid to being able to turn around quickly between pumping and turbine operation. Efficiencies of the system can be further increased by optimizing the design, such as the inclusion of adjustable blades to manage the efficiency in accordance to the head difference during turbine operation.

For the structural design, the elements of the pumping installation were integrated into a coastal dike. The dredging of the energy storage lake meant a lot of sand is recovered, which can be put to use for the dunes surrounding the lake, as well as for the dike. The construction sequence showed that it is beneficial to prefabricate the pumphouse structures and to then install them on the bottom. Due to the large distance between the pumphouse and the sea-side inlet (around 200 meters), a construction pit is not the preferred method. The depth of the bottom of the energy storage lake (27.5 meters below sea level) means that the embankments surrounding the construction pit would take up massive amounts of space, meaning large amounts of time would be spent dredging soil for installing and removing the embankments and then building the dike. Furthermore, due to its size, issues would likely be encountered during the dewatering of the construction pit. The cofferdam method was deemed the most suitable, however it was found that three levels of trusses would be needed for proper strength and stiffness. Although it was not checked, combination walls which have a higher degree of strength and stiffness would be a suitable alternative and decrease the amount and size of trusses needed.

The structural design also demonstrated that the sheltered location of the turbine-pumping station - on the south-western edge of the energy storage lake - was quite favorable. As shown in the Boundary Conditions, Subsection 3.4.2, the decrease in expected significant wave height of this location was 23% less than the design wave height if the turbine-pumping was located on the northern edge of the energy storage lake. For the design of the dike, the crest height was determined to be at NAP + 8.21 meters. The lower slope is covered in blocks with thickness of 0.37 meters, and the upper slope is covered in an asphalt layer 0.51 meter thick. The penstock between the pumphouse and sea-side inlet was also detailed, and it was calculated that for GFR a minimal thickness of 23 mm would be required to withstand the effects of water hammer, soil loading, and hydraulic loads.

11.2. Recommendations

The conceptual design of the turbine-pumping station for the Delta21 energy storage lake showed the overall feasibility of such a hydro-pumped storage installation, but also gave light to many issues that would need to be analysed in order to accomplish a full design.

Recommendations for further studies in connection with furthering the technical feasibility of the turbine-pumping station include:

- Simulation of the operation of the turbine-pumping station for energy storage with regards to the daily demand and supply of (renewable) energy. An optimization should be made to determine how to operate the pumps. Increasing the speed of the pumps would allow for a faster storage of renewable energy during surplus, but would decrease the efficiency of the system, and vice versa.
- Taking a closer look at the maintenance requirements of the turbine-pumping station, getting insight into how to best replace items from the pumphouse.
- Analysing the prefabrication and installation of the pumphouse elements, including a design of the work island and the transportation method.
- A financial study giving a detailed breakdown of the costs involved with construction and maintenance, and an analysis of the revenue which can be generated through the energy storage

lake, by means of saving costs for river dike maintenance and by selling energy to the grid. A calculation can be done of the net present value, and an internal rate of revenue prediction can be carried out.

- A life-cycle analysis should be done to get an exact of how this type of design compares with a more monolithic structure, such as the one conceptualized by Ansorena-Ruiz (2020).
- There is much uncertainty in terms of the soil properties of the site surrounding the Delta21 site. A model of the subsurface should be made, and the impact of this should be determined. Many major stability issues, such as the bursting of the bottom of the lake and piping underneath the structure currently depend on simple assumptions of the soil properties around the site.

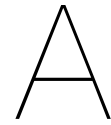
References

- Agarwal, T. (2012). Review of Pump as Turbine (PAT) for Micro-Hydropower. *International Journal of Emerging Technology and Advanced Engineering*.
- Amaya-Gomez, R., Sanchez-Silva, M., Bastidas-Arteagac, E., Schoefsc, F., & Munoz, F. (2018). Reliability assessments of corroded pipelines based on internal pressure - a review. *Engineering Failure Analysis*.
- Ansorena-Ruiz, R. (2020). *Conceptual design of the valmeer's pump storage station of the delta21 plan*. Unpublished master's thesis, TU Delft.
- Arbib, M. (2014). *Analysis of soft soil compression data for flevoland*. Unpublished master's thesis, TU Delft.
- Arnold, J., & Nijhuis, G. J. (2004). *Selection, design and operation of rotodynamic pumps* (Tech. Rep.). Nijhuis Pompen. doi: ISBN90-809393-1-5
- Atkinson, K. E. (1989). *An Introduction to Numerical Analysis (2nd Edition)*. John Wiley Sons, Inc.
- Battjes, J., & Labeur, R. J. (2017). *Unsteady Flow in Open Channels*. Cambridge University Press.
- Borm, W. (2018). *Het kierbesluit* (Tech. Rep.). Adviesgroep Borm Huijgens. Retrieved from <https://beet.nl/het-kierbesluit/>
- Boskalis. (2017). Equipment Sheet - Helios [Computer software manual].
- Bray, R. N. (2009). *A guide to cost standards for dredging equipment*. Construction Industry Research Information Association.
- Bretschneider, C. L. (1965). Generation of Waves by Wind. *NESCO Report*.
- Buitendijk, M. (2019). New anti-fouling solution uses uv light. *SWZ Maritime*.
- de Vilder, L. H. (2017). *Offshore Pumped Hydropower Storage*. Unpublished master's thesis, TU Delft.
- EurOtop. (2007). *Wave Overtopping of Sea Defences and Related Structures: Assessment Manual*.
- French Society for Trenchless Technology. (2004). *Microtunneling and Horizontal Drilling*. y Hermes Science Publishing Ltd.
- Fujihara, T., Imano, H., & Oshima, K. (1998). Development of pump turbine for seawater pumped storage power plant. *Hitachi Review Vol. 47*.
- Gouriou, O., Robin, L., & Wintzer, J. (2018). *Aluminium bronze: An alternative to duplex steels in pump design* (Tech. Rep.). Pump Engineer.
- Grundfos. (2004). *Pump Handbook*.
- Gubin, M. F. (1970). *Draft tubes of hydro-electric stations* (Energiya Press, Ed.).
- Gudonis, E., Timinskas, E., Gribniak, V., Kaklauskas, G., Arnautov, A. K., & Tamulėnas, V. (2013). Frp reinforcement for concrete structures: state-of-the-art review of application and design. *Engineering Structures and Technologies 5(4): 147–158*.
- Gunoz, A., Kepir, Y., & Kara, M. (2020). Tensile strength alteration of gfrp composite pipes under seawater-dominated conditions. *Journal of Failure Analysis and Prevention 20(1)*.
- Hegnauer, M., Beersma, J. J., van den Boogaard, H. F. P., Buishand, T. A., & Passchier, R. H. (2014). Generator of rainfall and discharge extremes (grade) for the rhineand meuse basins. *Final report of GRADE 2.0*.
- Hegnauer, M., Kwadijk, J., & Klijn, F. (2015). The plausibility of extreme highdischarges in the river rhine. *Deltares(1220042-004)*.
- Holthuisen, L. H. (2007). *Waves in Oceanic and Coastal Waters*. Cambridge University Press.
- Hop, J. (2011, May). *Vismigratie rijin-maasstroomgebied – samenvatting op hoofdlijnen* (Tech. Rep. No. 20110414001). RWS Zuid Holland.
- IJntema, J. (2021). *Initial morphodynamic changes in the voordelta in response to the delta21 interventions*. Unpublished master's thesis, TU Delft.
- Jin, C., & Randall, R. E. (2018). The Estimation of Production and Location of Pumps for a Cutter Suction Dredgeusing a Long Distance Pipeline. *Journal of Dredging, Vol. 16, No. 1*.
- Joshi, S., & Kulkarni, R. (2004). Advanced and conventional pumping technologies for power stations. *World Pumps, 2004(449), 50-55*. doi: [https://doi.org/10.1016/S0262-1762\(04\)00110-5](https://doi.org/10.1016/S0262-1762(04)00110-5)
- Ju, M., Lee, S., & Park, C. (2017). Response of glass fiber reinforced polymer (gfrp)-steel hybrid reinforcing bar in uniaxial tension. *International Journal of Concrete Structures and Materials*.
- Katsaprakakis, D. A., Christakis, D. G., Stefanakis, I., Spanos, P., & Stefanakis, N. (2013). Technical details regarding the design, the construction and the operation of seawater pumped storage systems. *Energy*.

- Klein Breteler, M. (1992). *Handboek voor dimensionering van gezette taludbekledingen*. Civieltechnisch Centrum Uitvoering Research en Regelgeving.
- Klein, Schanzlin Becker Aktiengesellschaft. (n.d.). *Centrifugal Pump Lexicon*. Website. (Retrieved on 05/05/2021 from <https://www.ksb.com/centrifugal-pump-lexicon/impeller/191094/>)
- Korff, M. (2018). *Cie4363 deep excavations – design, execution and monitoring of deep excavations with retaining walls*. Delft University of Technology.
- KWT Waterbeheersing. (2018). *Technische catalogus Schotbalkstuwten en overstortputten*.
- Laan, G. J. (1983). De toepasbaarheid van mijnsteen in de waterbouw. *Werkgroep I voor Keuring van Bouwstoffen voor de Waterbouw*.
- Laan, G. J. (1996). De relatie tussen eisen aan loskorrelige steentmaterialen en ontwerpparameters. *Ministerie van Verkeer en Waterstaat Directoraat-Generaal Rijkswaterstaat*.
- Lavooij, H., & Berke, L. (2019). Delta21 update 2019.
- Lechner, A. (2018). Pumped storage for the future. *HydroNews*, 32.
- Lin, M. M., & Hidayat, R. (2018). Jakarta, the fastest-sinking city in the world. *BBC Indonesian*.
- Lüdecke, H.-J., & Kothe, B. (2006). Water hammer. *KSB Know-how, Volume 1*.
- Molenaar, W. F., & Voorendt, M. Z. (2019). *Hydraulic structures - general lecture notes*. Delft University of Technology.
- Mooyaart, L. (2009). *De Energiepolder - Haalbaarheidsstudie naar een getijcentrale langs de Westerschelde*. Unpublished master's thesis, TU Delft.
- NEN-EN 1991-2+C1. (2015). *Eurocode 1: Actions on structures - part 2: Traffic loads on bridges* (Tech. Rep.). Koninklijk Nederlands Normalisatie-instituut.
- NEN-EN 1997-1. (2005). *Eurocode 7: Geotechnical design - part 1: General rules* (Tech. Rep.). Koninklijk Nederlands Normalisatie-instituut.
- NEN-EN 1997-1. (2019). *Nationale bijlage bij NEN-EN 1997-1 Eurocode 7: Geotechnisch ontwerp* (Tech. Rep.). Koninklijk Nederlands Normalisatie-instituut.
- Oppenheimer, M., Glavovic, B. C., Hinkel, J., van de Wal, R., Magnan, A. K., Abd-Elgawad, A., ... Sebesvari, Z. (2019). Sea level rise and implications for low-lying islands, coasts and communities. *IPCC Special Report on the Ocean and Cryosphere in a Changing Climate*.
- Paasman, Y. (2020). *Design for the in- and outlet structure of the energy storage lake within the delta21 plan*. Unpublished master's thesis, TU Delft.
- Pandey, P., Srivastav, A., Kulmi, P., & Prasad, A. K. (2016). Sea water pumped storage power plant-concept paper. *Global Energy Technology Summit*.
- Rajendran, S., Arkadu, J. P., Dinakaran, S. V., Ganapathy, D., & Murthy, M. V. R. (2018). Application of gfrp for unburied submarine pipeline in shallow water of coral islands. *Journal of Pipeline Systems Engineering and Practice*.
- Rijkswaterstaat. (n.d.). *Haringvlietsluizen*. Website. (Retrieved on 04/04/2021 from <https://www.rijkswaterstaat.nl/water/waterbeheer/bescherming-tegen-het-water/waterkeringen/deltawerken/haringvlietsluizen>)
- Rijkswaterstaat. (2020, June). *Project afsluitdijk*. Retrieved from <https://www.rijkswaterstaat.nl/water/projectenoverzicht/afsluitdijk>
- Schiereck, G. J. (2005). *Introduction to Bed, Bank and Shore Protection*. Delft University Press.
- Shakir Abbood, I., aldeen Odaa, S., Hasan, K. F., & Jasim, M. A. (2021). Properties evaluation of fiber reinforced polymers and their constituent materials used in structures – a review. *Materials Today: Proceedings*.
- Slagboom, A. (1965). *Bouwput middenin het Haringvliet en op de achtergrond het Rak van Scheelhoek*. Photograph. Retrieved from <https://www.nationaalarchief.nl/onderzoeken/fotocollectie/aacde756-d0b4-102d-bcf8-003048976d84>
- Soni, V., Roghelia, A., Desai, J., & Chauhan, V. (2010). Design development of optimum draft tube for high head francis turbine using cfc. *Proceedings of the 37th International 4th National Conference on Fluid Mechanics and Fluid Power*. doi: 10.13140/2.1.2786.8169
- Swane, H. (2007). *Tidal Power Plant in Saemangeum*. Unpublished master's thesis, TU Delft.
- TAW. (2002). Technisch Rapport Asfalt voor Waterkeren. *Technische Adviescommissie voor de Waterkeringen*.
- TAW - LZeM. (1999). Leidraad Zee- en Meerdijken. *Technische Adviescommissie Voor de Waterkeringen*.

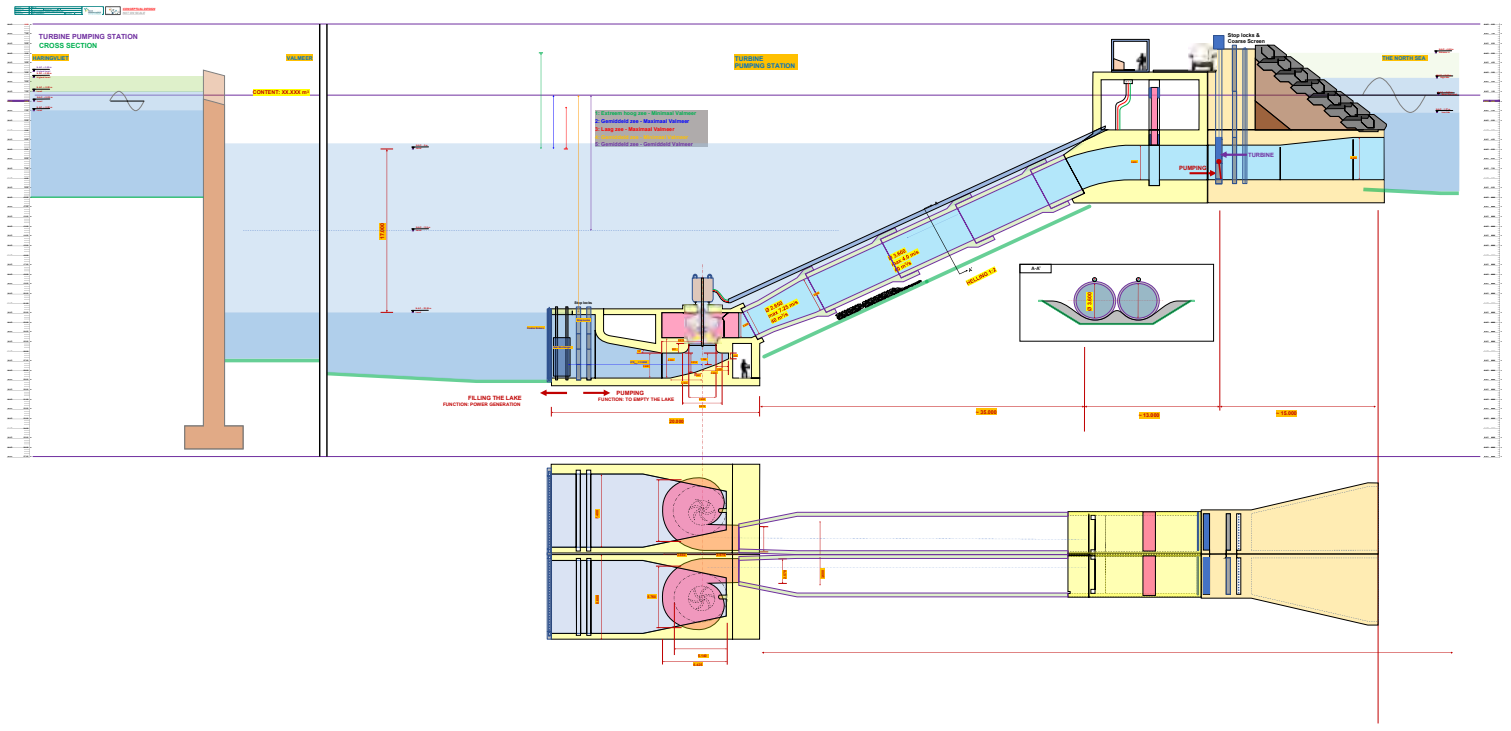
- TAW - WRWOD. (2002). Technical Report Wave Run-up and Wave Overtopping at Dikes. *Technical Advisory Committee on Flood Defence*.
- United States Steel. (1984). Steel sheet piling design manual.
- Van Der Ven. (2020). *Innamepompstation bergsche maas*. website. (Retrieved from <https://www.vanderven.nl/projecten/innamepompstation-bergsche-maas.html>)
- van Berkel, J., Beentjes, R., de Bijl, J., Bloemendal, W., Breukelaar, A., Captein, J., ... van 't Bosch, J. (2018). Fish safety of pumps, archimedean screws and pressure turbines used in pumping stations and hydroelectric plants. *NEN 8775*.
- van Stormbroek, J. (2008). *Development of a floor made from fiber reinforced polymers (frp) with integrated installations*. Unpublished master's thesis, TU Delft.
- Verruijt, A. (2001). *Soil mechanics*. Delft University of Technology.
- Vlasblom, W. J. (2005). *WB3408 Designing Dredging Equipment*. TU Delft.
- Voorendt, M. Z., & Molenaar, W. F. (2020). *Manual hydraulic structures*. Delft University of Technology.
- Vrijling, J. K., van Duivendijk, J., Jonkman, S. N., Gilles, A., & Mooyaart, L. F. (2008). Getijcentrale in de Brouwersdam - Een Verkennende Studie. *TU Delft*.
- WindEurope. (2020). *Offshore wind in europe: Key trends and statistics 2019* (Tech. Rep.). Author. Retrieved from <https://windeurope.org/about-wind/statistics/offshore/european-offshore-wind-industry-key-trends-statistics-2019/>

Appendices



Level Schematic

The level schematic is the base of the hydraulic design. It shows a cross section of the turbine-pumping installation and the water levels on either side are indicated. The combination of the various water levels on either side of the installation are the so-called 'levels' which govern the operation. The combination resulting in the largest head difference is when there is a storm surge on the North Sea side and the energy storage lake is empty. This is also the level to be expected when the installation is used for flood protection mode.



B

System Characteristic Calculations

The system characteristics are shown in Appendix D and E. This appendix shows the calculation of the head loss for various flow velocities. Hydraulic laws state that the head losses are usually quadratically proportional to the velocity, hence the parabolic shape. The topic of the calculations show the head losses that are to be expected for various bends, inflows, and outflows. Wall friction is also included.



Table with columns: No. below, Q (m³/s), Discharge, etc. Includes a small diagram of a channel cross-section.

Table with columns: No. below, Q (m³/s), Discharge, etc. Includes a small diagram of a channel cross-section.

FORM CALCULATING RESULT

Table 0: Flow characteristics including flow rate (1800.0 m³/s), velocity (0.50 m/s), and depth (3.60 m).

Table 2: Flow characteristics including flow rate (1800.0 m³/s), velocity (0.50 m/s), and depth (3.60 m).

Table 3: Flow characteristics including flow rate (1800.0 m³/s), velocity (0.50 m/s), and depth (3.60 m).

Table 5: Flow characteristics including flow rate (1800.0 m³/s), velocity (0.50 m/s), and depth (3.60 m).

Table 5: Flow characteristics including flow rate (1800.0 m³/s), velocity (0.50 m/s), and depth (3.60 m).

Table 5: Flow characteristics including flow rate (1800.0 m³/s), velocity (0.50 m/s), and depth (3.60 m).

Table 5: Flow characteristics including flow rate (1800.0 m³/s), velocity (0.50 m/s), and depth (3.60 m).

Table 5: Flow characteristics including flow rate (1800.0 m³/s), velocity (0.50 m/s), and depth (3.60 m).

Table 3: Flow characteristics including flow rate (1800.0 m³/s), velocity (0.50 m/s), and depth (3.60 m).

Table 6a: Flow characteristics including flow rate (1800.0 m³/s), velocity (0.50 m/s), and depth (3.60 m).

Table 6b: Flow characteristics including flow rate (1800.0 m³/s), velocity (0.50 m/s), and depth (3.60 m).

Table 8: Flow characteristics including flow rate (1800.0 m³/s), velocity (0.50 m/s), and depth (3.60 m).

Table 5: Flow characteristics including flow rate (1800.0 m³/s), velocity (0.50 m/s), and depth (3.60 m).

Table X: Flow characteristics including flow rate (1800.0 m³/s), velocity (0.50 m/s), and depth (3.60 m).

Table X: Flow characteristics including flow rate (1800.0 m³/s), velocity (0.50 m/s), and depth (3.60 m).

Table X: Flow characteristics including flow rate (1800.0 m³/s), velocity (0.50 m/s), and depth (3.60 m).

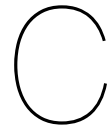
Table 6: Flow characteristics including flow rate (1800.0 m³/s), velocity (0.50 m/s), and depth (3.60 m).

Table 13: Flow characteristics including flow rate (1800.0 m³/s), velocity (0.50 m/s), and depth (3.60 m).

Table 13: Flow characteristics including flow rate (1800.0 m³/s), velocity (0.50 m/s), and depth (3.60 m).

Table 13: Flow characteristics including flow rate (1800.0 m³/s), velocity (0.50 m/s), and depth (3.60 m).

Right side of the page containing detailed hydraulic calculations, diagrams of various structures (weirs, gates, pumps), and summary tables for each case. Includes columns for 'Local pressure / head' and 'mOD'.



Pump Characteristic

This pump characteristic is provided by the equipment manufacturer Pentair. It is a realistic curve that can be manufactured. The impeller diameter for this curve is indicated, and is 2649 mm. This curve is for a rotational speed of 150 rpm, also known as the rated speed. However, the curve can be scaled according to the affinity laws to achieve something with the required head difference. As can be seen from the graph, a higher delivery head corresponds to a lower discharge, and vice-versa.

PUMP PERFORMANCE CURVE



Pumptype: *BMF1-250.265*
Serial n°:
Impeller n°: *L402065*
Diameter [mm]: *2649*
Max. / min.: *2649 / 2649*

Operational:
Rated speed [1/min]: *150*
Max. / min.:
Medium: *Water*
Temp. [°C]: *10*
Dens. [kg/m³]: *1000*
Visc. [mm²/s]: *1.31*

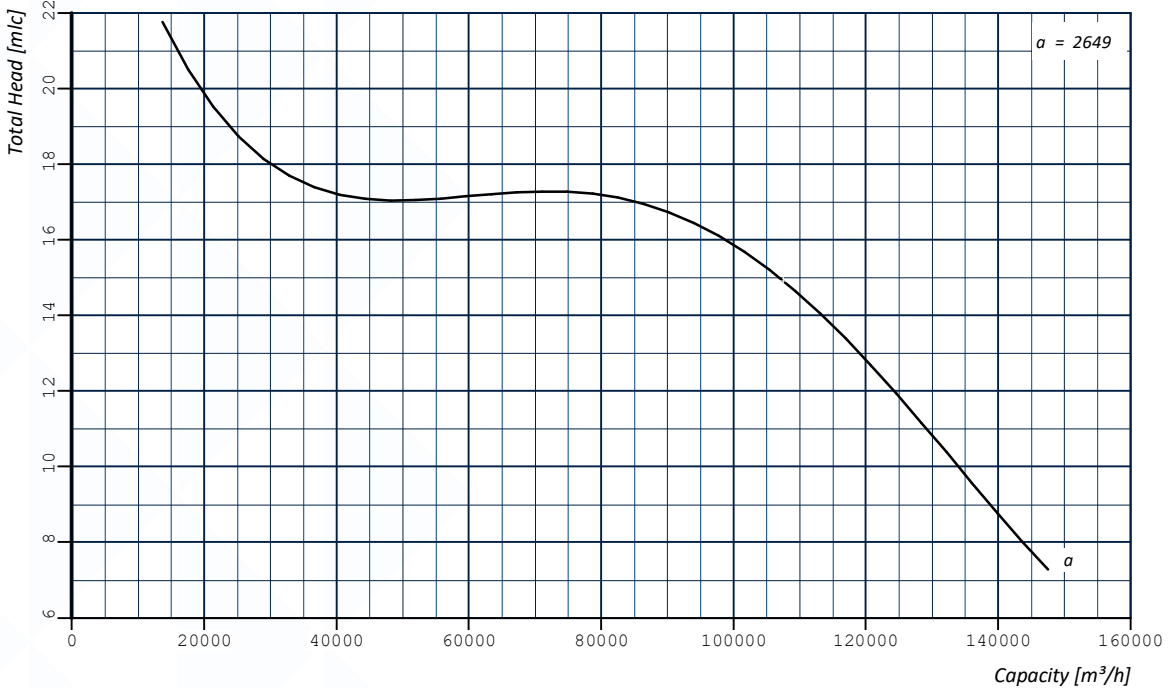
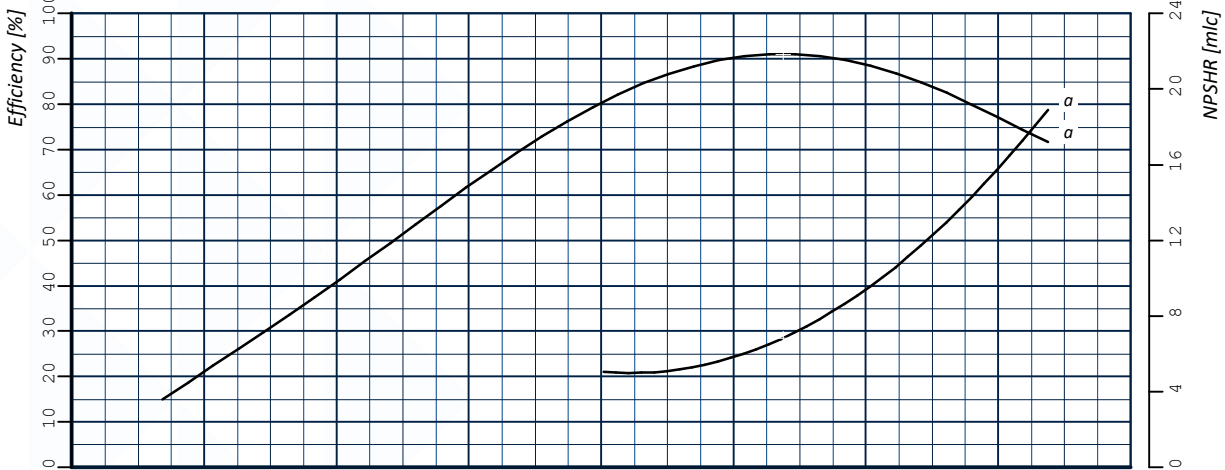
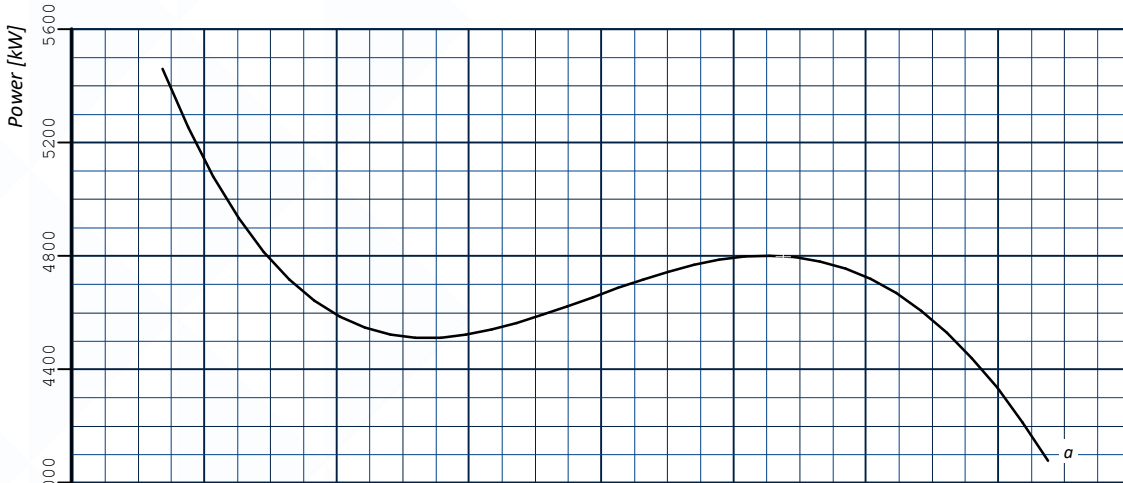
General:
Curve n°: *M0283-150*
Revision: *0*
Date: *16-02-21*
Customer: -
Project: -

Remarks:

Copyright reserved ©

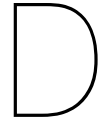
FAIRBANKS NIJHUIS / EARTH

Concrete Volute
Single suction



Curves as per:
ISO9906 gr.2B

Optimum point [0]:
 [2649]
Q : 107479 [m³/h]
H : 14.92 [mlc]
P : 4797 [kW]
eta : 91.0 [%]
NPSHR: 6.8 [mlc]



System & Pump Characteristics

The pump characteristic shown in Appendix C is combined with the calculated system characteristics (Appendix B) and results in the system and pump characteristics. The colors of the system characteristics correspond to the colors given to the various levels in the level schematic (Appendix A). As the flow rate (and thus the flow velocity) increases, the delivery head increases as well due to the head losses. Various pump characteristics can be found too, these are the characteristics for various rotational speeds. The speeds are indicated in the top right, and range from 113 to 190 rpm.

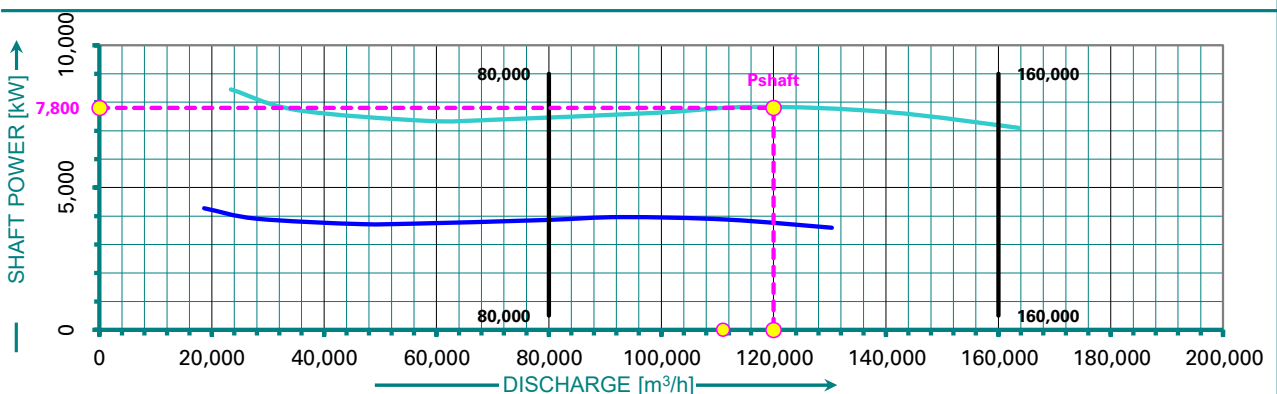
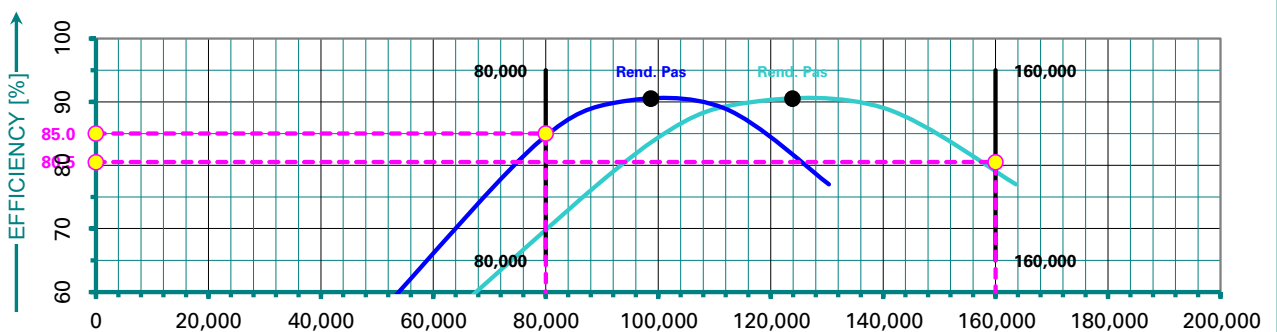
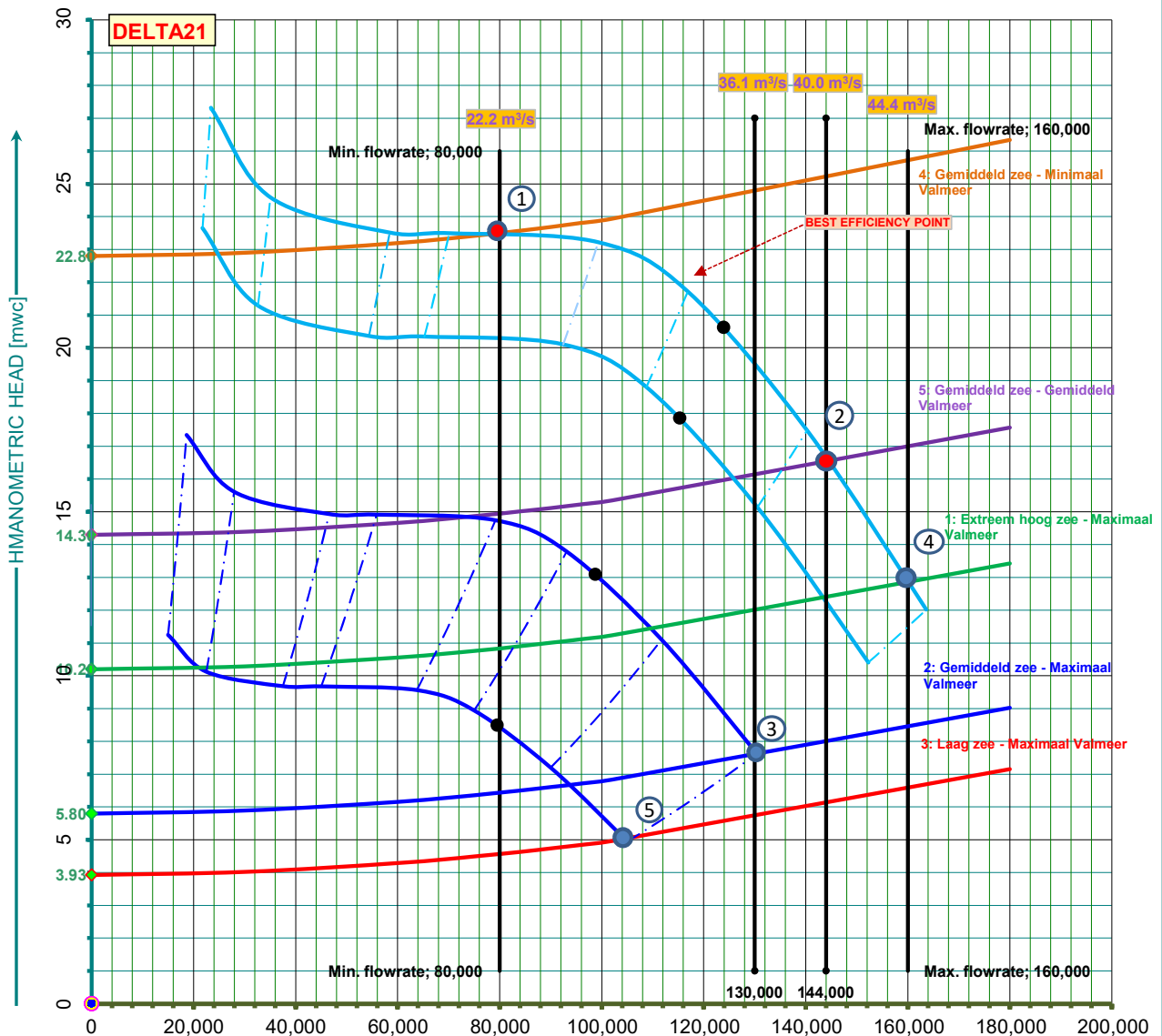
The intersections of the pump curve and the system characteristics are called working points. From these working points, the discharges for each level can be determined. These discharges are plotted in the black horizontal lines. Of course during operation the working points will constantly be moving in correspondence with the speed of the motor/impeller and the levels on either side of the lake.

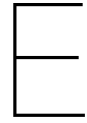
● optimal operation point pump ● System relevant operating points

PROJECT	PUMPING STATION DELTA 21		
PROJECT NO.	INITIALEN:	LJ	
SUBJECT	SYSTEM AND PUMP CHARACTERISTIC		
OPSTELLER	LOIC JACQUEMIN		

curve	min-1	%	Hz	curve	min-1	%	Hz
N1	175	93.5%	46.8	N5	92	49.3%	24.7
N2	163	87.0%	43.5	N6	87	46.4%	23.2
N3	140	74.5%	37.3	N7	84	45.0%	22.5
N4	113	60.0%	30.0	N8	80	42.8%	21.4

PUMP: CVP TYPE: Pump SPEED: 187.5 rpm FREE PASSAGE:





System & Turbine Characteristics

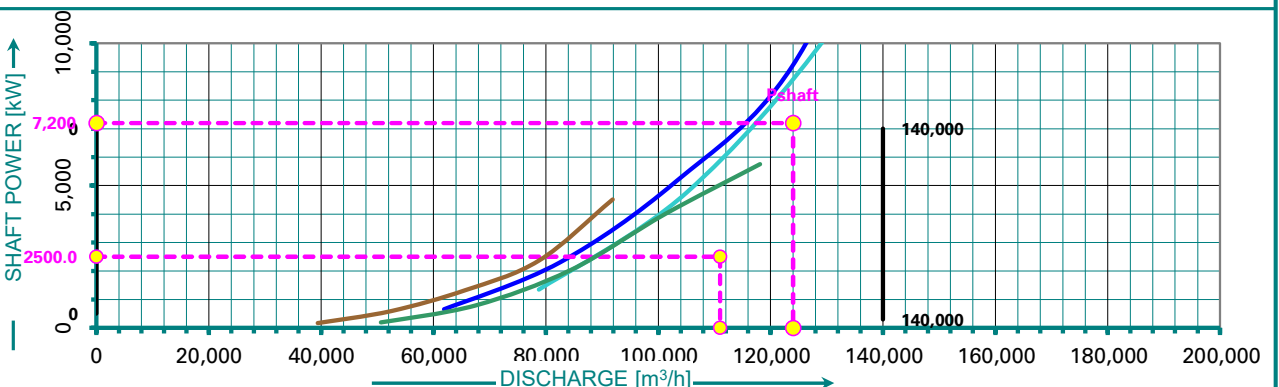
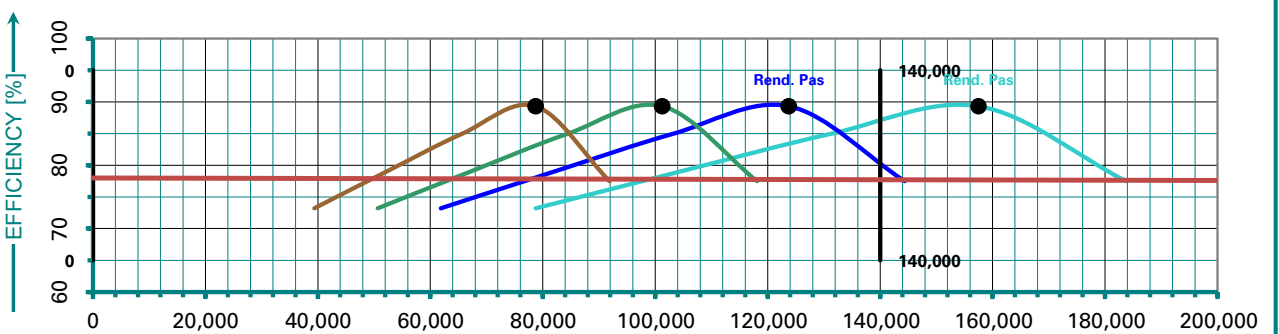
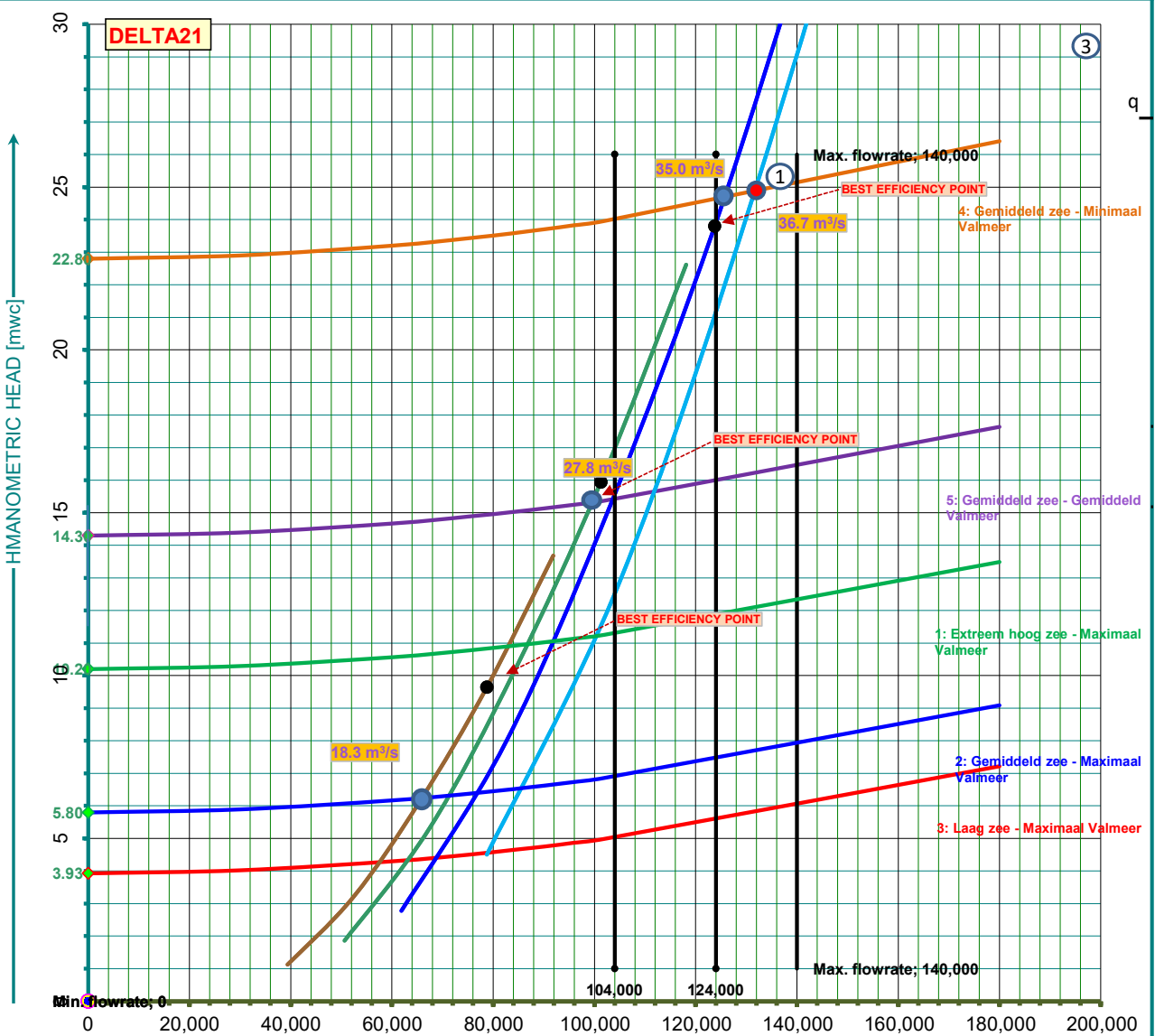
The principle of the system and turbine characteristic is the same as for the pump characteristic in Appendix D, however for the operation of the turbine. The system characteristic in this case is the opposite. Since head losses count against the working of the turbine, the system characteristic curves run downward. Again, the intersections of the turbine and system characteristics show the working points of the turbine system, and the colors of the turbine curve correspond to the speeds shown on the top right.

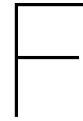
● optimal operation point pump ● System relevant operating points

PROJECT	PUMPING STATION DELTA 21		
PROJECT NO.	INITIALEN:	LJ	
SUBJECT	SYSTEM AND TURBINE CHARACTERISTIC		
OPSTELLER	LOIC JACQUEMIN		

curve	min-1	%	Hz	curve	min-1	%	Hz
N1	131.3	70.0%	35.0	N5	84	45.0%	22.5
N2	131.3	70.0%	35.0	N6	84	45.0%	22.5
N3	103	55.0%	27.5	N7	66	35.0%	17.5
N4	103	55.0%	27.5	N8	66	35.0%	17.5

PUMP: CVP TYPE: Turbine-pump SPEED: 144 rpm FREE PASSAGE:





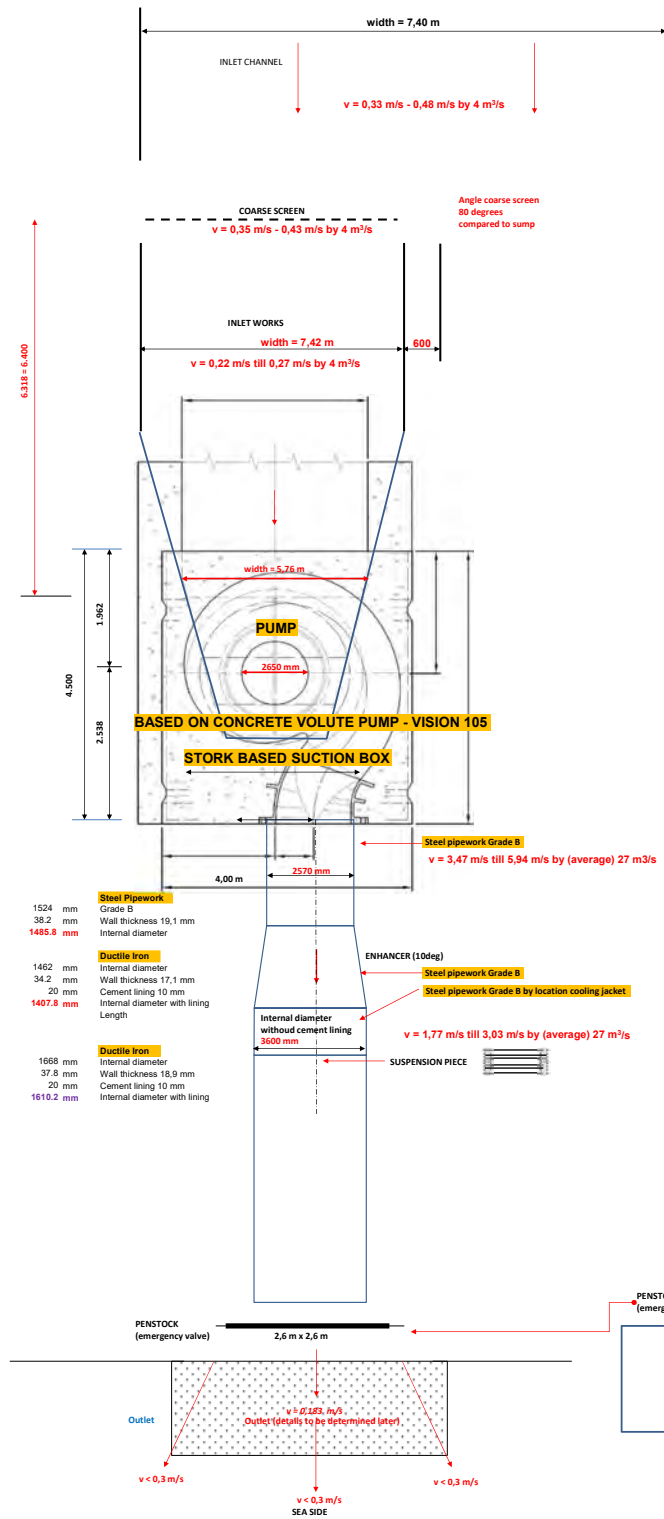
Flow Velocities Pump

For various levels the discharge and thus the flow velocities change. The color of the level is indicated, as well as the flow velocity through the installation. The flow velocity is a function of the flow rate (discharge) and the geometry of the respective section of the installation.

PROJECT	: POMPTURBINESTATION DELTA21
PROJECT NR.	: BG1930 TYPICAL NR. :
BESTREFF	: DESIGN WET PATH - POMP
OPSTELLER	: LOC JACQUEMIN INITIALEN: LJ



IPS-RHD-MS-Z2-RP-M-2115
Hydraulic sizing Vision 105
Number 2115



- Steel Pipework**
Grade B
Wall thickness 19,1 mm
Internal diameter
1485,8 mm
- Ductile Iron**
Internal diameter
Wall thickness 17,1 mm
Cement lining 10 mm
Internal diameter with lining
Length
1407,8 mm
- Ductile Iron**
Internal diameter
Wall thickness 15,9 mm
Cement lining 10 mm
Internal diameter with lining
1610,2 mm

Water level	-22 mOD	Water level	-22 mOD	Water level	-13,5 mOD	Water level	-13,5 mOD
Sump floor	-30 mOD	Sump floor	-30 mOD	Sump floor	-30 mOD	Sump floor	-30 mOD
Water depth	8 m	Water depth	8 m	Water depth	16,5 m	Water depth	16,5 m
Width	7,4 m	Width	7,4 m	Width	7,4 m	Width	7,4 m
Surface A	59,2 m ²	Surface A	59,2 m ²	Surface A	122,1 m ²	Surface A	122,1 m ²
Q	22,2 m ³ /s	Q	36,1 m ³ /s	Q	40 m ³ /s	Q	44,8 m ³ /s
v	0,35 m/s	v	0,61 m/s	v	0,33 m/s	v	0,35 m/s

Water level	-23,4 mOD	Water level	-23,4 mOD	Water level	-23,4 mOD	Water level	-23,4 mOD
Sump floor	-30 mOD	Sump floor	-30 mOD	Sump floor	-30 mOD	Sump floor	-30 mOD
Water depth	6,6 m	Water depth	6,6 m	Water depth	6,6 m	Water depth	6,6 m
Width	7,4 m	Width	7,4 m	Width	7,4 m	Width	7,4 m
Surface A	48,84 m ²	Surface A	48,84 m ²	Surface A	48,84 m ²	Surface A	48,84 m ²
Q	22,2 m ³ /s	Q	36,1 m ³ /s	Q	40 m ³ /s	Q	44,8 m ³ /s
v	0,45 m/s	v	0,74 m/s	v	0,82 m/s	v	0,91 m/s

Water level	-27,43 mOD
Sump floor	-30 mOD
Water depth	2,57 m
Width	5,76 m
Surface A	14,803 m ²
Q	18 m ³ /s
v	1,216 m/s

Water level	-27,43 mOD
Sump floor	-30 mOD
Water depth	2,57 m
Width	5,76 m
Surface A	14,803 m ²
Q	30,8 m ³ /s
v	2,081 m/s

Diameter (internal)	2,57 m
Surface A	5,19 m ²
Q	36,1 m ³ /s
v	4,28 m/s

Diameter (internal)	2,57 m
Surface A	5,19 m ²
Q	40 m ³ /s
v	6,96 m/s

Diameter (internal)	2,57 m
Surface A	5,19 m ²
Q	40 m ³ /s
v	7,71 m/s

Diameter (internal)	2,57 m
Surface A	5,19 m ²
Q	44,8 m ³ /s
v	8,56 m/s

Diameter (internal)	3,60 m
Surface A	10,18 m ²
Q	22,2 m ³ /s
v	2,18 m/s

Diameter (internal)	3,60 m
Surface A	10,18 m ²
Q	36,1 m ³ /s
v	3,55 m/s

Diameter (internal)	3,60 m
Surface A	10,18 m ²
Q	40 m ³ /s
v	3,93 m/s

Diameter (internal)	3,60 m
Surface A	10,18 m ²
Q	44,8 m ³ /s
v	4,36 m/s

Bocht naar uitstroom	3,60 m
Width	3,60 m
Height	3,60 m
Surface A	12,96 m ²
Q	22,2 m ³ /s
v	1,71 m/s

Width	3,60 m
Height	3,60 m
Surface A	12,96 m ²
Q	36,1 m ³ /s
v	2,79 m/s

Width	3,60 m
Height	3,60 m
Surface A	12,96 m ²
Q	40 m ³ /s
v	3,09 m/s

Width	3,60 m
Height	3,60 m
Surface A	12,96 m ²
Q	44,8 m ³ /s
v	3,43 m/s

Width	5,20 m
Height	4,40 m
Surface A	22,88 m ²
Q	22,2 m ³ /s
v	0,97 m/s

Width	5,20 m
Height	4,40 m
Surface A	22,88 m ²
Q	36,1 m ³ /s
v	1,58 m/s

Width	5,20 m
Height	4,40 m
Surface A	22,88 m ²
Q	40 m ³ /s
v	1,75 m/s

Width	5,20 m
Height	4,40 m
Surface A	22,88 m ²
Q	44,8 m ³ /s
v	1,94 m/s

Rooster 5.2

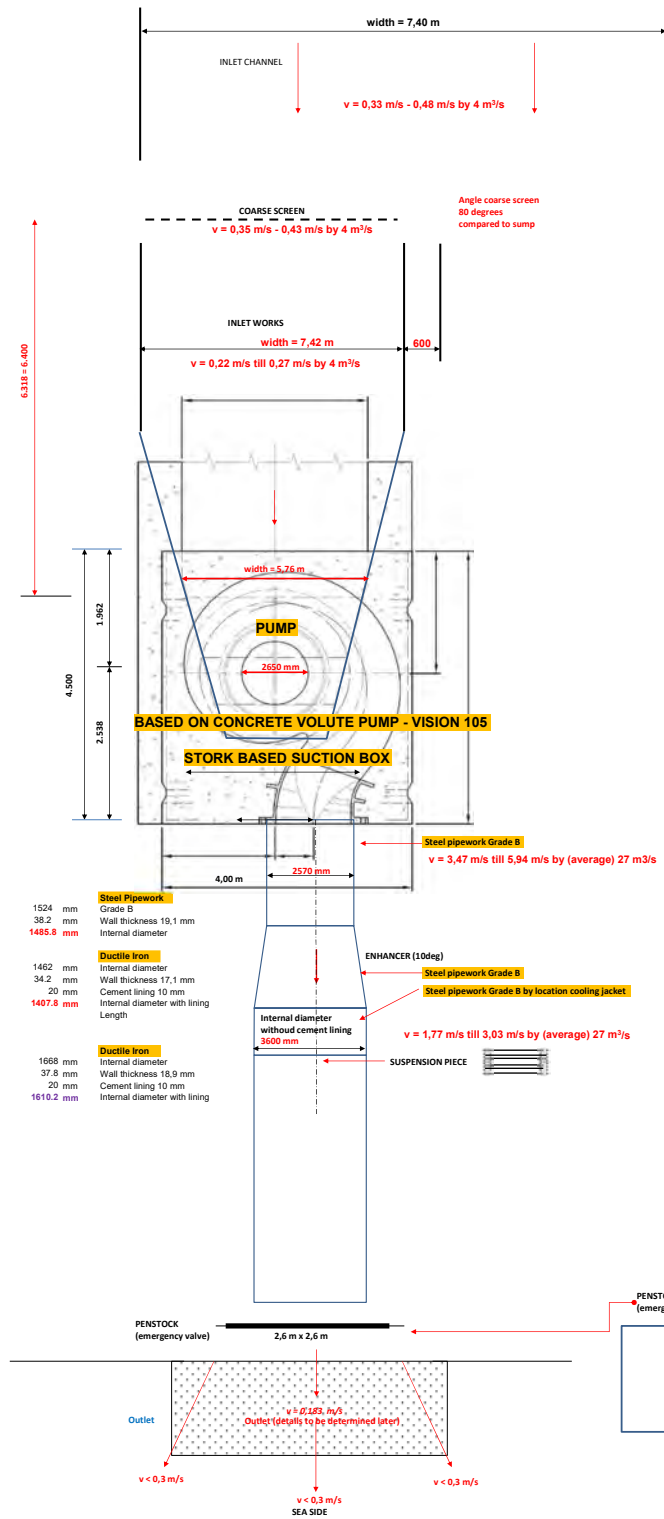
G

Flow Velocities Turbine

PROJECT	: POMPTURBINESTATION DELTA21
PROJECT NR.	: BG1930 TYPICAL NR. :
BETREFF	: DESIGN WET PATH - POMP
OPSTELLER	: LOC JACQUEMIN INITIALEN: LJ



IPS-RHD-MS-Z2-RP-M-2115
Hydraulic sizing Vision 105
Number 2115



- Steel Pipework**
Grade B
Wall thickness 19,1 mm
Internal diameter
1485,8 mm
- Ductile Iron**
Internal diameter
Wall thickness 17,1 mm
Cement lining 10 mm
Internal diameter with lining
Length
1407,8 mm
- Ductile Iron**
Internal diameter
Wall thickness 15,9 mm
Cement lining 10 mm
Internal diameter with lining
1610,2 mm

Water level	-22 mOD	Water level	-22 mOD	Water level	-13,5 mOD	Water level	-13,5 mOD
Sump floor	-30 mOD	Sump floor	-30 mOD	Sump floor	-30 mOD	Sump floor	-30 mOD
Water depth	8 m	Water depth	8 m	Water depth	16,5 m	Water depth	16,5 m
Width	7,4 m	Width	7,4 m	Width	7,4 m	Width	7,4 m
Surface A	59,2 m ²	Surface A	59,2 m ²	Surface A	122,1 m ²	Surface A	122,1 m ²
Q	36,7 m ³ /s	Q	35 m ³ /s	Q	27,8 m ³ /s	Q	18,3 m ³ /s
v	0,62 m/s	v	0,59 m/s	v	0,23 m/s	v	0,15 m/s

Water level	-23,4 mOD	Water level	-23,4 mOD	Water level	-23,4 mOD	Water level	-23,4 mOD
Sump floor	-30 mOD	Sump floor	-30 mOD	Sump floor	-30 mOD	Sump floor	-30 mOD
Water depth	6,6 m	Water depth	6,6 m	Water depth	6,6 m	Water depth	6,6 m
Width	7,4 m	Width	7,4 m	Width	7,4 m	Width	7,4 m
Surface A	48,84 m ²	Surface A	48,84 m ²	Surface A	48,84 m ²	Surface A	48,84 m ²
Q	36,7 m ³ /s	Q	35 m ³ /s	Q	27,8 m ³ /s	Q	18,3 m ³ /s
v	0,75 m/s	v	0,72 m/s	v	0,57 m/s	v	0,37 m/s

Water level	-27,43 mOD
Sump floor	-30 mOD
Water depth	2,57 m
Width	5,76 m
Surface A	14,803 m ²
Q	36,7 m ³ /s
v	2,479 m/s

Water level	-27,43 mOD
Sump floor	-30 mOD
Water depth	2,57 m
Width	5,76 m
Surface A	14,803 m ²
Q	18,3 m ³ /s
v	1,236 m/s

Diameter (internal)	2,57 m
Surface A	5,19 m ²
Q	36,7 m ³ /s
v	6,75 m/s

Diameter (internal)	2,57 m
Surface A	5,19 m ²
Q	35 m ³ /s
v	6,75 m/s

Diameter (internal)	2,57 m
Surface A	5,19 m ²
Q	27,8 m ³ /s
v	5,36 m/s

Diameter (internal)	2,57 m
Surface A	5,19 m ²
Q	18,3 m ³ /s
v	3,53 m/s

Diameter (internal)	3,60 m
Surface A	10,18 m ²
Q	36,7 m ³ /s
v	3,61 m/s

Diameter (internal)	3,60 m
Surface A	10,18 m ²
Q	35 m ³ /s
v	3,44 m/s

Diameter (internal)	3,60 m
Surface A	10,18 m ²
Q	27,8 m ³ /s
v	2,73 m/s

Diameter (internal)	3,60 m
Surface A	10,18 m ²
Q	18,3 m ³ /s
v	1,80 m/s

Bocht naar uitstroom	3,60 m
Width	3,60 m
Height	3,60 m
Surface A	12,96 m ²
Q	36,7 m ³ /s
v	2,85 m/s

Width	3,60 m
Height	3,60 m
Surface A	12,96 m ²
Q	35 m ³ /s
v	2,70 m/s

Width	3,60 m
Height	3,60 m
Surface A	12,96 m ²
Q	27,8 m ³ /s
v	2,15 m/s

Width	3,60 m
Height	3,60 m
Surface A	12,96 m ²
Q	18,3 m ³ /s
v	1,41 m/s

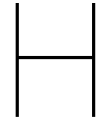
Width	5,20 m
Height	4,40 m
Surface A	22,88 m ²
Q	36,7 m ³ /s
v	1,60 m/s

Width	5,20 m
Height	4,40 m
Surface A	22,88 m ²
Q	35 m ³ /s
v	1,53 m/s

Width	5,20 m
Height	4,40 m
Surface A	22,88 m ²
Q	27,8 m ³ /s
v	1,22 m/s


Width	5,20 m
Height	4,40 m
Surface A	22,88 m ²
Q	18,3 m ³ /s
v	0,80 m/s

Rooster

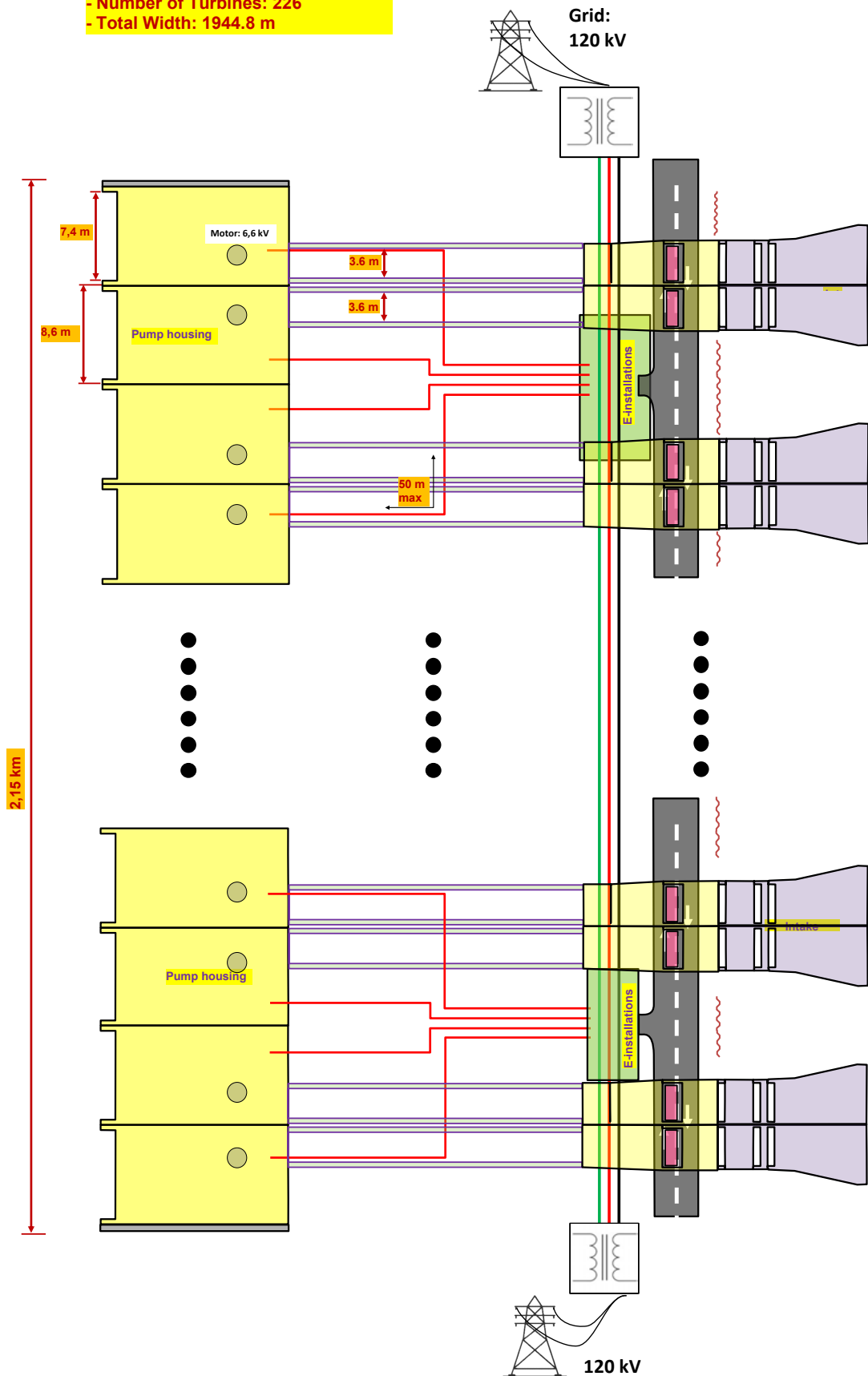


Overview Schematic

The overview schematic is a bird's-eye view of the total installation. It shows the required infrastructure as well as the separate turbine-pumping modules next to each other. Based on the intake width and the number of pumps the total width of the turbine-pumping station can be estimated. This is based on a wall width of 0.6 for each pumphouse.

PROJECT	: OVERVIEW DELTA21			
PROJECT NR.	: X	TYPICAL NR.		:
BETREFF.	: K			
OPSTELLER	: LOIC JACQUEMIN	INITIALEN:		: LJ

VERSION: 44 m³/s
- Impeller Diameter: Ø2.649 mm
- Intake Width: 7417 mm
- Overall Width (2x600mm): 8600 mm
- Number of Turbines: 226
- Total Width: 1944.8 m





NPSH Calculations

PROJECT	DELTA21		 
PROJECT NR	BF1709	DATUM & VERSIE : 19-12-2016, Versie 2.0	
SUBJECT	NPSH BEREKENING TURBINE POMP		
AUTHOR	LOIG JACQUEMEN	INITIALS:	

Temperatuur	10.0 °C
Centrifuge impeller	-21.00 mNAP
Atmospheric pressure	990.0 hPa

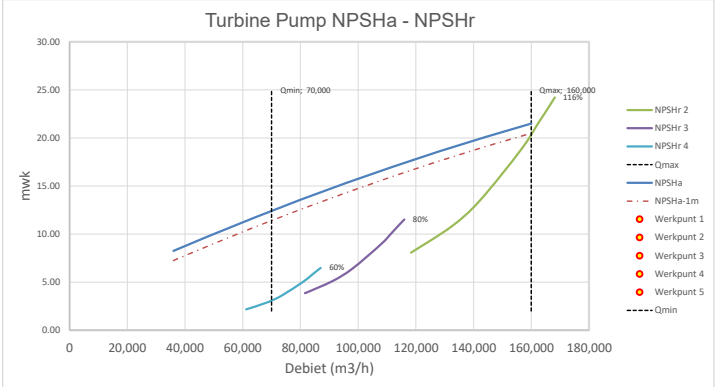
Regeling gemeal				
		m ³ /s	m ³ /h	
Qmin	36.000 [m ³ /h]		10	36000
Qmax	160.000 [m ³ /h]		31.8	114480
Instlagpeil	-22.5 [mNAP]		40	144000
Uitslagpeil	-22.5 [mNAP]		44.44444	160000
Max regelpeil	-5.0 [mNAP]			
Overstortpeil	-5.0 [mNAP]			

Plot grenzen	
Qmin	36.000
Qmax	160.000

NPSHr curve										
n-nom	Merk, type		150.00 n=		174.00 n=		120.00 n=		90.00 n=	
	100%	116%	80%				60%			
145.000	18.00	168.200	24.22	#####	11.52	87.000	6.48			
140.000	16.00	162.400	21.53	#####	10.24	84.000	5.76			
135.000	14.00	156.600	18.84	#####	8.96	81.000	5.04			
122.500	10.00	142.100	13.46	#####	6.40	73.500	3.60			
114.000	8.00	132.240	10.76	#####	5.12	68.400	2.88			
102.000	6.00	118.320	8.07	#####	3.84	61.200	2.16			
			0.00			0.00				
			0.00			0.00				
			0.00			0.00				
			0.00			0.00				
			0.00			0.00				

Verlies zuigleiding	
0	0
16000	0.0451
32000	0.1798
48000	0.404
64000	0.7177
80000	1.1208
96000	1.6133
112000	2.1953
128000	2.8668
144000	3.6276
160000	4.478
160000	4.478
160000	4.478
160000	4.478
160000	4.478
160000	4.478
160000	4.478
160000	4.478
160000	4.478
160000	4.478
160000	4.478
160000	4.478
160000	4.478
160000	4.478
160000	4.478
160000	4.478

Plotgrenzen Qmin		Plotgrenzen Qmax		Werpunten	
70.000	2.0	160.000	2.0	P1	114.480
70.000	25.0	160.000	25.0	P2	
				P3	
				P4	
				P5	



J

NPSH Head Losses

PROJECT	DEL TA21	TYPICAL_NL	
PROJECT NR.			
BETREFFT	LEIDINGWEERSTAND POMPTURBINE 30 MP'S		
OPTELLER	LOC. JACQUEM	INITIALEN	U



LAYOUT GEMAAL T.B.V. LEIDINGWEERSTANDBEREKENING

ALGEMENE GEGEVENS	
Materiaal	perlslabesteen
Volumieke massa	1.600 kg/m ³
Viscositeit	1.66E-06 m ² /s
Omax gemaal	160.000 m ³ /h
Omax gemaal	1 m ³ /h
Aantal pompen samenhangend	1 stuks
Zwaartekrachtversnelling	9.80665 m/s ²

ZUIGLEIDING	
Opomp	160.000 m ³ /h
Diameter	3.600 mm
Lengte	40,00 m
Materiaal	B
Wandruwheid [k]	0,2 mm

PERSLEIDING	
Opomp	160.000 m ³ /h
Diameter	3.600 mm
Lengte	40,00 m
Materiaal	B
Wandruwheid [k]	0,2 mm

GEZAMENLIJKE PERSLEIDING DEEL 1	
Opomp	160.000 m ³ /h
Diameter	3.600 mm
Lengte	0,00 m
Materiaal	GY
Wandruwheid [k]	0,2 mm

GEZAMENLIJKE PERSLEIDING DEEL 2	
Opomp(er)	160.000 m ³ /h
Diameter	10.000 mm
Lengte	0,00 m
Materiaal	
Wandruwheid [k]	0,0 mm

GEZAMENLIJKE PERSLEIDING DEEL 3	
Opomp(er)	160.000 m ³ /h
Diameter	10.000 mm
Lengte	0,00 m
Materiaal	
Wandruwheid [k]	0,0 mm

TERREIN PERSLEIDING DEEL 4	
Opomp(er)	160.000 m ³ /h
Diameter	10.000 mm
Lengte	0,00 m
Materiaal	Staal
Wandruwheid [k]	0,0 mm

FORMSTUKKEN/APPENDAGES			
Instroom	0,05	1	0,05
Knie	1,30	0	0,00
Bocht	0,15	0	0,00
T-stuk	1,50	0	0,00
Verloop	0,10	1	0,10
Afsluiter	0,30	1	0,30
Tenueplagklep	1,00	0	0,00
Uitstroom	1,00	0	0,00
Gedetailleerde verwijding	0,80	0	0,00
Totaal zeta	1,50	0,48	

Drukverval per meter leiding	249,83 Pa/m
Drukverval bij Omax	2,50 kPa
Drukverval bij Omax - totaal	1,84 kPa
Drukverval bij Omax - totaal	1,84 mW/k

FORMSTUKKEN/APPENDAGES			
Instroom	0,05	0	0,00
Knie	1,30	0	0,00
Bocht	0,15	2	0,30
T-stuk	1,50	0	0,00
Verloop	0,10	0	0,00
Afsluiter	0,30	0	0,00
Tenueplagklep	1,40	1	1,40
Uitstroom	1,00	1	1,00
Gedetailleerde verwijding	0,80	0	0,00
Totaal zeta	2,22	2,70	

Drukverval per meter leiding	54,02 Pa/m
Drukverval bij Omax	1,64 kPa
Drukverval bij Omax - totaal	2,84 kPa
Drukverval bij Omax - totaal	2,84 mW/k

FORMSTUKKEN/APPENDAGES			
Instroom	0,05	0	0,00
Knie	1,30	0	0,00
Bocht	0,15	0	0,00
T-stuk	1,50	0	0,00
Verloop	0,10	0	0,00
Afsluiter	0,30	0	0,00
Tenueplagklep	1,00	0	0,00
Uitstroom	1,00	0	0,00
Gedetailleerde verwijding	0,15	0	0,00
Totaal zeta	0,00	0,00	

Drukverval per meter leiding	0,00 Pa/m
Drukverval bij Omax	0,00 kPa
Drukverval bij Omax - totaal	0,01 kPa
Drukverval bij Omax - totaal	0,00 mW/k

FORMSTUKKEN/APPENDAGES			
Instroom	0,05	0	0,00
Knie	1,30	0	0,00
Bocht	0,15	0	0,00
T-stuk	1,50	0	0,00
Verloop	0,10	0	0,00
Afsluiter	0,30	0	0,00
Tenueplagklep	1,00	0	0,00
Uitstroom	1,00	0	0,00
Gedetailleerde verwijding	1,00	0	0,00
Totaal zeta	0,00	0,00	

Drukverval per meter leiding	0,00 Pa/m
Drukverval bij Omax	0,00 kPa
Drukverval bij Omax - totaal	0,01 kPa
Drukverval bij Omax - totaal	0,00 mW/k

FORMSTUKKEN/APPENDAGES			
Instroom	0,05	0	0,00
Knie	1,30	0	0,00
Bocht	0,15	0	0,00
T-stuk	1,50	0	0,00
Verloop	0,10	0	0,00
Afsluiter	0,30	0	0,00
Tenueplagklep	1,00	0	0,00
Uitstroom	1,00	0	0,00
Gedetailleerde verwijding	1,00	0	0,00
Totaal zeta	0,00	0,00	

Drukverval per meter leiding	0,00 Pa/m
Drukverval bij Omax	0,00 kPa
Drukverval bij Omax - totaal	0,01 kPa
Drukverval bij Omax - totaal	0,00 mW/k

FORMSTUKKEN/APPENDAGES			
Instroom	0,05	0	0,00
Knie	1,30	0	0,00
Bocht	0,15	0	0,00
T-stuk	1,50	0	0,00
Verloop	0,10	0	0,00
Afsluiter	0,30	0	0,00
Tenueplagklep	1,00	0	0,00
Uitstroom	1,00	0	0,00
Gedetailleerde verwijding	1,00	0	0,00
Totaal zeta	0,00	0,00	

Drukverval per meter leiding	0,00 Pa/m
Drukverval bij Omax	0,00 kPa
Drukverval bij Omax - totaal	0,01 kPa
Drukverval bij Omax - totaal	0,00 mW/k

Drukverval per meter leiding	0,00 Pa/m
Drukverval bij Omax	0,00 kPa
Drukverval bij Omax - totaal	0,01 kPa
Drukverval bij Omax - totaal	0,00 mW/k

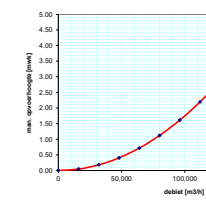
Drukverval per meter leiding	0,00 Pa/m
Drukverval bij Omax	0,00 kPa
Drukverval bij Omax - totaal	0,01 kPa
Drukverval bij Omax - totaal	0,00 mW/k

Drukverval per meter leiding	0,00 Pa/m
Drukverval bij Omax	0,00 kPa
Drukverval bij Omax - totaal	0,01 kPa
Drukverval bij Omax - totaal	0,00 mW/k

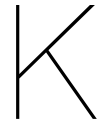
Drukverval per meter leiding	0,00 Pa/m
Drukverval bij Omax	0,00 kPa
Drukverval bij Omax - totaal	0,01 kPa
Drukverval bij Omax - totaal	0,00 mW/k

Drukverval per meter leiding	0,00 Pa/m
Drukverval bij Omax	0,00 kPa
Drukverval bij Omax - totaal	0,01 kPa
Drukverval bij Omax - totaal	0,00 mW/k

inwendige weerstand gemaal

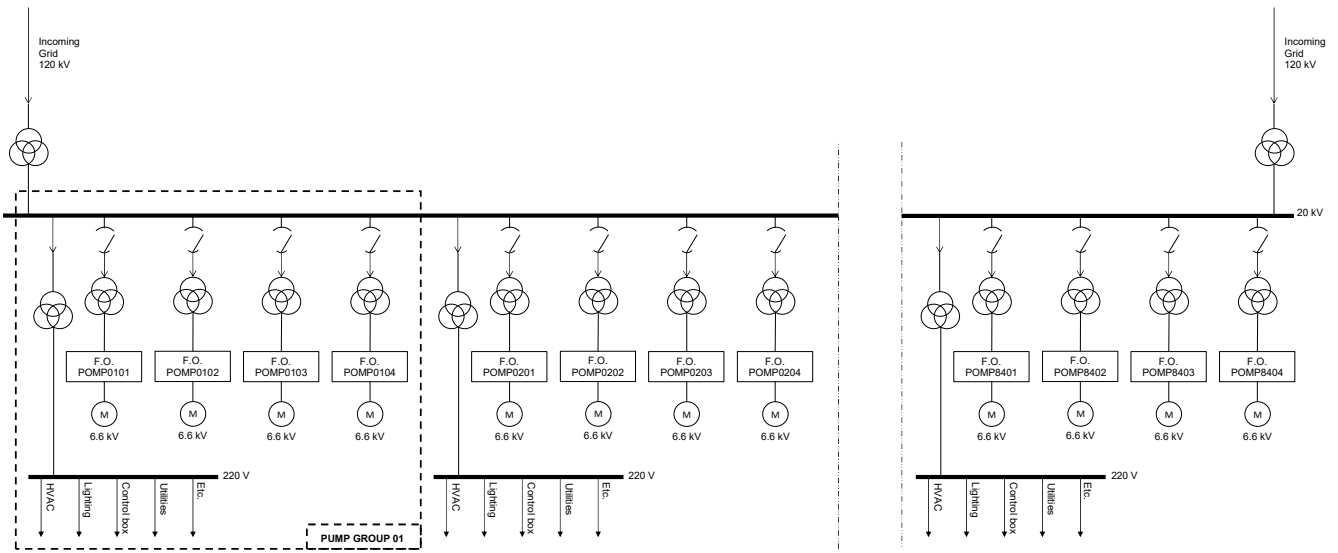


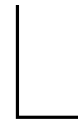
debiet [m³/h]	inwendige weerstand [mW/k]
0	0,00
10.000	0,00
32.000	0,18
48.000	0,40
64.000	0,72
80.000	1,12
96.000	1,61
112.000	2,20
128.000	2,87
144.000	3,63
160.000	4,48



Single-line Diagram

PROJECT	: DELTA21 POMTURBINE	1.60	Column
PROJECT NR.	: TYPICAL NR. :	13.80	Height
BETREFT	: ONE-LINE DIAGRAM		
OPSTELLER	: LOIC JACQUEMIN	INITIALEN: LJ	





System Efficiencies

PROJECT NR. :	PUMPING STATION DELTA21
BETREFT :	TYPICAL NR. :
OPSTELLER :	L. JACQUEMIN [INITIALEN] LJ



GUARANTEED POINT 1 ● 4. Gemiddeld zee/Minimaal Valmeer

Point 1

Q	1,332 [m³/min]	22.20 [m³/s]	79,920 [m³/h]
Rho		1,020 [kg/m³]	
$H_{manometric} = H_{static} + H_{dynamic}$		23.50 [mwc]	Calculated in hydraulic design
$\eta_{Pump, Motor, Vsd, Harmonic Filters}$		0.629 [%/100]	Calculated
η_{pump}		0.700 [%/100]	Fill in pump manufacturer
η_{motor}		0.945 [%/100]	Fill in pump manufacturer
η_{VSD}		0.965 [%/100]	Fill in pump manufacturer
$\eta_{Harmonic Filters}$		0.985 [%/100]	Fill in pump manufacturer
η_{total}		0.985 [%/100]	Fill in pump manufacturer

Speed $\omega_{motor} = 175 \text{ min}^{-1}$ (Star connected)

GUARANTEED POINT 2 ● 5. Gemiddeld Zee/Gemiddeld Valmeer

Best Efficiency Point

Q	2,400 [m³/min]	40.00 [m³/s]	144,000 [m³/h]
Rho		1,020 [kg/m³]	
$H_{manometric} = H_{static} + H_{dynamic}$		16.50 [mwc]	Calculated in hydraulic design
$\eta_{Pump, Motor, Vsd, Harmonic Filters}$		0.790 [%/100]	Calculated
η_{pump}		0.875 [%/100]	Fill in pump manufacturer
η_{motor}		0.945 [%/100]	Fill in pump manufacturer
η_{VSD}		0.970 [%/100]	Fill in pump manufacturer
$\eta_{Harmonic Filters}$		0.985 [%/100]	Fill in pump manufacturer
η_{total}		0.985 [%/100]	Fill in pump manufacturer

Speed $\omega_{motor} = 175 \text{ min}^{-1}$ (Star connected)

GUARANTEED POINT 3 ● 5. Gemiddeld Zee/Gemiddeld Valmeer

Lowest Discharge

Q	2,166 [m³/min]	36.10 [m³/s]	129,960 [m³/h]
Rho		1,020 [kg/m³]	
$H_{manometric} = H_{static} + H_{dynamic}$		7.70 [mwc]	Calculated in hydraulic design
$\eta_{Pump, Motor, Vsd, Harmonic Filters}$		0.640 [%/100]	Calculated
η_{pump}		0.720 [%/100]	Fill in pump manufacturer
η_{motor}		0.930 [%/100]	Fill in pump manufacturer
η_{VSD}		0.970 [%/100]	Fill in pump manufacturer
$\eta_{Harmonic Filters}$		0.985 [%/100]	Fill in pump manufacturer
η_{total}		0.985 [%/100]	Fill in pump manufacturer

Speed $\omega_{motor} = 140 \text{ min}^{-1}$ (Star connected)

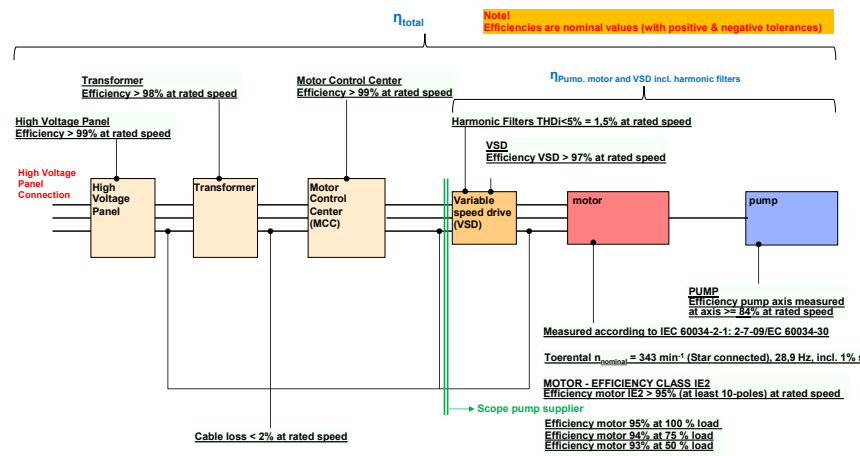
GUARANTEED POINT 4 ● 1. Extreem hoog zee/Maximaal Valmeer

Q	2,664 [m³/min]	44.40 [m³/s]	159,840 [m³/h]
Rho		1,020 [kg/m³]	
$H_{manometric} = H_{static} + H_{dynamic}$		13.00 [mwc]	Calculated in hydraulic design
$\eta_{Pump, Motor, Vsd, Harmonic Filters}$		0.723 [%/100]	Calculated
η_{pump}		0.805 [%/100]	Fill in pump manufacturer
η_{motor}		0.950 [%/100]	Fill in pump manufacturer
η_{VSD}		0.960 [%/100]	Fill in pump manufacturer
$\eta_{Harmonic Filters}$		0.985 [%/100]	Fill in pump manufacturer
η_{total}		0.985 [%/100]	Fill in pump manufacturer

Electrical VSD connection including Harmonic Filters **7,987 [kW]** Calculated

$$P_{exit\ transformer} [kW] = \frac{Q [m^3/s] \cdot \rho [kg/m^3] \cdot g [m/s^2] \cdot H_{manometric} [mwc]}{1.000 \cdot \eta_{hydraulic} \cdot \eta_{volumetric} \cdot \eta_{mechanical} \cdot \eta_{motor} \cdot \eta_{VSD} \cdot \eta_{Harmonic\ Filters} \cdot \eta_{MCC} \cdot \eta_{Transformer} \cdot \eta_{High\ Voltage\ Panel} \cdot \eta_{Cable\ losses}}$$

$\eta_{pump\ measured\ at\ axis}$



GUARANTEED POINT 5 ● 2. Gemiddeld zee

Q	1,734 [m³/min]	28.90 [m³/s]	104,040 [m³/h]
Rho		1,020 [kg/m³]	
$H_{manometric} = H_{static} + H_{dynamic}$		5.00 [mwc]	Calculated in hydraulic design
$\eta_{Pump, Motor, Vsd, Harmonic Filters}$		0.787 [%/100]	Calculated
η_{pump}		0.900 [%/100]	Fill in pump manufacturer
η_{motor}		0.925 [%/100]	Fill in pump manufacturer
η_{VSD}		0.960 [%/100]	Fill in pump manufacturer
$\eta_{Harmonic Filters}$		0.985 [%/100]	Fill in pump manufacturer
η_{total}		0.985 [%/100]	Fill in pump manufacturer

Speed $\omega_{motor} = 113 \text{ min}^{-1}$ (Star connected)

Electrical VSD connection including Harmonic Filters **1,637 [kW]** Calculated

M

Water Cooling Principle

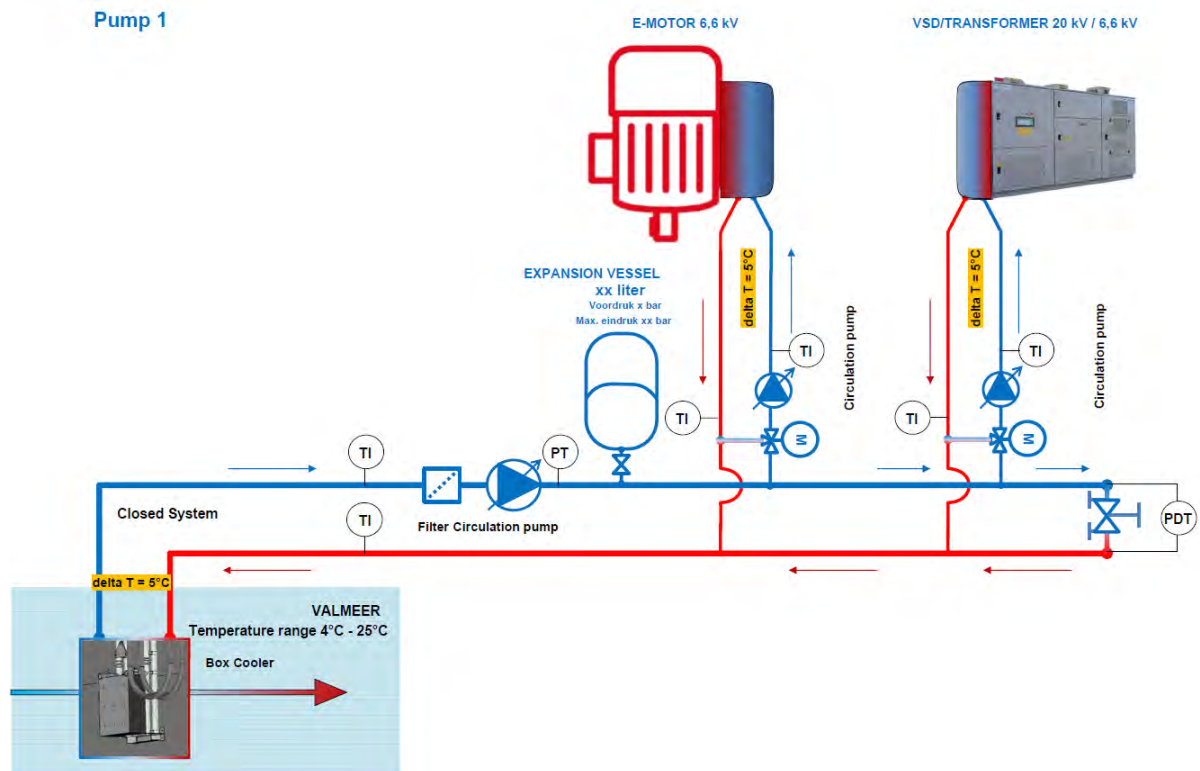


Figure M.1: Cooling Principle Schematic

N

NPSH Calculations: 180 rpm

PROJECT	DELTA21		
PROJECT NR	BF1789	DATUM & VERSIE	19-12-2016, Versie 2.0
SUBJECT	NPSH BEREKENING TURBINE POMP		
AUTHOR	LOIC JACQUEMEN	INITIALS	



Temperatuur	10.0	°C
Centrefline impeller	-25.00	mNAP
Atmospheric pressure	990.0	hPa

Regeling gemaal			
Qmin	36.000	[m3/h]	m3/s m3/h
Qmax	170.000	[m3/h]	
Instagpeil	-22.5	[mNAP]	40 144000
Uitslagpeil	-22.5	[mNAP]	44.44444 160000
Max regelpeil	-5.0	[mNAP]	
Overstortpeil	-5.0	[mNAP]	

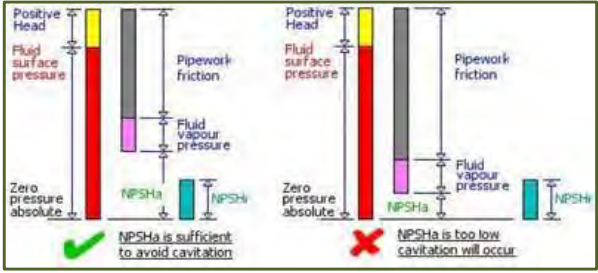
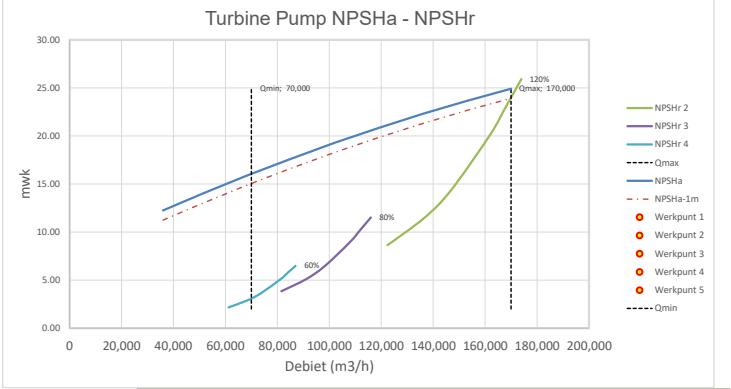
Plot grenzen	
Qmin	36.000
Qmax	180.000

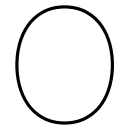
NPSHr curve						
n-nom	150.00	n=	180.00	n=	120.00	n=
	100%		120%		80%	60%
145.000	18.00	174.000	25.92	11.52	87.000	6.48
140.000	16.00	168.000	23.04	10.24	84.000	5.76
135.000	14.00	162.000	20.16	8.96	81.000	5.04
122.500	10.00	147.000	14.40	6.40	73.500	3.60
114.000	8.00	136.800	11.52	5.12	68.400	2.88
102.000	6.00	122.400	8.64	3.84	61.200	2.16
		0.00	0.00	0.00	0.00	0.00
		0.00	0.00	0.00	0.00	0.00
		0.00	0.00	0.00	0.00	0.00
		0.00	0.00	0.00	0.00	0.00

Verlies zuigleiding	
0	0
17000	0.0509
34000	0.203
51000	0.456
68000	0.8101
85000	1.2651
102000	1.8211
119000	2.4781
136000	3.236
153000	4.0949
170000	5.0548
170000	5.0548
170000	5.0548
170000	5.0548
170000	5.0548
170000	5.0548
170000	5.0548
170000	5.0548
170000	5.0548
170000	5.0548
170000	5.0548
170000	5.0548
170000	5.0548
170000	5.0548

Plotgrenzen Qmin	70.000	2.0
Plotgrenzen Qmax	170.000	2.0
Plotgrenzen Qmax	170.000	25.0

Werkpunten	
P1	114.480
P2	
P3	
P4	
P5	





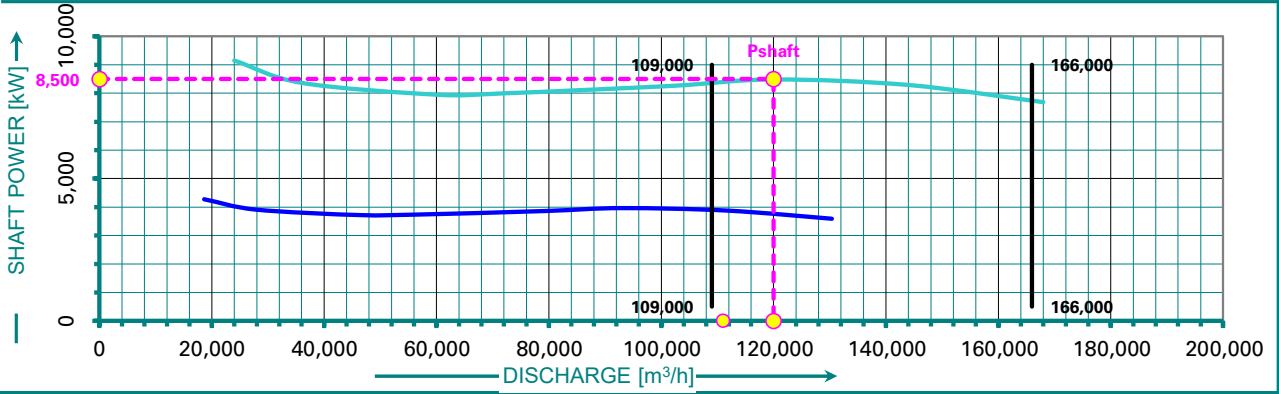
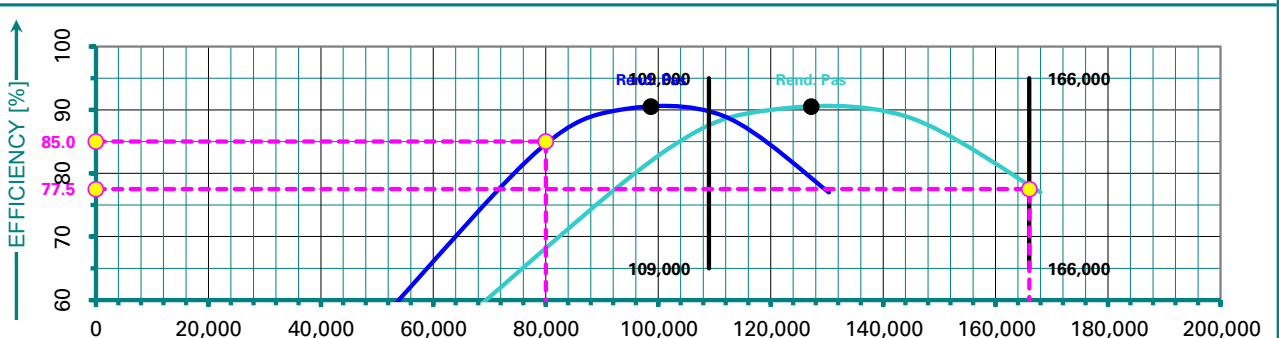
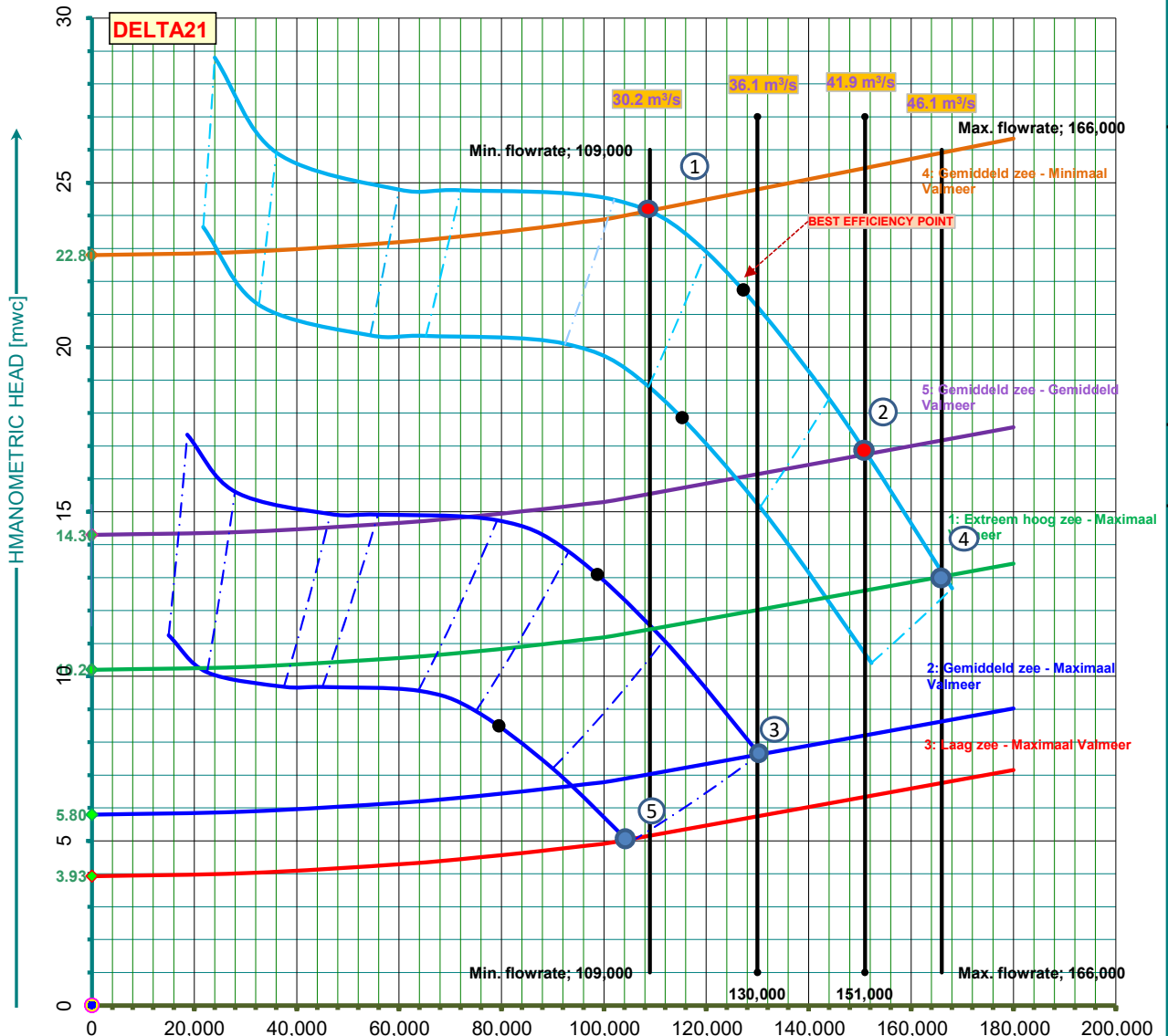
System and Pump Curve: 180 rpm

● optimal operation point pump ● System relevant operating points

PROJECT	PUMPING STATION DELTA 21		
PROJECT NO.	INITIALEN:	LJ	
SUBJECT	SYSTEM AND PUMP CHARACTERISTIC		
OPSTELLER	LOIC JACQUEMIN		

curve	min-1	%	Hz	curve	min-1	%	Hz
N1	180	96.0%	48.0	N5	92	49.3%	24.7
N2	163	87.0%	43.5	N6	87	46.4%	23.2
N3	140	74.5%	37.3	N7	84	45.0%	22.5
N4	113	60.0%	30.0	N8	80	42.8%	21.4

PUMP: CVP TYPE: Pump SPEED: 187.5 rpm FREE PASSAGE:



P

NPSH Calculations: 190 rpm

PROJECT	DELTA21		
PROJECT NR	BF1789	DATUM & VERSIE	19-12-2018, Versie 2.0
SUBJECT	NPSH BEREKENING TURBINE POMP		
AUTHOR	LOIC JACQUEMEN	INITIALS	



Temperatuur	10.0	°C
Centrifuge impeller	-30.00	mNAP
Atmospheric pressure	990.0	hPa

Regeling gemaal			
Qmin	36,000	[m3/h]	m3/s 10 36000
Qmax	190,000	[m3/h]	31.8 114480
Instagpeil	-22.5	[mNAP]	40 144000
Uitslagpeil	-22.5	[mNAP]	44.44444 160000
Max regelpeil	-5.0	[mNAP]	
Overstortpeil	-5.0	[mNAP]	

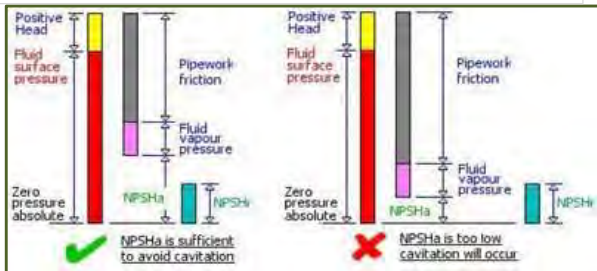
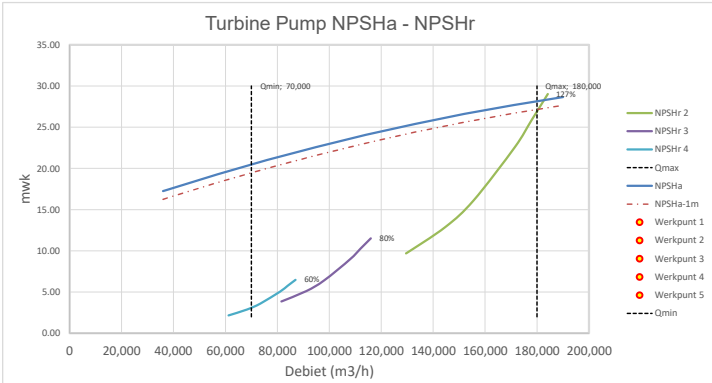
Plot grenzen	
Qmin	36,000
Qmax	200,000

NPSHr curve							
n-nom	150.00	n=	190.50	n=	120.00	n=	90.00
145,000	18.00	184.150	29.03	#####	11.52	87,000	6.48
140,000	16.00	177.800	25.81	#####	10.24	84,000	5.76
135,000	14.00	171.450	22.58	#####	8.96	81,000	5.04
122,500	10.00	155.575	16.13	38,000	6.40	73,500	3.60
114,000	8.00	144.780	12.90	91,200	5.12	68,400	2.88
102,000	6.00	129.540	9.68	81,600	3.84	61,200	2.16
		0.00	0.00		0.00		0.00
		0.00	0.00		0.00		0.00
		0.00	0.00		0.00		0.00
		0.00	0.00		0.00		0.00
		0.00	0.00		0.00		0.00

Verlies zuigleiding	
0	0
19000	0.0636
38000	0.2534
57000	0.5694
76000	1.0116
95000	1.5799
114000	2.2744
133000	3.0949
152000	4.0416
171000	5.1144
190000	6.3134
190000	6.3134
190000	6.3134
190000	6.3134
190000	6.3134
190000	6.3134
190000	6.3134
190000	6.3134
190000	6.3134
190000	6.3134
190000	6.3134
190000	6.3134
190000	6.3134

Plotgrenzen Qmin	
70,000	2.0
70,000	30.0
Plotgrenzen Qmax	
180,000	2.0
180,000	30.0

Werkpunten	
P1	114,480
P2	
P3	
P4	
P5	



Q

System and Pump Curve: 190 rpm

● optimal operation point pump ● System relevant operating points

PROJECT	PUMPING STATION DELTA 21		
PROJECT NO.	INITIALEN:	LJ	
SUBJECT	SYSTEM AND PUMP CHARACTERISTIC		
OPSTELLER	LOIC JACQUEMIN		

curve	min-1	%	Hz
N1	190	101.5%	50.8
N2	163	87.0%	43.5
N3	140	74.5%	37.3
N4	113	60.0%	30.0

curve	min-1	%	Hz
N5	92	49.3%	24.7
N6	87	46.4%	23.2
N7	84	45.0%	22.5
N8	80	42.8%	21.4

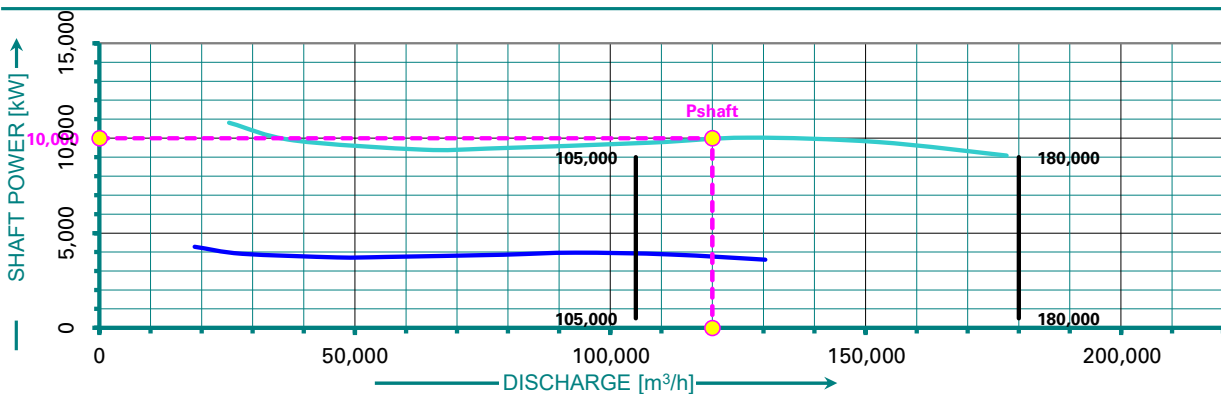
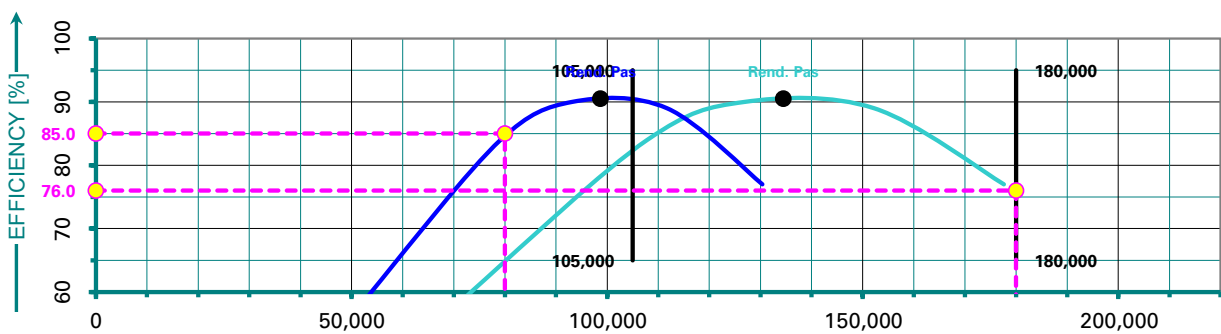
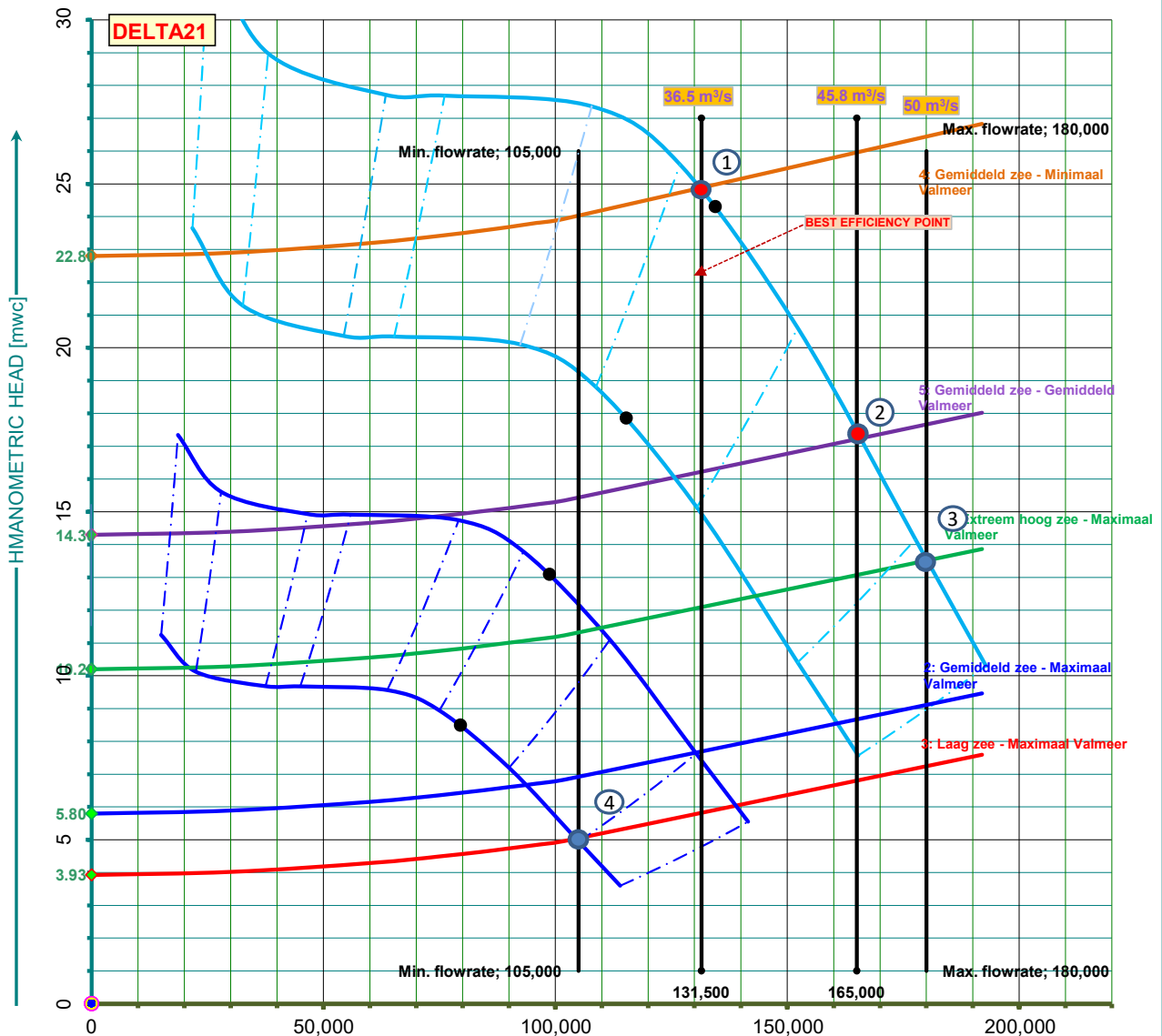
PUMP: CVP

TYPE: Pump

SPEED:

187.5 rpm

FREE PASSAGE:



R

Cost Calculations

Characteristics																						
Concept	D Impeller [m]	H Impeller [m - N/A]	Stroke	n_max [rpm]	n_pumps	Total Width [m]	Extra Depth Impeller	Extra Depth Draft	Extra Depth Total [m]	Time [min]	Power [MW]	Time [min]	Power [MW]	Cycle Duration [sec]	Efficiency [%]	Max. Power [jumping] [MW]	Concept 1	Concept 2	Concept 3	Concept 4	Concept 5	Concept 6
Concept 1	2.600	-25	Surfcon Box	175	208	2221.56	0.0	0.00	0.0	400	18923.24180	360	14400.00000	2560	62.7	8.20	44.4	8.20	18597.20000	12687.00000	12687.00000	12687.00000
Concept 2	2.400	-25	Drift Tube	180	313	2638.56	4.0	2.75	6.7	906	28261.49738	1014	12378.95045	1620	43.9	7.80	46.1	7.80	28164.81878	12781.95000	12781.95000	12781.95000
Concept 3	2.600	-25	Drift Tube	175	208	2221.56	0.0	0.00	0.0	400	18923.24180	360	12318.70000	2120	66.2	8.80	46.4	8.80	28287.00000	12218.20000	12218.20000	12218.20000
Concept 4	2.800	-25	Surfcon Box	180	237	2023.28	4.0	0.00	4.0	547	18462.61700	865	10980.08828	1432	59.7	11.36	46.1	11.36	18462.61700	10980.08828	10980.08828	10980.08828
Concept 5	2.600	-20	Surfcon Box	180	226	2064.22	8.0	0.00	8.0	574	18458.42112	960	10467.43460	2120	59.9	10.15	50	10.15	18458.42112	10467.43460	10467.43460	10467.43460
Concept 6	2.600	-25	Drift Tube	180	247	2130.34	4.0	0.00	7.0	583	18168.10171	918	12116.70000	1501	67.7	9.13	44.4	9.13	18168.10171	12116.70000	12116.70000	12116.70000

Evaluation										
Criteria	Performance (D-D)	Performance (D-S)	Power Generated (D-S)	Height + 0.2Z	Height + 0.1Z	Height + 0.0Z	Sensitivity to Failure	Total Score		
Concept 1	4	4	4	4	4	4	4.00		-10.0	33.0
Concept 2	1	1	4	3	4	4	2.50		-36.7	36.7
Concept 3	5	4	5	5.5	4	5	4.75		-10.0	31.0
Concept 4	1	2	1	1	1	1	1.00		-34.0	34.0
Concept 5	3	3	3	3	3	3	2.50		-39.0	39.0
Concept 6	6	5	5	5.5	4	5	4.50		-37.0	37.0

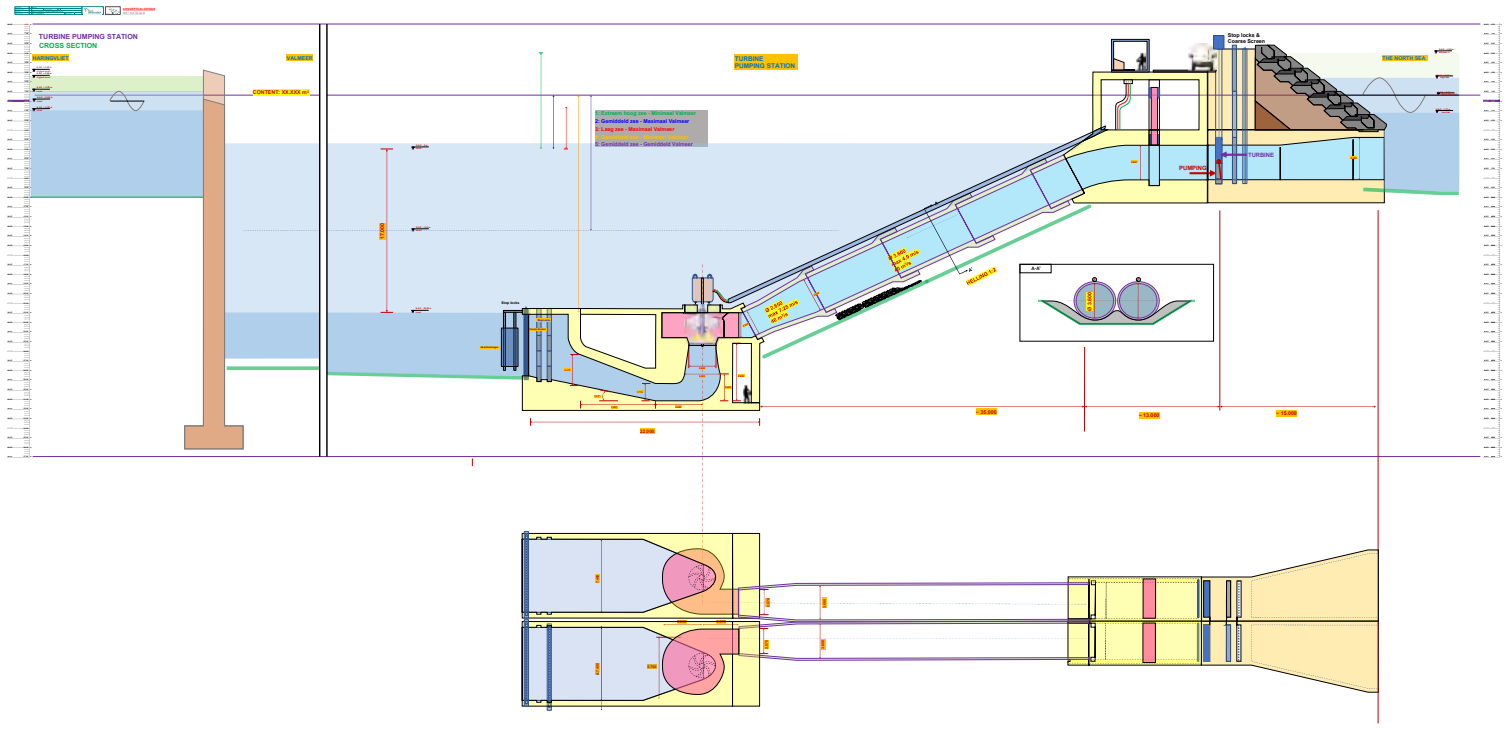
Costs														
Per Unit	Machinery		Excavation		Powerhouse (reinforced concrete)				Penstock		Bed Protection		Ground Improvement	
	Unit cost	Volume [m³]	Unit cost	Volume [m³]	Unit cost	Volume [m³]	Unit cost	Volume [m³]	Unit cost	Volume [m³]	Unit cost	Volume [m³]	Unit cost	Volume [m³]
Concept 1	€ 4,311,121.00	€ 1,020,000,000.00	€ 1,111,442.8	€ 14,111,442.8	€ 248.4	€ 613,786.00	€ 632.32	€ 372,487.40	€ 24,000.00	€ 216,000.00	€ 10,000.00	€ 100,000.00	€ 1,000.00	€ 10,000.00
Concept 2	€ 4,026,376.48	€ 1,130,466,428.00	€ 1,111,442.8	€ 14,111,442.8	€ 248.4	€ 613,786.00	€ 632.32	€ 372,487.40	€ 24,000.00	€ 216,000.00	€ 10,000.00	€ 100,000.00	€ 1,000.00	€ 10,000.00
Concept 3	€ 4,391,162.19	€ 1,020,000,000.00	€ 1,111,442.8	€ 14,111,442.8	€ 248.4	€ 613,786.00	€ 632.32	€ 372,487.40	€ 24,000.00	€ 216,000.00	€ 10,000.00	€ 100,000.00	€ 1,000.00	€ 10,000.00
Concept 4	€ 4,376,611.11	€ 1,118,970,088.27	€ 1,111,442.8	€ 14,111,442.8	€ 248.4	€ 613,786.00	€ 632.32	€ 372,487.40	€ 24,000.00	€ 216,000.00	€ 10,000.00	€ 100,000.00	€ 1,000.00	€ 10,000.00
Concept 5	€ 4,361,376.19	€ 1,020,347,390.00	€ 1,111,442.8	€ 14,111,442.8	€ 248.4	€ 613,786.00	€ 632.32	€ 372,487.40	€ 24,000.00	€ 216,000.00	€ 10,000.00	€ 100,000.00	€ 1,000.00	€ 10,000.00
Concept 6	€ 4,631,508.19	€ 1,020,466,600.24	€ 1,111,442.8	€ 14,111,442.8	€ 248.4	€ 613,786.00	€ 632.32	€ 372,487.40	€ 24,000.00	€ 216,000.00	€ 10,000.00	€ 100,000.00	€ 1,000.00	€ 10,000.00

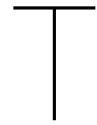
Total Costs									
Concept	Cost [€]	Mechanical	Electrical	Total	Ratio				
Concept 1	€ 174,427,111.00	€ 1,020,000,000.00	€ 1,111,442.8	€ 1,291,538,543.14	0.898				
Concept 2	€ 331,350,477.96	€ 1,138,466,428.00	€ 1,111,442.8	€ 1,470,928,348.76	0.433				
Concept 3	€ 376,580,605.02	€ 1,020,000,000.00	€ 1,111,442.8	€ 1,397,692,047.82	0.921				
Concept 4	€ 373,828,602.14	€ 1,118,470,088.27	€ 1,111,442.8	€ 1,493,409,133.28	0.615				
Concept 5	€ 382,576,678.53	€ 1,020,347,390.00	€ 1,111,442.8	€ 1,404,035,511.53	0.643				
Concept 6	€ 373,358,821.48	€ 1,020,466,600.24	€ 1,111,442.8	€ 1,394,836,864.52	0.868				

Value vs. Cost									
Concept	Cost [€]	Value [€]	Ratio						
Concept 1	€ 1,395,455,653.14	€ 1,395,455,653.14	1.000						
Concept 2	€ 1,472,918,577.86	€ 637,000,000.00	0.433						
Concept 3	€ 1,395,455,653.14	€ 1,395,455,653.14	1.000						
Concept 4	€ 1,380,461,586.51	€ 856,200,000.00	0.615						
Concept 5	€ 1,389,465,475.16	€ 856,200,000.00	0.615						
Concept 6	€ 1,385,161,463.92	€ 1,111,200,000.00	0.868						

S

Level Schematic Selected Hydraulic Design





Construction Sequence: Construction Pit Method

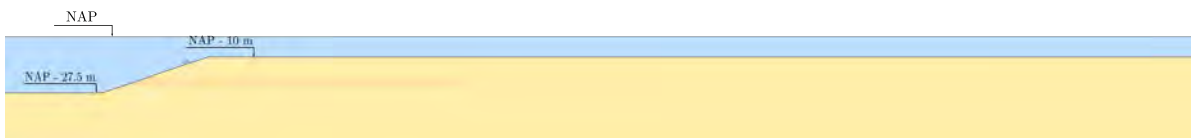


Figure T.1: Initial situation

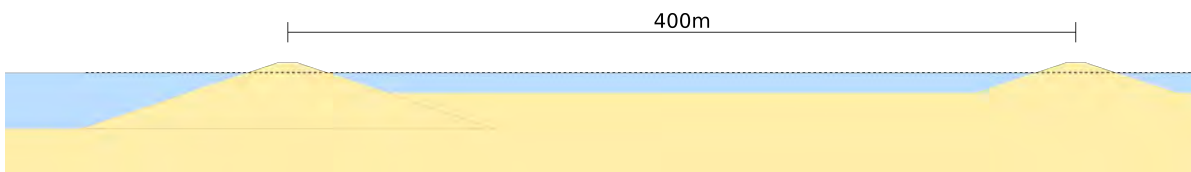


Figure T.2: Dredging of embankments

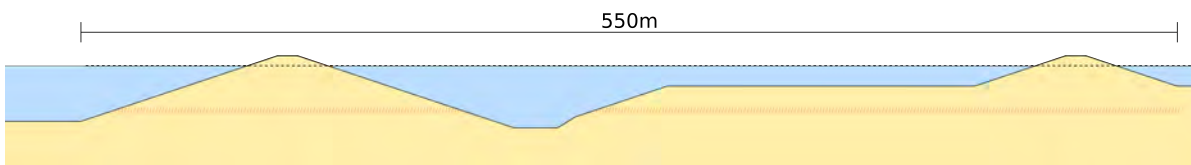


Figure T.3: Excavation inside construction pit

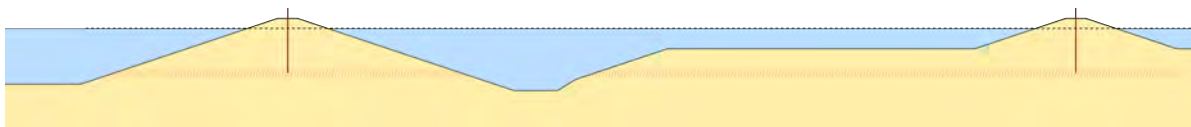


Figure T.4: Installation of sheet piles

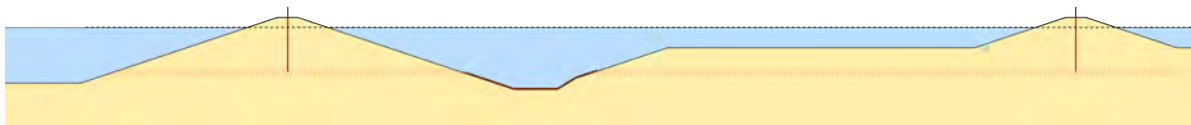


Figure T.5: Waterproof membrane at bottom of construction pit

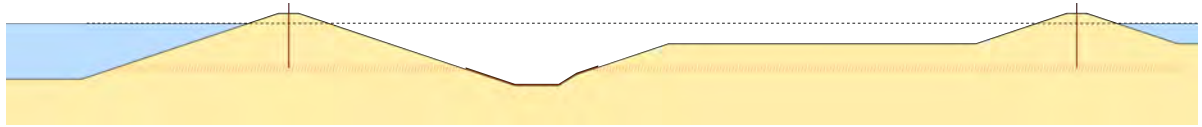


Figure T.6: Dewatering of construction pit

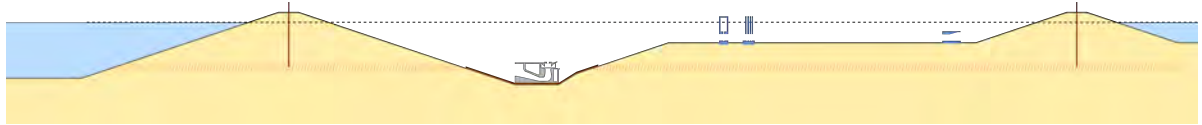


Figure T.7: In-situ construction of pumphouse, emergency gate housing, and sea-side inlet

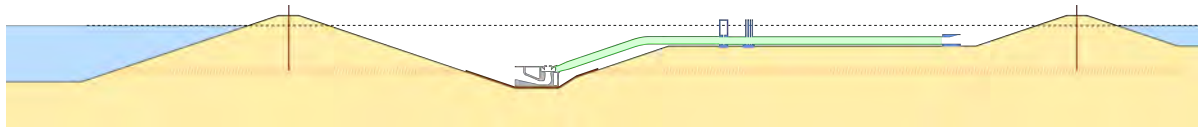


Figure T.8: Construction of penstock

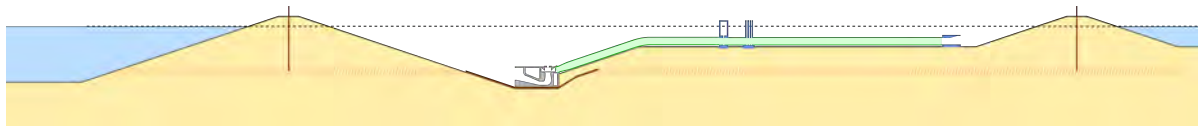


Figure T.9: Backfilling inner slope

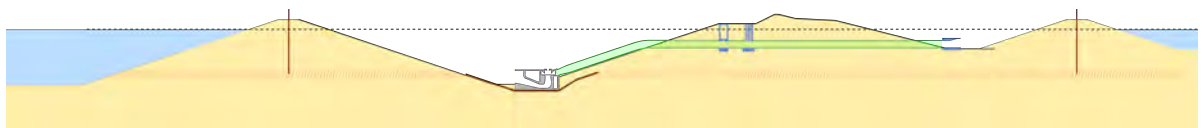


Figure T.10: Backfilling of dike core

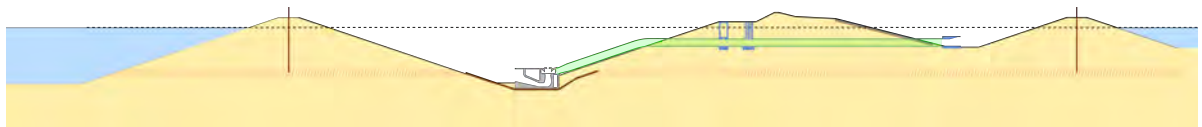


Figure T.11: Placement of dike revetment

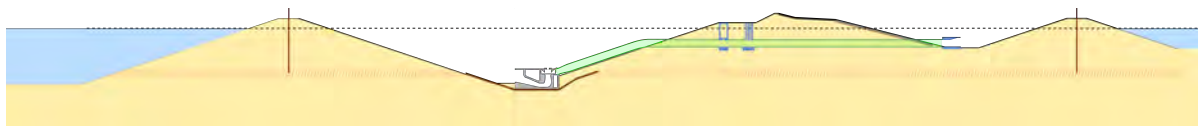


Figure T.12: Asphaltting dike upper slope

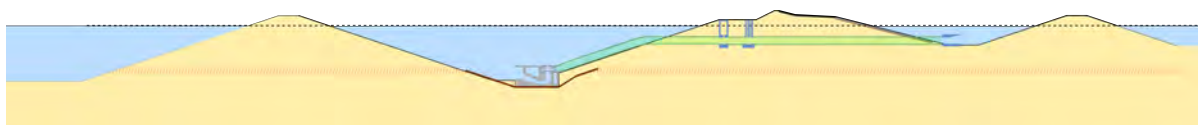


Figure T.13: Extrusion of sheet piles and flooding of construction pit

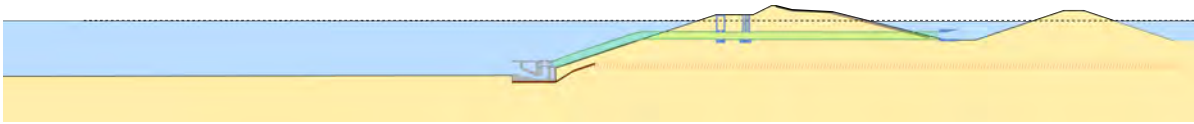


Figure T.14: Dredging of lake-side embankment

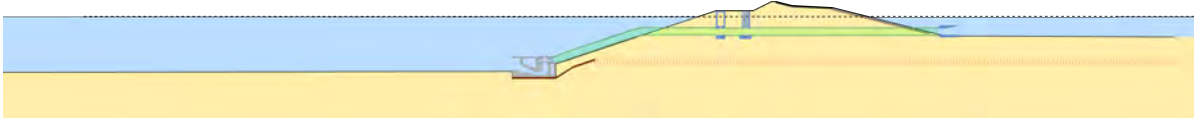
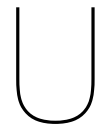


Figure T.15: Dredging of sea-side embankment



Construction Sequence: Cofferdam Method

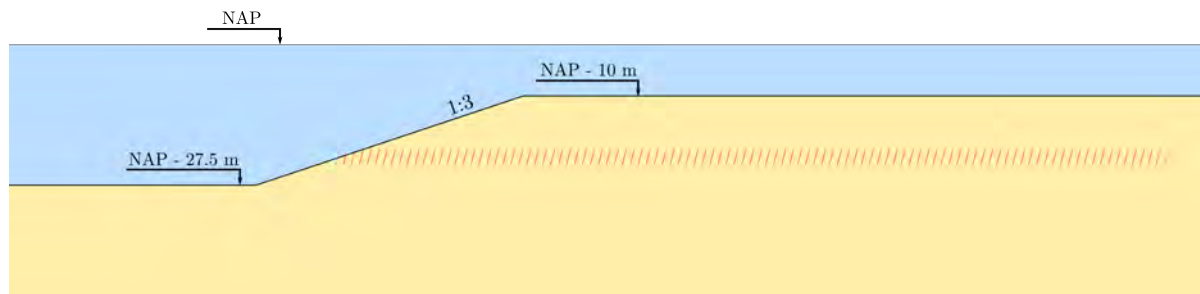


Figure U.1: Initial situation

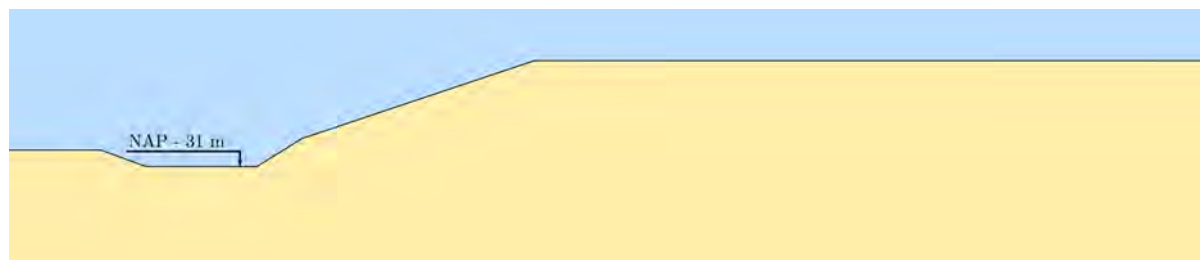


Figure U.2: Excavation Until NAP - 31 m

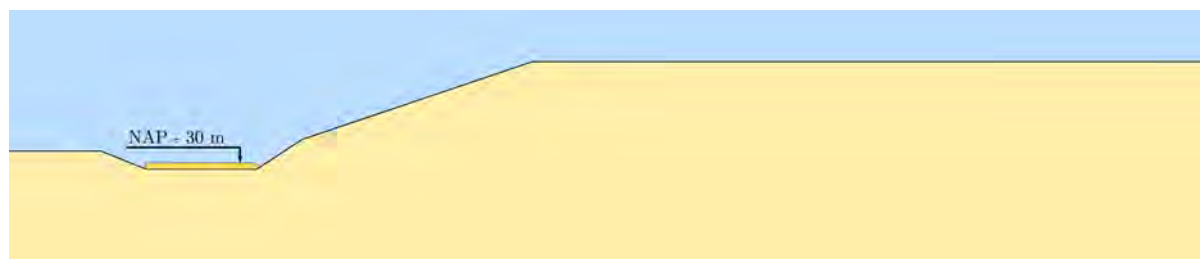


Figure U.3: Ground Improvement and Compaction Underneath Pumphouse

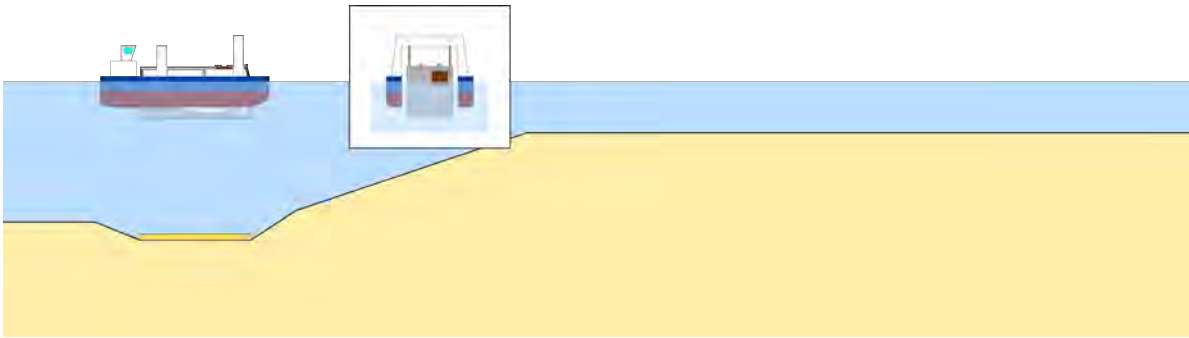


Figure U.4: Transportation of Prefabricated Pumphouse from Work Island

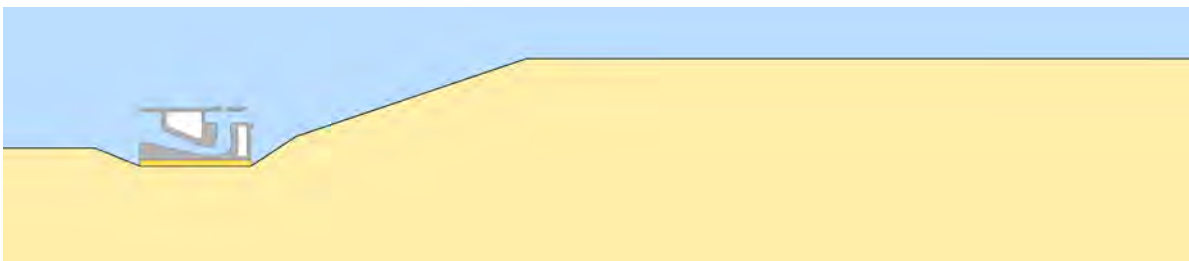


Figure U.5: Installation (sinking) of Pumphouse

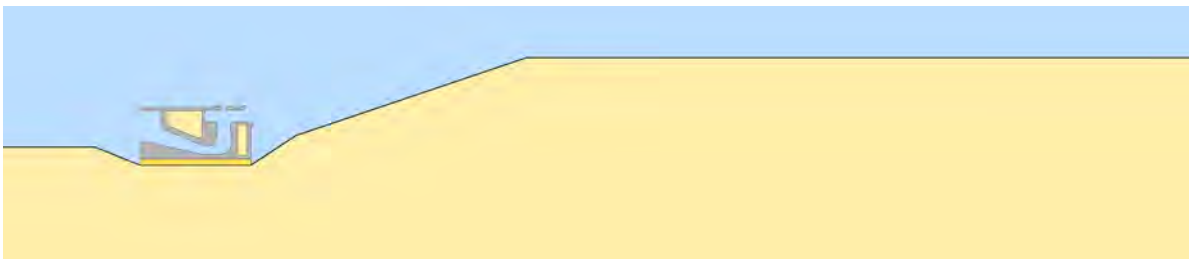


Figure U.6: Filling voids of pumphouse with sand



Figure U.7: Backfilling around pumphouse

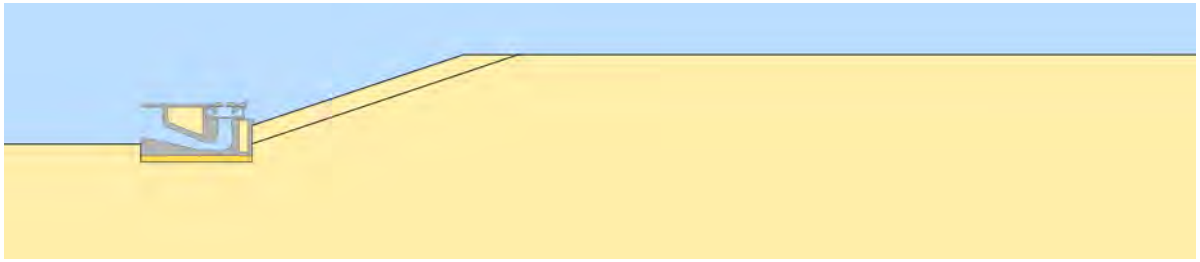


Figure U.8: Backfilling inner slope



Figure U.9: Initial situation

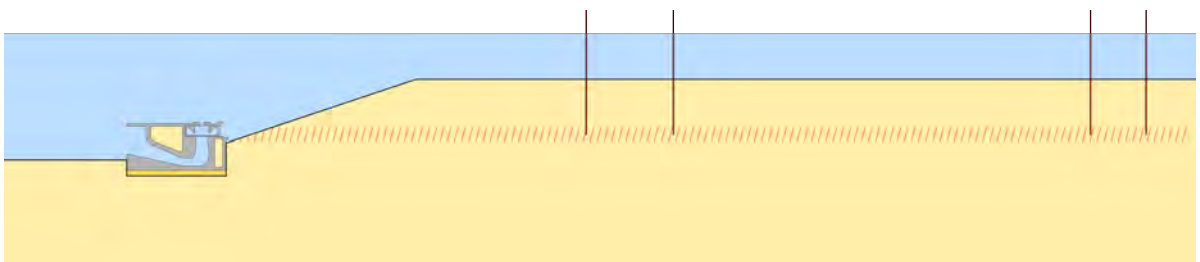


Figure U.10: Installation of sheet piles

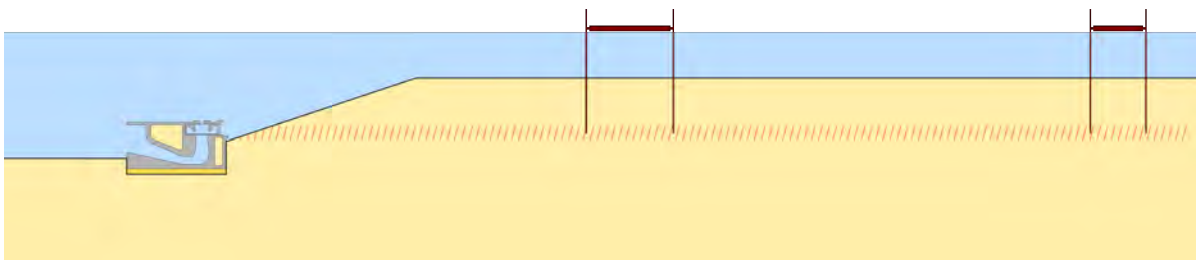


Figure U.11: Installation of Struts

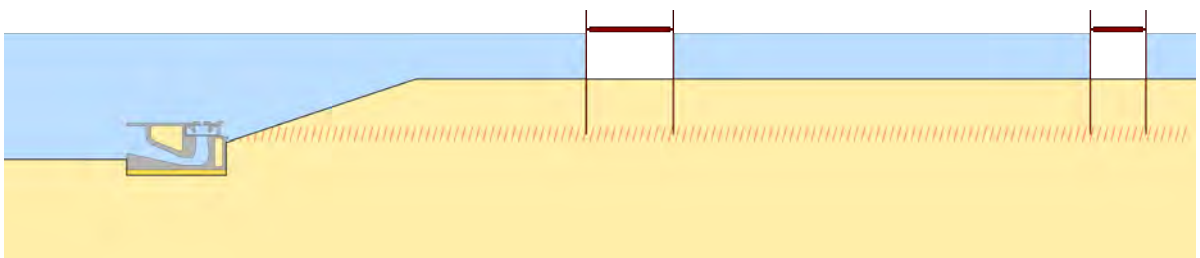


Figure U.12: Emptying cofferdam

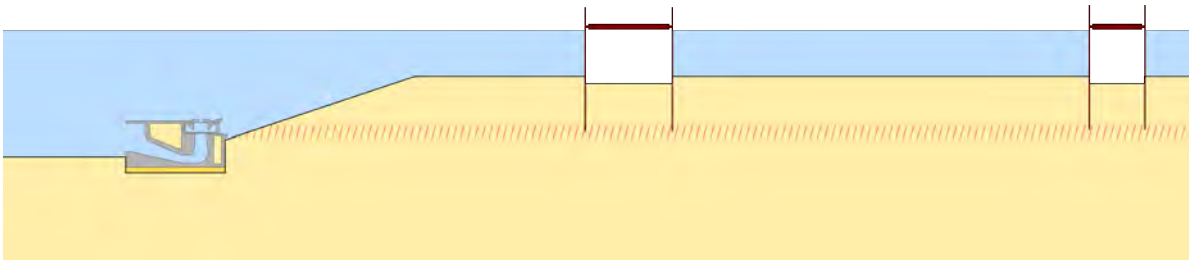


Figure U.13: Excavation of cofferdam to NAP - 10.5 m

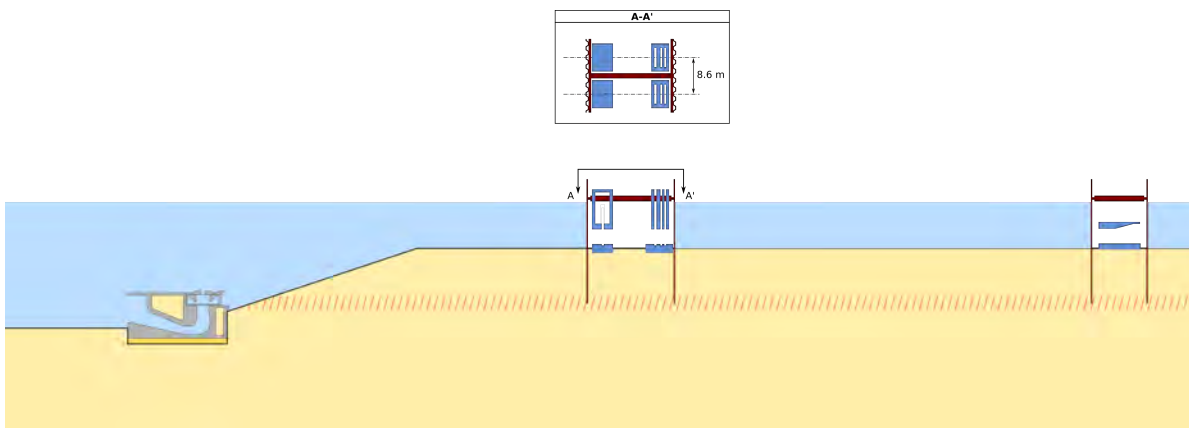


Figure U.14: In-situ construction of emergency gate housing and sea-side inlet

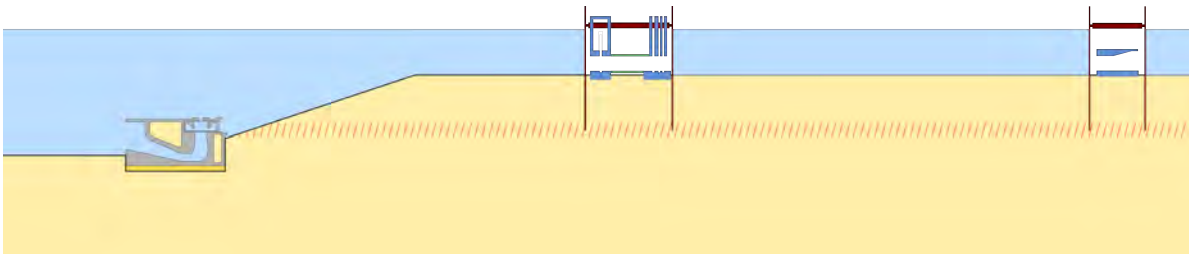


Figure U.15: Installation of penstock

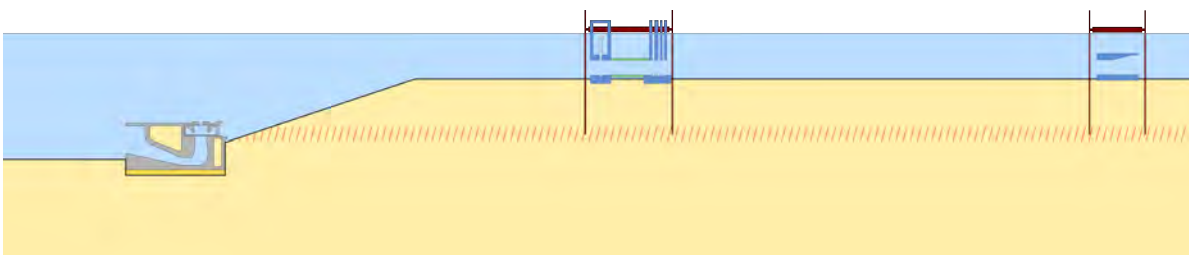


Figure U.16: Flooding of cofferdam

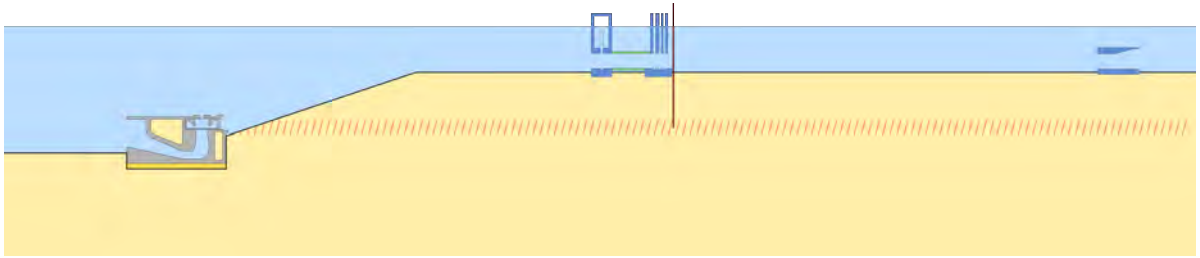


Figure U.17: Removal of struts and sheet piles

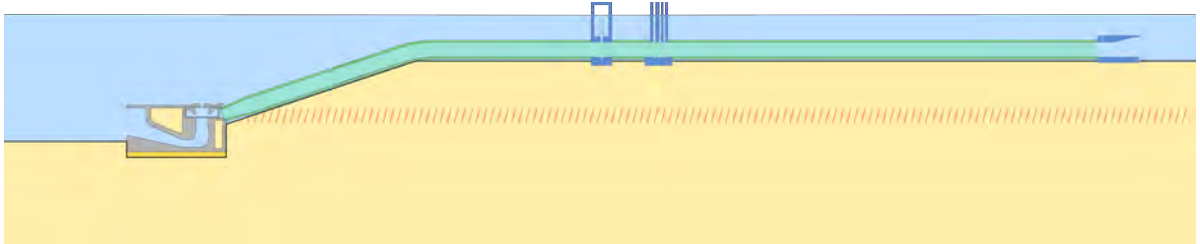


Figure U.18: Underwater installation of penstock

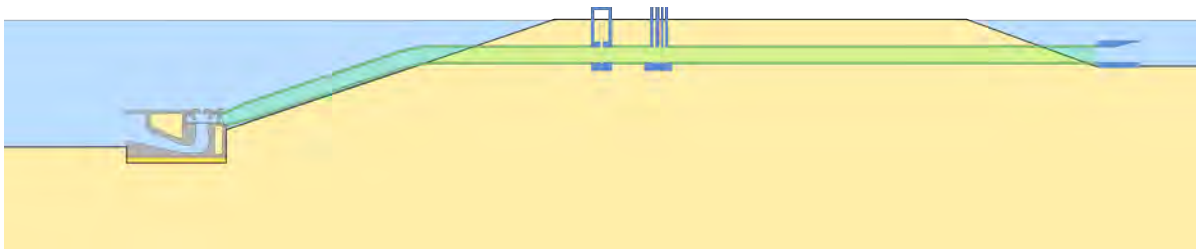


Figure U.19: Backfilling of dike

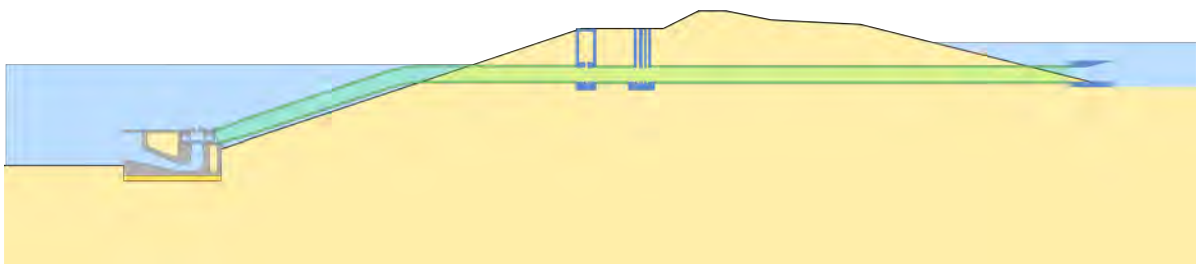


Figure U.20: Construction of rest of dike

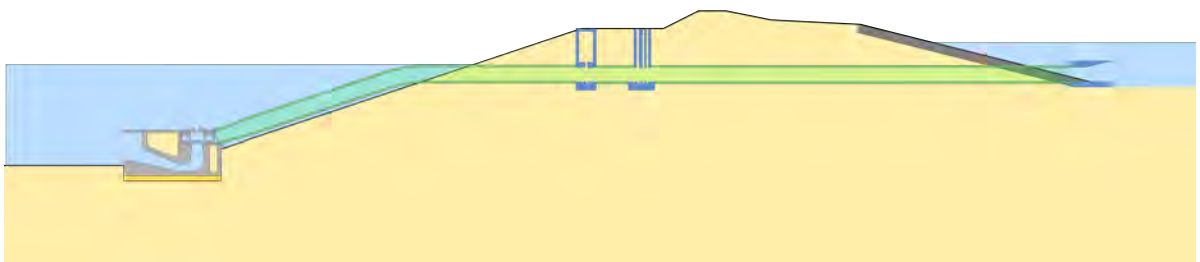


Figure U.21: Laying of revetment lower slope

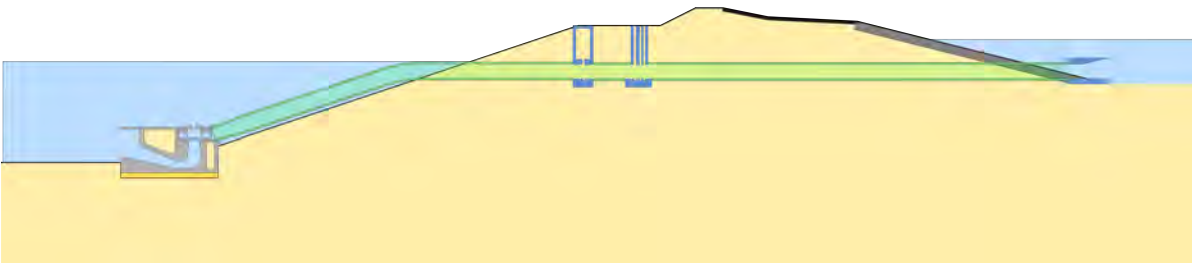


Figure U.22: Asphaltting upper slope

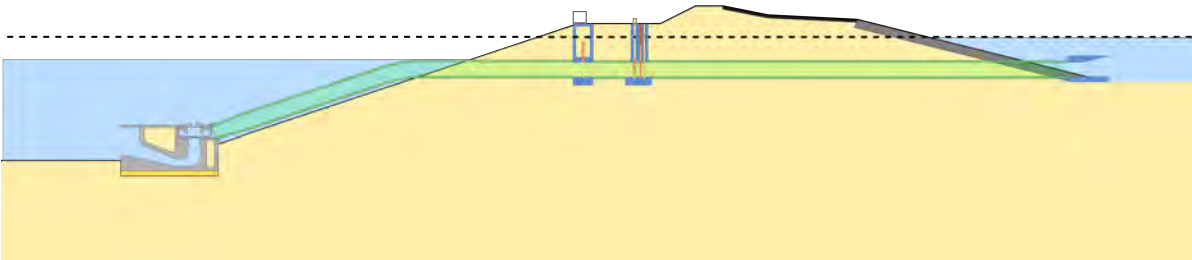


Figure U.23: Construction of electrical installation and standard equipment



Construction Sequence: Caisson Method

The steps between the initial situation and the first step in this method are identical to the first 9 steps of the Cofferdam Method, shown in Appendix U, Figures U.1 to U.9.



Figure V.1: Initial situation



Figure V.2: Installation of sheet piles

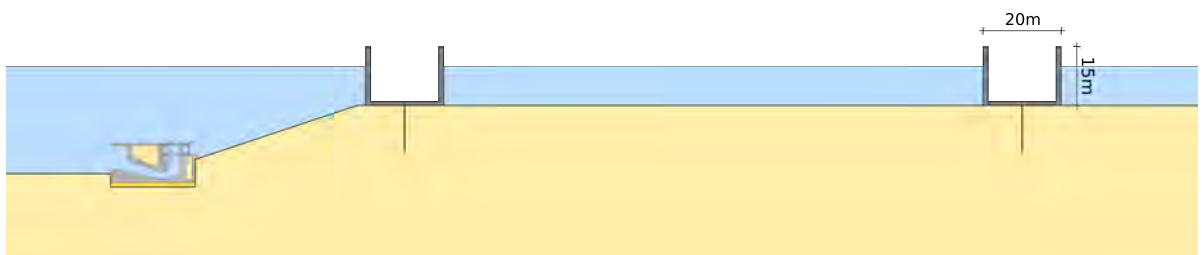


Figure V.3: Sinking of caissons on top of sheet piles

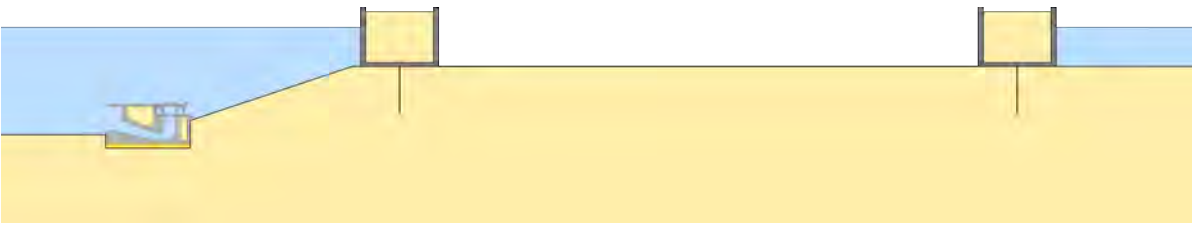


Figure V.4: Filling caissons with ballast material

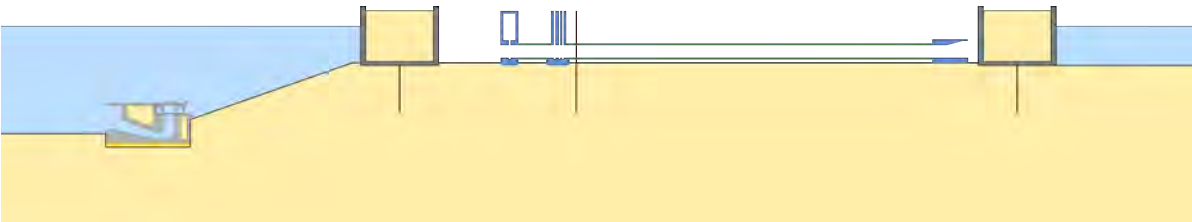


Figure V.5: In-situ construction of emergency gate housing and sea-side inlet. Installation of seepage screen

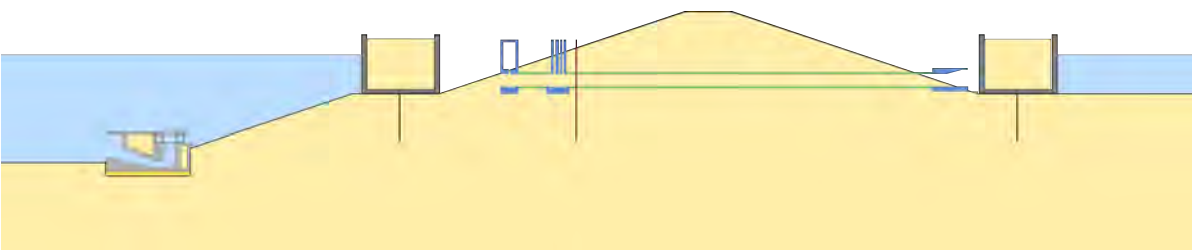


Figure V.6: Backfill of dike core

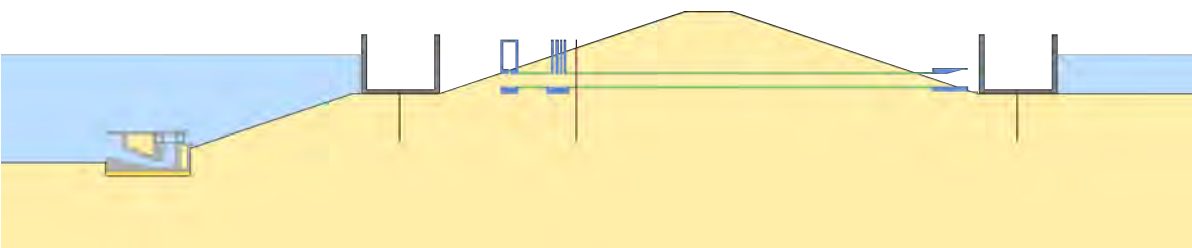


Figure V.7: Emptying caissons

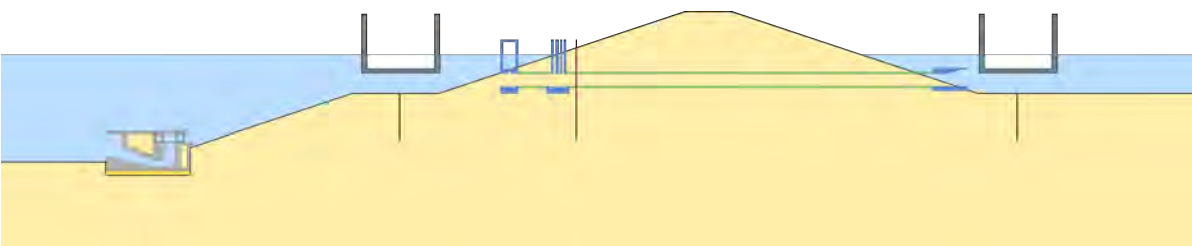


Figure V.8: Floating and removal of caissons

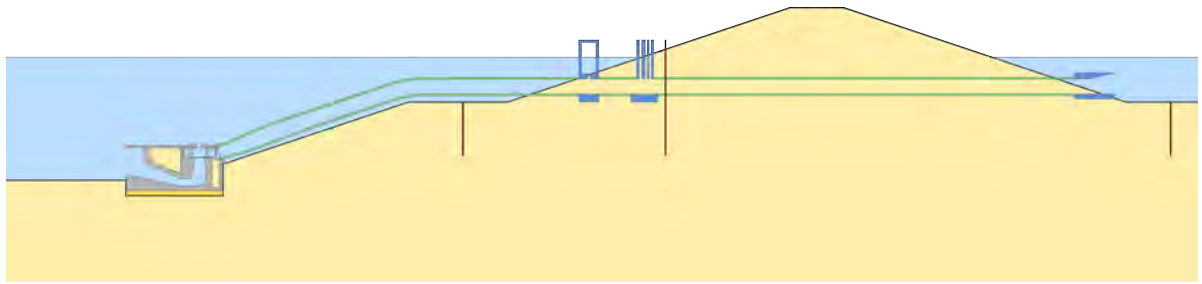


Figure V.9: Installation of penstocks

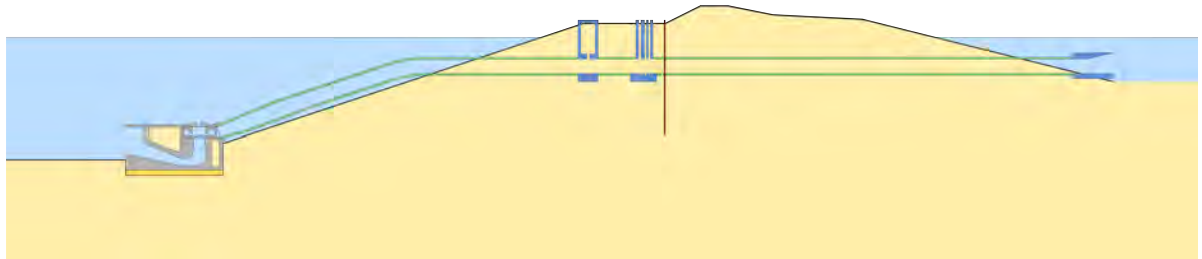


Figure V.10: Shaping of dike core

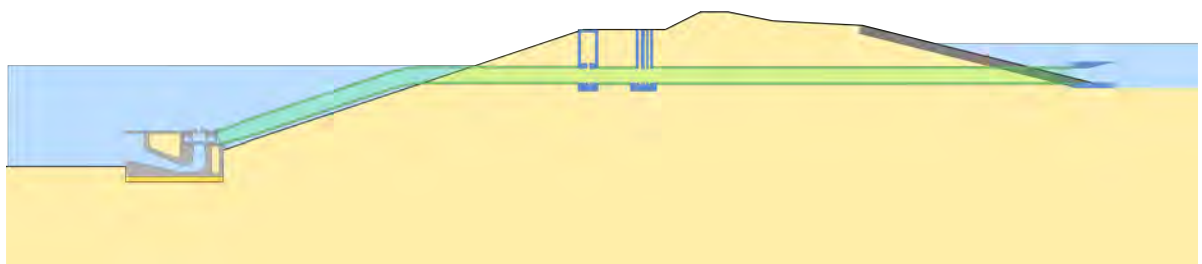


Figure V.11: Placing revetment on lower slope

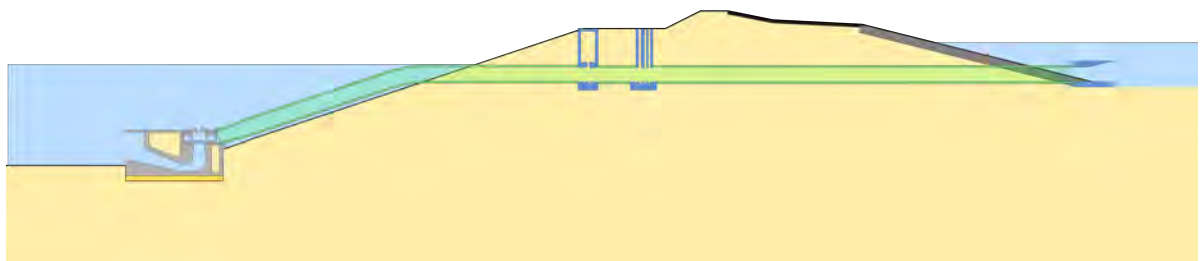


Figure V.12: Asphaltting upper slope

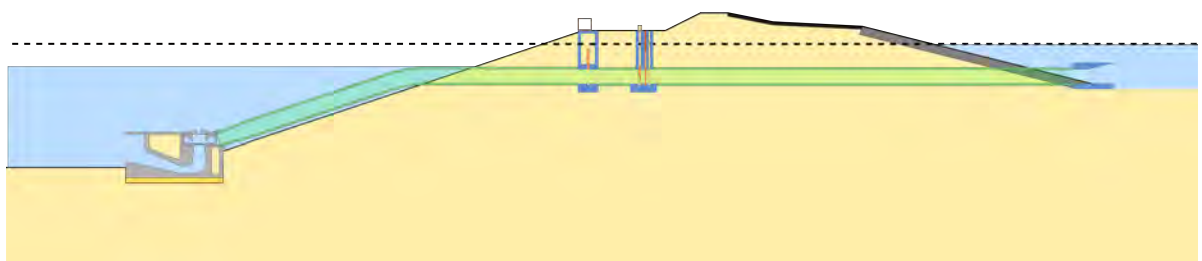
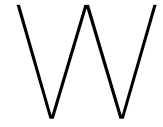
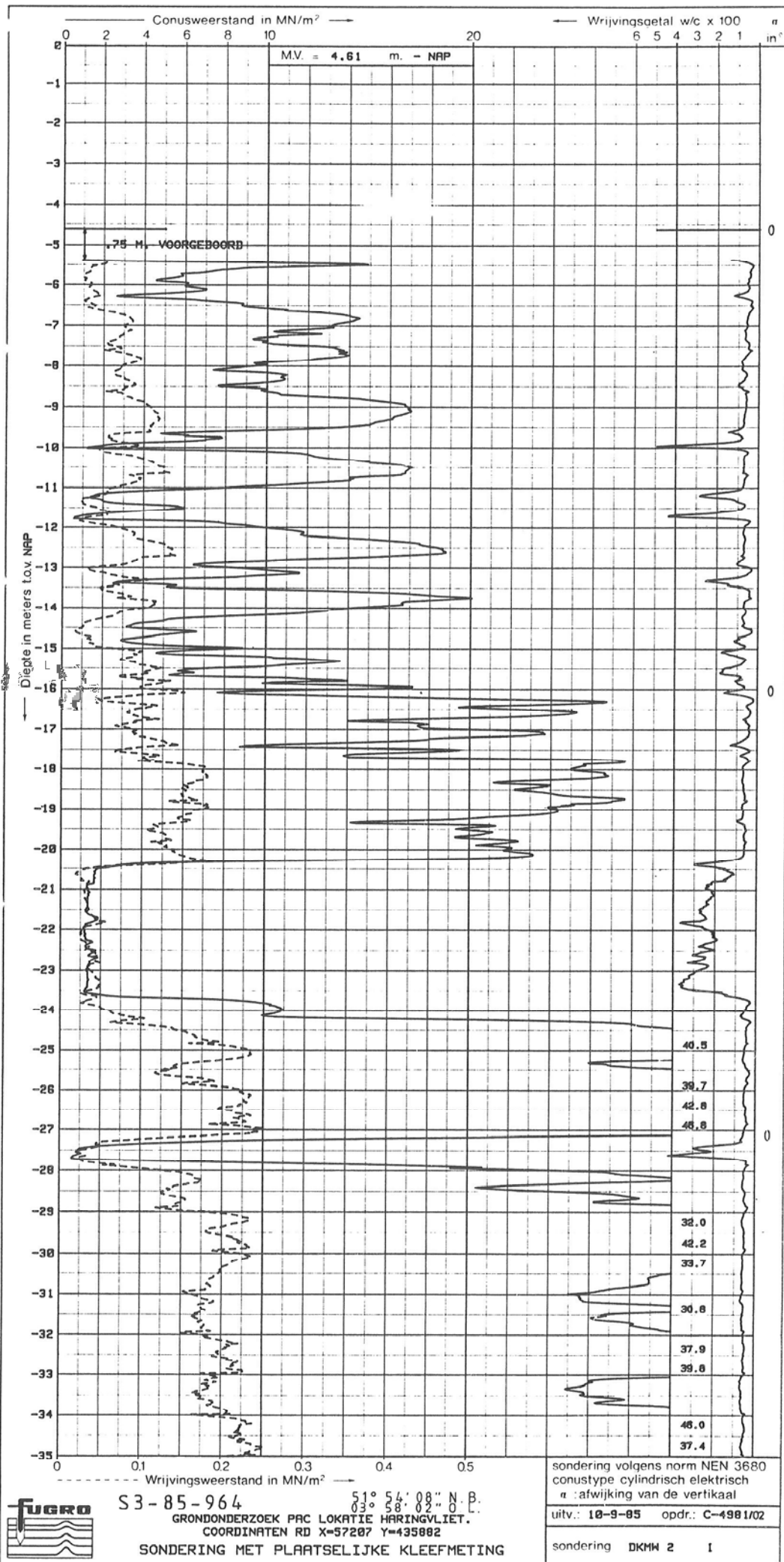


Figure V.13: Construction of powerhouse and installation of standard equipment



Cone Penetration Test



S3-85-964 51° 54' 08" N. B.
 03° 58' 02" O. L.
 GRONDONDERZOEK PAC LOKATIE HARINGVLIET.
 COORDINATEN RD X=57207 Y=435802
 SONDERING MET PLAATSELIJKE KLEEFMETING



Loads Acting on the Cofferdam

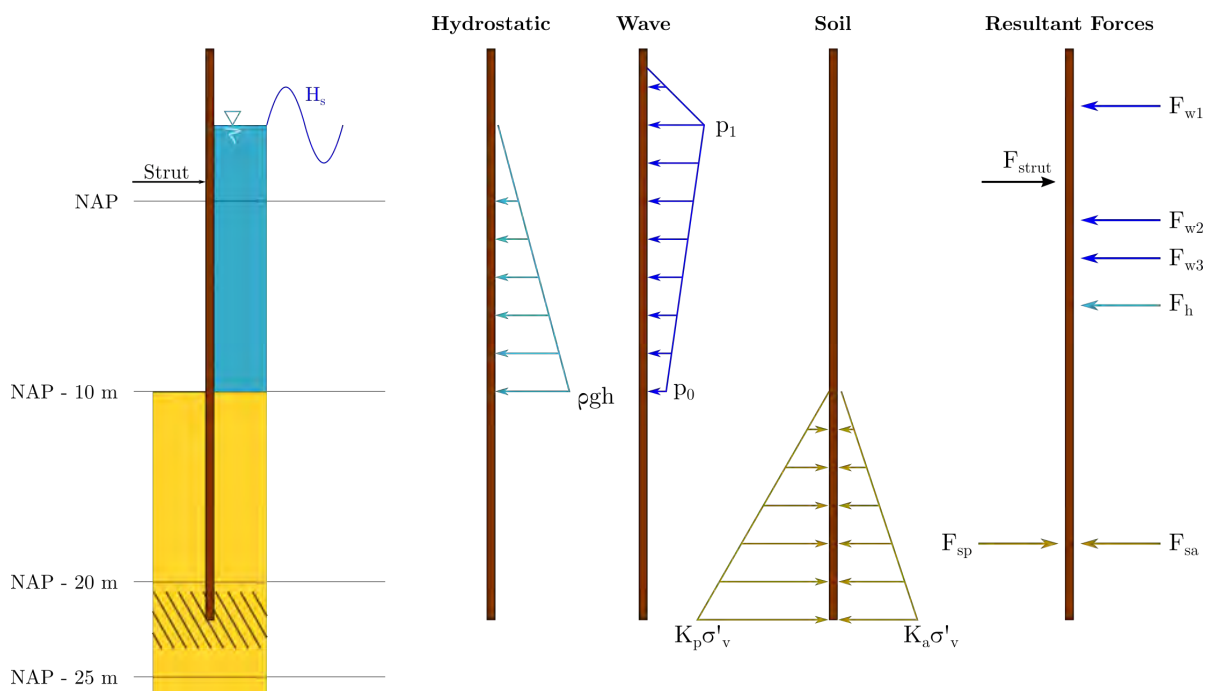


Figure X.1: Loads on the Cofferdam

The loads acting on the sheet piles during the cofferdam execution are represented in Figure X.1. The pore pressure on either of the sheet pile is neglected as it is the same and cancels each other out.

X.1. Hydrostatic Pressure

The maximal hydrostatic pressure on the sheet pile is given by the Equation X.1, h being the maximal depth.

$$p_{hydrostatic} = \rho \cdot g \cdot h \quad (X.1)$$

The governing hydrostatic pressure is given by the level during the expected storm surge, this being NAP + 3.85 meters. This returns a total depth of 13.85 meters, and thus a maximal pressure of 139.6 kN/m² or a point load of F_h 959.8 kN/m', m' being the distance width normal to the page in Figure X.1.

X.2. Wave Pressure

The calculation of the wave load follows from the theory of Sainflou. For this formula to be valid the wave must not be breaking, but at a depth of 10 meters, (or 13.85 meters in the governing situation) this is not the case. The significant wave height and period are 2.08 meters and 5.56 seconds, respectively. This returns a wavelength (in transitional depth) of 62.6 meters.

The wave pressures (p_0 and p_1) for Sainflou are given in Equations X.2 and X.3, while the expected increase in water level due to the wave (h_0) is given in Equation X.4 (Voorendt & Molenaar, 2020).

$$p_1 = \rho \cdot g \cdot (H_{in} + h_0) = 22.2 \text{ kN/m}^2 \quad (\text{X.2})$$

$$p_0 = \frac{\rho \cdot g \cdot H_{in}}{\cosh(k \cdot d')} = 13.45 \text{ kN/m}^2 \quad (\text{X.3})$$

$$h_0 = \frac{1}{2} \cdot k \cdot H_{in}^2 \cdot \coth(k \cdot d) = 0.14 \text{ m.} \quad (\text{X.4})$$

X.3. Soil Pressures

The majority of the forces are acting on the wet side of the cofferdam, inward. This means the soil pressure on the inside of the cofferdam will be of the passive nature, while those acting on the cofferdam from the outside, in the same direction as the hydrostatic pressure, are active pressures.

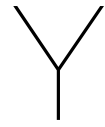
Lateral soil pressure coefficients for cohesionless soils (sand) are calculated with the Equations X.5 and X.6, ϕ being the angle of friction for the corresponding soil type (Verruijt, 2001).

$$K_a = \frac{1 - \sin \phi}{1 + \sin \phi} \quad (\text{X.5})$$

$$K_p = \frac{1 + \sin \phi}{1 - \sin \phi} \quad (\text{X.6})$$

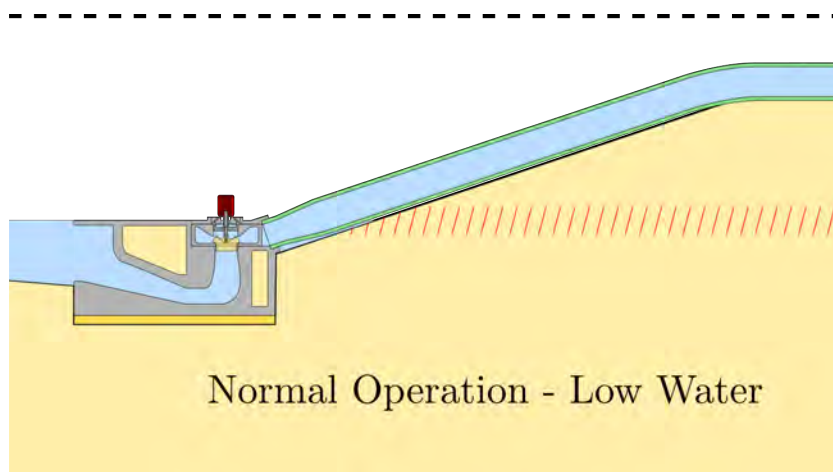
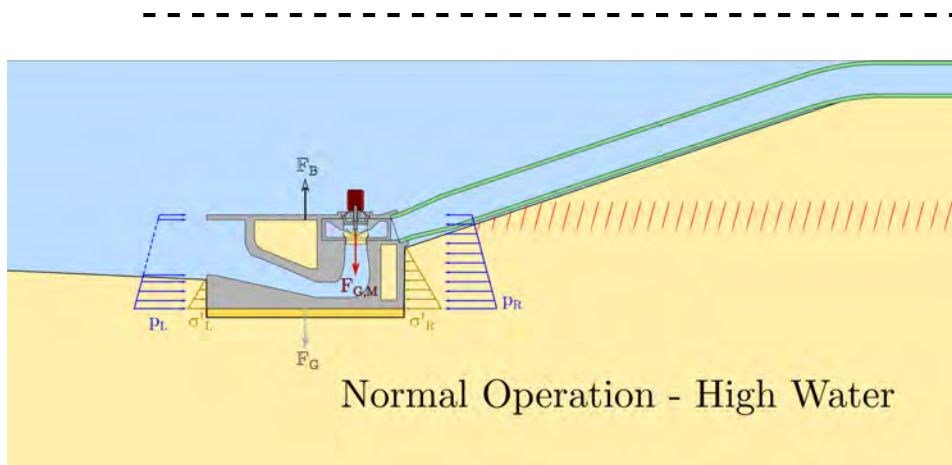
The sand at the location of the turbine pumping station has a relatively dense packing so the value of ϕ is 35° . This returns $K_a = 0.27$ and $K_p = 3.69$.

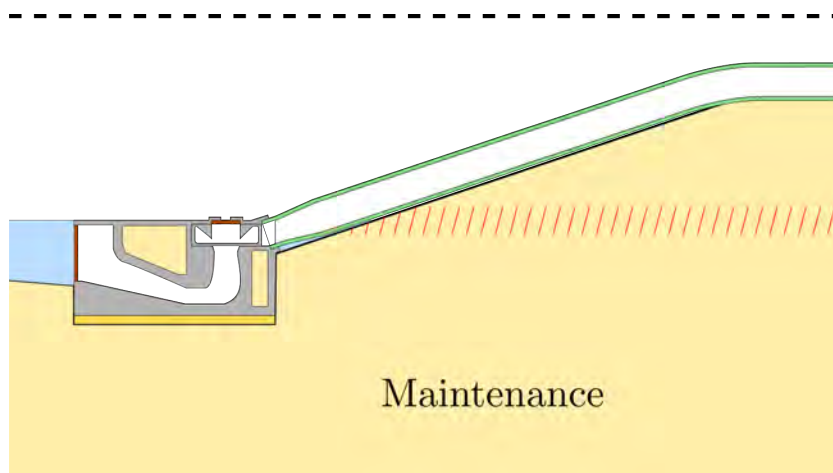
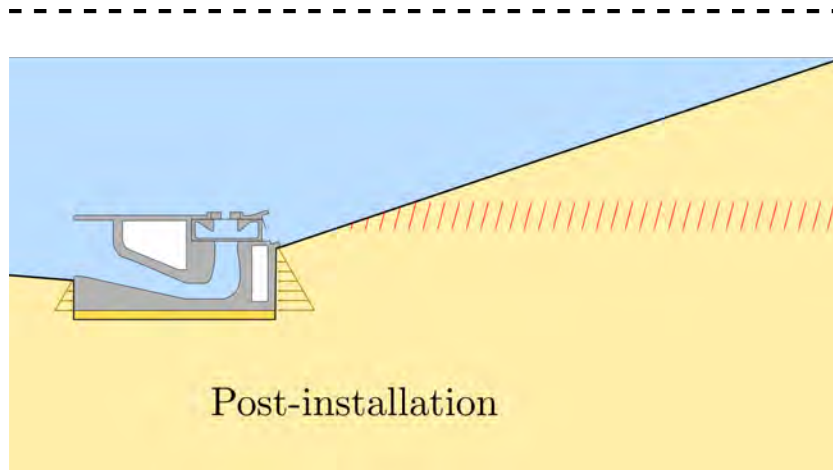
It should also be noted that the inside of the cofferdam will likely experience a surcharge due to the construction occurring inside, however since the surcharge on the passive side is favorable for the stability it will be neglected.



Loads Acting on the Pumphouse

Y.1. Scenario's





The four scenario's for which the forces acting on the pumphouse are shown. During maintenance the pumphouse is not sealed off when the water level is brought back to a maximum, as the hydrostatic pressures would be very large, and the pumphouse is not required to stay dry after removal of the motor and blades.

Y.2. Self-Weight

The volumes of the pumphouse can be estimated with the dimensions given in Figure Y.1. For this it is assumed the walls of the pumphouse on either side are 0.6 meters thick, resulting a space 7.4 meters wide at the outlet and total width of 8.6 meters.

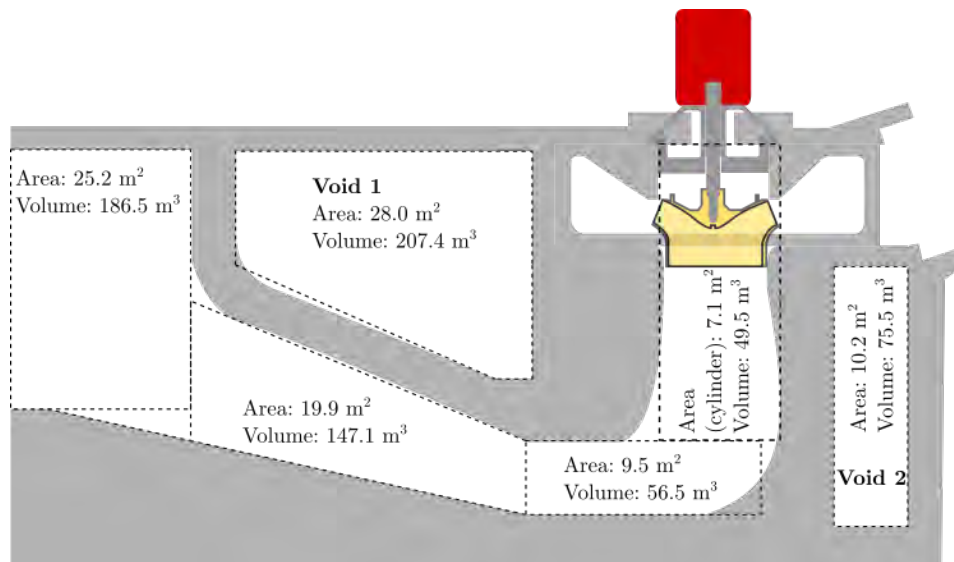


Figure Y.1: Dimensions of the Cross Section of the Pumphouse

The voids are filled with sand when the pumphouse is installed. Table Y.1 shows the respective volumes of all the parts of the pumphouse. The total volume is determined by assuming a caisson with dimensions 8.6 by 10 by 22 meters.

	Volume [m^3]
Total	1892
Concrete	1169.5
Voids	282.9
Waterway	439.6

Table Y.1: Volumes of the Parts of the Pumphouse

As well as this, the motor and the pump impeller are also included in the self weight of the pumphouse. The mass of these combined is 25,000 kg.

The self weights are collected as follows:

- Pumphouse, only concrete: 28,682 kN
- Pumphouse, voids filled: 34,232 kN
- Pumphouse, voids filled, motor: 34,478 kN

Y.3. Center of Gravity

Depending on the scenario, the center of gravity changes due to a redistribution of the masses. As a reference point, the bottom left of the cross section of the pumphouse is used as the origin. The x and y coordinates (with respect to the origin) of the center of mass for each scenario is given in Table Y.2. This is calculated by dividing the pumphouse into smaller parts as shown in Figure Y.2. It is assumed that the pumphouse is symmetrical in the y-plane (normal to the page). The results show that the center of mass is very close to the middle of the bottom of the structure.

	x-coordinate [m]	y-coordinate [m]
Empty caisson	11.1	4.1
Voids filled	11.2	2.8
Voids filled, with motor	11.6	2.9

Table Y.2: Location of the Center of Mass

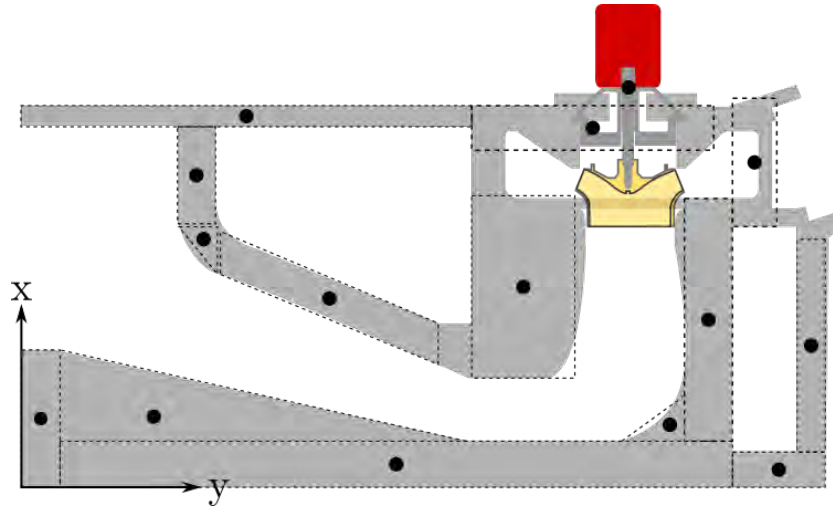


Figure Y.2: Center of Mass

Y.4. Buoyant Forces

The buoyancy of an item at rest is determined by the amount of water that it displaces. The pumphouse can either be full of water, or during maintenance and installation, emptied. During normal operation when the chamber is filled, the upward buoyant forces total 11,702 kN. When the pumphouse is sealed off and emptied the buoyant forces are equal to 16,101 kN.

During installation, when the voids are not yet filled with sand, the total buoyant forces are 18,932 kN. However, the self weight of just the concrete is 28,682 kN, so this gives an effective mass of about 1000 tons.

Y.5. Soil Pressures

The soil on the sea-side of the pumphouse has a slope, therefore to calculate the active lateral earth pressure coefficient, the formula given in Equation Y.1 is used (Verruijt, 2001).

$$K_a = \frac{\sin^2(\alpha + \phi)}{\sin^2 \alpha \sin(\alpha - \delta) [1 + \sqrt{\{\sin(\phi + \delta) \sin(\phi - \beta)\} / \{\sin(\alpha - \delta) \sin(\alpha + \beta)\}}]^2} \quad (\text{Y.1})$$

Angles α and δ in this case are 90° , while β is the inner slope, which is 1:3. The variable ϕ is the friction angle and is taken as 35° . This results in an active earth pressure coefficient of 0.344.

A neutral pressure is used at the lake-side of the pumphouse, equal to 0.5 for sand. For saturated sand underwater this returns a horizontal pressure of 15 kPa at the based of the pumphouse.



Loads Acting on the Penstock

Z.1. Scenario's and Load Combinations

The main loads acting on the penstock can be split up into two categories: soil loads and hydraulic loads. Since the loads act in different directions they will be analysed separately in order to get the governing combination of loads.

The loads from the soil pressure are largest in the section of penstock underground.

Z.2. Loads

Z.2.1. Soil Pressure and Surcharges

The access road for the electrical installations is the biggest surcharge load on the soils, and is shown in Figure ?? as Section A-A'.

The load of the traffic on the road deck is determined using NEN-EN 1991-2+C1 (2015). The load combination for a single lane 3 meters wide is 4 point loads (Q_{ik}) of 300 kN, and a distributed load (q_{ik}) of 9 kN/m². Distributing the 4 point loads over the width of the road and 4 meters length gives a surcharge of 100 kPa. The self-weight of the concrete would be 2.5 kPa for a layer thickness of 0.1 meters, but is neglected in this case.

For the load combination in Section A-A', the ground will be considered unsaturated and free from groundwater, as this section is located behind the piping screen. The ground level is located at NAP + 3 m, while the middle of the penstock is at NAP - 7 meters. For an unsaturated sand, the 8 meters above the penstock create 144 kPa of pressure, as well as the surcharge of 100 kPa. The resultant earth pressure on the top of the pipeline is determined using the Terzaghi method shown in Figure Z.1 (French Society for Trenchless Technology, 2004). The effects of ovality and the pressure underneath the pipeline are neglected.

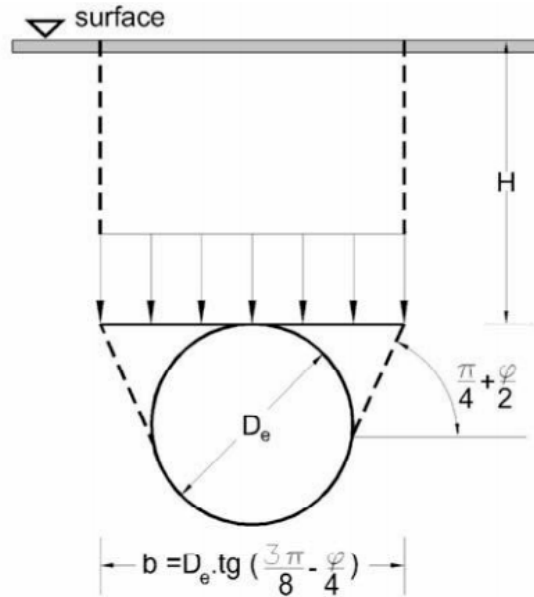


Figure Z.1: Terzaghi Method for Determining Soil Stresses on Underground Pipelines (French Society for Trenchless Technology, 2004)

The value b in Figure Z.1 is equal to 6.9 meters. The formula defining the earth pressure atop the pipeline (σ'_v) is given in Equation Z.1 (French Society for Trenchless Technology, 2004).

$$\sigma'_v = \frac{b \cdot \left(\gamma - \frac{2 \cdot c}{b} \right)}{2 \cdot K \cdot \tan \varphi} \left(1 - e^{-\frac{2 \cdot K \cdot \tan \varphi \cdot H}{b}} \right), \text{ where (for sand): } K = 1 \quad (\text{Z.1})$$

The combined pressure of soil and surcharge results in a pressure of 197 kPa on top of the pipeline.

Z.2.2. Flow Through the Penstock

The pressure in the penstock due to the hydrostatic pressure and the flow pressure is determined using Bernoulli's equation (Equation 5.3).

The largest difference in head for the pumping station is during storm surge levels and when the energy storage lake is at its lowest level. This results in a head difference of 27.5 meters.

The largest head difference results in a pressure of 275 kPa. The highest flow velocity (during turbine operation) results in an extra pressure of 5 kPa.

Z.2.3. Water Hammer

As discussed in Section 4.15 there exists a region in the pump characteristic where the discharge can fluctuate suddenly. This change in discharge is largest at the maximum impeller speed, and as stated in Section 4.15, the maximum change in flow rate is 12 m³/s. For the narrowest area of the penstock, where $D = 2650$ mm, this results in a velocity change of 2.2 m/s.

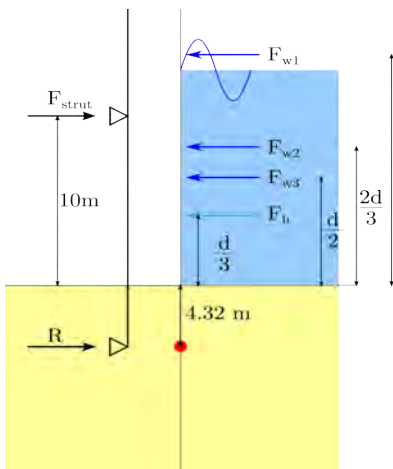
Jouwkowsky studied the effects of water hammer and gave an equation which determines the over-pressure (Δp_{Jou}) created for a change in velocity (Δv). The formula, in Equation Z.2 depends also on the density of the fluid (ρ) and the wave speed inside the pipeline (a), given in Equation Z.3 (Lüdecke

& Kothe, 2006).

$$\Delta p_{\text{Jou}} = \rho \cdot a \cdot \Delta v \quad (\text{Z.2})$$

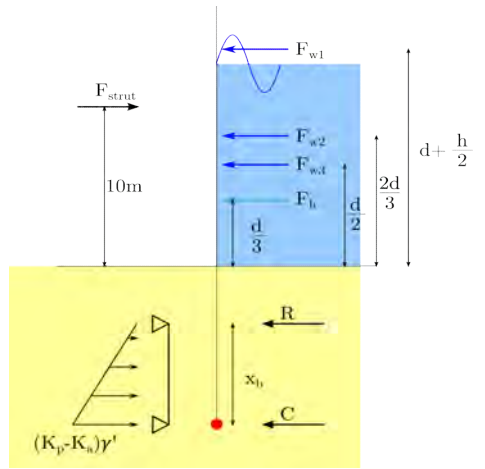
$$a = \sqrt{\frac{1}{\frac{\rho}{E_F} + \frac{\rho \cdot d_i \cdot (1 - \mu^2)}{E_A \cdot s}}} \quad (\text{Z.3})$$

Equivalent Beam Calculations



$d + \frac{h}{2}$
 $\frac{2d}{3}$
 $\frac{d}{2}$
 $\frac{d}{3}$
 4.32 m

$K_p - K_a$	3.42
d	13.84 m
h	2.22 m
t0	5 m
γ'	10 kN/m ³
E	2.1E+08 kN/m ²
I_{yy}	130140 cm ⁴
I_{yy}	0.001301 m ⁴
Waves 1	Force
	arm
Waves 2	Force
	arm
Waves 3	Force
	arm
Hydrostatic	Force
	arm
Soil	Force
	arm
distance	to strut
Contraflexure	depth
Moment T	Σu_{tot}
	R
Moment T	Σu_{tot}
	F_{strut}
	x_b
	Moment



$d + \frac{h}{2}$
 $\frac{2d}{3}$
 $\frac{d}{2}$
 $\frac{d}{3}$
 x_b
 $(K_p - K_a)\gamma'$

Forces, Moments, and Displacements During Cofferdam Staging

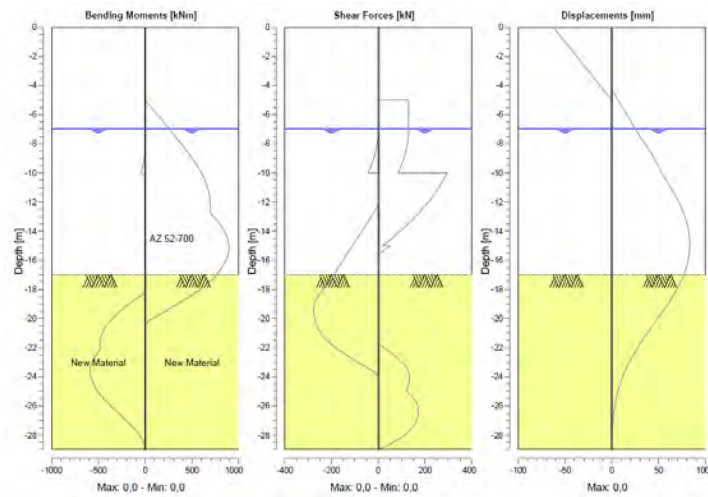


Figure .1: Stage 1

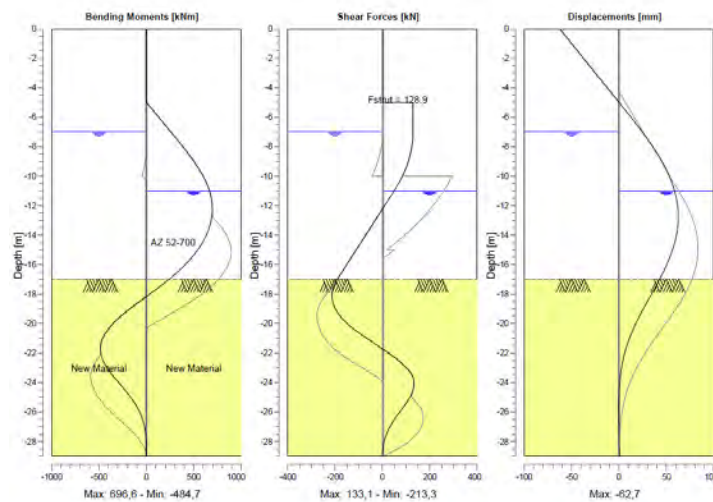


Figure .2: Stage 2

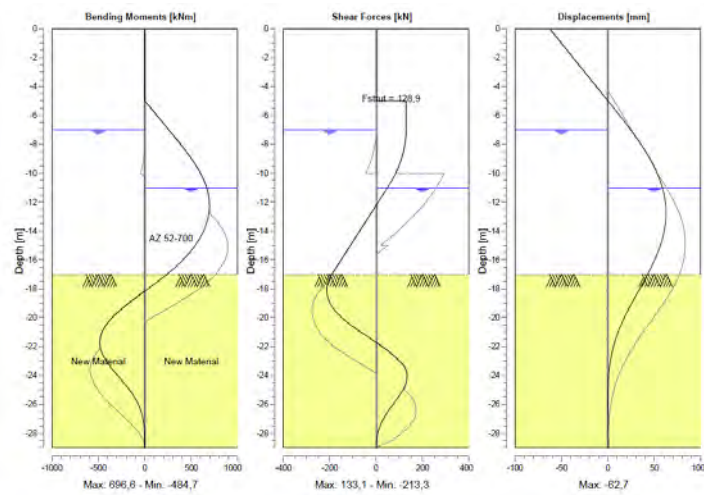


Figure .3: Stage 3

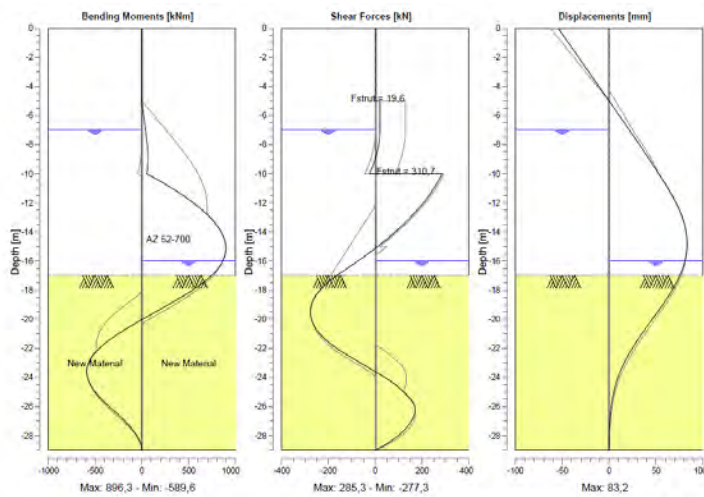


Figure .4: Stage 4

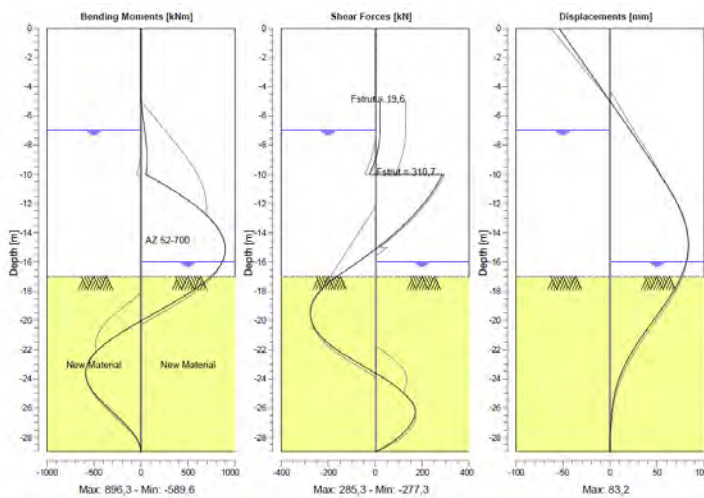


Figure .5: Stage 5

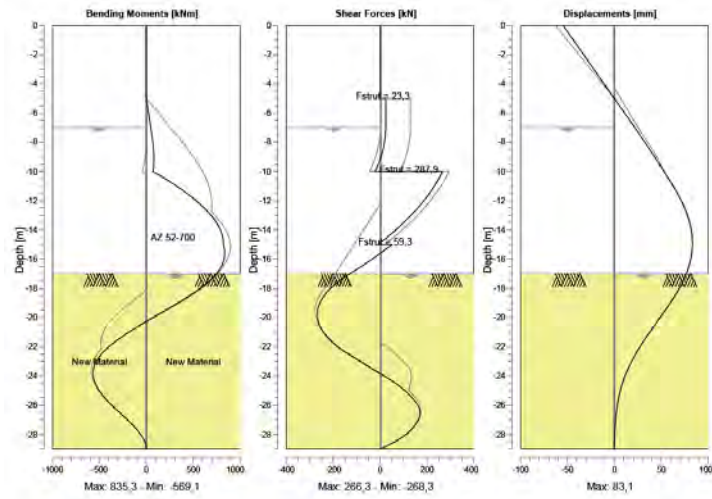


Figure .6: Stage 6

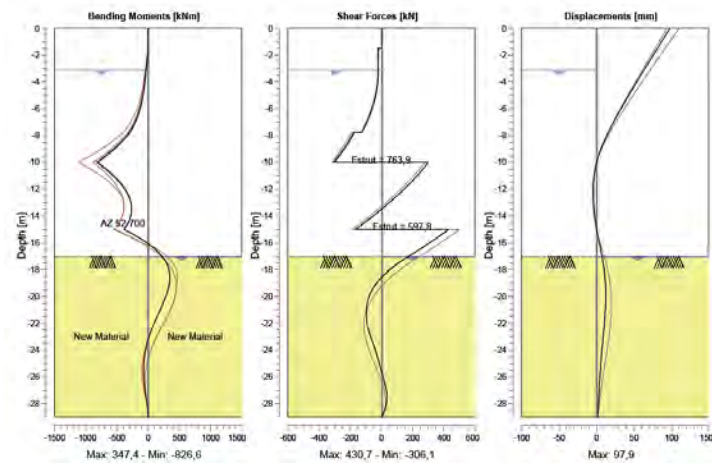


Figure .7: Governing Load Combination: SLS

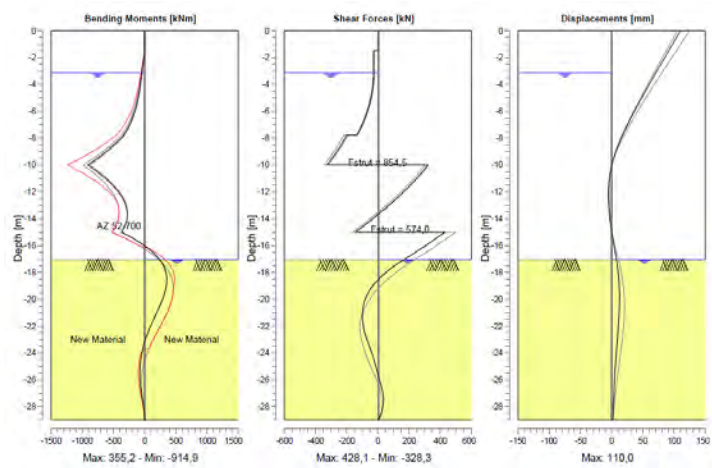


Figure .8: Governing Load Combination: ULS